Philipps Universität Marburg

NEW PERSPECTIVES ON THE SIGNIFICANCE OF BROWN ADIPOSE TISSUE IN MAMMALS

NEUE EINBLICKE IN DIE EVOLUTION DES BRAUNEN FETTGEWEBES DER SÄUGETIERE

Dissertation
zur
Erlangung des Doktorgrades
der Naturwissenschaften
(Dr. rer. nat.)

dem Fachbereich Biologie
der Philipps-Universität Marburg
vorgelegt von

REBECCA ÖLKRUG

aus Winterberg
Marburg/Lahn
Februar 2013

Vom Fachbereich Biologie der Philipps-Universität Marburg als
Dissertation am 30.04.2013 angenommen.

Erstgutachter: Prof. Dr. Gerhard Heldmaier
Zweitgutachter: Prof. Dr. Lothar Beck

Tag der mündlichen Prüfung am: 23.05.2013

Für meine treuen Weggefährten

“The important thing in science is not so much to obtain new facts as to discover new ways of thinking about them.”

(Sir William Lawrence Bragg)

CONTENTS

GLOSSARY OF TERMS

ANT	adenine nucleotide translocase
ATGL	adipose triglyceride lipase
ATP	adenosine triphosphate
BAT	brown adipose tissue
BCA	bicinchoninic acid assay
BSA	bovine serum albumin
CA	cold acclimated
cAMP	cyclic adenosine monophosphate
CAT	carboxyatractylate
CET	central European time
Cyt c	cytochrome c
COX	cytochrome c oxidase
cDNA	complementary desoxyribonucleic acid
CRE	cAMP response element
CREB	cAMP response element binding protein
E.coli	*Escherichia coli*
ETF	electron transfer flavoprotein
EGTA	ethylene glycol tetraacetic acid
^{18}F-FDG	^{18}F-fluorodeoxyglucose
FCCP	carbonyl cyanide-phenylhydrazone
FFA	free fatty acid
Fig	figure
G3Pdh	glycerol-3-phosphate dehydrogenase
GDP	guanosine diphosphate
HP	heat production
HEK	human embryo kidney
HSL	hormone sensitive lipase
ICDH	isocitrate dehydrogenase
LPL	lipoprotein lipase
mRNA	messenger ribonucleic acid
MYA	million years ago
MR	metabolic rate
NADH	nicotinamide adenine dinucleotide
$NADP^+$	nicotinamide adenine dinucleotide phosphate
NST	nonshivering thermogenesis
PCR	polymerase chain reaction
PET-CT	positron emission tomography - computed tomography
PKA	protein kinase A
PPARγ	peroxisome proliferator-activated receptor
PuNu	purine nucleotides
RACE-PCR	rapid amplification of cDNA ends - PCR
qPCR	quantitative PCR
ROS	reactive oxygen species
Ta	ambient temperature
Ta_{min}	minimum ambient temperature
Tb	body temperature
Tb_{min}	minimum body temperature
TGL	triglycerides
TPMP	triphenylmethylphosphonium
TR	thyroid hormone receptor
UCP	uncoupling protein
UCP1-KO	UCP1-knockout
UTR	untranslated region
VLDL	very low density lipoproteins
WA	warm acclimated
WT	wild-type

INTRODUCTION

REGULATORY THERMOGENESIS IN MAMMALIAN ENDOTHERMS

Mammals are able to maintain relatively constant body temperatures of 30-37°C by means of endogenous heat production (Hayes and Garland 1995), a thermoregulatory behavior that is referred to as endothermy (IUPS-Thermal-Commission 2003). Endothermy facilitates optimum temperatures for most biochemical processes and thereby high levels of sustained activity, irrespective of daily and seasonal environmental temperature fluctuations (Heldmaier et al. 1990). This is an energetically costly behavior, which is illustrated by the fact that the resting metabolic rate of an endotherm is approximately 8-10 fold higher compared to an ectotherm of the same size and body temperature (Else and Hulbert 1981).

Endotherms spend a substantial proportion of their lives in thermal environments that are well below body temperature levels. Consequently, most thermal sensors are cold sensitive and cold sensation induces a rapid activation of regulatory thermogenesis and decreased skin blood flow by cutaneous vasoconstriction. These autonomous responses ensure that body temperature remains homeothermic within physiological limits (Nakamura and Morrission 2008).

Mammals possess two major mechanisms of regulatory heat production, shivering and nonshivering thermogenesis (NST, Cannon and Nedergaard 2004). During shivering thermogenesis temperature sensitive neurons of the cervical spinal cord respond to a cold stimulus and mediate the activation of antagonistically working muscle groups, a no-load contraction that converts chemical energy into heat instead of mechanical work (IUPS-Thermal-Commission 2003). This form of heat production provides additional heat on a short term scale; but hinders locomotion, increases thermal conduction by disrupting fur insulation and ultimately causes an increase in heat loss (Hart 1952, Heldmaier et al. 1989). In contrast, nonshivering thermogenesis is mainly initiated by cutaneous cold sensation and relies on biochemical, non-contractile processes. NST neither hinders locomotion nor increases heat loss, and it is therefore considered a more efficient way of regulatory thermogenesis (Cannon and Nedergaard 2004).

BROWN ADIPOSE TISSUE: ANATOMY AND MORPHOLOGY

Brown adipose tissue is a major thermogenic organ and the key source of nonshivering thermogenesis in mammals (BAT, Nicholls and Locke 1984). It was first discovered in hibernators, but increasing evidence suggests a more widespread distribution among the mammalian lineage, including humans (Nedergaard et al. 2007). In small mammals such as rats, mice and hamsters, brown adipose tissue is expressed in distinct depots predominantly in the front parts of the body (thorax; Fig. 2). The subcutaneous depots of the interscapular, dorso-cervical, axillary and suprasternal region are often

referred to as a "heating jacket" due to their anatomic location (Heldmaier et al. 2012). The interscapular brown fat depot has been most intensively studied in the past and is claimed as the most important depot as it transports warmed blood via the Sulzer's vein directly to the heart.

Brown adipose tissue is densely vascularised for the optimal distribution of heat, possesses multilocular fat droplets for rapid mobilization and burning of fatty acids and has a high mitochondrial density. Unlike white adipose tissue, brown fat mitochondria contain only minor amounts of ATP-synthase to convert nutritional energy into cellular energy equivalents (Cannon and Vogel 1977).

UNCOUPLING PROTEIN 1 IS CENTRAL TO BROWN ADIPOSE TISSUE MEDIATED NONSHIVERING THERMOGENESIS

The neuronal circuits and subcellular pathways by which cold sensation triggers brown adipose tissue thermogenesis have been intensively studied in the past: Cold-sensitive thermoreceptors on the skin or in the body core, spine and brain, transmit thermal afferent signals to the preoptic area in the hypothalamus (Morrison et al. 2008) or to brain stem control regions (Bartness et al. 2010, Nautiyal et al. 2008), leading to the activation of postganglionic sympathetic fibres that release noradrenaline to the brown adipose tissue (reviewed by Klingenspor and Fromme 2012). Noradrenaline binds to specific β3-adrenergic receptors on the surface of brown adipocytes leading to the activation of a G-protein coupled signalling pathway that stimulates lipolysis and the subsequent release of free fatty acids (Fig. 1). These free fatty acids can serve as substrates for cellular beta oxidation, while they also act as direct activators of the unique brown fat protein, the uncoupling protein 1 (UCP1, Echtay et al. 2002, Echtay et al. 2003). UCP1 is a mitochondrial protein located in the inner mitochondrial membrane of brown adipocytes. Once activated, it acts like a proton channel and mediates the dissipation of the mitochondrial proton motive force as heat. Therefore, the presence and functionality of UCP1 is crucial for brown adipose tissue thermogenesis (Enerback et al. 1997, Golozobouva et al. 2001).

UCP1 (previously known as UCP or thermogenin) belongs to the family of mitochondrial anion carrier proteins and accounts for up to 8% of the total mitochondrial protein content (Rousset et al. 2004). UCP1 consists of monomers formed by approximately 300 amino acids with a molecular weight of 32kDa (Ricquier and Kader 1976). Six transmembrane α-helices (Miroux et al. 1993) form three repeats and both, the N- and C-terminal amino acids, face the intermembrane space. Based on structural and sequence similarities, several UCP1 paralogues have been identified: UCP2 (Fleury et al. 1997) and UCP3 (Boss et al. 1998) in vertebrates and UCP in birds (Vianna et al. 2001) and plants (Laloi et al. 1997). Even though an explicit description of the regulation and physiological function of UCP2 (ubiquitously expressed) and UCP3 (expressed in skeletal muscle, heart and brown fat) is lacking, the uniqueness of UCP1 in mediating brown adipose tissue nonshivering thermogenesis has

been confirmed on UCP1-ablated mice that are unable to defend their body temperature under acute cold exposure (Enerback et al. 1997).

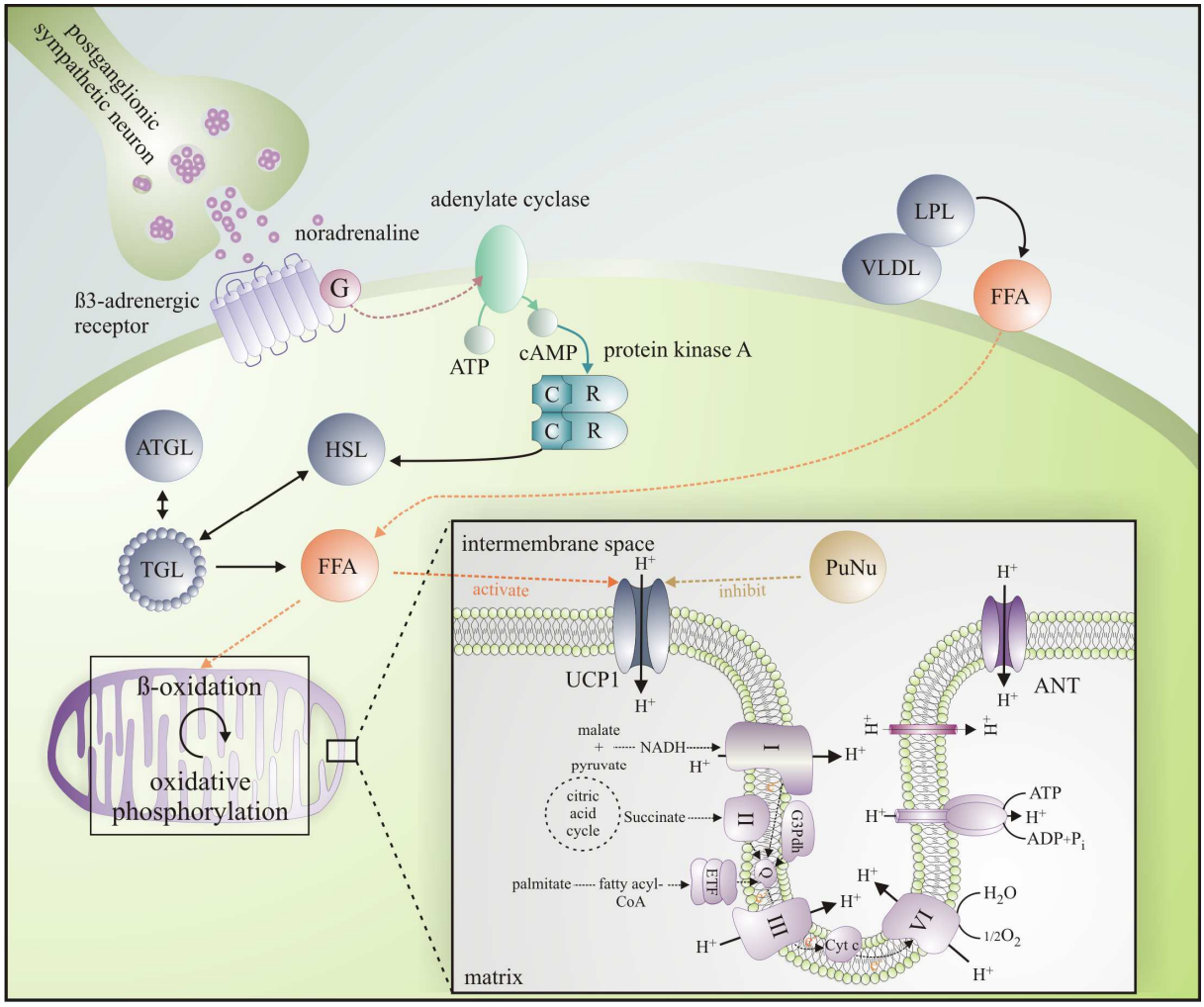

Figure 1: Sympathetic activation of UCP1-mediated nonshivering thermogenesis. Cold stimulates the sympathetic nervous system which in response releases the neuronal transmitter noradrenaline that binds to β3-adrenergic receptors on the plasma membrane of brown adipocytes. Subsequently, the adenylate cyclase is activated and converts ATP to cyclic AMP. cAMP activates the protein kinase A (PKA) whereupon the catalytic subunit detaches from the regulatory subunit. As a result the hormone sensitive lipase (HSL) and the adipose triglyceride lipase (ATGL) break down triglycerides (TGL) to free fatty acids (FFA). FFA serve, on the one hand, as substrates for β-oxidation and on the other hand are potent activators of the uncoupling protein 1 (UCP1) which uncouples the proton motive force from oxidative phosphorylation by generating a proton leak - dissipating the proton motive force as heat. The proton motive force is an electrochemical gradient generated by electron transfer that facilitates pumping of protons (complex I, III and IV) from the matrix to the intermembrane space. The lipoprotein lipase (LPL) releases FFA from very low density lipoprotein (VLDL), when the cellular storage of triglycerides is depleted. UCP1 is persistently inhibited by purine nucleotides (PuNu). The adenine translocase (ANT) and a basal proton leak additionally participate to the, ATP-synthases independent, reduction of the proton gradient. The glycerol-3-phosphat dehydrogenase (G3Pdh), complex I and complex III are the most potent sites of mitochondrial reactive oxygen species production. ETF: electron transport flavoprotein, Cyt c: cytochrom c.

At thermoneutral ambient temperatures, i.e. thermal conditions obviating thermoregulatory heat production, uncoupling through UCP1 is inhibited by physiologically relevant concentrations (up to 10mM) of purine nucleoside di- and triphosphates. Following adrenergic stimulation, long-chain fatty

acids can overcome this inhibition (Nicholls and Locke 1984, Shabalina et al. 2004, Jastroch et al. 2012) but the underlying mechanism still remains elusive (Klingenberg 2010, Divakaruni and Brand 2011). Currently three competing models are discussed: 1.) fatty acids are obligatory cofactors, which are required to transport protons across the inner mitochondrial membrane (Klingenberg and Winkler 1985, Winkler and Klingenberg 1994, Klingenberg and Huang 1999, Fedorenko et al. 2012: the long-chain fatty acid/proton shuttling model). 2.) The cycling of fatty acids is required for proton transport. Specifically, UCP1 transports fatty acid anions from the matrix to the intermembrane space, followed by protonation and flip-flop of the acids back to the matrix (Garlid et al. 1996, Garlid et al. 1998, Breen et al. 2006). 3.) Fatty acids induce an allosteric change to overcome persistent nucleotide inhibition of an inherently active UCP1 by simple competitive kinetics (Winkler and Klingenberg 1994, Rial et al. 2004, Shabalina et al. 2004). Even though the exact mechanism of UCP1 activation remains unclear, the analysis of UCP1 activity in *in vitro* experiments, using purine nucleotides as inhibitors and free fatty acids as activators, is a well-established method (Jastroch et al. 2012).

THE PHYSIOLOGICAL ROLE OF BROWN ADIPOSE TISSUE

Brown adipose tissue is inevitably associated with cold environmental temperatures and thermogenesis. This is substantiated by the fact that long term cold exposure leads to a proliferation of brown adipose tissue and improves its thermogenic capacity by enhancement of UCP1 expression and recruitment of its oxidative capacity (Klingenspor 2003, Fig. 2), a process termed *adaptive thermogenesis* (Lowell and Spiegelman 2000). Adaptive thermogenesis allows animals to appropriately adjust their thermoregulatory capacities to the seasonal requirements. The capacity for BAT-NST and its seasonal plasticity can be assessed *in vivo* by pharmacologically mimicking a cold stimulus (Heldmaier 1971, Heldmaier and Buchberger 1985) The Djungarian hamster, for example, increases its maximal noradrenaline induced thermogenic capacity from 55mW/g to 90mW/g during the winter months (Heldmaier and Klingenspor 2003).

Oxidative phosphorylation is incompletely coupled, since protons can leak across the inner membrane and relieve the proton potential independent of the production of ATP (Fig. 1). Accordingly, all metabolic processes that maintain the proton gradient require an up regulation, i.e. the electron flux over the complexes of the respiratory chain increases to counter the reduction in proton motive force. This so called basal proton leak thereby contributes significantly to the resting metabolic rate of an animal (up to 20%, Rolfe and Brown 1997, Lowell and Spiegelmann 2000). During thermogenesis UCP1 activity additionally enlarges the mitochondrial protein leak and indirectly enhances the respiratory activity of brown adipose tissue mitochondria (Nicholls 2001). Thereby nonshivering thermogenesis can account for as much as one third of the metabolic rate of small mammals under acute cold exposure (Foster 1984).

Historically, brown adipose tissue was first discovered in hibernators (“hibernation gland”, Freake and Oppenheimer 1987, Rasmussen 1923). It is now confirmed that brown adipose tissue is involved

in the generation of endogenous heat during arousal from hypometabolic and hypothermic states such as torpor and hibernation (Cannon and Nedergaard, 2004). Nonshivering thermogenesis is especially important during arousal at low body temperatures which are not permissive for shivering.

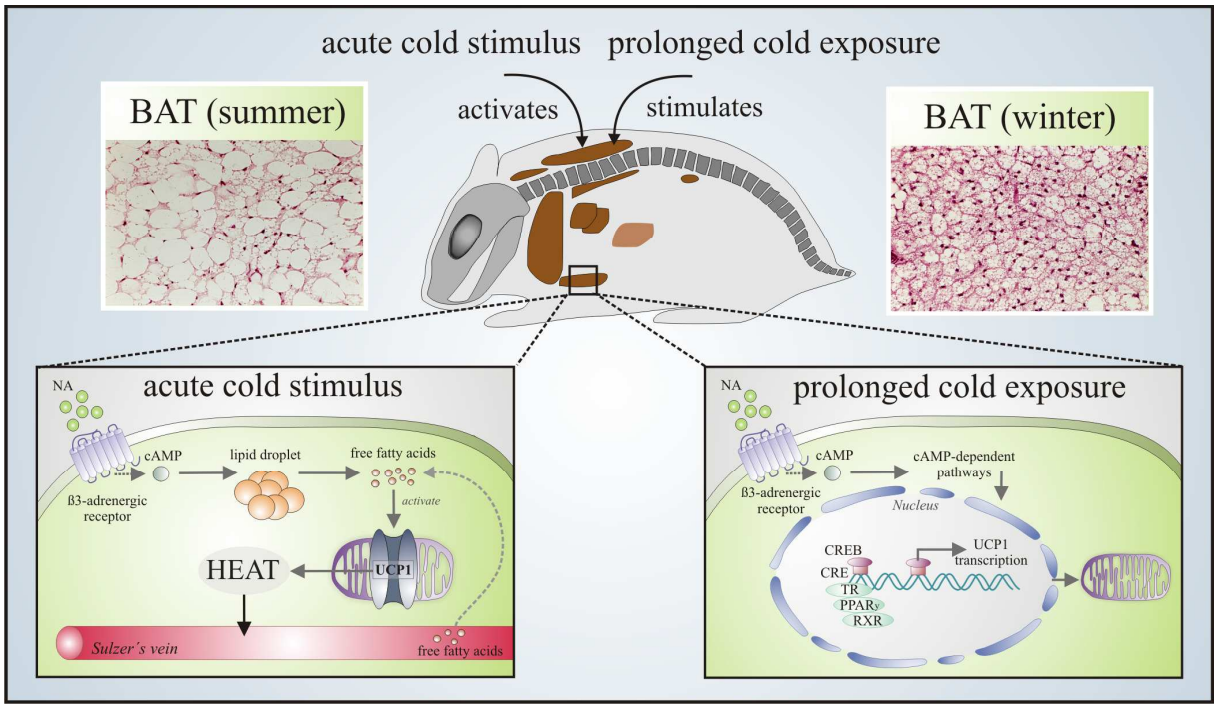

Figure 2: Anatomical location and physiological regulation of brown adipose tissue (BAT) activity. Brown adipose tissue is mainly located in the dorso-cervical area of modern Eutherian mammals (here: *Phodopus sungorus*). Noradrenergic stimulation of ß3-adrenergic receptors triggers different cAMP responsive pathways depending on the duration of the cold stimulus. Following an acute cold stimulus, cAMP initiates the production of heat which is directly transported to the heart via the Sulzer´s vein and from there distributed to the brain and the rest of the body. Under prolonged cold exposure cAMP enhances the transcription of UCP1 and the proliferation of brown adipose tissue (here: histology sections of brown adipose tissue from *Phodopus sungorus* acclimatzed to summer and winter, stained with hematoxyl and eosin). CREB: cAMP response element binding protein, CRE: cAMP response element, TR: thyroid hormone receptor, PPARγ: peroxisome proliferator-activated receptor.

Torpor and hibernation are efficient mechanisms to periodically save energy in periods of food scarcity and decreasing ambient temperatures (up to 98%, Wang 1989, Ruf and Heldmaier 1992, Fig. 3). Hibernation, estivation and torpor are not restricted to cold (Holartic) regions, on the contrary, torpor and hibernation were currently found in several species from warm temperate (Afrotropical) regions (Dausmann et al. 2004, Mzilikazi and Lovegrove 2004, Hallam and Mzilikazi 2010). While daily torpor is defined as a hypometabolic and hypothermic state of less than 24 hours, hibernation is a sequence of multiple torpor bouts, whereas a single bout can last up 30 days (Bieber and Ruf 2009). Animals capable of expressing torpor or hibernation are also termed as heterothermic endotherms (Grigg et al. 2004, Lovegrove 2012), as they are endothermic animals that allow their body temperature to fluctuate over a wide temperature range (from -3.6°C to ~37°C in arctic ground squirrels (*Spermophilus parryii*), Barnes 1989).

Even through the importance of brown adipose tissue for rewarming from torpor seems straight forward the quantitative contribution of UCP1 activity on torpor behavior has not been determined. This is especially intriguing as several species display torpor without the expression of functional UCP1 (see below and Fig. 3D). I therefore sought to investigate the significance of functional BAT in the context of torpor, using a transgenic UCP1-knockout mouse model (chapter I)

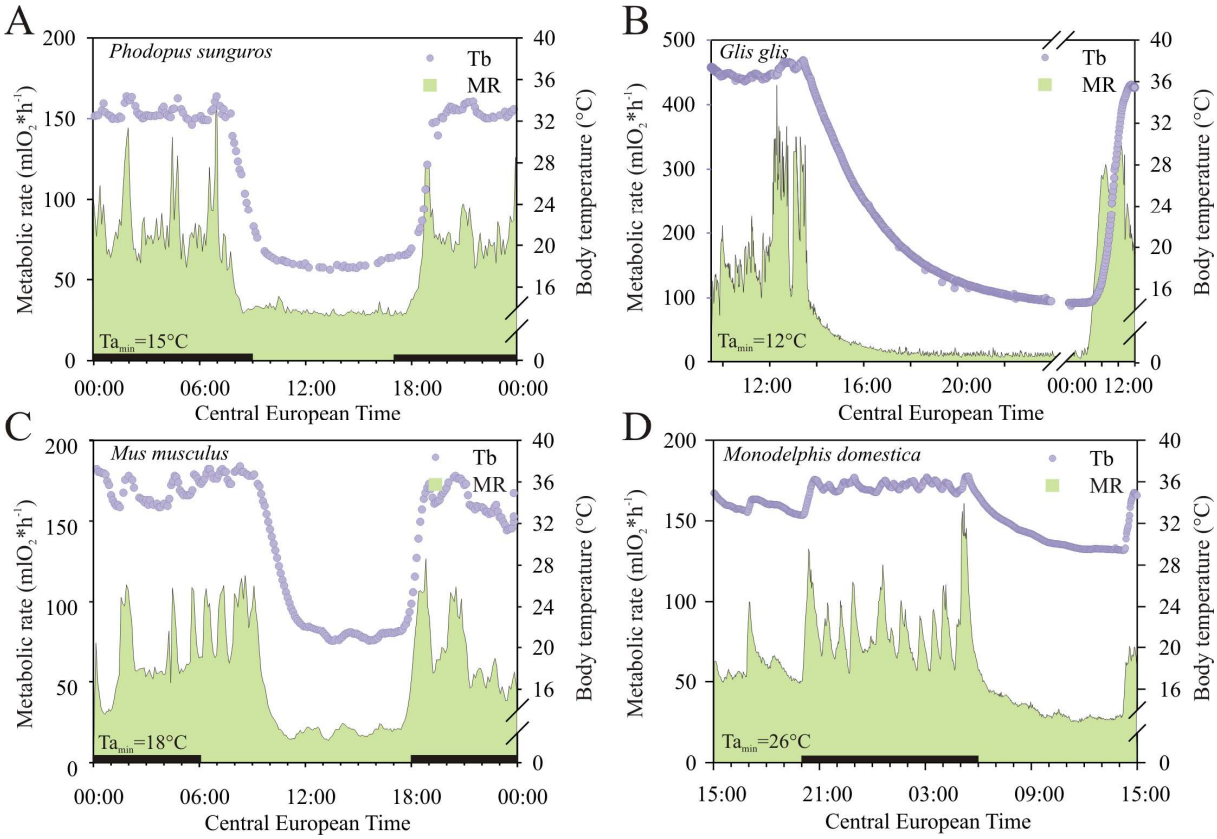

Figure 3: Torpor a versatile mechanism to save energy. A) Djungarian hamster (*Phodopus sungorus*) enter daily torpor in response to environmental cues; a facultative behavior. B) In contrast hibernation (a combination of multiple torpor bouts) in the Edible dormouse (*Glis glis*) is an obligate behavior in response to endogenous physiological cues, larger energy savings can be achieved up to 98%. C) Torpor in laboratory mice (*Mus musculus*) is facultative and can be induced by a cold stimulus or a combination of cold and food restriction. D) The gray short-tailed opossum is a great example of torpor without UCP1 and at relatively high ambient temperatures (Ta_{min}: 26°C). Ta_{min}: minimum ambient temperature, black bars: night (dark) phase, all data were kindly provided by Prof. Dr. G. Heldmaier and Dr. C.W. Meyer.

More recently a role of UCP1- mediated uncoupling of the respiratory chain in the prevention of reactive oxygen species (ROS) has been proposed. Potent superoxide and reactive oxygen species are caused by overleaping electrons from the mitochondrial respiratory chain complexes, mainly at complex I, III and the glycerol-3-phosphatdehydrogenase. Different studies on UCP1 and the UCP1 orthologues (UCP2 and UCP3) demonstrated that uncoupling activity can be induced by superoxide and peroxidation metabolites (Echtay et al. 2002, 2003), claiming direct feedback of oxidative by-products to UCP action and associating UCPs with a potential role in the prevention of superoxide production. This so called “mild uncoupling” is currently intensively and controversially discussed in

the literature, as others studies refute a role of UCP1 in the protection against cellular ROS (Silva et al. 2005, Shabalina et al. 2006). A higher oxidative capacity, e.g. after cold induced stimulation of the tissue, is always accompanied by an elevated proton flux and it is commonly accepted that this elevated proton flux results in an increased production of reactive oxygen species. This raises the possibility that uncoupling of the respiratory chain by UCP1 serves to prevent the production of reactive oxygen species during thermogenesis, an assumption that will be validated in chapter II.

EVOLUTIONARY TRAITS OF BROWN ADIPOSE TISSUE

The UCP1 gene has been found in all so far investigated Eutherian mammals, including humans. Only in pigs the UCP1 gene is naturally disrupted (Berg et al. 2006). Although it has been stated that "*the acquisition of brown adipose tissue with its new protein, uncoupling protein-1 (UCP1, thermogenin), may have been the one development that gave us as mammals our evolutionary advantage, i.e., to survive and especially to be active during periods of nocturnal or hibernal cold, to survive the cold stress of birth…" (Cannon and Needergaard 2004)*, an ultimate cause favoring the evolution of a distinct anatomical energy depot with specific thermogenic properties has yet to be revealed. This is especially interesting, as the evolutionary history of UCP1 dates back to teleost fishes, demonstrating that UCP1 pre-cursors were already present before the divergence of ray-finned and lobe-finned vertebrate lineages about 420 million years ago (chapter IV, Jastroch et al. 2005, 2008).

Implicit to "modern" functional brown adipose tissue is not just the presence of UCP1, but also its uncoupling activity in response to a pharmacological stimulation of uncoupling, the ability of free fatty acids to stimulate proton leak, and the increase of its thermogenic capacity with seasonal cold acclimation (adptive thermogenesis, see above). In amphibians (Trzcionka et al. 2008) and fish UCP1 is therefore likely without a thermogenic function, even though fish UCP1 shows the same uncoupling characteristics as Eutherian UCP1 (Jastroch et al. 2005, 2007). In marsupials, gene expression of UCP1 is found in adipose tissue (Jastroch et al. 2008) but does not contribute to NST or adaptive thermogenesis (Polymeropoulos et al. 2012).

In Afrotherians, the closest relative group to Eutherian mammals, UCP1 is expressed and shows typical kinetics, enabling them to utilize nonshivering thermogenesis *in vivo* (Mzilikazi et al. 2007). However, their brown adipose tissue seems non-adaptive in captivity, suggesting that Afrotherian brown adipose tissue may convey primitive thermogenic features. The only Afrotherian species in which seasonal adaptive nonshivering thermogenesis has been previously described is the Hottetot golden mole (Amblysomus hottentotus longiceps, Scantleburry et al. 2008). Hottentot golden moles live in thermally buffered underground burrows without access to exogenous heat sources (i. e. sun basking), therefore they are reliant on endogenous mechanism of heat production and maybe not representative for the Afrotherian clade. The evolutionary trait of brown adipose tissue and

nonshivering thermogenesis has thus remained unenlightened and the specific function of brown adipose tissue in Afrotherians will be further investigated in this study (chapter III).

THERMOREGULATION IN PROTOENDOTHERMIC MAMMALS

There is one group of mammals that can be placed between the evolutionary stage of facultative endothermic reptiles and endothermic mammals, using a classification that distinguishes between different thermoregulatory strategies. This so called “protoendothermic” mammals are very flexible in their thermoregulatory precision and minimize energetic costs by using ectothermy facultatively when entering daily torpor or hibernation (Grigg et al. 2004). An interesting protoendothermic member of the Afrotherian order is the Lesser hedgehog tenrec (*Echinops telfairi*). The thermoregulatory behavior of this species is unique. For most of their lifespan, their body temperature closely tracks the ambient temperature and shows reptilian like patterns (Poppit et al. 1994, Lovegrove and Genin 2008). Strikingly, female *E. telfairi* are reported to maintian constantly high body temperatures during periods of reproduction and parental care (~33°C). In summary, these observations raise the question if brown adipose tissue is present in protoendothermic species.

The parental care theory of the evolution of endothermy postulates that endothermy evolved as a consequence of increased body temperatures during periods of offspring incubation (Farmer 2000). As increasing incubation temperatures decrease juvenile mortality and accelerate growth to maturity, the parental care theory supports a profound evolutionary scenario that directly leads to an improvement of species fitness (Kozlowski 1992, Stearns 1992, Kozlowski and Weiner 1997). In front of this background, a role of brown adipose tissue mediated thermogenesis in protoendothermic animals not only provides novel insights on the evolutionary scenario supporting its development but also on the evolution of endothermy in general (chapter IV).

AIM OF THE PHD-THESIS

Although textbook knowledge inevitable associates brown adipose tissue with cold and body temperature regulation (regulatory thermogenesis), we are far from understanding how, why and when Eutherian mammals gained full UCP1-mediated thermogenic support. Brown adipose tissue is also present in humans, and it is currently considered a major therapeutic target in the treatment of obesity. To fully appreciate and to potentially modulate the function of this unique tissue, comparative studies from nature's toolbox will prove invaluable new insights. In my PhD-thesis I therefore sought to expand our knowledge on brown adipose tissue thermogenesis and its significance in various mammalian orders, spanning from the *in vitro* to the *in vivo* level. In doing so, I aimed to uncover novel aspects regarding the evolution of its thermogenic function.

In my studies, I used artificially generated UCP1-ablated mice to evaluate further benefits of UCP1 expression on brown adipose tissue function (ROS prevention) and the torpor behavior of Eutherian mammals from Holartic regions. Furthermore I tried to clarify the function of UCP1-mediated nonshivering thermogenesis in more "ancient" mammals from Afrotropical regions, is brown adipose tissue of Afrotherians seasonally regulated? Therefore I worked with two members of the Afrotherian clade, Western rock elephant shrews (*Elephantulus rupestris*) and protoendothermic Lesser hedgehog tenrecs (*Echinops telfairi*). The later additionally provided me the perfect model organism for another approach; the function of brown adipose tissue in protoendothermic mammals and the revealing of selection constraints that supported the evolution of brown adipose tissue and mammalian endothermy. Specifically, the following questions were addressed:

1. What are the effects of UCP1 activity on the torpor behavior of Eutherian mammals, can they arouse from hypometabolic and hypothermic states (torpor) without UCP1-mediated nonshivering thermogenesis? If so, what are the benefits of UCP1 activity for arousal?

2. Does UCP1 play a role in the prevention of reactive oxygen species during nonshivering thermogenesis? Was the prevention of ROS the ancient function of UCP1?

3. Do species from the Afrotropics adjust their thermoregulatory capacities during winter? Is nonshivering thermogenesis in Western rock elephant shrews adaptive and a common feature of the Afrotherian clade?

4. Do protoendothermic Lesser hedgehog tenrecs possess functional brown adipose tissue and adaptive thermogenesis? If so, is the specific function of UCP1 comparable between protoendothermic and endothermic mammals?

5. Was brown adipose tissue involved in the evolution of endothermy?

METHODS

In this thesis, standard physiological and molecular methods were used and are briefly summarized in this section. Further information about the exact methodology can be found in the material and methods section of chapter I-IV.

ANIMAL EXPERIMENTS

All animal experiments were approved by the German animal welfare authorities. Experiments on Western rock elephant shrews in South Africa were permitted by the Western Cape Nature Conversation board (South Africa).

- Writing protocols and applying for animal ethic approvals
- Capturing of free-ranging animals using Sherman traps
- Marking of free-ranging animals with ID-Transponders
- Breeding and maintenance of UCP1-knockout mice and Lesser hedgehog tenrecs
- Implantation of temperature sensitive transmitters for body temperature recordings
- Acclimation of study animals to different ambient temperatures
- Indirect calorimetry for the determination of metabolic rates
- Injections of noradrenaline and the β3 adrenergic receptor antagonist SR 59230A to test for nonshivering thermogenesis capacities
- Dissection of animals to collect tissues and to identify brown fat depots
- Preparation of brown adipose tissue, white adipose tissue, heart, liver, kidney, skeletal muscle, spleen

MOLECULAR TECHNIQUES

- Genotyping of UCP1-knockout mice using polymerase chain reaction
- Cloning of tenrec UCP1: Isolation of mRNA and Northern blot analysis, qPCR, RACE-PCR experiments to identify the 5'- and 3'-UTR of the UCP1 transcript, amplification of tenrec UCP1 cDNA using reverse transcriptase polymerase chain reaction, cloning in PGEMTeasy and pcDNA 3 vector systems, plasmid preparations
- Cell culture techniques to grow, maintain and harvest HEK293 cells
- Stable expression of tenrec UCP1 in HEK293 cells
- Determination of UCP1 and β3 adrenoreceptor protein concentrations in tissue homogenates and isolated mitochondria using standard immunoblotting techniques (Western blot)
- Generation of tenrec UCP1 inclusion bodies, using a pMW172 vector and the *E.coli* strain C41 (DE3), as a protein standard

- Determination of protein concentration using the BCA, Bradford and Biuret method

BIOCHEMICAL ANALYSIS

- Isolation of brown adipose tissue and skeletal muscle mitochondria by differential centrifugation
- Polarographic measurements of cytochrome c oxidase activity in tissue homogenates and mitochondria to analyze changes in oxidative capacity
- Measurement of mitochondrial respiration rates in a temperature regulated chamber with a Clark-type oxygen electrode
- Determination of proton leak kinetics using a Clark- and a TPMP-electrode
- Measurements of mitochondrial hydrogen peroxide releasing rates using the fluorescence assay Amplex Red
- Cell metabolism analyses using a Seahorse extracellular flux analyzer

STATISTICAL ANALYSIS

All statistical analyses were performed using Sigma Stat 3.5, Sigma Plot 10.0 (both from Jandel Scienti Wc, San Rafael, California) or the statistical package R (library nIme). The Students T-Test or One Way Anova were used to test for differences between groups and the paired T-Tests, Two Way Anova or Wilcoxon Test to test for differences within a group. In data sets were normal distribution of data could not be assumed the Mann Whitney U-Test was performed for analysis. In single cases the dynamic regression wizard function or a linear mixed effect model was used to calculate best fitting standard curves. All mean values are reported as mean values ± standard deviation (chapter I, III) or ± standard error (chapter II, IV and supplements). The 0.05 level of probability was accepted as indicating statistical significance. In chapter II the effective P-Values were adjusted according to Bonferroni.

SCOPE OF THE PHD-THESIS

UCP1 EXPRESSION: AN EFFECTIVE WAY OF ENDOGENOUS HEAT PRODUCTION (CHAPTER I)

Torpor is not intrinsically linked to the expression of brown fat, even though it contributes to the arousal process (Cannon and Nedergaard 2004). Members of phylogenetically ancient mammalian groups (e.g. monotremes and marsupials) display torpor and hibernation although lacking classical brown adipose tissue thermogenesis (Hayward and Lisson 1992, Jastroch et al. 2008, Nicol et al. 2008). In these species rewarming to normothermia cannot be supported by UCP1-mediated thermogenesis, raising the question on the significance of brown adipose tissue and UCP1 in the context of torpor (Lyman and O´Brien 1986, Stone and Purvis 1992).

In order to directly assess the quantitative magnitude by which the presence or absence of UCP1 affects torpor patterns, rewarming and arousal rates within one species, I compared induced torpor behavior in wild-type and UCP1-deficient (UCP1-KO) mice. Mice belong to modern Eutherian mammals and are thought to rely on nonshivering thermogenesis during arousal from torpor. Torpor was induced by depriving mice of food for up to 48 hours combined with a reduction of ambient temperature from 30°C (thermoneutral zone) to 18°C (moderate cold). In response to the energetic and thermoregulatory challenge, both genotypes were able to enter and, more importantly, to arouse (rewarm) from torpor only by means of endogenous heat production mechanisms. The degree of hypometabolism and hypothermia was comparable in wild-type and UCP1-KO mice. But, in contrast to UCP1-KO mice, wild-type mice were able to enter and to arouse from multiple torpor bouts within 48 hours. Occasionally UCP1-KO mice entered a second torpor bout but were unable to regain normothermia unless passively rewarmed with an infrared lamp. Arousal in UCP1-KO mice took significantly longer (+50%) and required 60% more energy, which may explain the inability of UCP1-KO mice to display multiple torpor bouts per day. A result that clearly supports previous predictions that rapid rewarming from torpor is energetically less demanding compared to slow rewarming (Stone and Purvis 1992, McKechnie and Wolff 2004). The magnitude by which the artificial ablation of UCP1 influenced rewarming from torpor was within the range of results from pharmacological suppression of nonshivering thermogenesis in bats (-50%, Heldmaier 1970).

In phylogenetically more ancient species rewarming to normothermia is largely achieved through shivering thermogenesis and, especially in animals from the southern hemisphere, arousal is assisted by the selection of a warmer thermal environment (for example sun basking, Ortmann et al. 1997, Lovegrove et al. 1999, Mzilikazi et al. 2002, Warnecke and Geiser 2010). This form of behavioral thermoregulation reduces arousal costs in animals not capable of nonshivering thermogenesis. Nevertheless it should be kept in mind that exogenous passive heating involves certain risks. First, animals have to leave their burrows and therewith are directly exposed to their predators; excluding animals that hibernate in poorly insulated tree holes (Dausmann et al. 2004). Secondly, arousal takes

longer and animals shiver more intensively which hinders locomotion and decreases chances of a successful escape which ultimately leads to a decrease of species fitness. The development of a thermogenic organ (like brown adipose tissue) might have been particularly beneficial for the migration to Holarctic regions, where sun basking cannot be used as efficient as in Afrotropical regions. However, Eutherian mammals can display normal torpor behavior without UCP1-mediated thermogenesis albeit increased arousal costs.

IS TORPOR IN MICE LINKED TO ENDOGENOUS RHYTHMS (CHAPTER I)?

In contrast to Djungarian hamsters (*Phodopus sungorus*) or mouse lemurs (*Microcebus murinus*), torpor in mice is not a physiological behavior of seasonal acclimation, e.g. in response to decreasing day length (Fig. 3 Introduction). Torpor in mice is a facultative, physiological response to energetic challenge which can be induced by a combination of food restriction and cold in the laboratory (Hudson and Scott 1979, Webb et al. 1982, Swoap et al. 2006, Dikic et al. 2008). In animals that show seasonal torpor behavior, a direct link between preparedness for torpor entry and the circadian system has been discussed in several studies (Heldmaier and Steinlechner 1981, Ortmann et al. 1997, McKechnie and Lovegrove 2001, Ehrhardt et al. 2005). In order to investigate the influence of the circadian system on torpor in laboratory mice, I induced torpor at different time points (6:00, 12:00, 18:00, 24:00 CET) by lowering the ambient temperature from 30°C to 18°C. At 6:00, 12:00 and 24:00 CET, animals entered torpor within 20 minutes after the temperature change, i.e. torpor entry could be "switched on". Interestingly, when the cold exposure started at 18:00 CET (*lights off*), the start of the animals nocturnal activity period, torpor entry was delayed by 6 hours to midnight, the common onset of torpor in laboratory mice. Torpor bouts expressed during the light phases lasted 3-6 hours while significantly longer torpor bouts were recorded when mice entered torpor during the dark phase (~16 hours).

The differential responses to the interaction of cold and time of day suggested a functional link to an ultradian rhythm, which is permissive for torpor entry in laboratory mice. This hypothesis is supported by two independent findings. Ablation of the SCN, the pacemaker of the circadian rhythm, abolishes torpor timing and peripheral sympathetic inhibition by 6-hydroxydopamine (6-OHDA) suppresses torpor and ultradian rhythms of body temperature in Djungarian hamsters (*Phodopus sungorus*, Ruby and Zucker 1992, Braulke and Heldmaier 2010). Additionally, several recent findings support a strong relationship between energetic challenges and the activity or rather the torpor behavior of different Eutherian species (Daan et al. 2011, Hut et al. 2011, Grimpo et al. 2012) thereby underlining our hypothesis that facultative torpor in mice might be based on a tight ultradian rhythm. Further experiments will be necessary to verify this assumption.

SUPEROXIDE PRODUCTION IN BROWN ADIPOSE TISSUE MITOCHONDRIA IS SENSITIVE TO MILD UNCOUPLING (CHAPTER II)

Mitochondria are the main source of cellular reactive oxygen species (ROS) and therefore often play an important role in cell damage and degradation processes (Cadenas et al. 2000), that cause a decrease in life span ("free radical of aging theory" Harman 1956, 1972). Altering the mitochondrial membrane potential can prevent a large proportion of mitochondrial ROS and attenuate cellular aging processes (Boveris et al. 1976, Nohl et al. 1996, Herrero et al. 1998). UCP1 expression and activity influences the membrane potential and conclusively might be a highly effective *in vivo* "antioxidant" that prevents the production of mitochondrial ROS and thereby reduces cellular damage. Interestingly, UCP1-ablated mice die after several weeks in the cold, with no obvious signs of physical deterioration (Golozobouva et al. 2006); raising the possibility that lack of UCP1 not just impairs thermogenesis, but may also lead to detrimental accumulation of ROS. However, a function of UCP1 activity in the prevention of ROS is highly disputed (see introduction, Echtay et al. 2002, Echtay et al. 2003, Silva et al. 2005, Shabalina et al. 2006).

The availability of UCP1-ablated mice enabled me to dissociate UCP1 dependent and independent effects on mitochondrial ROS production rates and allowed us to ultimately determine the role of UCP1 in "mild uncoupling" mitochondria. I investigated the impact of different substrates (succinate, glycerol-3-phosphate, pyruvate/malate) on mitochondrial respiration and superoxide production rates in isolated brown adipose tissue mitochondria of wild-type mice and UCP1-KO littermates. As suggested by Echtay et al. (2002, 2003) superoxide production rates at state 4 (basal or leak respiration) were lower in wild-type mitochondria than in UCP1-KO mice mitochondria, even though maximal inducible respiration rates were similar. This reduction in superoxide production was attributable to UCP1, because the addition of the UCP1 inhibitor guanosindiphosphate (GDP) abolished genotype differences by increasing superoxide production rates of wild-type mitochondria.

Our experimental setup allowed the further determination of the exact superoxide production sites and how they were influenced by UCP1 activity. This analysis revealed that UCP1 activity decreases superoxide production at the I_Q-site of complex I by ~40-50%, at the glycerol-3-phosphate dehydrogenase by 20% and at residual sites such as the Q pool and complex III by 50-70%. Next to UCP1 activity, other proteins may also influence the mitochondrial membrane potential, leading to an elevated superoxide production rate independent of UCP1. The adenine translocase, for example, has been shown to significantly contribute to the basal proton leak (Brand et al. 2005) and as regulator of mitochondrial uncoupling (Khailova et al. 2006). However, the adenosines translocase (ANT) had no effect on superoxide production rates in our experiments and conclusively the observed effects were all attributable to UCP1 uncoupling activity.

The direction of the electron flow causing electron leak and superoxide formation is still controversially discussed. Superoxide formation with NADH-linked substrates, like pyruvate and malate, is generally associated with forward electron transport. Under these conditions I found nearly

no generation of superoxide but in another approach, with succinate as substrate for complex II, I found a rotenone (inhibits complex I) and GDP (inhibits UCP1) sensitive formation of superoxide. ROS production was reduced when UCP1 was active and electron transport was predominantly forward. Conclusively I suggest diminished probability of "reverse electron transport" facilitated by uncoupled respiration as the underlying mechanism of reactive oxygen species suppression in brown adipose tissue. This suggestion has been recently contested by Schönfeld et al. (2012), who argued that superoxide production in brown adipose tissue mitochondria is not caused by reverse electron transport and is not influenced by UCP1 activity. However, their isolated mitochondria could not establish a membrane potential respiring on succinate, a hint that mitochondria were damaged during the isolation process and less integrative. The same arguments can be raised for data in Shabalina et al. (2006), where it was proposed that UCP1 has no effect on superoxide production; these were measured rates in the presence of complex I and III inhibitors. For these conditions, however, the magnitude of membrane potential is negligible. Nevertheless, a role of UCP1 in the prevention of ROS production has been meanwhile confirmed and approved by additional studies on UCP1-ablated mice (Dlaskova et al. 2010) and on transgenic mice that ectopically express UCP1 in skeletal muscle mitochondria (Keipert et al. 2010).

Conclusively, these results clearly demonstrate that mild uncoupling activity catalyzed by UCP1 reduces the production of deleterious oxygen species in brown adipose tissue mitochondria.

UNCOUPLING ALLOWS HIGH SUBSTRATE TURNOVER RATES DURING NONSHIVERING THERMOGENESIS SIMULTANEOUSLY LOWERING ROS PRODUCTION (CHAPTER II)

In the upper part, I approved a role of UCP1 in mild uncoupling mitochondria and itemized the underlying mechanism. However this thesis aims to unravel the significance of brown adipose tissue in mammals, wherefore it is insufficient to solely describe functions of UCP1 under non-physiological conditions. Therefore I designed an advanced approach where I mimicked physiological conditions in my experimental setup. Again I isolated brown adipose tissue mitochondria of wild-type mice and UCP1-KO littermates, but this time animals were previously acclimated to either 30°C (thermoneutral conditions) or 5°C (cold) to mimick cold stress. Respiration was stimulated using substrates for beta oxidation (palmitate).

Cold stress causes the activation of brown adipose tissue and induces its proliferation to produce additional heat. Accordingly I detected an increase in UCP1 protein levels and wild-type mitochondria leak respiration. The UCP1-dependent proton turnover rate in response to cold was increased by 1.6µmol protons per minute or 300%. Under these conditions the probability of electrons to leak from the respiratory chain to form superoxide should increase, but my results showed that UCP1 blunts this increase (-96% of potential superoxide production). Interestingly UCP1-ablated mice failed to increase

their oxidative capacity in response to cold acclimation, maybe a protection mechanism to avoid toxic superoxide levels in the brown adipocytes.

During nonshivering thermogenesis, triglycerides are broken down by lipolytic activity and free fatty acids are released to serve as substrates for β-oxidation, the major pathway of substrate oxidation in brown adipose tissue during cold-induced thermogenesis. To highlight and analyze the relevance of UCP1 in a physiological scenario I stimulated respiration with palmitate to reproduce a situation of cold-stimulated lipolysis. Similar to what I have observed previously, UCP1 expression increased mitochondria respiration rates by simultaneously lowering superoxide production rates. Therefore I finally conclude that mammalian UCP1 allows high oxidation rates in the absence of mitochondrial ROS production during nonshivering thermogenesis.

Evolution may have promoted the presence of UCP1 in adaptive nonshivering thermogenesis of mammals because of its dual role in heat production and superoxide prevention. The role of ancient UCP1 orthologues in ectotherms (Jastroch et al. 2005) may therefore be the prevention of superoxide production before nonshivering thermogenesis evolved. While specific accumulation of ROS in brown adipocytes may not be directly causative for the decreased survival rates of UCP1-ablated mice in the cold, other sources of heat production may have recruited and increased systemic radical damage, therefore affecting life span (supplements chapter II).

SEASONAL METABOLIC ADJUSTMENTS OF WESTERN ROCK ELEPHANT SHREWS (CHAPTER III)

As outlined above, brown adipose tissue and torpor are not a prerogative of Eutherian mammals from the Holartic region. To better understand the function of brown adipose tissue in phylogenetically more ancient mammalian orders from Afrotropical regions, I analyzed the thermoregulatory capacity of an Afrotherian mammal from South Africa under natural conditions. Based on my main research interest, the significance of brown adipose tissue in mammals (not only in modern Eutherians) and the evolutionary patterns of its development, I sought to address the following questions: 1) How flexible are the seasonal metabolic adjustments in small sized mammals from the southern hemisphere in comparison to mammals from the northern hemisphere? 2) How common is adaptive thermogenesis in Afrotherian species?

Therefore, I worked with free ranging Western rock elephant shrews (*Elephantulus rupestris*) that naturally occur in the Western Cape of South Africa. Western rock elephant shrews belong to the superorder Afrotheria, phylogenetically “basal” Eutherian mammals which separated from the mammalian lineage over 100 mya (Springer et al. 1997, Fig. 4). They are an excellent model organism to investigate seasonal metabolic adjustments, as they belong to the smallest members of the Afrotherian superorder and live in a highly seasonal environment with winter rainfall (Fig. 4).

Figure 4: The natural habitat of Western rock elephant shrews (*Elephantulus rupestris*) during summer and winter. Pictures were taken at the Gamkaberg Nature reserve (S 33°40.245; E 21°53.164, altitude: 378 m) in South Africa where the study was conducted. The reserve is located between the winter and summer rainfall regions with gentle rain in winter and thundershowers in summer. Summers are dry and plants flower only during the winter months (C). The annual rainfall averages 500 mm at the summits and 200 mm on the lower slopes of the mountain, light snow occasionally falls during winter (T_a: summer >40°C and winter <5°C; T. Barry, Cape Nature, pers. comm.).

Additionally several members of Afrotheria have been previously reported to show daily torpor (Scholl 1974, Fielden et al. 1990, Lovegrove et al. 1999, Mzilikazi and Lovegrove 2004, Scantleburry et al. 2008, Geiser and Mzilikazi 2011). So far no study on seasonal metabolic adjustments in elephant shrews has been conducted under natural conditions in the field. Only one study recorded body temperatures of free-ranging animals, showing a pronounced use of torpor (*Elephantulus myurus*, Mzilikazi and Lovegrove 2004). With this study, I provided the first physiological data set of Western rock elephant shrews in their natural habitat during winter and summer (resting metabolic rate and body temperature patterns). Surprisingly, elephant shrews were extremely flexible in their seasonal adjustments to counteract adverse environmental conditions. Their basal metabolic rate during winter was decreased and the slope of the linear increase in resting metabolic rate below thermoneutrality was shallower. This may indicate an improvement of fur insulation or a lowered body temperature. Both lead to a lower thermal conductance and consequently, to a decrease in thermoregulatory costs during winter. Notably, males and females entered torpor not only in winter; they also displayed torpor in summer. However, in winter the incidence of torpor was higher and torpor episodes were longer and deeper (Tb min: 11.9°C).

In facultative heterotherms, heterothermy is a physiological response that is usually associated with cold conditions, a short photoperiod and food scarcity. From personal observations I can exclude that torpor was induced by low prey abundance or a drought year. Nevertheless I detected another physical parameter that occurred as a predictor of torpor in elephant shrews, namely air humidity e.g. rain. High air humidity moistens the fur, collapses the insulating air layer and thereby increases thermal conduction. To my knowledge only one previous study reports on a correlation between the occurrence of rain and torpor (Körtner and Geiser 2000). It will be important to further assess the impact of air humidity on life history traits in future studies.

The flexibility of torpor behavior in Western rock elephant shrews was further visible in a flexible timing of torpor entry and the capacity to arouse in winter without exogenous heating sources, unlike Eastern rock elephant shrews (*Elephantulus myurus*, Mzilikazi et al. 2002). Eastern rock elephant

shrews live in a summer rainfall area and it is possible that the harsher environmental conditions in my study favored adaptive thermogenesis that assisted arousal, which will be further evaluated below.

ADAPTIVE THERMOGENESIS IS A COMMON FEATURE IN AFROTHERIANS (CHAPTER III)

So far published data on adaptive thermogenesis in Afrotherians are controversial. Absence of an increased thermogenic response following cold acclimation could be a plesiomorphic feature, as the African endemic species were not exposed to highly seasonal cold climates during the Late Cenozoic (Lovegrove 2012). This would confirm an evolutionary scenario in which brown adipose tissue indeed evolved to survive the cold. I therefore aimed to elucidate if adaptive thermogenesis is in fact restricted to Afrotherian mammals that live in subterranean burrow systems or if the laboratory study of Mzilikazi et al. 2007 was insufficient to trigger the seasonal changes that Eastern rock elephant shrews exhibit in the wild.

I determined the capacity for nonshivering thermogenesis of Western rock elephant shrews, acclimatized to summer and winter, by injecting animals with noradrenaline (Fig. 2). Adrenergic stimulation of thermogenesis is an established method to quantify the magnitude of nonshivering thermogenesis *in vivo* (Heldmaier 1971, Cannon and Nedergaard 2011). Following noradrenaline injection, both groups increased their metabolic rate. Nevertheless maximum metabolic rates were reached faster and were 1.8 fold higher in winter acclimatized animals, than in summer acclimatized animals. This represents a clear proof for the presence of adaptive thermogenesis in Western rock elephant shrews. In free-ranging animals environmental factors like photoperiod or rain may enforce the development of a higher nonshivering thermogenesis capacity during harsher season (Heldmaier et al. 1981, Haim 1982, Kronfeld-Schor et al. 2000). This might explain why Mzilikazi et al. 2007 could not detect adaptive thermogenesis in Eastern rock elephant shrews.

On the basis of an allometric relationship between body mass and nonshivering thermogenesis of modern Eutherians from cold climates (Heldmaier 1971), the maximum metabolic rate after noradrenaline injection was 36% lower than predicted. At first sight this may indicate that Afrotherians have reduced thermoregulatory capacities. Using a regression which includes 19 species from the southern hemisphere and accounts for phylogeny (Mzilikazi and Lovegrove 2006), however the capacity for nonshivering thermogenesis of Western rock elephant shrews is only slightly (-14%) below the predicted value. Taken together Western rock elephant shrews exhibit seasonal metabolic adjustments comparable to Holartic rodents (compare to Geiser and Mzilikazi 2011). Moreover adaptive thermogenesis occurs in Afrotropical regions and is a widespread feature of the Afrotherian superorder, thereby disproving an evolutionary scenario in which brown adipose tissue primarily evolved to colonize Holartic regions.

PROTOENDOTHERMIC MAMMALS POSSESS FULLY FUNCTIONAL BROWN ADIPOSE TISSUE (CHAPTER IV)

It is possible that brown adipose tissue was first invented to assist protoendothemic mammals in defending a temporarily high body temperature. Together with Mzilikazi et al. (2007) and Scantleburry et al. (2008) I could confirm full functional brown fat and the occurrence of adaptive thermogenesis in Afrotherian mammals. In the next step I investigated the link between protoendothermy and brown adipose tissue in Lesser hedge tenrecs (*Echinops telfairi*), protoendothermic members of the Afrotheria (Fig. 5).

Figure 5: Lesser hedgehog tenrecs (*Echinops telfairi*) are protoendothermic mammals belonging to the subfamily of Tenrecinae within the Afrotherians. It is a small insectivorous mammal endemic to south-western parts of Madagascar, where it inhabits deciduous, gallery and xerophytic spiny forests. Minimum ambient temperatures during winter are reported to be around 10°C (Lovegrove and Genin 2008). In external appearance it resembles a European hedgehog with a sparsely haired abdomen and a spiny back.

As it has been previously reported for free ranging tenrecs (Lovegrove and Genin 2008), all investigated tenrecs showed pronounced daily body temperature fluctuations (21°C-33°C) with only a few hours of high body temperatures, irrespective of the surrounding ambient temperature (T_a: 20-27°C). In my experimental setup no exogenous heat sources were available, nevertheless animals were capable of rewarming only by the means of endogenous heat production mechanisms on a daily basis (shivering or nonshivering thermogenesis). Even though Lesser hedgehog tenrecs appeared very opportunistic in their thermoregulatory behavior, I detected brown adipose tissue and could confirm the expression of UCP1 on the mRNA and protein level. A cold acclimation study could additionally confirm the occurrence of adaptive thermogenesis *in vivo* and *in vitro*. Cold acclimated animals had significantly reduced rewarming rates from torpor after inhibition of the β3-signalling pathway, supporting inhibition of adaptive nonshivering thermogenesis that classically replaces shivering thermogenesis during cold acclimation. Furthermore cold acclimation led to a proliferation of brown adipose tissue resulting in 2 fold higher UCP1 levels in tissue homogenates and mitochondria which was accompanied by an increase in oxidative capacity (higher cytochrome c oxidase (COX) activity) and mitochondrial respiration rates in state 4. Inhibition of UCP1 with GDP re-coupled mitochondria, leading to a higher membrane potential and a lower respiration rate thereby demonstrating that UCP1 expression significantly contributes to the proton leak of brown adipose tissue mitochondria.

For further comparative biochemical characterization of tenrec UCP1, tenrec and mouse UCP1 orthologues were cloned and stably transfected in HEK293 cells to measure protein function in front of the same cellular background. Interestingly, the specific activity of tenrec and mouse UCP1 did not differ, despite their large evolutionary distance and the different thermoregulatory strategies of both species. In fact, it is currently a matter of debate if the thermoregulatory behavior of modern

heterothermic endotherms and ancient protoendotherms cannot be ascribed to a joint origin. As Grigg et al. stated in 2004: "*However, noting that hibernation and torpor are almost certainly plesiomorphic (= ancestral, primitive), and that heterothermy is very common among endotherms, we propose that homeothermic endothermy evolved via heterothermy, with the earliest protoendotherms being facultatively endothermic and retaining their ectothermic capacity for "constitutional eurythermy"*." An assumption that was further promoted by Lovegrove in 2012. If heterothermy in modern Eutherian mammals is a plesiomorphic or apomorphic feature needs further investigation in future projects. However, for the first time, I could show the presence of functional brown adipose tissue in a protoendothermic mammal and could therefore design a new scheme illustrating the significance of brown adipose tissue across the animal kingdom (Fig. 6).

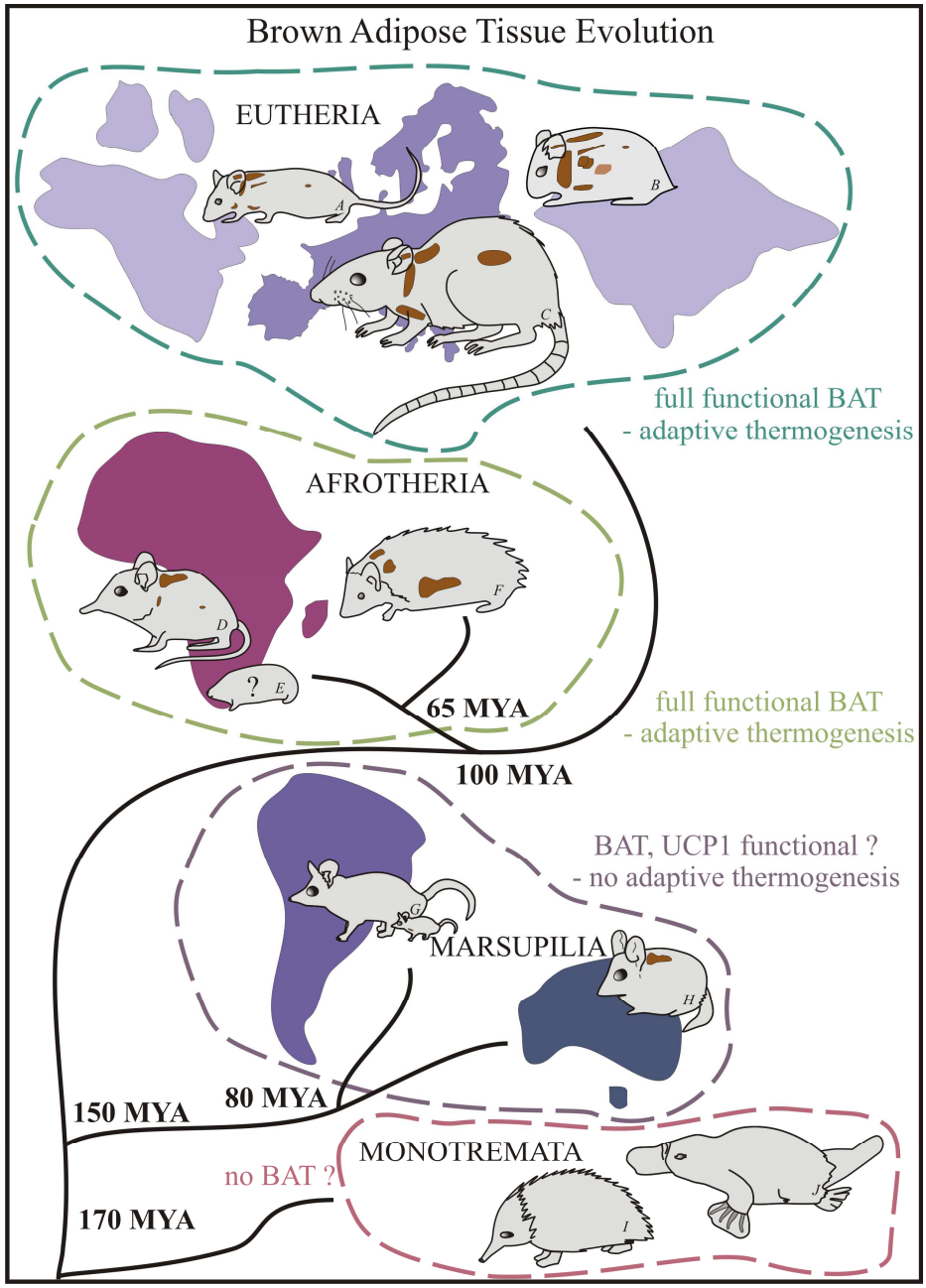

Figure 6. Emergence of brown adipose tissue (BAT) traits along the mammalian lineage. The uncoupling protein 1 (UCP1) is the critical protein for brown adipose tissue mediated nonshivering thermogenesis. Its expression dates back to the evolutionary stage of teleost fish and amphibians more than 400mya, even though functional, a thermogenic function has been excluded as unlikely in this species (Jastroch et al. 2005, 2007, Trzcionka et al. 2008). During mammalian evolution the order Monotremata separated from the mammalian lineage around a 170mya in late Jurassic (Wesley et al. 2008). UCP1 orthologues can be found in the Platypus (J) genome, but anatomical inspections of Echidnas (I) and Platypus so far failed to detect brown adipose tissue *in vivo*. South American marsupials express brown adipose tissue at the juvenile stage in Gray short-tailed opossums (G), whereas the Australian members of this clade possess large brown fat depots during adulthood in the Fat-tailed dunnart (Jastroch et al. 2008). However, brown adipose tissue thermogenesis seems to be non-adaptive (Polymeropolous et al. 2012) and the full functionality of marsupial UCP1 remains to be approved. According to this thesis and the findings of Mzilikazi et al. 2007 and Scantleburry et al. 2008 brown adipose tissue in Afrotropical Afrotherians is functional and adaptive in elephant shrews (D, Mzilikazi et al. 2007, Oelkrug et al. 2012) and Lesser hedgehog tenrecs (F, Oelkrug et al. 2013 in revision), and is possibly responsible for adaptive thermogenesis in Hottentot golden moles (E, Scantleburry et al. 2008). Holartic Eutherians are the best investigated mammalian group in which the most pronounced form of adaptive thermogenesis can be found in small mammals and newborns, for example in mice (A), hamsters (B) and rats (C), with the exception of pigs where a naturally disrupted UCP1 gene results in poor thermoregulation (Berg et al. 2006).

DID ENDOTHERMY EVOLVE AS A CONSEQUENCE OF OFFSPRING INCUBATION? (CHAPTER IV)

Even though mammals and birds are regarded as the classic endotherms, heterothermia or local endothermy can also be found in insects, fishes, reptiles and even some plants (Seymour 2010). Birds and mammals maintain constant high body temperatures by, among others, minimizing their thermal conductance with fur or feathers. However, covering a reptile with an insulating layer does not result in high body temperature, as it has been demonstrated in lizards dressed in custom-cut mink coats (Cowles 1958), suggesting more profound physiological changes that encompass endothermic homeothermy. The evolution of mammalian endothermy still is a central research subject for many evolutionary biologists, physiologists and ecologists (Koteja 2000, Lovegrove 2012). Interestingly, even though brown adipose tissue is a very important thermogenic organ that is discussed as a therapeutic target for many human metabolic disorders, the context between brown adipose tissue development and the evolution of endothermy has not been reviewed.

A phylogenetic analysis of UCP1 sequences from different mammalian orders revealed that the tenrec UCP1 orthologue is among the most modern existing forms of UCP1 (supplements: Evolutionary tree of UCP1), whereas UCP1 of the "modern" Eutherian clade seems to be already modified. This is especially interesting as anatomical inspections of tenrecs post mortem identified the major brown adipose tissue depot in the area around the gonads (~60-70% of total organ weight) whereas only small brown fat patches could be found in the typical axillary and dorso-cervical region. This is an unusual location for the major brown fat depot that normally is predominantly expressed in the intrascapular and dorso-cervical region (~ 50-60% in mice and rats, Bal et al. 2012) or axillary and subscapular region (~50% in hamster, Heldmaier et al. 2012). Active gonadal brown adipose tissue in males and females, together with sustained homeothermy during periods of parental care may point towards a use BAT-derived thermogenesis during periods of parental care.

Interestingly, a role of brown adipose tissue in reproduction is not supported considering studies in modern Eutherian mammals (Trayhurn et al. 1982, Trayhurn and Wusteman 1987). As modern mammals have high body temperatures around 36-37°C, the thermogenic capacity of BAT is decreased during pregnancy and lactation, possibly to avoid overheating (reviewed by Cannon and Nedergaard 2004). Rats are the only modern mammals where relatively large renal-abdominal BAT depots have been reported (25% of total BAT, Smith and Roberts 1964). The interscapular BAT of rats is inactive during pregnancy and lactation (Villarroya et al. 1987, Abelenda and Puerta 1987), unfortunately there are no data available about physiological activity of renal BAT.

Cold exposure does not lead to any activation of brown adipose tissue for body temperature defense in Lesser hedgehog tenrecs. Wünnenberg et al. postulated in 1974 that the dorsal brown adipose tissue of European hedgehogs is functionally non-uniform and that there is a catcholamine (noradrenaline) independent mode of nonshivering thermogenesis. Catecholamines appeared to activate the interscapular brown adipose tissue during arousal from hibernation whereas

desoxycorticosterone-like compounds activated a dorsal brown fat layer during cold exposure. The same may account for the specific activation of tenrec renal brown adipose tissue during periods of parental care, the regulatory pathway may be different from the commonly accepted pathway.

If brown adipose tissue thermogenesis is indeed important for reproduction in female tenrecs, what could be a thermogenic role in males? Interestingly, incubation temperature of reproductive cells is temperature-sensitive. In modern Eutherian mammals, spermatogenesis is maintained at 2 °C (humans) to 8 °C (mouse) below body temperature while in reptiles, the rate of spermatogenesis increases with increasing temperatures (Licht 1972, Joly and Saint Girons 1975). In hibernating ground squirrels, the testicular androgen production also is highly temperature sensitive and inhibited during deep torpor (Ta: 5°C; Barnes et al. 1987). Conclusively spermatogenesis in male tenrecs might be as well temperature sensitive and more efficient at higher body temperature (Tb~33°C). In an evolutionary scenario, brown fat may have assisted in selection advantages by incubating reproductive cells of males and females independently of ambient temperature and thereby increasing the reproduction success. Conclusively this study indirectly supports the parental care theory of the evolution of endothermy (Fig. 7).

CONCLUSION

My PhD-thesis aimed to provide new perspectives on the significance of brown adipose tissue in mammals and maybe to emphasize a novel and more profound evolutionary scenario of its development. I was particularly interested in UCP1s quantitative contribution to torpor arousal and its role in the protection against ROS in Eutherian mammals. Furthermore I sought to clarify the function of brown adipose tissue in Afrotherians and especially protoendotherms. By combining state of the art physiological, molecular and biochemical techniques I could clearly demonstrate that:

1) UCP1 expression facilitates accelerated arousal rates from hypometabolic and hypothermic states while requiring 60% less energy. A clear advantage considering that torpor is a physiological behavior to save energy in periods of limited food and water resources. Nevertheless, UCP1 is not essential for normal torpor behavior of Eutherian mammals but might have been particularly beneficial for the migration to Holarctic regions, where sun basking cannot be used as efficient as in Afrotropical regions.
2) Furthermore, UCP1 allows high substrate turnover rates during nonshivering thermogenesis without the production of deleterious reactive oxygen species. Conclusively UCP1 has a dual role in heat production and superoxide production in modern Eutherians. The role of recently discovered ancient UCP1 orthologues in ectotherms could therefore be the prevention of superoxide production prior to the acquisition of nonshivering thermogenesis.
3) Following the trait of the evolutionary history of adaptive thermogenesis, I finally confirmed that adaptive thermogenesis is already present at the evolutionary stage of Afrotherians and is a widespread feature within this clade and, consequently, in Afrotropical regions. Therefore it is unlikely that brown adipose tissue evolved its thermogenic function solely during migration to Holartic regions.
4) Additional studies on the Lesser hedgehog tenrec showed for the first time the expression of full functional brown adipose tissue and adaptive thermogenesis in a protoendothermic mammal. Unexpectedly, the tenrec UCP1 orthologue appeared as a modern form of UCP1 in phylogenetic analysis. The correlative evidence suggests that the evolution of brown adipose tissue is linked to selection for increased incubation temperatures during periods of parental care.

Based on these findings we designed a scheme of an evolutionary scenario in which brown adipose tissue developed as a consequence of selection for improved offspring incubation in protoendotherms (Fig. 7). This promoted the radiation of ancient Eutherian mammals and the evolution of the first obligate endothermic mammals. The development and functional expansion of brown adipose tissue towards defending a high body temperature facilitated a further niche expansion and the migration into

cold environments, leading to a more successful radiation of modern Eutherian mammals.

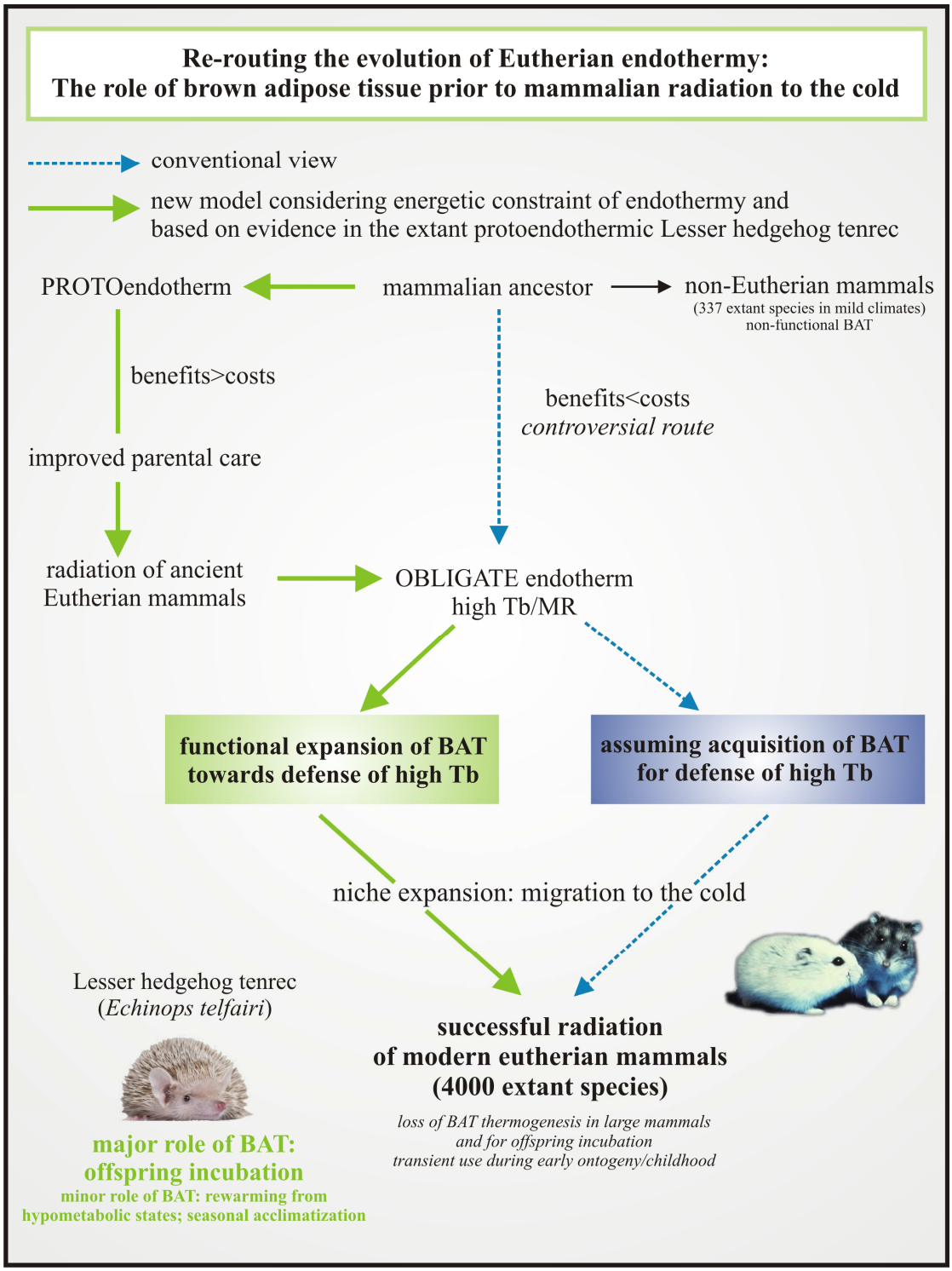

Figure 7: Re-routing the evolution of Eutherian endothermy. The role of brown adipose tissue (BAT) prior to mammalian radiation to the cold. The conventional view of the evolution of brown adipose tissue mediated thermogenesis predicts that brown fat primarily evolved (directly or indirectly) for body temperature (Tb) defense to display obligate endothermy. An evolutionary scenario in which the metabolic costs (MR: metabolic rate) clearly exceed the benefits of the new invention. Therefore we propose that brown adipose tissue gained a thermogenic function first in protoendothermic mammals to increase body temperature during periods of parental care. The only scenario in which the metabolic costs were lower than the benefits of the new invention. Later on brown adipose tissue was used for a defense of body temperature, leading to a niche expansion to Holartic regions and the successful radiation of modern Eutherian mammals.

TRANSLATIONAL VALUE

BROWN ADIPOSE TISSUE AND UCP1 AS A THERAPEUTIC TARGET TO COMBAT OBESITY AND COMORBIDITIES

Epidemiological studies forecasted that by 2030, 2.16 billion people worldwide will be overweight and 1.12 billion people will be obese (Kastorini et al. 2011). Type 2 diabetes and the associated beta-cell failure is up to 90% attributable to weight gain and will increase in parallel with the pandemic of obesity. These forecasts are serious and thus the investigation of new therapeutic targets regarding obesity is indispensable. The definite confirmation of human brown adipose tissue in 2007 promoted the brown fat research sector (Fig. 8, Nedergaard et al. 2007) and established a broader interest of the scientific community in this research field (222 publications in 2007 to 413 in 2012, source: www.pubmed.com). Several studies could show that human brown fat is similarly regulated as it has been previously postulated for murine models (Fig. 8G) and brown fat became the focus of attention as a new potential therapeutic target for the treatment of human body weight disorders (Cypress et al. 2009, van Marken Lichtenbelt et al. 2009, Virtanen et al. 2009). Already the selective activation of 50g brown fat could account for a 20% daily increase in energy expenditure (Rothwell and Stock, 1983), a promising and minimal invasive way to counteract obesity and to successfully fight many serious diseases of the new world. Therefore this study not only provides important results for the further clarification of brown adipose tissue function in small or ancient mammals; it is also helpful to fully elucidate the function and regulation of brown adipose tissue pathways in humans.

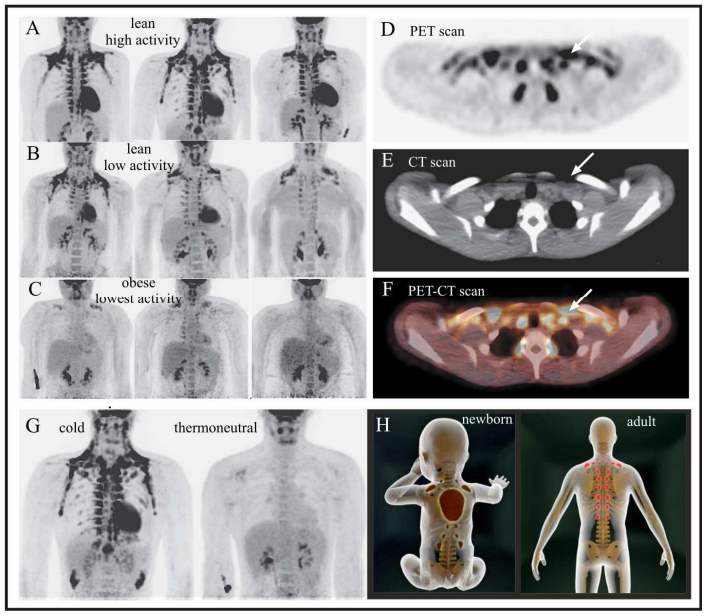

Figure 8. Brown adipose tissue activity in humans as assessed by PET–CT with ^{18}F-FDG. Brown fat in humans can be activated upon weight loss and cold exposure. A) Lean subjects with the highest levels of brown-adipose-tissue activity, B) lean subjects with median levels of activity, and C) obese or overweight subjects with the lowest levels of activity (C). D-F) The supraclavicular region has the greatest amount of brown adipose tissue. G) Comparative PET–CT scans reveal the patterns of ^{18}F-FDG uptake in a subject from the lean group after exposure to cold and under thermoneutral conditions. Panel H shows the distribution of brown adipose tissue in newborn and adult humans (red-brown patches, http://www.daserste.de/information/wissen-kultur/w-wie-wissen/sendung/2012/braunes-fettgewebe-100.html). Figure (A-G) and text modified after van Marken Lichtenbelt et al. 2009.

REFERENCES

Abelenda M. and Puerta M.L. (1987) *Inhibition of diet-induced thermogenesis during pregnancy in the rat.* Pflugers Arch 409: 314-317.

Aydin J., Shabalina I.G., Place N., Reiken S., Zhang S. et al. (2008) *Nonshivering thermogenesis protects against defective calcium handling in muscle.* FASEB J 22: 3919-3924.

Bal N.C., Sabtosj M.K., Danesh S.H., Sanjaya S.K., Subash G.C. et al. (2012) *Sarcolipin is a newly identified regulator of muscle-based thermogenesis in mammals*. Nat Med 18: 1575-1579.

Barnes B.M., Licht P. and Zucker I. (1987) *Temperature dependence of in vitro androgen production in testes from hibernating ground squirrels, Spermophilus lateralis.* Can J Zool 65: 3020 - 3023.

Barnes B.M. (1989) *Freeze avoidance in a mammal: body temperatures below 0 degree C in an Arctic hibernator.* Science 244:1593-1595.

Bartness T.J., Vaughan C.H. and Song C.K. (2010) *Sympathetic and sensory innervation of brown adipose tissue.* Int J Obesity 1: 36-42.

Berg F., Gustafson U. and Andersson L. (2006) *The uncoupling protein 1 gene (UCP1) is disrupted in the pig lineage: a genetic explanation for poor thermoregulation in piglets.* PLoS Genetics 2: e129.

Bieber C. and Ruf T. (2009) *Summer dormancy in edible dormice (Glis glis) without energetic constraints.* Naturwissenschaften 96: 165-171.

Boss O., Samec S., Kuhne F., Bijlenga P., Assimacopoulos-Jeannet F. et al. (1998) *Uncoupling protein-3 expression in rodent skeletal muscle is modulated by food intake but not by changes in environmental temperature.* J Biol Chem 273: 5-8.

Boveris A., Cadenas E. and Stoppani A.O. (1976) *Role of ubiquinone in the mitochondrial generation of hydrogen peroxide.* Biochem J 156: 435-444.

Brand M.D., Pakay J.L., Ocloo A., Kokoszka J., Wallace D.C. et al. (2005) *The basal proton conductance of mitochondria depends on adenine nucleotide translocase content.* Biochem J 392: 353-362.

Braulke L.J. and Heldmaier G. (2010) *Torpor and ultradian rhythms require an intact signalling of the sympathetic nervous system.* Cryobiol 60: 198-203.

Breen E.P., Gouin S.G., Murphy A.F., Haines L.R., Jackson A.M. et al. (2006) *On the mechanism of mitochondrial uncoupling protein 1 function.* J Biol Chem 281: 2114-2149.

Cannon B. and Nedergaard J. (2004) *Brown adipose tissue: function and physiological significance.* Physiol Rev 84: 277-359.

Cannon B. and Nedergaard J. (2011) *Nonshivering thermogenesis and its adequate measurement in metabolic studies.* J Exp Biol 214: 242-253.

Cannon B and Vogel G (1977) *The mitochondrial ATPase of brown adipose tissue. Purification and comparison with the mitochondrial ATPase from beef heart.* FEBS Lett 76: 284-289.

Cowles R.B. (1958) *Possible origin of dermal temperature regulation.* Evolution 12: 347-357.

Cypess A.M., Lehman S., Williams G., Tal I., Rodman D. et al. (2009) *Identification and importance of brown adipose tissue in adult humans.* N Engl J Med 360: 1509-1517.

Daan S., Spoelstra K., Albrecht U., Schmutz I., Daan M. et al. (2011) *Lab mice in the field: unorthodox daily activity and effects of a dysfunctional circadian clock allele.* J Biol Rhythms 26: 118-129.

Dausmann K.H., Glos J., Ganzhorn J.U. and Heldmaier G. (2004) *Physiology: hibernation in a tropical primate.* Nature 429: 825-826.

Dikic D., Heldmaier G. and Meyer C.W. (2008) *Induced torpor in different strains of laboratory mice*. In: Hypometabolism in Animals: Torpor, Hibernation and Cryobiology, eds. Lovegrove B.G. and McKechnie A.E., University of KwaZulu-Natal, Pietermaritzburg: 223-230.

Divakaruni A.S. and Brand M.D. (2011) *The regulation and physiology of mitochondrial proton leak.* Physiology 26: 192-205.

Dlaskova A., Clarke K.J. and Porter R.K. (2010) *The role of UCP 1 in production of reactive oxygen species by mitochondria isolated from brown adipose tissue.*Biochim Biophys Acta 1797: 1470-1476.

Echtay K.S., Roussel D., St-Pierre J., Jekabsons M.B., Cadenas S. et al. (2002) *Superoxide activates mitochondrial uncoupling proteins.* Nature 415: 96-99.

Echtay K.S., Esteves T.C., Pakay J.L., Jekabsons M.B,. Lambert A.J. et al. (2003) *A signalling role for 4-hydroxy-2-nonenal in regulation of mitochondrial uncoupling.* EMBO J 22: 4103-4110.

Ehrhardt N., Heldmaier G. and Exner C. (2005) *Adaptive mechanisms during food restriction in Acomys russatus: the use of torpor for desert survival.* J Comp Physiol B 175: 193-200.

Else P.L and Hulber A.J. (1981) *Comparison of the "mammal machine" and the "reptile machine": energy production.* Am J Physiol 240: R3-9.

Enerback S., Jacobsson A., Simpson E.M., Guerra C., Yamashita H. et al. (1997) *Mice lacking mitochondrial uncoupling protein are cold-sensitive but not obese.* Nature 387: 90-94.

Farmer C.G. (2000) *Parental Care: The Key to Understanding Endothermy and Other Convergent Features in Birds and Mammals.* Am Nat 155: 326-334.

Fedorenko A., Lishko P.V. and Kirichok Y. (2012) *Mechanism of fatty-acid-dependent UCP1 uncoupling in brown fat mitochondria.* Cell 151: 400-413.

Fielden L.J., Perrin M.R. and Hickman G.C. (1990) *Water metabolism in the Namib Desert golden mole, Eremitalpa granti namibensis (Chrysochloridae).* Comp Biochem Physiol A 96: 227-234.

Fleury C., Neverova M., Collins S., Raimbault S., Champigny O. et al. (1997) *Uncoupling protein-2: a novel gene linked to obesity and hyperinsulinemia.* Nat Genet 15: 269-272.

Foster D.O. (1984) *Quantitative contribution of brown adipose tissue thermogenesis to overall metabolism.* Can J Biochem Cell Bio*l* 62: 618-622.

Freake H.C. and Oppenheimer J.H. (1987) *Stimulation of S14 mRNA and lipogenesis in brown fat by hypothyroidism, cold exposure, and cafeteria feeding: evidence supporting a general role for S14 in lipogenesis and lipogenesis in the maintenance of thermogenesis.* P Natl Acad Sci USA 84: 3070-3074.

Garlid K.D., Orosz D.E., Modriansky M., Vassanelli S. and Jezek P. (1996) On the mechanism of fatty acid-induced proton transport by mitochondrial uncoupling protein. J Biol Chem 271: 2615-2620.

Garlid K.D., Jaburek M. and Jezek P. (1998) *The mechanism of proton transport mediated by mitochondrial uncoupling proteins.* FEBS Lett 438: 10-14.

Geiser F. and Mzilikazi N. (2011) *Does torpor of elephant shrews differ from that of other heterothermic mammals.* J Mammol 92: 444-451.

Golozoubova V., Hohtola E., Matthias A., Jacobsson A., Cannon B. et al. (2001) *Only UCP1 can mediate adaptive nonshivering thermogenesis in the cold.* FASEB J 15: 2048-2050.

Golozoubova V., Cannon B. and Nedergaard J. (2006) *UCP1 is essential for adaptive adrenergic nonshivering thermogenesis.* Am J Physiol Endocrinol Metab 291: E350-357.

Grigg G.C., Beard L.A. and Augee M.L. (2004) *The evolution of endothermy and its diversity in mammals and birds.* Physiol Biochem Zool 77: 982-997.

Grimpo K., Legler K., Heldmaier G. and Exner C. (2012) *That's hot: golden spiny mice display torpor even at high ambient temperatures.* J Comp Physiol B, DOI 10.1007/s00360-012-0721-4.

Haim A. (1982) *Effects of long scotophase and cold acclimation on heat production in two diurnal rodents.* J Comp Physiol B 148: 77-81.

Hallam S. and Mzilikazi N. (2010) *Heterothermy in the southern African hedgehog, Atelerix frontalis.*J Comp Physiol B 181: 437-445.

Harman D. (1956) *Aging: a theory based on free radical and radiation chemistry.* J Gerontol 11: 298-300.

Harman D. (1972) *Free radical theory of aging: dietary implications.* Am J Clin Nutr 25: 839-843.

Hart J.S. (1952) *Effects of temperature and work on metabolism, body temperature, and insulation: results with mice.* Can J Zool 30: 90-98.

Hayes J.P. and Garland T. (1995) *The evolution of endothermy: testing the aerobic capacity Model.* Evolution 49: 836-847.

Hayward J.S. and Lisson P.A. (1992) *Evolution of brown fat: its absence in marsupials and monotremes.* Can J Zool 70: 171 - 179.

Heldmaier G. (1970) *Die Thermogenese der Mausohrfledermaus (Myotis myotis) beim Erwachen aus dem Winterschlaf.* Z Vergl Physiol 63: 59-84.

Heldmaier G. (1971) *Zitterfreie Wärmebildung und Körpergröbe bei Säugetieren.* Z vergl Physiol 73: 222-248.

Heldmaier G. and Steinlechner S. (1981) *Seasonal control of energy requirements for thermoregulation*

in the Djungarian hamster (Phodopus sungorus), living in natural photoperiod. J Comp Physiol B 142:429–437.

Heldmaier G. and Buchberger A. (1985) *Sources of heat during nonshivering thermogenesis in Djungarian hamsters: a dominant role of brown adipose tissue during cold adaptation.* J Comp Physiol B 156: 237-245.

Heldmaier G., Steinlechner S., Ruf T., Wiesinger H. and Klingenspor M. (1989) *Photoperiod and thermoregulation in vertebrates: body temperature rhythms and thermogenic acclimation.* J Biol Rhythms 4: 251-265.

Heldmaier G., Klaus S. and Wiesinger H. (1990) *Seasonal adaptation of thermoregulatory heat production in small mammals.* In: Thermoreception and Temperature Regulation, eds. Bligh J. and Voigt K., Springer, Berlin, Heidelberg, New York: 235-243.

Heldmaier G. and Klingenspor M. (2003) *Role of Photoperiod During Seasonal Acclimation in Winter-Active Small Mammals.* In: Environmental Signal Processing and Adaptation, eds. Heldmaier G. and Werner D., Springer, Berlin, Heidelberg, New York: 251-279.

Heldmaier G., Neuweiler G. and Rössler W. (2012) *Vergleichende Tierphysiologie.* Springer, Berlin, Heidelberg.

Herrero A. and Barja G. (1998) *H2O2 production of heart mitochondria and aging rate are slower in canaries and parakeets than in mice: sites of free radical generation and mechanisms involved.* Mech Ageing Dev 103: 133-146.

Hut R.A., Pilorz V., Boerema A.S., Strijkstra A.M. and Daan S. (2011) *Working for food shifts nocturnal mouse activity into the day.* PloS one 6: e17527.

IUPS-Thermal-Commission (2003) *Glossary of terms for thermal physiology.* Thermal Biol: 75-106.

Jastroch M., Wuertz S., Kloas W. and Klingenspor M. (2005) *Uncoupling protein 1 in fish uncovers an ancient evolutionary history of mammalian nonshivering thermogenesis.* Physiol Genomics 22: 150-156.

Jastroch M., Buckingham J.A., Helwig M., Klingenspor M. and Brand M.D. (2007) *Functional characterisation of UCP1 in the common carp: uncoupling activity in liver mitochondria and cold-induced expression in the brain.* J Comp Physiol B 177: 743-752.

Jastroch M., Withers K.W., Taudien S., Frappell P.B., Helwig M. et al. (2008) *Marsupial uncoupling protein 1 sheds light on the evolution of mammalian nonshivering thermogenesis.* Physiol Genomics 32: 161-169.

Jastroch M., Hirschberg V. and Klingenspor M. (2012) Functional characterization of UCP1 in mammalian HEK293 cells excludes mitochondrial uncoupling artefacts and reveals no contribution to basal proton leak. Biochim Biophys Acta 1817: 1660-1670.

Joly J. and Saint-Girons H. (1975) *Influence de la temperature sur la vitesse de la spermatogenese, la duree de l'activite spermatogenetique et l'evolution des caracteres sexuels secondaires du lezard des murailles, Lacerta muralis L. (Reptilia, Lacertidae).* Archives d'anatomie microscopique et de morphologie experimentale 64: 317-36.

Kastorini C., Milionis H.J., Esposito K., Giugliano D., Goudevenos J.A. et al. (2011) *The effect of Mediterranean diet on metabolic syndrome and its components: a meta-analysis of 50 studies and 534,906 individuals.* J Amer Coll Cardiol 57: 1299-1313.

Keipert S., Klaus S., Heldmaier G. and Jastroch M. (2010) *UCP1 ectopically expressed in murine muscle displays native function and mitigates mitochondrial superoxide production.* Biochim Biophys Acta 1797: 324-330.

Khailova L.S., Prikhodko E.A., Dedukhova V.I., Mokhova E.N., Popov V.N. et al. (2006) *Participation of ATP/ADP antiporter in oleate- and oleate hydroperoxide-induced uncoupling suppressed by GDP and carboxyatractylate.* Biochim Biophys Acta 1757: 1324-1329.

Klingenberg M. and Winkler E. (1985) *The reconstituted isolated uncoupling protein is a membrane potential driven H+ translocator.* EMBO J: 3087-3092.

Klingenberg M. and Huang S.G. (1999) *Structure and function of the uncoupling protein from brown adipose tissue.* Biochim Biophys Acta 1415: 271-296.

Klingenberg M. (2010) *Wanderings in bioenergetics and biomembranes.* Biochim Biophys Acta: 579-594.

Klingenspor M. (2003) *Cold-induced recruitment of brown adipose tissue thermogenesis.* Exp Physiol 88: 141-148.

Klingenspor M. and Fromme T. (2012) *Brown adipose tissue.* In: Adipose Tissue Biology, ed.

Symonds M.E., Springer Science+Business Media.

Koteja P. (2000) *Energy assimilation, parental care and the evolution of endothermy.* Proc Biol Sci 267: 479-484.

Kozlowski J. (1992) *Optimal allocation of resources to growth and reproduction: implications for age and size at maturity.* Trends Ecol Evol 7: 15-19.

Kozlowski J. and Weiner J. (1997) *Interspecific Allometries Are by-Products of Body Size Optimization.* Amer Nat 149: 352-380.

Kronfeld-Schor N., Haim A., Dayan T., Zisapel N., Klingenspor M. et al. (2000) *Seasonal thermogenic acclimation of diurnally and nocturnally active desert spiny mice.* Physiol Biochem Zool 73: 37-44.

Körtner G. and Geiser F. (2000) *Torpor and activity patterns in free-ranging sugar gliders Petaurus breviceps (Marsupialia).* Oecologia 123: 350 - 357.

Laloi M., Klein M., Riesmeier J.W., Muller-Rober B., Fleury C. et al. (1997) *A plant cold-induced uncoupling protein.* Nature 389: 135-136.

Licht P. (1972) *Actions of mammalian pituitary gonadotropins (FSH and LH) in reptiles. 1. Male snakes.* Gen Comp Endocrinol 19: 273-281.

Lovegrove B.G., Lawes M.J. and Roxburgh L. (1999) *Confirmation of pleisiomorphic daily torpor in mammals: the round-eared elephant shrew Macroscelides proboscideus (Macroscelidea).* J Comp Physiol B 169: 453-460.

Lovegrove B.G. and Genin F. (2008) *Torpor and hibernation in a basal placental mammal, the Lesser Hedgehog Tenrec Echinops telfairi.* J Comp Physiol B 178:691–698.

Lovegrove B.G. (2012) *The evolution of endothermy in Cenozoic mammals: a plesiomorphic-apomorphic continuum.* Biol Rev 87: 128-162.

Lowell B.B. and Spiegelman B.M. (2000) *Towards a molecular understanding of adaptive thermogenesis.* Nature 404:652–660.

Lyman C.P. and O'Brian R.C. (1986) *Is brown fat necessary?* In: Living in the Cold: Physiological and Biochemical Adaptations, eds. Heller H.C., Musacchia X.J. and Wang L.H.C. Elsevier, New York: 116-119.

McKechnie A.E. and Wolf B.O. (2004) *The energetics of the rewarming phase of avian torpor.* In: Life in the Cold: Evolution, Mechanism, Adaptation and Application, eds. Barnes B.M. and Carey H.V., University of Alaska, Fairbanks: 265-273.

McKechnie A.E. and Lovegrove B.G. (2001) *Heterothermic responses in the speckled mousebird (Colius striatus).* J Comp Physiol B 171: 507-518.

Miroux B., Frossard V., Raimbault S., Ricquier D. and Bouillaud F. (1993) *The topology of the brown adipose tissue mitochondrial uncoupling protein determined with antibodies against its antigenic sites revealed by a library of fusion proteins.* EMBO J 12: 3739-3745.

Morrison S.F., Nakamura K. and Madden C.J. (2008) *Central control of thermogenesis in mammals.* Exp Physiol 93: 773-797.

Mzilikazi N., Lovegrove B. and Ribble D.O. (2002) *Exogenous Passive Heating during Torpor Arousal in Free-Ranging Rock Elephant Shrews, Elephantulus myurus.* Oecologica 133: 307-314.

Mzilikazi N. and Lovegrove B.G. (2004) *Daily torpor in free-ranging rock elephant shrews, Elephantulus myurus: a year-long study.* Physiol Biochem Zool 77: 285-296.

Mzilikazi N. and Lovegrove B.G. (2006) *Noradrenalin induces thermogenesis in a phylogenetically ancient eutherian mammal, the rock elephant shrew, Elephantulus myurus.* J Comp Physiol B 176: 75-84.

Mzilikazi N., Jastroch M., Meyer C.W. and Klingenspor M. (2007) *The molecular and biochemical basis of nonshivering thermogenesis in an African endemic mammal, Elephantulus myurus.* Amer J Physiol 293: R2120-1227.

Nakamura K. and Morrison S.F. (2008) *A thermosensory pathway that controls body temperature.* Nat Neurosci 11: 62-71.

Nautiyal K.M., Dailey M., Brito N., Brito M.N., Harris R.B. et al. (2008) *Energetic responses to cold temperatures in rats lacking forebrain-caudal brain stem connections.* Am J Physiol Regul Integr Comp Physiol 295(3): R789–R798.

Nedergaard J., Bengtsson T. and Cannon B. (2007) *Unexpected evidence for active brown adipose tissue in adult humans.* Amer J Physiol 293: E444-452.

Nicholls D.G. and Locke R.M. (1984) *Thermogenic mechanisms in brown fat.* Physiol Rev 64: 1-64.

Nicholls D.G. (2001) *A history of UCP1.* Biochem Soc Trans 29: 751-755.

Nicol S.C., Morrow G. and Andersen N.A. (2008)

Hibernation in monotremes: a review. In: Hypometabolism in Animals: Hibernation, Torpor and Cryobiology, eds. Lovegrove B.G. and McKechnie A.E. University of KwaZulu-Natal, Pietermaritzburg: 251-262.

Nohl H., Gille L., Schonheit K. and Liu Y. (1996) *Conditions allowing redox-cycling ubisemiquinone in mitochondria to establish a direct redox couple with molecular oxygen.* Free Radical Biol Med 20: 207-213.

Oelkrug R., Meyer C.W., Heldmaier G. and Mzilikazi N. (2012) *Seasonal changes in thermogenesis of a free-ranging afrotherian small mammal, the Western rock elephant shrew (Elephantulus rupestris).*J Comp Physiol B 182: 715-727.

Oelkrug R., Goetze N., Exner C., Yang L., Ganjam G.K. et al. (2013) *Brown fat in a ´protoendothermic´ mammal fuels the parental care model of mammalian evolution.* Nat Comm, in revision.

Ortmann S., Heldmaier G., Schmid J. and Ganzhorn J.U. (1997) *Spontaneous daily torpor in Malagasy mouse lemurs.* Naturwissenschaften 84: 28-32.

Polymeropoulos E.T., Jastroch M. and Frappell P.B. (2012) *Absence of adaptive nonshivering thermogenesis in a marsupial, the fat-tailed dunnart (Sminthopsis crassicaudata).* J Comp Physiol B 182: 393-401.

Poppit S.D., Speakman J.R. and Racey P.A. (1994) *Energetics of reproduction in the lesser hedgehog tenrec, Echinops telfairi (Martin).* Physiol Zool 67: 976-994.

Rasmussen A.T. (1923) *The so-called hibernating gland*. J Morphol 38: 147-205.

Rial E., Aguirregoitia E., Jimenez-Jimenez J. and Ledesma A. (2004) *Alkylsulfonates activate the uncoupling protein UCP1: implications for the transport mechanism.* Biochim Biophys Acta 1608: 122-130.

Ricquier D. and Kader J.C. (1976) *Mitochondrial protein alteration in active brown fat: a soidum dodecyl sulfate-polyacrylamide gel electrophoretic study*. Biochem Biophys Res Commun 73: 577-583.

Rolfe D.F. and Brown G.C. (1997) *Cellular energy utilization and molecular origin of standard metabolic rate in mammals.* Physiol Rev 77: 731-758.

Rothwell N.J. and Stock M.J. (1983) *Luxuskonsumption, diet-induced thermogenesis and brown fat: the case in favour*. Clin Sci 64: 19-23.

Rousset S., Alves-Guerra M., Mozo J., Miroux B., Cassard-Doulcier A. et al. (2004) *The biology of mitochondrial uncoupling proteins.* Diabetes 53: 130-135.

Ruby N.F. and Zucker I. (1992) *Daily torpor in the absence of the suprachiasmatic nucleus in Siberian hamsters.* Amer J Physiol 263: R353-362.

Ruf T and Heldmaier G (1992) *The Impact of Daily Torpor on Energy Requirements in the Djungarian Hamster, Phodopus sungorus.* Physiol Zool 65: 994 - 1010.

Scantlebury M., Lovegrove B.G., Jackson C.R., Bennett N.C. and Lutermann H. (2008) *Hibernation and non-shivering thermogenesis in the Hottentot golden mole (Amblysomus hottentottus longiceps).* J Comp Physiol B 178: 887-897.

Schönfeld P. and Wojtczak L. (2012) *Brown adipose tissue mitochondria oxidizing fatty acids generate high levels of reactive oxygen species irrespective of the uncoupling protein-1 activity state.* Biochim Biophys Acta 1817: 410-418.

Shabalina I.G., Jacobsson A., Cannon B. and Nedergaard J. (2004) *Native UCP1 displays simple competitive kinetics between the regulators purine nucleotides and fatty acids.* J Biol Chem 279: 38236-38248.

Shabalina I.G., Petrovic N., Kramarova T.V., Hoeks J., Cannon B. et al. (2006) *UCP1 and defense against oxidative stress. 4-Hydroxy-2-nonenal effects on brown fat mitochondria are uncoupling protein 1-independent.* J Biol Chem 281: 13882-13893.

Scholl P. (1974) *Temperaturregulation beim madegassischen Igeltanrek Echinops telfairi (Martin, 1838).* 89: 175-195.

Seymour R.S. (2010) *Scaling of heat production by thermogenic flowers: limits to floral size and maximum rate of respiration.* Plant Cell Environ 33: 1474-1485.

Silva J.P., Shabalina I.G., Dufour E., Petrovic N., Backlund E.C. et al. (2005) *SOD2 overexpression: enhanced mitochondrial tolerance but absence of effect on UCP activity.* EMBO J 24: 4061-4070.

Smith R.E. and Roberts J.C. (1964) *Thermogenesis of brown adipose tissue in cold-acclimated rats.* Amer J Physiol 206: 143-148.

Springer M.S., Cleven G.C., Madsen O., de Jong W.W., Waddell V.G. et al. (1997) *Endemic African mammals shake the phylogenetic tree.* Nature 388: 61-64.

Stearns S.C. (1992) *The evolution of life histories.* Oxford University Press, Oxford.

Stone G.N. and Purvis A. (1992) *Warm-up rates during arousal from torpor in heterothermic mammals: physiological correlates and a comparison with heterothermic insects.* J Comp Physiol B 162: 284-295.

Swoap S.J., Gutilla M.J., Liles L.C., Smith R.O. and Weinshenker D. (2006) *The full expression of fasting-induced torpor requires beta 3-adrenergic receptor signaling.* J Neurosci 26: 241-5.

Trayhurn P. and Wusteman M.C. (1987) *Sympathetic activity in brown adipose tissue in lactating mice.* Amer J Physiol 253: E515-520.

Trayhurn P., Douglas J.B. and McGuckin M.M. (1982) *Brown adipose tissue thermogenesis is 'suppressed' during lactation in mice.* Nature 298: 59-60.

Trzcionka M., Withers K.W., Klingenspor M. and Jastroch M. (2008) *The effects of fasting and cold exposure on metabolic rate and mitochondrial proton leak in liver and skeletal muscle of an amphibian, the cane toad Bufo marinus.* J Exp Biol 211: 1911-1918.

van Marken Lichtenbelt W.D., Vanhommerig J.W., Smulders N.M., Drossaerts J.M.A.F.L., Kemerink G.J. et al. (2009a) *Cold-activated brown adipose tissue in healthy men.* N Engl J Med 360: 1500-1508.

Vianna C.R., Hagen T., Zhang C.Y., Bachman E., Boss O. et al. (2001) *Cloning and functional characterization of an uncoupling protein homolog in hummingbirds.* Physiol Genomics 5: 137-145.

Villarroya F., Felipe A. and Mampel T. (1987) *Reduced noradrenaline turnover in brown adipose tissue of lactating rats.* Comp Biochem Phys A 86: 481-3.

Virtanen K.A., Lidell M.E., Orava J., Heglind M., Westergren R. et al. (2009) *Functional brown adipose tissue in healthy adults.* N Engl J Med 360: 1518-1525.

Wang L.C.H. (1989) *Ecological, physiological and biochemical aspects of torpor in mammals and birds.* In: Animal Adaptation to Cold. Advances in Comparative and Environmental Physiology, ed.Wang L.C.H., Springer Verlag, Heidelberg: 361-401.

Warnecke L. and Geiser F. (2010) *The energetics of basking behaviour and torpor in a small marsupial exposed to simulated natural conditions.* J Comp Physiol B 180: 437-445.

Webb G.P., Jagot S.A. and Jakobson M.E. (1982) *Fasting-induced torpor in Mus musculus and its implications in the use of murine models for human obesity studies.* Comp Biochem Phys A 72: 211-219.

Wesley W.C., Hillier L.W., Marshall Graves J.A., Birney E., Ponting C.P. et al. (2008) *Genome analysis of the platypus reveals unique signatures of evolution.* Nature 453: 175-183.

Winkler E. and Klingenberg M. (1994) *Effect of fatty acids on H+ transport activity of the reconstituted uncoupling protein.* J Biol Chem 269: 2508-15.

Wünnenberg W., Merker G., Brück K. (1974) *Do corticosteroids control heat production in hibernators?* Pflugers Arch 352: 11-16.

TORPOR PATTERNS, AROUSAL RATES, AND TEMPORAL ORGANIZATION OF TORPOR ENTRY IN WILDTYPE AND UCP1-ABLATED MICE

R. OELKRUG ∞ G. HELDMAIER ∞ C. W. MEYER

J Comp Physiol B (2011) 181:137–145
DOI 10.1007/s00360-010-0503-9

ORIGINAL PAPER

Torpor patterns, arousal rates, and temporal organization of torpor entry in wildtype and UCP1-ablated mice

R. Oelkrug · G. Heldmaier · C. W. Meyer

Received: 18 April 2010 / Revised: 19 July 2010 / Accepted: 20 July 2010 / Published online: 1 August 2010

Abstract In eutherian mammals, uncoupling protein 1 (UCP1) mediated non-shivering thermogenesis from brown adipose tissue (BAT) provides a mechanism through which arousal from torpor and hibernation is facilitated. In order to directly assess the magnitude by which the presence or absence of UCP1 affects torpor patterns, rewarming and arousal rates within one species we compared fasting induced torpor in wildtype ($UCP1^{+/+}$) and UCP1-ablated mice ($UCP^{-/-}$). Torpor was induced by depriving mice of food for up to 48 h and by a reduction of ambient temperature (T_a) from 30 to 18°C at four different time points after 18, 24, 30 and 36 h of food deprivation. In most cases, torpor bouts occurred within 20 min after the switch in ambient temperature (30–18°C). Torpor bouts expressed during the light phase lasted 3–6 h while significantly longer bouts (up to 16 h) were observed when mice entered torpor during the dark phase. The degree of hypometabolism (5–22 ml h^{-1}) and hypothermia (19.5–26.7°C) was comparable in wildtype and UCP1-ablated mice, and both genotypes were able to regain normothermia. In contrast to wildtype mice, UCP1-ablated mice did not display multiple torpor bouts per day and their peak rewarming rates from torpor were reduced by 50% ($UCP1^{+/+}$: 0.24 ± 0.08°C min^{-1}; $UCP1^{-/-}$: 0.12 ± 0.04°C min^{-1}). UCP1-ablated mice therefore took significantly longer to rewarm from 25 to 32°C (39 vs. 70 min) and required 60% more energy for this process. Our results demonstrate the energetic benefit of functional BAT for rapid arousal from torpor. They also suggest that torpor entry and maintenance may be dependent on endogenous rhythms.

Keywords Hypometabolism · Hypothermia · Brown adipose tissue

Abbreviations

BAT	Brown adipose tissue
CET	Central European time
NST	Non-shivering thermogenesis
UCP	Uncoupling protein
T_a	Ambient temperature
T_b	Body temperature

Introduction

Endotherms employ daily torpor to reduce their daily energy expenditure on a day to day basis (Geiser 2004; Heldmaier et al. 2004). In daily heterotherms, such as short day acclimated Djungarian hamsters (*Phodopus sungorus*), or mouse lemurs (*Microcebus murinus*), daily torpor is observed as an obligatory behaviour during seasonal acclimation, e.g. in response to decreasing day length. Daily torpor also occurs as a facultative behaviour in response to acute energy shortfalls. An example is the mouse (*Mus musculus*), in which torpor is only displayed when animals are confronted with food deprivation or a combination of food deprivation and cold (Hudson and Scott 1979; Webb et al. 1982; Swoap et al. 2006; Dikic et al. 2008; Brown and Staples 2010).

Communicated by H. V. Carey.

R. Oelkrug · G. Heldmaier · C. W. Meyer (✉)
Department of Animal Physiology, Faculty of Biology, Philipps-Universität, Karl-von-Frisch Strasse 8, 35043 Marburg, Germany
e-mail: meyerc@staff.uni-marburg.de

Arousal from torpor is usually accompanied by a rapid rewarming of body temperature. In order to rewarm from hypothermia, small mammals can recruit heat by two major thermogenic mechanisms, shivering thermogenesis (ST) and non-shivering thermogenesis (NST). It is well known that a large proportion of the latter is derived from the dissipation of heat mediated by uncoupling protein 1 (UCP1) in brown adipose tissue (BAT) mitochondria (Cannon and Nedergaard 2004), although other tissues may also contribute to NST (Foster and Frydman 1978; Heldmaier and Buchberger 1985; Granneman et al. 2003; Ukropec et al. 2006; Shabalina et al. 2010). In contrast to shivering muscle, BAT is considered a highly efficient site of heat production for rewarming from torpor because of its central location in the cervicothoracic region. The heat generated in BAT is readily distributed in the body core while peripheral temperatures can still be low, thereby facilitating the full rewarming process (Jansky 1973).

Daily torpor and hibernation are also observed in monotremes or adult marsupials which lack classical BAT (Rowlatt et al. 1971; Hayward and Lisson 1991; Jastroch et al. 2008; Nicol et al. 2008). In members of these taxonomic groups rewarming to normothermia cannot be supported by UCP1-mediated thermogenesis, raising the question on the significance of BAT in the context of torpor (Lyman and O'Brian 1986; Geiser and Baudinette 1990; Stone and Purvis 1992). A comparison of deep torpor in the short beaked echidna (*Tachyglossus aculeatus*; Monotremata, no BAT) with the similar sized marmot (*Marmota marmota*, BAT present) suggested that the peak rewarming rates in echidnas were 50% lower than in marmots (Nicol et al. 2009). Rewarming from torpor through mechanisms other than BAT UCP1-mediated NST, therefore, appears to be less efficient.

The total time and effort required for arousal, however, depends upon body mass and overall thermogenic capacity and it may be facilitated by high burrow temperature, insulative properties of the burrow and the presence of burrow mates. Torpid animals may also seek warmer microclimates or even bask to support arousal (Ortmann et al. 1997; Lovegrove et al. 1999; Mzilikazi et al. 2002; Warnecke and Geiser 2010). All of these parameters may conceal the specific extent by which BAT and UCP1-mediated NST assists in rewarming. In order to directly assess the contribution of UCP1-mediated NST for arousal from shallow torpor we investigated mice that genetically lack functional brown adipose tissue (UCP1-ablated mice, UCP1$^{-/-}$; Enerback et al. 1997). The examination of wildtype and UCP1-ablated mice allows a direct comparison of torpor behaviour and arousal in the presence or absence of UCP1-mediated NST within the same species. We hypothesized that UCP1-ablated mice should be reluctant to express torpor, or rewarm from torpor at substantially lower rates as compared to wildtype mice.

For torpor induction, warm acclimated mice (30°C) were deprived of food for up to 48 h and in addition, the ambient temperature (T_a) was reduced from 30 to 18°C on the second day of fasting. Torpor behaviour appears tightly linked to the circadian system in most species studied so far (Heldmaier and Steinlechner 1981; Ortmann et al. 1997; McKechnie and Lovegrove 2001; Ehrhardt et al. 2005). Therefore, the reduction of ambient temperature was started at four different experimental time-points. We thereby aimed to elucidate if torpor entry and its duration is an immediate (facultative) response to the cold stimulus, or if this behaviour depends on time of day.

Materials and methods

Mice and maintenance

Wildtype and UCP1-ablated mice (genetic background C57Bl/6J) were derived from our breeding colony at the Philipps-Universität of Marburg. In the founder animals (originally provided by L. Kozak, Pennington Medical Research Centre, Baton Rouge, USA) the UCP1 gene had been inactivated by homologous recombination with a deletion vector in which exon 2 and parts of exon 3 had been replaced with a neomycin resistance gene (Enerback et al. 1997). Genotypes were identified using a PCR-based strategy (Oelkrug et al. 2010) and only female UCP1$^{+/+}$ and UCP1 $^{-/-}$ mice were included in the experiments.

Mice were bred and raised at an ambient temperature of 24°C. Except for the days on which torpor was induced, mice always received food (Ssniff 1534, Soest, Germany) ad libitum. They were kept on a 12:12 h light:dark cycle (lights on 6:00 CET). At the age of 2–6 months, they were surgically implanted with temperature sensitive transmitters (series 3000; model XM-FH; Mini Mitter Company, Inc., USA) for the monitoring of abdominal core body temperature (T_b). Following surgery mice were maintained in individual cages at an ambient temperature of 24°C. Hereafter they were warm acclimated at 30°C for at least 3 weeks before the onset of the first torpor trial.

Experimental set-up and protocol

For the metabolic measurements, individual mice were transferred to metabolic cages (modified home cages, ~5 l volume) which were connected to an open circuit respirometry system for continuous monitoring of oxygen consumption (VO_2) and carbondioxide production (VCO_2). The basic set-up of the respirometric system has been described previously (Heldmaier and Ruf 1992). In parallel, body

temperature was recorded using TR 3000 receiver plates running on the Vital View software (Mini Mitter Company Inc., USA). The metabolic parameters (VO_2, VCO_2, T_b) were determined in each mouse during 24 h at 5 min intervals.

In $n = 7$ wildtype and $n = 5$ UCP1-ablated mice four successive torpor trials were performed, each separated by a 3-day recovery period. For torpor induction, mice were initially deprived of food at 12:00 CET and then continued to be maintained at 30°C T_a. After 18, 24, 30 or 36 h of food deprivation at 30°C (i.e. at 6:00, 12:00, 18:00 and 24:00 CET), the ambient temperature was lowered to 18°C for different periods of time (Fig. 1a). Trials were terminated after a maximum of 48 h without food, and mice still torpid at this time point were induced to arouse by vibration and acoustic stimulation (knocking on the cage). Individuals clearly unable to regain normothermia by themselves were removed from the cages and re-warmed using an infrared lamp. All experimental procedures were approved by the German Animal Welfare Authorities.

Arousal heat production, peak rewarming rates and energy expenditure during rewarming

For the calculation of arousal heat production, oxygen consumption data (VO_2) from the beginning of an arousal to the highest oxygen consumption value were obtained. A mouse was considered torpid if its oxygen consumption decreased below 25 ml h^{-1} for more than 2 h. This threshold was chosen to distinguish torpor episodes from periodic fluctuations in metabolic rate (Dikic et al. 2008). In case of multiday torpor, only the first bout of hypometabolism was considered for the evaluation, because UCP1-ablated mice frequently failed to arouse from the second bout of torpor. Altogether 41 torpor episodes were observed (Fig. 1a, dark fillings) from which 39 arousal periods could be analyzed (excluding one disturbed registration and 6 arousals from second bouts in the 12:00 h trial). For each arousal period VO_2-data were converted to HP rates (J s^{-1}) using the respiratory quotient (RQ; volumes of CO_2 produced/volumes of O_2 consumed) and the caloric equivalents given by (Heldmaier 1975): HP (J s^{-1}) = (4.44 + 1.43 × RQ) × VO_2 (ml h^{-1}). Cumulative HP (J) was calculated from summated HP rates (J s^{-1}) and the total time (s) required for rewarming or arousal.

In order to compare the efficiency of rewarming from torpor, we used two different approaches. One approach was to calculate peak rewarming rates (PWR, °C min^{-1}) from the body temperature time course during an arousal, assuming a four-parameter sigmoid curve (for details see Nicol et al. 2009). For these calculations, the Regression Wizard function of SigmaPlot was used (SigmaPlot 10 for Windows, Systat Software Inc, San Jose, CA, USA). Average R^2_{adj} was 0.995 for all tested trials with SD 0.003 ($n = 36$ torpor bouts; T_b was not available for three bouts from a wildtype mouse). In the second approach, we selected the arousal period during which each mouse rewarmed from 25 to 32°C T_b. This body temperature range was chosen because minimal body temperature (T_b min) in all but two torpor bouts was below 25°C, and $T_b = 32$°C is often used as the threshold temperature below which an animal is called torpid (Barclay et al. 2001). Oxygen consumption during rewarming from 25 to 32°C was converted to HP rates and cumulative HP as outlined above.

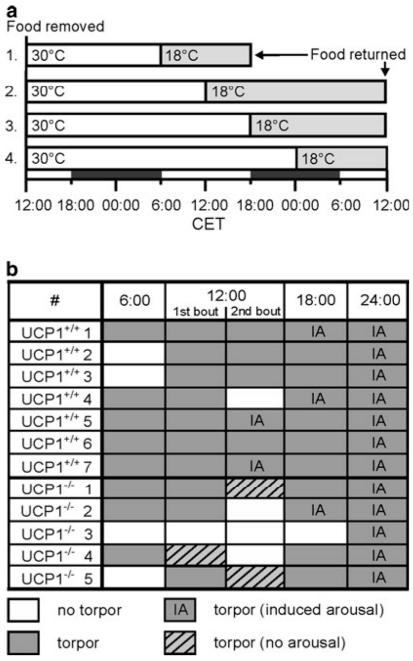

Fig. 1 **a** The experimental time schedule for torpor induction in wildtype and UCP1-ablated mice. Mice were food deprived for up to 48 h and additionally challenged with cold at different experimental time points (switch from 30 to 18°C, as indicated by the *shaded areas*). Periods of *lights off* are indicated by the *dark bars* at the bottom. **b** Individual torpor responses to different schedules of food deprivation and cold (switch from 30 to 18°C) in 7 wildtype ($UCP1^{+/+}$) and 5 UCP1-ablated mice ($UCP1^{-/-}$). The *top row* indicates the time of day (CET, central European time) when ambient temperature was changed. When the cold period started at 12:00 CET on the second day of food deprivation, the wildtype mice displayed two bouts of torpor during the subsequent 24 h

Statistical analyses

All data are expressed as mean ± standard deviation (SD). Differences in metabolic parameters between wildtype and UCP1-ablated mice were analyzed using Student's *t* test.

Results

Metabolic responses to food deprivation and cold

Figure 2 shows representative individual tracings of body temperature (T_b) and oxygen consumption in wildtype and UCP1-ablated mice challenged with food deprivation and a switch to cold ambient temperatures (18°C) at different experimental time points (at 6:00, 12:00, 18:00 and 24:00 CET, i.e. after 18, 24, 30 and 36 h of FD, exemplified in a–d). In all four trials and in both genotypes, clear bouts of hypometabolism and hypothermia could be observed. Altogether, we obtained 24 full torpor bouts from the wildtype mice and 15 full torpor bouts from the UCP1-ablated mice during which $\dot{V}O_2$ decreased below 23 ml h^{-1} and T_b was below 28°C. An overview on the individual torpor responses is given in Fig. 1b. In all trials, the body mass of the wildtype and UCP1-ablated mice was comparable ($UCP1^{+/+}$: 24.1 ± 1.3 g; $UCP1^{-/-}$: 24.2 ± 1.4 g). On average, mice lost between 1.8 and 7.0 g of body mass during each trial, with no differences between genotypes ($UCP1^{+/+}$: −4.5 g; $UCP1^{-/-}$: −4.4 g).

A reduction of ambient temperature from 30 to 18°C occurring at 6:00, 12:00, or 24:00 CET, induced a bout of hypometabolism and hypothermia in most mice within ~20 min after the onset of cold (Figs. 2a, b, d, 3a). When the cold exposure started at 18:00 CET (30 h without food), i.e. the time around *lights off*, torpor entry was delayed by 6 h (i.e. to midnight) relative to the cold onset and all mice entered torpor spontaneously (Figs. 2c, 3a). Nocturnal torpor bouts usually lasted longer than 6 h (up to 16 h) and on the next morning, we frequently induced an arousal by knocking on the cage in order to terminate the experiment (Fig. 3b). The longest bout from which an individual rewarmed by itself lasted almost 14 h in a wildtype mouse and 15 h in an UCP1-ablated mouse.

In the trial during which cold onset occurred at 12:00 CET (i.e. after mice had been without food for 24 h; Fig. 2b) clear genotype differences in the patterns of oxygen consumption and body temperature were evident. Initially, all wildtype mice and four UCP1-ablated mice readily entered a short bout of hypometabolism and hypothermia in acute response to cold. With the exception of one UCP1-ablated mouse, all individuals were able to arouse from torpor. After resuming normometabolism and normothermia all but one wildtype mouse spontaneously exhibited another long second bout of torpor around 9–12 h later (i.e. entry around midnight). In contrast, either the UCP1-ablated mice did not enter a second torpor bout, or they were clearly unable to arouse from a second torpor bout on their own (Figs. 1b, 2b). The fifth UCP1-ablated mouse did not enter any torpor and instead displayed a constant shallow body temperature (T_b ~ 33°C) without pronounced fluctuations in metabolic rate.

Arousal heat production, peak rewarming rates and energy expenditure during rewarming

The minimal oxygen consumption values observed in torpor ranged from 22.2 to 5.1 ml h^{-1} in wildtype and 22.0 to 4.8 ml h^{-1} in UCP1-ablated mice (Fig. 3c). Minimal body temperatures were 21.8 ± 2.4 and 21.2 ± 2.1°C, respectively (Fig. 3d).

The comparison of cumulative heat production during the full arousal period revealed that this process was energetically more costly in UCP1-ablated mice ($UCP1^{+/+}$: 2.33 ± 0.67 kJ; $UCP1^{-/-}$: 2.94 ± 0.90 kJ; $P = 0.019$; Fig. 4a). The time required to increase heat production from the onset of arousal to terminal values took significantly longer in UCP1-ablated mice compared with wildtype mice ($UCP1^{+/+}$: 127 ± 59 min; $UCP1^{-/-}$: 190 ± 65 min; $P = 0.004$; Fig. 4b).

Peak rewarming rates (PWR) were 0.24 ± 0.08°C min^{-1} in wildtype mice, while UCP1-ablated mice reached rewarming rates of only 0.12 ± 0.04°C min^{-1} (Fig. 4c). Body temperature during PWR was significantly lower in UCP1-ablated (28.2 ± 0.1°C) mice than in wildtype mice (29.6 ± 0.9°C; $P < 0.001$).

In order to elucidate the efficiency of BAT during rewarming, we analyzed the period of increase in body temperature from 25 to 32°C (highlighted Fig. 5a) which was available from all but two torpor bouts ($n = 34$). Rewarming from 25 to 32°C took almost twice as long in the UCP1-ablated mice ($UCP1^{+/+}$: 38.5 ± 12.5 min; $UCP1^{-/-}$: 70.1 ± 24.0 min, Fig. 5b) and required an additional 590 Joules ($UCP1^{+/+}$: 0.969 ± 0.209 kJ; $UCP1^{-/-}$: 1.59 ± 0.317 kJ; Fig. 5c, shaded area in Fig. 5a). Mean heat production (J s^{-1}) during rewarming from 25 to 32°C was not significantly different between wildtype and UCP1-ablated mice ($UCP1^{+/+}$: 0.376 ± 0.049 J s^{-1}; $UCP1^{-/-}$: 0.367 ± 0.063 J s^{-1}; Fig. 5d). Assuming a linear increase in heat production (J s^{-1}) with the time required for rewarming form 25 to 32°C (s), the rate of heat production change (J s^{-2}) during this process was significantly higher in the wildtype as compared to the UCP1-ablated mice ($UCP1^{+/+}$: 0.123 ± 0.055 mJ s^{-2}; $UCP1^{-/-}$: 0.051 ± 0.030 mJ s^{-2}; $P \leq 0.001$; Fig 5e).

Discussion

The comparison of wildtype and UCP1-ablated mice allowed us to investigate the role of UCP1-mediated NST during induced torpor behaviour. Clearly, absence of UCP1 (absence of functional BAT) did not impair the full expression of a single bout of torpor. Peak rewarming rates from torpor, however, were 50% lower in UCP1-ablated mice. The magnitude by which absence of uncoupled BAT

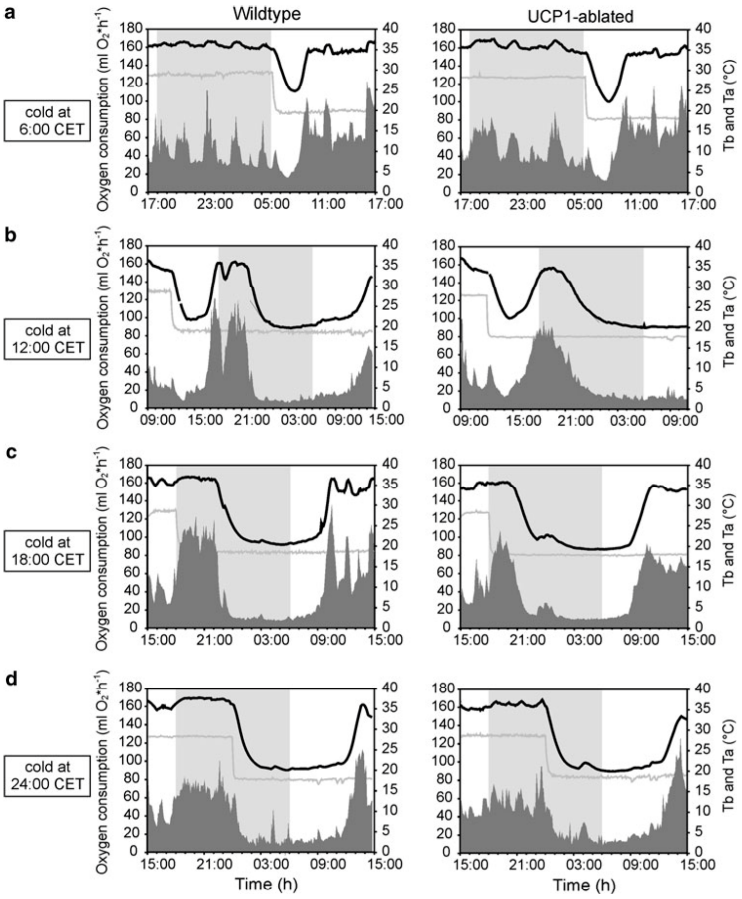

Fig. 2 Representative 24 h tracings of oxygen consumption (*dark area plot*) and body temperature (*black line*) from individual wildtype and UCP1-ablated mice in response to different experimental schedules of food deprivation (FD) and cold (see Fig. 1). **a** Mice had previously experienced 18 h of FD, and ambient temperature (T_a) was reduced to 18°C at 6:00 CET, as indicated by the *grey line*. **b** Mice had been held without food for 24 h and T_a was reduced to 18°C at noon. **c**, **d** The reduction of T_a occurred at 18:00 CET and 24:00 CET, respectively. Each experimental treatment induced bouts of hypometabolism and hypothermia in both genotypes. The *shaded area* represents the dark phase of the light–dark cycle (*lights off*: 18:00 CET, *lights on*: 6:00 CET)

thermogenesis compromised rewarming from torpor in the artificial system of the UCP1-ablated mouse is within the range of what has been previously suggested from suppression of NST through beta adrenergic blockade in wildtype mice (−30%; Swoap and Weinshenker 2008) or in hibernating bats (−50%; Heldmaier 1970). A 50% difference in peak rewarming rates could also be observed from the rates of emergence from torpor during the hibernation season in the echidna (no BAT; PWR: ~0.1°C min^{-1}) compared with the marmot (BAT present; PWR: 0.2°C min^{-1}) (Nicol et al. 2009).

The parallel recording of oxygen consumption enabled us to calculate total heat production during the rewarming period. In the absence of UCP1-mediated NST, arousal was less efficient, as rewarming for the same increase in body temperature (here: from 25 to 32°C T_b) required an additional 590 Joules (+60%) in UCP1-ablated mice. One possible explanation for the increment in thermogenesis in the absence of functional BAT is the need to compensate increased heat loss to the environment arising from thermogenesis of peripheral muscles. As we observed no difference in minimal metabolic rate or T_b min during torpor, and as the mean heat production during rewarming from 25 to 32°C did not differ between genotypes (Fig. 5c), our results do not support increased thermal conductance in UCP1-ablated mice. If anything, the UCP1-ablated mice reduce heat loss (decrease thermal conductance), e.g. by restricting blood flow to the tail (Wang et al. 2006). We conclude that heat dissipation rates outside BAT cannot fully compensate for the loss of uncoupled thermogenesis. As a result, the arousal process is less rapid, and it becomes energetically more costly because in addition to the

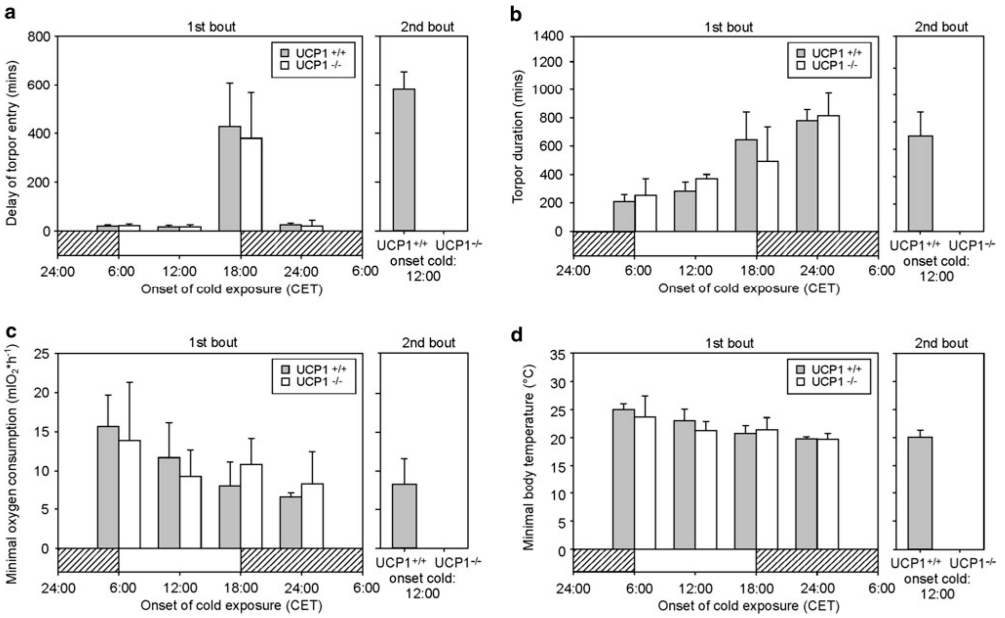

Fig. 3 Onset of torpor relative to the onset of cold (**a**), duration of induced torpor (**b**), minimal rates of oxygen consumption during torpor (**c**) and minimal body temperature in torpor (**d**) recorded from previously food deprived wildtype ($UCP^{+/+}$) and UCP1-ablated mice ($UCP^{-/-}$). Each *bar* represents the mean ± SD of 3–7 mice

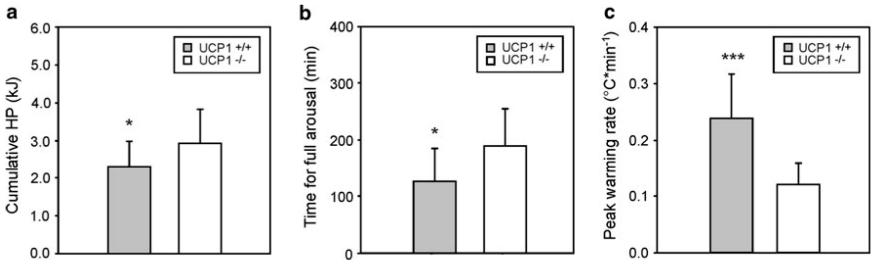

Fig. 4 Cumulative heat production (**a**), time required for arousal (**b**) and peak rewarming rates (PWR; **c**) during arousal from torpor in wildtype ($UCP1^{+/+}$) and UCP1-ablated mice ($UCP^{-/-}$). *Bars* represent mean ± SD from $n = 24$ torpor bouts (21 in **c**) obtained from $n = 6$ or 7 wildtype mice and 15 torpor bouts from $n = 5$ UCP1-ablated mice. $^{***}P < 0.001$; $^{*}P < 0.05$

metabolic effects for rewarming the body twice the amount of maintenance metabolism is required (Fig. 5a). Thereby, our results support previous predictions that rapid rewarming rates from torpor should be less expensive in terms of energetic costs than slow rewarming rates (Stone and Purvis 1992; McKechnie and Wolf 2004).

Another transgenic murine model in which BAT thermogenesis is severely impaired is the β-hydroxylase knockout ($Dbh^{-/-}$) mouse which lacks the ability to synthesize adrenalin and noradrenalin (Swoap et al. 2006). Unexpectedly, these mice failed to enter torpor when fasted, revealing the necessity for an intact sympathetic nervous system for full torpor expression. Dbh-$^{-/-}$ mice regained their ability to enter torpor when treated with L-3,4-dihydroxyphenlserine (DOPS) a synthetic precursor restoring central adrenalin synthesis, but the maximal rates of temperature gain during emergence from torpor were 75% lower (0.06°C min^{-1}) as compared to wildtype controls (0.26°C min^{-1}). It is likely that the slower rewarming rates in Dbh-$^{-/-}$ mice relative to UCP1-ablated mice may

J Comp Physiol B (2011) 181:137–145

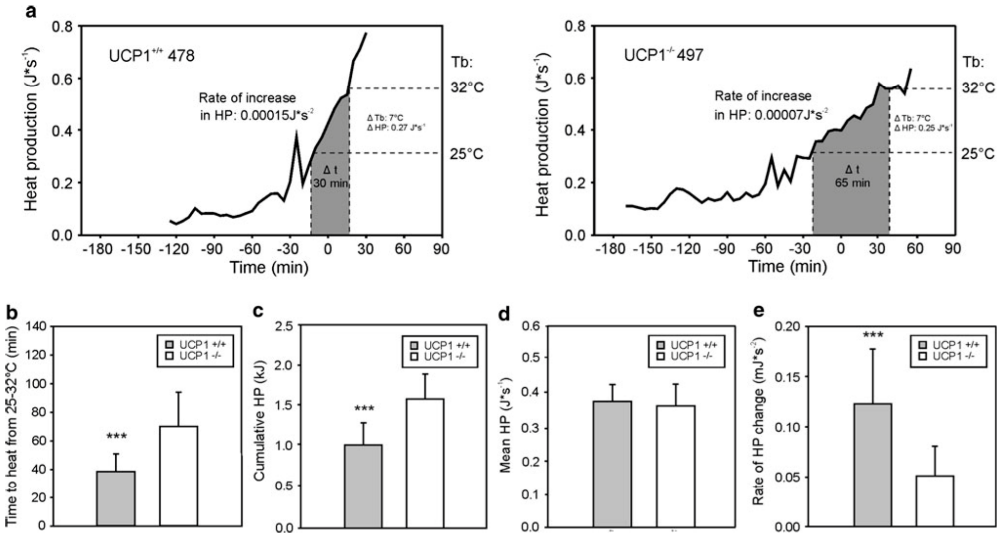

Fig. 5 **a** Body temperature and heat production rates during arousal from torpor in a wildtype (*left*) and a UCP1-ablated mouse (*right*). Minimal body temperature (T_b) in torpor was 19.6°C in the wildtype mouse and 19.8°C in the UCP1-ablated mouse. Minimal HP in torpor was 0.035 J s^{-1} (6.2 ml O_2 h^{-1}) and 0.038 J s^{-1} (6.7 ml O_2 h^{-1}), respectively. Data were aligned according to the point of peak rewarming rate. In each panel, the *shaded areas* highlight the specific amount of heat production necessary for rewarming the body from 25 to 32°C (+50% in the UCP1 ablated mouse). **b–d** *Bars* represent mean ± SD of 23 torpor bouts obtained from $n = 6$ wildtype mice and 14 torpor bouts from $n = 5$ UCP1-ablated mice. ***$P < 0.001$

result not only from their inability to activate BAT, but also because WAT derived lipolysis is compromised, and additionally the sympathetic control of heat loss is impaired.

The onset of fasting induced torpor in mice is usually observed during the second half of the night, irrespective of the duration of previous food deprivation (Hudson and Scott 1979; Webb et al. 1982; Gavrilova et al. 1999; Dikic et al. 2008; Jethwa et al. 2008; Brown and Staples 2010). When we challenged the fasted mice with cold onset during the light phase, we were, however, able to dissociate torpor entry from its normal timing. Fasted mice which experienced the transition from thermoneutral ambient temperature to cold at 6:00 CET (after 18 h FD) or at midday (12:00 CET; after 24 h FD) entered torpor within ~20 min, i.e. torpor entry could be "switched on" in the light phase. The diurnal bouts were shorter (3–6 h) and T_b was less deep, yet the minimal oxygen consumption values in torpor were on average ~16 ml h^{-1} (Fig. 3b, approximately −50% BMR; Golozoubova et al. 2006) and therefore justify the classification as torpor. In contrast, the mice did not enter torpor when the change in T_a coincided with the timing of *lights off*, indicating that the circadian onset of the nocturnal activity period could not be overridden.

The ability of cold exposed mice to actively suppress metabolic rate below BMR (operational: resting metabolic rate (RMR) at thermoneutrality) as a direct response to decreasing T_a was unexpected because endotherms normally recruit thermoregulatory heat production in order to maintain normothermia (Scholander et al. 1950). The differential responses to the interaction of cold and time of day have led us to speculate that torpor may also be functionally linked to an ultradian rhythm, which facilitates the entry into a state of suspended animation. The hypothesis that an ultradian rhythm may be permissive for torpor entry is supported by two independent findings. (1) It has been observed that following ablation of the SCN, the pacemaker of the circadian rhythm, food restricted Djungarian hamsters (*Phodopus sungorus*) lose their distinct circadian activity rhythm but they continue display torpor. The occurrence of these torpor bouts is irregular, and multiple torpor bouts per day could be observed, indicating that an ablation of the circadian pacemaker does not inhibit fasting induced torpor behaviour but abolishes its timing (Ruby and Zucker 1992). (2) In the same species, peripheral sympathetic inhibition by 6-hydroxydopamine (6-OHDA) not just suppressed torpor for 1 week, but hamsters also lost their ultradian rhythm of body

temperature for 2–6 days (Braulke and Heldmaier 2010). These results not just imply that an intact adrenergic system is a prerequisite for body temperature fluctuations, but the sequence of events also indicated that restoration of (daily) torpor was linked to the re-establishment of ultradian T_b rhythmicity. The interrelations of ultradian rhythmicity, circadian system, and metabolism remain to be elucidated. Interestingly, ultradian rhythms of body temperature fluctuations in the rat have recently been associated with rhythmic BAT thermogenesis (Ootsuka et al. 2009). The significance of this finding in the context of torpor is, however, debatable as rats do not enter torpor (Exner et al. 2000).

During hypothermia which is frequently associated with hibernation or daily torpor, the heat produced in BAT can be rapidly distributed to warm up vital organs such as the brain and the heart and thereby facilitate a coordinated return to normothermic body temperatures and agility. Nevertheless, birds, monotremes and some adult marsupials do not possess BAT, and yet they are able to rewarm from (deep) hypothermia. In species from these three groups rewarming to normothermia is largely achieved through shivering thermogenesis and may also be assisted by selection a warmer thermal environment. Our study shows that although UCP1-mediated NST constitutes a most potent mechanism of endogenous heat production in small mammals (0.3–0.4 J s^{-1} g^{-1} tissue mass in the Djungarian hamster *Phodopus sungorus*; Puchalski et al. 1987), its presence is not essential for the expression of a single torpor bout. In the absence of UCP1-mediated NST, however, the rate of heat production (efficiency of rewarming) is lower and more energy is required for arousal. The latter may account for the inability of UCP1-ablated mice to display multiple torpor bouts per day (Fig. 2b).

Acknowledgments This work was supported by DFG (grant #HE-990 to GH and CWM).

References

Barclay RM, Lausen CL, Hollis L (2001) What's hot and what's not: defining torpor in free-ranging birds and mammals. Can J Zool 79:1885–1890

Braulke LJ, Heldmaier G (2010) Torpor and ultradian rhythms require an intact signalling of the sympathetic nervous system. Cryobiology 60:198–203

Brown JC, Staples JF (2010) Mitochondrial metabolism during fasting-induced daily torpor in mice. Biochim Biophys Acta 1797:476–486

Cannon B, Nedergaard J (2004) Brown adipose tissue: function and physiological significance. Physiol Rev 84:277–359

Dikic D, Heldmaier G, Meyer CW (2008) Induced torpor in different strains of laboratory mice. In: Lovegrove BG, McKechnie AE (eds) Hypometabolism in animals: torpor. hibernation and cryobiology. Pietermaritzburg, University of KwaZulu-Natal, pp 223–230

Ehrhardt N, Heldmaier G, Exner C (2005) Adaptive mechanisms during food restriction in *Acomys russatus*: the use of torpor for desert survival. J Comp Physiol [B] 175:193–200

Enerback S, Jacobsson A, Simpson EM, Guerra C, Yamashita H, Harper ME, Kozak LP (1997) Mice lacking mitochondrial uncoupling protein are cold-sensitive but not obese. Nature 387:90–94

Exner C, Hebebrand J, Remschmidt H, Wewetzer C, Ziegler A, Herpertz S, Schweiger U, Blum WF, Preibisch G, Heldmaier G, Klingenspor M (2000) Leptin suppresses semi-starvation induced hyperactivity in rats: implications for anorexia nervosa. Mol Psychiatry 5:476–481

Foster DO, Frydman ML (1978) Brown adipose tissue: the dominant site of nonshivering thermogenesis in the rat. Experientia Suppl 32:147–151

Gavrilova O, Leon LR, Marcus-Samuels B, Mason MM, Castle AL, Refetoff S, Vinson C, Reitman ML (1999) Torpor in mice is induced by both leptin-dependent and -independent mechanisms. Proc Natl Acad Sci USA 96:14623–14628

Geiser F (2004) Metabolic rate and body temperature reduction during hibernation and daily torpor. Annu Rev Physiol 66:239–274

Geiser F, Baudinette RV (1990) The relationship between body mass and rate of rewarming from hibernation and daily torpor in mammals. J Exp Biol 151:349–359

Golozoubova V, Cannon B, Nedergaard J (2006) UCP1 is essential for adaptive adrenergic nonshivering thermogenesis. Am J Physiol Endocrinol Metab 291:E350–E357

Granneman JG, Burnazi M, Zhu Z, Schwamb LA (2003) White adipose tissue contributes to UCP1-independent thermogenesis. Am J Physiol Endocrinol Metab 285:E1230–E1236

Hayward JS, Lisson PA (1991) Evolution of brown fat: its absence in marsupials and monotremes. Can J Zool 70:171–179

Heldmaier G (1970) Die Thermogenese der Mausohrfledermaus (*Myotis myotis*) beim Erwachen aus dem Winterschlaf. Z Vergl Physiol 63:59–84

Heldmaier G (1975) Metabolic and thermoregulatory responses to heat and cold in the Djungarian hamster, *Phodopus sungorus*. J Comp Physiol 102:115–122

Heldmaier G, Buchberger A (1985) Sources of heat during nonshivering thermogenesis in Djungarian hamsters: a dominant role of brown adipose tissue during cold adaptation. J Comp Physiol [B] 156:237–245

Heldmaier G, Ruf T (1992) Body temperature and metabolic rate during natural hypothermia in endotherms. J Comp Physiol [B] 162:696–706

Heldmaier G, Steinlechner S (1981) Seasonal control of energy requirements for thermoregulation in the Djungarian hamster (*Phodopus sungorus*), living in natural photoperiod. J Comp Physiol 142:429–437

Heldmaier G, Ortmann S, Elvert R (2004) Natural hypometabolism during hibernation and daily torpor in mammals. Respir Physiol Neurobiol 141:317–329

Hudson JW, Scott IM (1979) Daily torpor in the laboratory mouse, *Mus musculus* var. albino. Physiol Zool 52:205–218

Jansky L (1973) Non-shivering thermogenesis and its thermoregulatory significance. Biol Rev 48:85–132

Jastroch M, Withers KW, Taudien S, Frappell PB, Helwig M, Fromme T, Hirschberg V, Heldmaier G, McAllan BM, Firth BT, Burmester T, Platzer M, Klingenspor M (2008) Marsupial uncoupling protein 1 sheds light on the evolution of mammalian nonshivering thermogenesis. Physiol Genomics 32:161–169

Jethwa PH, I'anson H, Warner A, Prosser HM, Hastings MH, Maywood ES, Ebling FJ (2008) Loss of prokineticin receptor 2

signaling predisposes mice to torpor. Am J Physiol Regul Integr Comp Physiol 294:R1968–R1979

Lovegrove BG, Koertner G, Geiser F (1999) The energetic cost of arousal from torpor in the marsupial *Sminthopsis macroura*: benefits of summer ambient temperature cycles. J Comp Physiol [B] 169:11–18

Lyman CP, O'Brian RC (1986) Is brown fat necessary? In: Heller HC, Musacchia XJ, Wang LHC (eds) Living in the cold: physiological and biochemical adaptations. Elsevier, New York, pp 116–119

McKechnie AE, Lovegrove BG (2001) Heterothermic responses in the speckled mousebird (*Colius striatus*). J Comp Physiol [B] 171:507–518

McKechnie AE, Wolf BO (2004) The energetics of the rewarming phase of avian torpor. In: Barnes BM, Carey HV (eds) Life in the cold, evolution, mechanism, adaptation and application. Alaska University of Alaska Fairbanks, Institute of Arctic Biology, Fairbanks, pp 265–273

Mzilikazi N, Lovegrove BG, Ribeiro MO (2002) Exogenous passive heating during torpor arousal in free-ranging rock elephant shrews, *Elephantulus myurus*. Oecologia 133:307–314

Nicol SC, Morrow G, Andersen NA (2008) Hibernation in monotremes: a review. In: Lovegrove BG, McKechnie AE (eds) Hypometabolism in animals: hibernation, torpor and cryobiology. University of KwaZulu-Natal, Pietermaritzburg, pp 251–262

Nicol SC, Andersen NA, Arruda AP, Ruf T (2009) Rewarming rates of two large hibernators: comparison of a monotreme and a eutherian. J Therm Biol 34:155–159

Oelkrug R, Kutschke M, Meyer CW, Heldmaier G, Jastroch M (2010) Uncoupling protein 1 decreases superoxide production in brown adipose tissue mitochondria. J Biol Chem (PMID: 20466728)

Ootsuka Y, de Menezes RC, Zaretsky DV, Alimoradian A, Hunt J, Stefanidis A, Oldfield BJ, Blessing WW (2009) Brown adipose tissue thermogenesis heats brain and body as part of the brain-coordinated ultradian basic rest-activity cycle. Neuroscience 164:849–861

Ortmann S, Heldmaier G, Schmid J, Ganzhorn JU (1997) Spontaneous daily torpor in Malagasy mouse lemurs. Naturwissenschaften 84:28–32

Puchalski W, Bockler H, Heldmaier G, Langefeld M (1987) Organ blood flow and brown adipose tissue oxygen consumption during noradrenaline-induced nonshivering thermogenesis in the Djungarian hamster. J Exp Zool 242:263–271

Rowlatt U, Mrosovsky N, Englisch A (1971) A comparative survey of brown fat in the neck and axilla of mammals at birth. Biol Neonate 17:53–83

Ruby NF, Zucker I (1992) Daily torpor in the absence of the suprachiasmatic nucleus in Siberian hamsters. Am J Physiol 263:R353–R362

Scholander PF, Hock R, Walters V, Irving L (1950) Adaptation to cold in arctic and tropical mammals and birds in relation to body temperature insulation, and basal metabolic rate. Biol Bull 99:259–271

Shabalina IG, Hoeks J, Kramarova TV, Schrauwen P, Cannon B, Nedergaard J (2010) Cold tolerance of UCP1-ablated mice: A skeletal muscle mitochondria switch toward lipid oxidation with marked UCP3 up-regulation not associated with increased basal, fatty acid- or ROS-induced uncoupling or enhanced GDP effects. Biochim Biophys Acta 1797(6–7):968–980

Stone GN, Purvis A (1992) Warm-up rates during arousal from torpor in heterothermic mammals: physiological correlates and a comparison with heterothermic insects. J Comp Physiol [B] 162:284–295

Swoap SJ, Weinshenker D (2008) Norepinephrine controls both torpor initiation and emergence via distinct mechanisms in the mouse. PLoS One 3:e4038

Swoap SJ, Gutilla MJ, Liles LC, Smith RO, Weinshenker D (2006) The full expression of fasting-induced torpor requires beta 3-adrenergic receptor signalling. J Neurosci 26:241–245

Ukropec J, Anunciado RP, Ravussin Y, Hulver MW, Kozak LP (2006) UCP1-independent thermogenesis in white adipose tissue of cold-acclimated Ucp1$^{-/-}$ mice. J Biol Chem 281:31894–31908

Wang Y, Kimura K, Inokuma K, Saito M, Kontani Y, Kobayashi Y, Mori N, Yamashita H (2006) Potential contribution of vasoconstriction to suppression of heat loss and homeothermic regulation in UCP1-deficient mice. Pflugers Arch 452:363–369

Warnecke L, Geiser F (2010) The energetics of basking behaviour and torpor in a small marsupial exposed to simulated natural conditions. J Comp Physiol [B] 180:437–445

Webb GP, Jagot SA, Jakobson ME (1982) Fasting-induced torpor in Mus musculus and its implications in the use of murine models for human obesity. Comp Biochem Physiol 72A:211–219

UNCOUPLING PROTEIN 1 DECREASES SUPEROXIDE PRODUCTION IN BROWN ADIPOSE TISSUE MITOCHONDRIA

R. OELKRUG ∞ M. KUTSCHKE ∞ G. HELDMAIER
C. W. MEYER ∞ M. JASTROCH

THE JOURNAL OF BIOLOGICAL CHEMISTRY VOL. 285, NO. 29, pp. 21961–21968, July 16, 2010

Uncoupling Protein 1 Decreases Superoxide Production in Brown Adipose Tissue Mitochondria*[S]

Received for publication, March 12, 2010, and in revised form, April 28, 2010 Published, JBC Papers in Press, May 13, 2010, DOI 10.1074/jbc.M110.122861

Rebecca Oelkrug, Maria Kutschke, Carola W. Meyer, Gerhard Heldmaier, and Martin Jastroch[1]

From the Department of Animal Physiology, Faculty of Biology, Philipps-Universität Marburg, 35043 Marburg, Germany

In thermogenic brown adipose tissue, uncoupling protein 1 (UCP1) catalyzes the dissipation of mitochondrial proton motive force as heat. In a cellular environment of high oxidative capacity such as brown adipose tissue (BAT), mitochondrial uncoupling could also reduce deleterious reactive oxygen species, but the specific involvement of UCP1 in this process is disputed. By comparing brown adipose tissue mitochondria of wild type mice and *UCP1*-ablated litter mates, we show that UCP1 potently reduces mitochondrial superoxide production after cold acclimation and during fatty acid oxidation. We address the sites of superoxide production and suggest diminished probability of "reverse electron transport" facilitated by uncoupled respiration as the underlying mechanism of reactive oxygen species suppression in BAT. Furthermore, ablation of *UCP1* represses the cold-stimulated increase of substrate oxidation normally seen in active BAT, resulting in lower superoxide production, presumably avoiding deleterious oxidative damage. We conclude that UCP1 allows high oxidative capacity without promoting oxidative damage by simultaneously lowering superoxide production.

The physiological role of endogenous heat production by nonshivering thermogenesis in brown adipose tissue (BAT)[2] of mammals, in particular small mammals, hibernators, and neonates, is the maintenance of a constant high body temperature (T_b) independent of daily and seasonal temperature fluctuations (1). Heat production by BAT is, however, also activated by high calorie diets (2), and because the presence of BAT has been recently shown in adult humans, it is in the focus as a potential therapeutic target for the treatment of human body weight disorders (3–5).

BAT is characterized by an exceptionally high presence of mitochondria that possess only a minor amount of ATP synthase to convert nutritional into cellular energy equivalents (6). Instead, brown adipose tissue mitochondria are specialized by a high content of mitochondrial uncoupling protein 1 (UCP1), up to 8% of total mitochondrial protein (7), which generates a proton leak in the mitochondrial inner membrane dissipating proton motive force as heat (8). UCP1 can be inhibited by physiological concentrations of purine nucleoside di- and triphosphates before free fatty acids can overcome inhibition (8).

Cold exposure stimulates lipolysis in BAT, thereby activating UCP1. Long term cold acclimation further increases the thermogenic capacity of BAT by enhanced UCP1 expression and recruitment of oxidative capacity (9). The importance of UCP1 for brown adipose tissue-derived heat production has been confirmed in *UCP1*-ablated mice, which are unable to defend their body temperature when acutely exposed to the cold (4 °C) (10). Successive acclimation improves the cold tolerance of *UCP1*-ablated mice, suggesting that other sources of heat production partially compensate for the loss of functional BAT, namely muscle shivering (11, 12) and accelerated metabolic flux in white adipose tissue (13, 14). These alternative thermogenic mechanisms appear to be less efficient and are disadvantageous because the median survival rate of *UCP1*-ablated mice decreases in the cold from >24 to ~13 weeks as compared with wild type mice, raising the question about the advantages of UCP1-mediated thermogenesis.

The cold recruitment of oxidative capacity increases the chance of oxidative damage. According to the free radical theory of aging, an increase of radical production could potentially decrease life span (15, 16). Superoxide and reactive oxygen species are potently caused by mitochondria; escaping electrons from respiratory chain complexes are the major source of cellular superoxide and its derived reactive oxygen species (17, 18). Complex I (NADH:ubiquinone oxidoreductase) (19) and complex III (ubiquinol:cytochrome *c* oxidoreductase) (20) are postulated as the major producers of cellular superoxide, but also the mitochondrial glycerophosphate dehydrogenase, which is highly abundant in BAT (21, 22), appears to produce superoxide (23–25).

Functional studies on UCPs (UCP1, 2, and 3) showed activation of uncoupling activity by superoxide and peroxidation metabolites like 4-hydroxy-2-nonenal (26, 27), associating UCPs with a potential role in the prevention of superoxide production. These observations were highly disputed (28–30), and specifically the involvement of UCP1 in cellular reactive oxygen species regulation is questioned (29, 30). Studies comparing BAT from wild type and *UCP1*-ablated mice found no activation of UCP1 with 4-hydroxy-2-nonenal, unaltered uncoupling function with manipulated matrix superoxide levels, identical rates of superoxide release, and no difference in markers of oxidative damage (29, 30). Together with unchanged superoxide scavenging systems (29), these results led to the conclusion that conditions of high oxygen tension and high substrate sup-

* This work was supported by Deutsche Forschungsgemeinschaft Grants HE 990/15-1 (to G. H. and C. W. M.) and JA 1884/2-1.

[S] The on-line version of this article (available at http://www.jbc.org) contains supplemental Figs. S1–S3.

[1] To whom correspondence should be addressed: Buck Institute for Age Research, 8001 Redwood Blvd., Novato, CA 94945. Fax: 415-209-2232; E-mail: mjastroch@buckinstitute.org.

[2] The abbreviations used are: BAT, brown adipose tissue; CA, cold-acclimated; FCCP, carbonyl cyanide *p*-trifluoromethoxyphenylhydrazone; UCP, uncoupling protein; WA, warm-acclimated; TES, 2-{[2-hydroxy-1,1-bis(hydroxymethyl)ethyl]amino}ethanesulfonic acid; G3P, glycerol-3-phosphate.

ply in brown adipose tissue do not necessarily lead to increased oxidative stress.

Using mitochondria sampled from wild type and *UCP1*-ablated mice, we here show that the presence of UCP1 potently lowers mitochondrial superoxide production during cold acclimation and fatty acid oxidation. Our results therefore demonstrate that uncoupling is a physiologically relevant mechanism to reduce oxidative stress in a mammalian organ of high oxidative capacity.

EXPERIMENTAL PROCEDURES

Animals—Wild type and *UCP1*-ablated mice were provided by Dr. Leslie Kozak (Pennington Medical Research Center), and littermates (genetic background C57Bl/6J) were derived from heterozygous breeding pairs in the animal facility of the Philipps-Universität of Marburg. In these mice *UCP1* was inactivated by homologous recombination with a deletion vector in which exon 2 and parts of exon 3 had been replaced with a neomycin resistance gene. In brown adipose tissue of these mice, no UCP1 could be detected with polyclonal antibodies (10). For experimental procedures, only homozygotes for *UCP1* (wild type; $UCP1^{+/+}$) and *UCP1*-ablated ($UCP1^{-/-}$) mice were used. The mice were fed *ad libitum* (Sniff 1534) with free access to water and kept on a 12 h of light/12 h of dark cycle. For experiments, the animals were kept in single cages. Warm-acclimated mice (WA) were maintained at 30 °C at least 3 weeks prior to sacrifice, whereas wild type and *UCP1*-ablated adult mice were cold-acclimated (CA) by first transferring them to 18 °C for 3 weeks followed by 3 weeks at 5 °C (11). The final body mass of the mice did not differ between the experimental groups (WA, $UCP1^{+/+}$, 23.5 ± 1.0 g, and $UCP1^{-/-}$, 24.5 ± 1.0 g; CA, $UCP1^{+/+}$, 24.7 ± 0.3 g, and $UCP1^{-/-}$, 24.4 ± 0.4 g). All of the experimental procedures were approved by the German Animal Welfare Authorities.

Genotyping—The mice were genotyped by amplifying 201-bp ($UCP1^{+/+}$) and 409-bp ($UCP1^{-/-}$) fragments from the *UCP1* gene using the primers 8265-5F (GGT AGT ATG CAA GAG AGG TGT), E2Rev (CCT AAT GGT ACT GGA AGC CTG), and NeoRev (CCT ACC CGC TTG CAT TGC TCA) according to a protocol kindly provided by L. Kozak. Additionally the presence or absence of UCP1 protein was validated post mortem by immunological detection in brown adipose tissue mitochondria (as published previously in Ref. 31). The membranes were probed with a rabbit anti-UCP1 polyclonal antibody (1:30,000 dilution; 3046; Chemicon), followed by the relevant peroxidase-conjugated secondary antibody (goat anti-rabbit-IgG at 1:10,000 dilution; Dako). The antigens were visualized on x-ray film (Super RX; Fuji) using an ECL Plus Western blotting detection system (SRX-101A; Konika Minolta).

Mitochondria Isolation—Mitochondria were prepared by homogenization and differential centrifugation as described previously (32). Mitochondria from one wild type and one *UCP1*-ablated mouse were always isolated in parallel to control for possible day-by-day variability of mitochondrial quality. All available brown adipose tissue depots were removed (interscapular, dorsal cervical, axillar, suprasternal, and subcostal) and immediately placed in ice-cold isolation medium. Protein concentration was determined photometrically using the Bradford method (33).

Measurement of Oxygen Consumption—Mitochondrial oxygen consumption was measured using a Clark-type oxygen electrode (Rank Brothers Ltd.) maintained at 37 °C and calibrated with air-saturated medium (50 mM KCl, 5 mM TES, 2 mM $MgCl_2 \times 6H_2O$, 4 mM KH_2PO_4, 1 mM EGTA, 0.4% bovine serum albumin (w/v), pH 7.2 at room temperature) that was assumed to contain 406 nmol of O ml^{-1} (34). Mitochondrial respiration was measured in 500 μl of medium at a concentration of 0.1 mg ml^{-1} incubated with 4.8 μM rotenone (inhibiting complex I of the respiratory chain) and 2 μM oligomycin (inhibiting the ATP synthase). Mitochondria were energized by the addition of glycerol-3-phosphate (G3P, titrating up to 16 mM) or 4 mM succinate (state 4 respiration). Subsequently GDP was titrated to a final concentration of 5 mM. The ability of GDP to establish respiratory control in wild type mice also confirmed the integrity of the mitochondria after the isolation process. At the end of each respiration measurement, the artificial uncoupler FCCP was titrated in ~1 μM steps to estimate the maximal substrate oxidation rate. State 4 respiration in some cases was directly translated into the proton leak rate, assuming that 6 protons were transported (and leaked back to the matrix) per atomic oxygen when respiring on succinate or glycerol-3-phosphate.

Measurements of Mitochondrial Hydrogen Peroxide Release—Measurements of hydrogen peroxide production of isolated mitochondria were performed similarly to the procedures of Lambert *et al.* (35). 10–20 μg of brown adipose tissue mitochondria were incubated in assay buffer (50 mM KCl, 5 mM TES, 2 mM $MgCl_2 \times 6H_2O$, 4 mM KH_2PO_4, 1 mM EGTA, bovine serum albumin 0.4% (w/v), pH 7.2 at room temperature) containing a mixture of the fluorescent probe Amplex Red (50 μM; Invitrogen), 30 units ml^{-1} superoxide dismutase (to convert superoxide to hydrogen peroxide), 6 units ml^{-1} horseradish peroxidase (catalyzing the reaction of hydrogen peroxide with Amplex Red resulting in fluorescent resorufin), and 2 μM oligomycin (to inhibit ATP synthase). Amplex Red reacts with H_2O_2 at a 1:1 stoichiometry, whereas the stoichiometry of conversion from superoxide to H_2O_2 is assumed to be 1:2.

H_2O_2 formation was initiated by the addition of glycerol-3-phosphate (15 mM), succinate (5 mM), or a mixture of pyruvate (5 mM) and malate (3 mM). Experiments aimed to measure the H_2O_2 formation after palmitate addition were performed according to the protocol/substrates of the mitochondrial respiration measurements (see below). Fluorescence was detected at 37 °C in a microplate reader (BMG Labtech, FLUOstar Optima) in 96-well microplates (Greiner 96-Well μClear, F-Bottom, black). The excitation wavelength was set to 560–10 nm, and the fluorescence emission was detected at 590 nm. Fluorescence was calibrated using known amounts of H_2O_2 at each experimental day. Optionally, superoxide production was measured in the presence of rotenone (2 μM, inhibiting complex I-derived reactive oxygen species production), GDP (5 mM, to inhibit UCP1), and carboxyatractylate (2.5 nM) to distinguish from adenine nucleotide transporter-dependent effects.

Supplemental Material can be found at:
http://www.jbc.org/content/suppl/2010/05/13/M110.122861.DC1.html

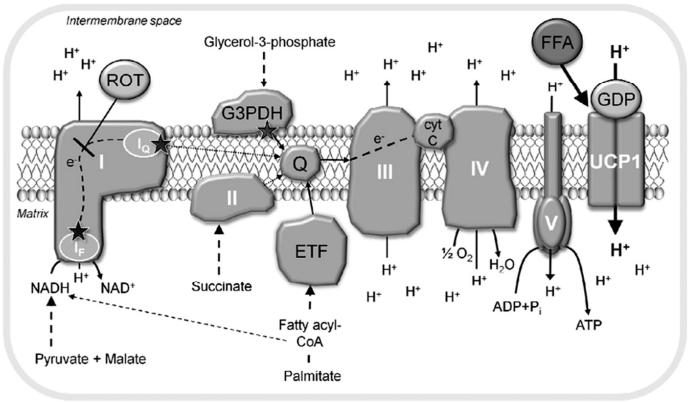

FIGURE 1. **Sites of substrate entry and superoxide production in the respiratory chain of BAT mitochondria.** NADH-linked substrates donate their electrons to complex I. Further substrate entry sites, which are investigated in this study, are the mitochondrial glycerol-3-phosphate dehydrogenase (*G3PDH*), the succinate dehydrogenase (*complex II*), and the electron transfer flavoprotein (*ETF*), which is fueled by β-oxidation respectively. β-Oxidation also generates NADH, which enters *complex I* in parallel. The electrons from the entry complexes are transferred to ubiquinone (*Q*), forming QH_2. In the normal electron forward transfer, the electrons are donated to *complex III* and then *complex IV* before finally reducing oxygen to water. Electrons may leak from the I_F site and the I_Q site of complex I. These sites can be distinguished by using the complex I inhibitor rotenone (*ROT*). A substantial amount of superoxide production can also derive from the glycerol-3-phosphate dehydrogenase and the electron transfer flavoprotein. The sites of superoxide production are indicated with *stars* in the figure. Proton motive force, generated by *complexes I*, *III*, and *IV*, is dissipated by either the ATP synthase (*complex V*) or UCP1. UCP1 is activated by free fatty acids (*FFA*) and inhibited by purine nucleoside di- and triphosphates (here, *GDP*).

Measurement of Oxygen Consumption and Hydrogen Peroxide Release during β-Oxidation of Palmitoyl-CoA—To measure the palmitate-dependent mitochondrial respiration and hydrogen peroxide release, we incubated the mitochondria with 5 μM coenzyme A and 2 mM L-carnitine in a measuring buffer without bovine serum albumin. The mitochondria were energized with 3 mM malate. After 7 min we added 1 mM ATP (to allow the activation of residual free fatty acids). After a further 15 min, 20 μM palmitate (equilibrated in a final concentration of 0.02% bovine serum albumin) was added that activated β-oxidation and UCP1 in parallel (36).

Statistics—In figures and text, the data are expressed as the means ± S.E. In some cases, normal distribution of data could not be assumed. Therefore, to reveal significant differences in respiration rates or reactive oxygen species production rates between genotypes, Student's *t* test or Mann Whitney *U* test was used, as indicated. To assess the effect of different substrates or inhibitors within genotypes, a paired *t* test or Wilcoxon test was used. All of the calculations were performed using SigmaStat 3.5. The overall level of significance was set to $p < 0.05$. To account for type one errors in multiple comparisons, the effective *p* values were adjusted according to Bonferroni.

RESULTS

In the following experiments, we investigated the impact of different substrates on mitochondrial respiration and superoxide production in isolated BAT mitochondria from warm-acclimated (30 °C) and cold-acclimated (5 °C) wild type and *UCP1*-ablated mice. Fig. 1 gives an overview on the respiratory chain complexes in the mitochondrial inner membrane, potential sites of substrate entry and electron leak, the latter resulting in superoxide production.

UCP1 Reduces Superoxide Production in BAT Mitochondria of Warm-acclimated Mice—Initially, we investigated mitochondria respiring on G3P because BAT has substantial amounts of glycerol-3-phosphate dehydrogenase (Fig. 2*a*). Because the affinity of the G3P dehydrogenase to its substrate is comparably low, we titrated G3P to saturating amounts (supplemental Fig. S1). State 4 respiration in wild type and *UCP1*-ablated mice up to 7 mM G3P was similar. More than 7 mM G3P resulted in a further increase of respiration rates of wild type but not of *UCP1*-ablated mice, before saturating at concentrations above 13 mM (Fig. 2*a*). Then GDP was added to inhibit UCP1 and to induce respiratory control. The concentration of 5 mM GDP, which fully inhibited UCP1, was determined in the mitochondria of CA wild type animals (supplemental Fig. S1). By addition of GDP and recoupling of wild type mitochondria, we also assured mitochondrial integrity (because brown adipose tissue mitochondria possess very little ATP synthase, state 3 respiration is not applicable to show respiratory control, and oligomycin had minor or no effect on respiration). The addition of 5 mM GDP strongly recoupled wild type mitochondria but had only minor effects in UCP1-ablated mitochondria (Fig. 2*a*). At the end of each measurement, FCCP was added to induce maximal uncoupled respiration. FCCP-induced respiration was similar between wild type and UCP1-ablated mitochondria.

We then measured the hydrogen peroxide release rate from isolated brown adipose tissue mitochondria, which is established to report mitochondrial superoxide production rates (37, 38). Mitochondrial superoxide production rates were directly calculated from hydrogen peroxide concentrations. Superoxide production rates at state 4 (leak) respiration were lower in wild type mitochondria than in UCP1-ablated mitochondria (Fig. 2*b*). This reduction was attributable to UCP1 because the addition of the UCP1 inhibitor GDP abolished genotypic differences. The administration of rotenone allowed determination of the amount of superoxide production by the I_Q site of complex I (Fig. 1). G3P-dependent superoxide production was only slightly sensitive to rotenone (Fig. 2*b*), indicating that the major proportion of superoxide was produced independently of complex I. Superoxide production rates and the associated effect of GDP were highly dependent on substrate concentration and only slightly sensitive to rotenone (supplemental Fig. S1), supporting the idea that the G3P dehydrogenase itself generates

Supplemental Material can be found at:
http://www.jbc.org/content/suppl/2010/05/13/M110.122861.DC1.html

UCP1 Decreases Superoxide Production in BAT Mitochondria

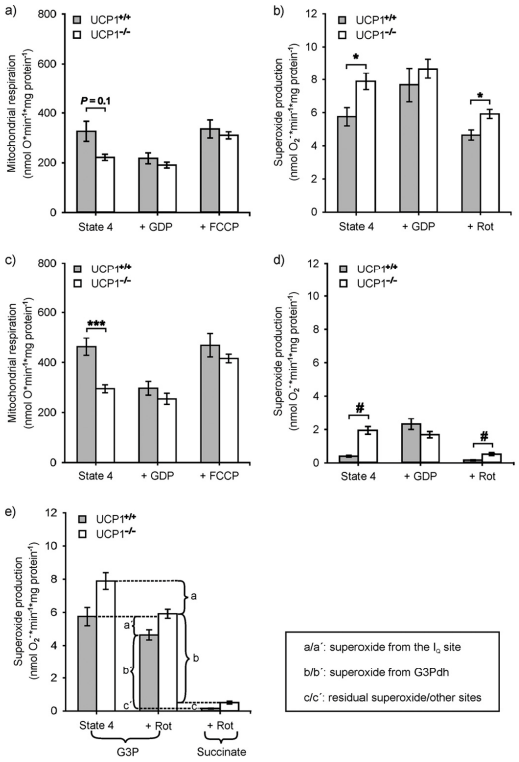

FIGURE 2. **Respiration and superoxide production rates of brown adipose tissue mitochondria from warm-acclimated wild type (*UCP1*$^{+/+}$) and *UCP1*-ablated (*UCP1*$^{-/-}$) mice energized with glycerol-3-phosphate (*a* and *b*) or with succinate (*c* and *d*).** The effect of UCP1 on superoxide derived from different sites is illustrated in *e*. Mitochondrial respiration of 0.1 mg ml^{-1} mitochondrial protein was measured in a temperature-controlled chamber with a Clark-type electrode at 37 °C. 2 μM oligomycin, 4.8 μM rotenone, and 16 mM G3P (*a*) or 4 mM succinate (*c*) were added to establish state 4 respiration, 5 mM GDP was added to inhibit UCP1 and recouple mitochondria and at the end of each run, FCCP was added to artificially uncouple mitochondria and estimate maximum substrate oxidation. Comparing succinate with G3P respiration, succinate respiration was higher in every treatment. State 4 respiration with G3P tended to be higher in wild type as compared with UCP1-ablated mitochondria ($p = 0.1$, Student's *t* test, $n = 8$/group) but was significantly different during succinate respiration. (***, $p < 0.001$, Student's *t* test, $n = 7$/group). Superoxide production was calculated from hydrogen peroxide release assayed with Amplex Red in the presence of superoxide dismutase (30 units ml^{-1}). Superoxide production was measured in mitochondria incubated with oligomycin (2 μM, state 4), 5 mM GDP was added to inhibit UCP1, and 4.8 μM rotenone was added to inhibit complex I. Genotype differences in superoxide production were found in state 4 and in the presence of rotenone (inhibiting complex I) (*, $p < 0.05$, Student's *t* test, $n = 7$/group). Superoxide production after the addition of succinate (*d*) was generally lower, but rotenone addition resulted in a greater decrease, demonstrating that the major proportion of superoxide was produced at complex I (#, $p < 0.05$, Mann Whitney *U* test, *UCP1*$^{+/+}$, $n = 11$, and *UCP1*$^{-/-}$, $n = 15$ (12 with GDP)). In *e*, rotenone inhibits superoxide production from the I_Q site of complex I. The superoxide leaving from the I_Q site (*brackets a'* and *a*) when respiring on glycerol-3-phosphate is ~40–50% lower in brown adipose tissue mitochondria of wild type mice as compared with *UCP1*-ablated mice. Respiring on succinate with rotenone, the residual superoxide production rate (*brackets c'* and *c*) derives from other sites such as the Q radical and complex III. This residual superoxide production rate is ~50% lower in wild type mice. Subtracting *c* and *c'* from the rotenone-insensitive rate with glycerol-3-phosphate determines superoxide generated by the glycerol-3-phosphate dehydrogenase (*brackets b* and *b'*). This rate was ~20% lower in *UCP1*-wild type mice. All of the experiments were performed from brown adipose tissue mitochondria of individual animals kept at 30 °C.

superoxide. In particular, when aiming to compare superoxide levels from warm- and cold-acclimated animals, membrane potential and UCP1-sensitive effects on superoxide production may be overwritten by differences in G3P dehydrogenase content and its self-generated superoxide (25). Therefore, we chose to further investigate mitochondria respiring on succinate (Fig. 2*c*), because the succinate dehydrogenase possesses high substrate affinity and is a weak producer of superoxide.

When respiring on succinate, leak respiration was ~1.5-fold higher in wild type than in UCP1-ablated BAT mitochondria (Fig. 2*c*). In wild type mitochondria, leak respiration could be reduced to UCP1-ablated levels by administration of GDP. FCCP respiration was indistinguishable between wild type and UCP1-lacking mitochondria. Superoxide production rates of wild type mitochondria respiring on succinate were barely detectable but GDP-sensitive, whereas in UCP1-ablated mitochondria, the production rate was ~5-fold higher and GDP-insensitive (Fig. 2*d*).

In the presence of GDP, superoxide production increased in wild type to levels as high as in *UCP1*-ablated mice that showed no GDP effect on superoxide production. Although superoxide production with G3P could only be slightly inhibited in the presence of rotenone, the potent inhibition in the presence of succinate demonstrated that the major proportion was produced by complex I (Fig. 2*d*).

The Sites of UCP1-dependent Superoxide Generation—The experimental setup measuring superoxide production with G3P and succinate, as well as the administration of rotenone, allowed for the determination of superoxide producing sites in BAT mitochondria. The rotenone-sensitive proportion of superoxide can be attributed to the I_Q site of complex I. Superoxide generated by the G3P dehydrogenase can be calculated by subtracting the rotenone-insensitive superoxide production rate of succinate (residual superoxide) from the rate with G3P energization. Analyzing this (Fig. 2*e*), UCP1 decreases superoxide production at the I_Q site by ~40–50%, decreases superoxide production at the G3P dehydrogenase just ~20%, and decreases superoxide production at residual sites such as the Q pool and complex III by 50–70%.

Mitochondrial Respiration and Superoxide Production during Cold Acclimation—Although brown adipose tissue should be inactive in the thermoneutral zone (30 °C) of the mouse, cold temperatures should lead to proliferation and activation of brown adipose tissue to produce heat. To examine this physiological condition, we acclimated the two genotypes (*UCP1*$^{+/+}$/*UCP1*$^{-/-}$) to 5 °C as described under "Experimental Procedures." We then investigated thermoregulatory effects on respiration and superoxide production of isolated brown adipose tissue mitochondria.

Cold acclimation caused an increase in UCP1 protein levels (Fig. 3*a*) and in leak respiration in wild type mitochondria (compare Fig. 2*c* with Fig. 3*b*) but had no increasing effect in *UCP1*-ablated mice. The genotype difference in succinate respiration observed in WA animals was further increased in

Supplemental Material can be found at:
http://www.jbc.org/content/suppl/2010/05/13/M110.122861.DC1.html

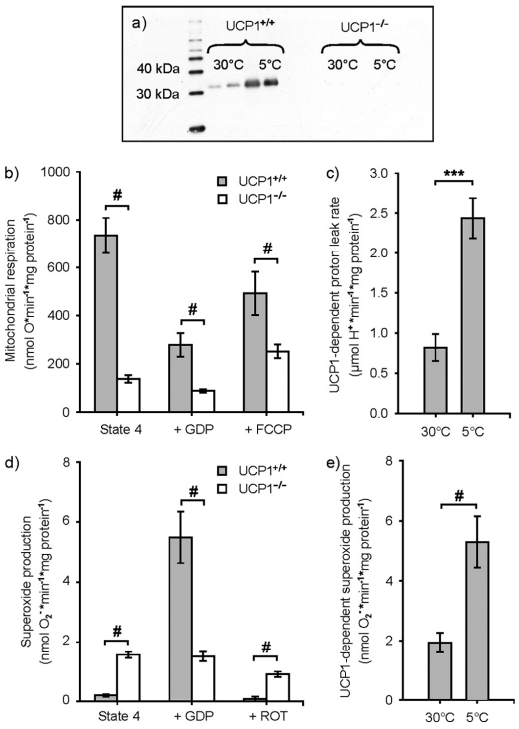

FIGURE 3. **Cold-induced adaptive changes in mitochondrial physiology.** Succinate respiration rates/UCP1-dependent proton leak rate and superoxide production rates/UCP1-dependent superoxide production of brown adipose tissue mitochondria from cold-acclimated wild type (*UCP1*$^{+/+}$) and *UCP1*-ablated (*UCP1*$^{-/-}$) mice are shown. The ablation and cold-induced protein levels of UCP1 were confirmed by immunological detection of UCP1 in brown adipose tissue with an anti-hamster UCP1 antibody (*a*). Experiments on mitochondrial respiration were performed on 0.1 mg of mitochondrial protein/ml from wild type ($n = 7$) and *UCP1*-ablated mice mitochondria ($n = 5$) incubated in an air-saturated medium at 37 °C (*b*). Respiration was started in state 4 with 2 μM oligomycin, 4.8 μM rotenone (*ROT*), and 4 mM succinate. The addition of GDP (5 mM) acted as an inhibitor of UCP1, and a final addition of 2–4 μM FCCP was made to compare maximum substrate oxidation rates. State 4 respiration of CA wild type mitochondria was higher than of UCP1-lacking mitochondria, and the difference persisted after GDP addition (*b*) (#, $p < 0.05$, Mann Whitney *U* test). The UCP1-dependent proton leak rate (*c*) was calculated based on the assumption that 6 protons are transported per molecule of oxygen and increased by 1.6 μmol min^{-1} mg^{-1} in response to cold acclimation. The data for WA mice were taken from Fig. 1 (***, $p < 0.001$, Student's *t* test). Superoxide production was assessed by measurement of the hydrogen peroxide release rate, determined fluorometrically over the reduction of Amplex Red to resorufin in the presence of superoxide dismutase (30 units ml^{-1}) and horseradish peroxidase (6 units ml^{-1}). In state 4 conditions (with 2 μM oligomycin), superoxide production was higher in *UCP1*-ablated mitochondria ($n = 5$). Administration of GDP increased wild type ($n = 7$) mitochondrial superoxide production, exceeding the levels found for UCP1-ablated mitochondria as well as WA wild type mitochondria (see Fig. 1*d*) (Fig. 1; #, $p < 0.05$, Mann Whitney *U* test) (*d*). The UCP1-dependent superoxide production rate was calculated as superoxide production after GDP inhibition minus the respective state 4 superoxide production, resulting in a 2.7-fold increase of UCP1-dependent superoxide production of wild type mitochondria in response to cold (#, $p < 0.05$, Mann Whitney *U* test) (*e*).

response to cold acclimation (Fig. 3*b*). Surprisingly, state 4 respiration in the CA *UCP1*-ablated mice (Fig. 3*b*) was decreased in contrast to WA *UCP1*-ablated mice (Fig. 2*c*), whereas in wild type mitochondria, cold acclimation led to an increase of state 4 respiration (Fig. 3*b*). The addition of 5 mM GDP inhibited UCP1 and decreased state 4 respiration of cold-acclimated wild type mice mitochondria (Fig. 3*b*). Similar to WA animals, GDP had only minor effects on UCP1-lacking mitochondria (Fig. 3*b*). The maximal substrate oxidation rate of CA *UCP1*-ablated mice determined with FCCP was not increased, suggesting that their mitochondria were unable to recruit oxidative capacity in the cold. The state 4 superoxide production rate of BAT mitochondria from CA animals was ~7.5-fold lower in wild type than in UCP1-ablated mitochondria (Fig. 3*d*). The addition of GDP increased superoxide production of wild type mitochondria by 30-fold, exceeding values found for *UCP1*-ablated mice.

UCP1-sensitive Changes in Proton Leak Rate—Mitochondrial oxygen consumption in state 4 can be directly translated to proton leak rate, assuming that with complex II substrates, 6 protons are transported out of the matrix (and leak back) per reduced oxygen atom. Calculated from Fig. 2*c*, GDP led to a decrease of proton leak rate by 1.00 μmol of protons min^{-1} mg^{-1} protein in WA wild type but only by 0.18 μmol of protons min^{-1} mg^{-1} mitochondrial protein in *UCP1*-ablated mice (UCP1-independent effects). The UCP1-dependent proportion of proton leak rate of mitochondria respiring on succinate in state 4 can therefore be given as 0.82 μmol of protons min^{-1} mg^{-1} (Fig. 3*c*). To investigate the physiological relevance of UCP1-mediated proton leak during cold acclimation, we also determined the UCP1-dependent proportion of proton leak from CA wild type brown adipose tissue mitochondria (Fig. 3*b*), which was ~2.74 and ~0.30 μmol of protons min^{-1} mg^{-1} for UCP1-lacking mitochondria. Consequentially 2.44 μmol of protons min^{-1} mg^{-1} of the proton leak was GDP-dependent. Taken together, the UCP1-dependent proton turnover rate in response to cold was increased by ~1.6 μmol of protons min^{-1} mg^{-1} or 300% (Fig. 3*c*).

UCP1-dependent Changes in Superoxide Production—What is the contribution of UCP1 in reducing mitochondrial superoxide? Inhibiting UCP1 with GDP should give a differential value of superoxide production rate that reflects the production rate depending on UCP1. This value can be further corrected with the effect of GDP in the *UCP1*-ablated mice. The calculation of the UCP1-dependent superoxide production (Fig. 3*d*) showed that under warm conditions UCP1 blunts 83% of potential mitochondrial superoxide production. During cold stress, when the respiration rate and the flow of electrons through the respiratory chain are elevated, the protective function of UCP1 increased and mitigated more than 96% of potential superoxide production (calculated as the difference of values ± GDP).

Other Potential Sources of Uncoupling Affecting Mitochondrial Superoxide Production—The adenine nucleotide translocase contributes significantly to basal proton leak (39) and can also regulate uncoupling (40–42), albeit less than UCP(s). In BAT mitochondria of our experiments, the adenine nucleotide translocase, inhibited with carboxyatractylate, did not affect superoxide production rates (supplemental Fig. S2), although it

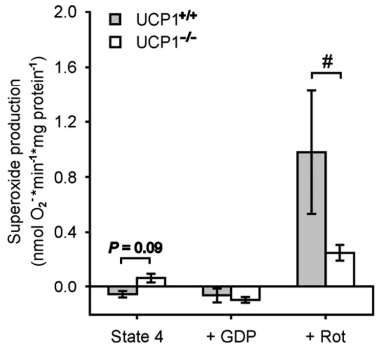

FIGURE 4. **Superoxide production of brown adipose tissue mitochondria from cold-acclimated wild type (*UCP1*$^{+/+}$) and *UCP1*-ablated (*UCP1*$^{-/-}$) mice mitochondria by complex I (pyruvate/malate).** A mixture of pyruvate (5 mM) and malate (3 mM) was used to provide complex I with NADH. By supplemental addition of rotenone (*Rot*), we showed that UCP1 provides superoxide production by reverse electron transfer. Independent experiments were performed with wild type mitochondria ($n = 4$) and *UCP1*-ablated mice mitochondria ($n - 8$) (#, $p < 0.05$ Mann Whitney *U* test).

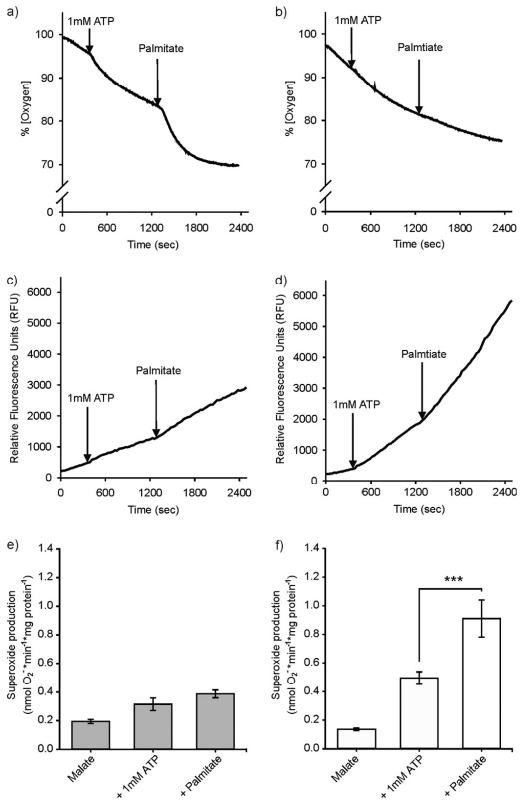

FIGURE 5. **Effects of UCP1 ablation on superoxide production during fatty acid oxidation in brown adipose tissue mitochondria of cold-acclimated animals.** *a* and *b*, palmitatoyl-CoA oxygen consumption response curve of a wild type mouse (*a*) and of a *UCP1*-ablated mouse (*b*). The *arrows* indicate the time points when substrates were added. *c* and *d*, superoxide production of the same wild type mouse as shown above measured as fluorescence (*c*) and of the same *UCP1*-ablated mouse (*d*). At $t = 0$ the mitochondria were respiring on malate (3 mM) in all of the performed measurements. *e* and *f*, the mean values ± S.E. of wild type mice ($n = 4$) and UCP1-ablated mice ($n = 8$) for every treatment (***, $p < 0.001$, one-way RM analysis of variance (Bonferroni-adjusted)).

has been shown previously that isoforms may contribute to uncoupling in BAT mitochondria (29).

Superoxide Production with the Complex I Substrates Pyruvate/Malate—Using pyruvate and malate as substrate of BAT mitochondria from both CA genotypes, we found barely detectable superoxide production rates (Fig. 4) that were not increased by GDP. Substantial superoxide production could only be provoked by adding rotenone (produced at the I_F site, see Fig. 1) and was higher in the mitochondria of CA wild type compared with *UCP1*-ablated mice (Fig. 4).

UCP1 Mitigates Mitochondrial Superoxide during Fatty Acid Oxidation—During adaptive nonshivering thermogenesis, triglycerides are broken down by lipolytic activity, and fatty acids are delivered to brown adipose tissue mitochondria. Free fatty acids activate UCP1, but in the presence of CoA and ATP, they are subsequently converted to acyl-CoA clearing this physiological UCP1 activator. To highlight the relevance of UCP1 in preventing superoxide production in a physiological scenario by mimicking cold-stimulated lipolysis, we incubated brown adipose tissue mitochondria from cold-acclimated mice with compounds of the carnitine cycle (L-carnitine, CoA), let them respire on malate to provide C4-bodies for β-oxidation, and then added ATP to activate and oxidize residual free fatty acids as described previously (Ref. 43 and Fig. 5). The addition of ATP increased mitochondrial respiration in all mice (Fig. 5, *a* and *b*), clearly demonstrating that fatty acids were oxidized despite the absence or partial purine nucleotide-related inhibition of UCP1. After subsequent addition of a 20 μM pulse of equilibrated palmitate (containing 512 nM free fatty acids according to Ref. 44), the initial respiratory burst appeared to be larger in wild type mice. This increase of respiration is likely caused by a combination of palmitoyl-CoA oxidation and uncoupled respiration and was, however, depressed in UCP1-ablated mitochondria.

Although superoxide production rates of mitochondria from both genotypes energized with malate were similar, the activation of endogenous free fatty acids induced by adding 1 mM ATP resulted in a more pronounced increase of superoxide production of UCP1-ablated mitochondria as compared with wild type mitochondria (Fig. 5, *c–f*). Although the following palmitate pulse induced a stronger respiration rate of CA wild type mitochondria, the superoxide production rate remained on a constant level, whereas it further increased in UCP1-ablated mitochondria.

DISCUSSION

Cold stress causes the activation of brown adipose tissue mitochondria, which quantitatively increases the influx of electrons, the reduction state of the respiratory chain, and the amount of respiratory complexes. This is seen in our experiments by an increase of UCP1-dependent proton leak rate (Fig.

3*c*). The probability of electrons to leak from the respiratory chain to form superoxide should increase, but our results show that this increase is blunted by UCP1. Major sites of superoxide production that are affected by the presence of UCP1 are the I_Q site (~40–50% lower) and other sites in the respiratory chain like the Q pool or complex III (~50–70% lower).

In contrast, a previous study (29) concluded no effect of UCP1 on superoxide production but measured rates in the presence of rotenone (inhibiting complex I) and antimycin A (inhibiting complex III). Under these conditions, however, there is reduced electron flow, and membrane potential is negligible (Fig. 1). Therefore, no effect of UCP1 under those conditions is expected.

We show that the glycerol-3-phosphate dehydrogenase, which is highly abundant in brown adipose tissue, produces a major proportion of superoxide that can only be mildly reduced (~20%) by uncoupling. Previous reports confirm that the glycerol-3-phosphate dehydrogenase *per se* generates high levels of superoxide under *in vitro* conditions (24).

The oxidative capacity of BAT mitochondria from warm-acclimated animals, as measured by maximal uncoupling with FCCP, shows no genotype differences. However, during cold acclimation, it appears that only BAT of wild type mice can derive the typical cold-induced oxidative capacity requiring the presence of UCP1.

In fact, superoxide production in *UCP1*-ablated mice is lower than expected from wild type mitochondria with inhibited UCP1. The unexpectedly low superoxide production rates in cold-acclimated UCP1-ablated mitochondria can be explained by compensatory lower respiratory chain activity. There is evidence for lower complex I content in UCP1-ablated mitochondria (seen in Fig. 4), because the electron leak provoked by rotenone at the complex I flavin site is lower in UCP1-ablated than in wild type mitochondria. Other downstream components of the respiratory chain are also affected, because maximal succinate respiration in the presence of FCCP is also reduced in CA UCP1-ablated mitochondria (Fig. 2*b*). The failure to increase oxidative capacity in *UCP1*-ablated mice may protect the brown adipocytes from toxic superoxide levels. Indeed, we show that the protective function of UCP1 on potential superoxide production increases in the cold, and despite higher substrate turnover rates, superoxide production in wild type mitochondria is further reduced in the cold.

The direction of electron flow causing electron leak and superoxide formation is still controversially discussed. Superoxide production with NADH-linked substrates is generally associated with forward electron transfer. Measuring autofluorescence of NAD(P)H, the mitochondrial $NAD(P)^+$ pool was ~70% reduced by supplying a mixture of pyruvate/malate (100% in the presence of rotenone; see supplemental Fig. S3). Under these conditions, we found almost no generation of superoxide. Considering that superoxide production with the complex II-linked succinate was sensitive to GDP and diminished by rotenone, it may be suggested by current state-of-art definitions that superoxide in BAT mitochondria is likely caused by "reverse electron transport," which can be potently diminished by UCP1 (Figs. 2*d* and 3*d*).

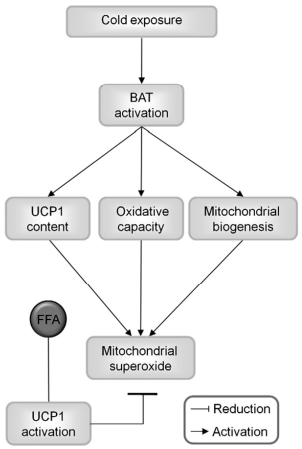

FIGURE 6. **Physiological significance of mitochondrial uncoupling on mitochondrial superoxide production in brown adipose tissue mitochondria.** Cold exposure activates brown adipose tissue for heat production, which is generally referred to as adaptive nonshivering thermogenesis. The heat output of the brown adipocytes is increased by stimulation of oxidative capacity and mitochondrial biogenesis. These factors would usually potently increase the probability of mitochondrial superoxide production. In BAT mitochondria, however, cold acclimation also stimulates UCP1 gene transcription and protein levels, and cold-induced free fatty acid (*FFA*) release activates UCP1, which dissipates proton motive force as heat. Based on our study, we put forward a model that proposes an additional physiological role of UCP1 by preventing cellular damage through the decrease of superoxide formation.

When respiring on palmitate with malate, we found a similar reduction state of the $NAD(P)^+$ pool (~70%) as with pyruvate/malate. Oxidizing palmitate in the presence of malate, 70% of the electrons are transferred to NAD^+, whereas 30% of them are transferred to the electron transfer flavoprotein and complex II. Because complex I is unlikely to produce a significant amount of superoxide during forward transport in BAT mitochondria (as shown with pyruvate/malate) most of the superoxide during β-oxidation in *UCP1*-ablated mice can be addressed to reverse electron transport. Generation of superoxide by electron transfer flavoprotein *per se* may be of minor significance because UCP1-ablated mitochondria have less respiration/oxidative capacity in the cold but substantially produce more superoxide (Fig. 5).

Our data support physiological significance of UCP1 in blunting enhanced superoxide production during β-oxidation, the major pathway of substrate oxidation in brown adipose tissue during cold-induced thermogenesis. Pertaining to superoxide and the lack of cold-induced substrate oxidation in CA *UCP1*-ablated mice, superoxide may also act as a signaling molecule reporting the redox status of mitochondria, thereby adjusting mitochondrial biogenesis, as recently hypothesized (45). It has been emphasized that some reactive oxygen species are required to induce mitochondrial biogenesis via PGC-1α (46), but our results suggest that pathologically high reactive oxygen species concentrations inhibit respiration. Initial superoxide bursts during cold acclimation in *UCP1*-ablated mice may compromise the function of respiratory chain complexes,

as seen for superoxide dismutase 2 knock-out mice (47). Further indirect evidence that superoxide negatively controls oxidative capacity was derived from superoxide dismutase 2 overexpression, which resulted in enhanced oxidative capacity (30).

The survival rates of *UCP1*-ablated mice are markedly reduced in the cold (11). Although local oxidative damage in BAT could be responsible for the shorter life span, the absence of UCP1 requires recruitment of other tissues for heat production with less mitochondrial uncoupling capacity. This might increase systemic radical damage, affecting life span.

Our results show the interrelationship of brown adipose tissue UCP1, energy dissipation, and superoxide production, which may become instrumental when considering human brown adipose tissue for the treatment of obesity. A model proposing activation of UCP1 directly by superoxide as a negative feedback, thereby preventing further superoxide production (27), is highly disputed (28–30). Independent of such a mechanism, we here demonstrate that UCP1 regulates mitochondrial superoxide production upon physiological challenge. We comprise our results in a model shown in Fig. 6. Mammalian UCP1 allows high oxidation rates in the absence of deleterious oxidative stress, and because of this dual role in heat production and superoxide reduction, evolution may have selected for the implementation of UCP1 in adaptive nonshivering thermogenesis of mammals. The role of recently discovered ancient UCP1 orthologues in ectotherms (48) may well be prevention of superoxide production prior to evolution of nonshivering thermogenesis.

Acknowledgments—We thank Sigrid Stöhr and Sebastian Busse for excellent technical assistance and Prof. Martin Brand for helpful discussion.

REFERENCES

1. Heldmaier, G., Klaus, S., and Wiesinger, H. (1990) *Seasonal Adaptation of Thermoregulatory Heat Production in Small Mammals*, Springer-Verlag, Berlin
2. Rothwell, N. J., and Stock, M. J. (1983) *Adv. Nutr. Res.* **5,** 201–220
3. Cypess, A. M., Lehman, S., Williams, G., Tal, I., Rodman, D., Goldfine, A. B., Kuo, F. C., Palmer, E. L., Tseng, Y. H., Doria, A., Kolodny, G. M., and Kahn, C. R. (2009) *N. Engl. J. Med.* **360,** 1509–1517
4. van Marken Lichtenbelt, W. D., Vanhommerig, J. W., Smulders, N. M., Drossaerts, J. M., Kemerink, G. J., Bouvy, N. D., Schrauwen, P., and Teule, G. J. (2009) *N. Engl. J. Med.* **360,** 1500–1508
5. Virtanen, K. A., Lidell, M. E., Orava, J., Heglind, M., Westergren, R., Niemi, T., Taittonen, M., Laine, J., Savisto, N. J., Enerbäck, S., and Nuutila, P. (2009) *N. Engl. J. Med.* **360,** 1518–1525
6. Cannon, B., and Vogel, G. (1977) *FEBS Lett.* **76,** 284–289
7. Rousset, S., Alves-Guerra, M., Mozo, J., Miroux, B., Cassard-Doulcier, A., Bouillaud, F., and Ricquier, D. (2004) *Diabetes* **53,** (Suppl. 1) 130–135
8. Nicholls, D. G., and Locke, R. M. (1984) *Physiol. Rev.* **64,** 1–64
9. Klingenspor, M. (2003) *Exp. Physiol.* **88,** 141–148
10. Enerback, S., Jacobsson, A., Simpson, E. M., Guerra, C., Yamashita, H., Harper, M. E., and Kozak, L. P. (1997) *Nature* **387,** 90–94
11. Golozoubova, V., Hohtola, E., Matthias, A., Jacobsson, A., Cannon, B., and Nedergaard, J. (2001) *FASEB J.* **15,** 2048–2050
12. Aydin, J., Shabalina, I. G., Place, N., Reiken, S., Zhang, S. J., Bellinger, A. M., Nedergaard, J., Cannon, B., Marks, A. R., Bruton, J. D., and Westerblad, H. (2008) *FASEB J.* **22,** 3919–3924
13. Granneman, J. G., Burnazi, M., Zhu, Z., and Schwamb, L. A. (2003) *Am. J. Physiol. Endocrinol. Metab.* **285,** E1230–E1236
14. Ukropec, J., Anunciado, R. P., Ravussin, Y., Hulver, M. W., and Kozak, L. P. (2006) *J. Biol. Chem.* **281,** 31894–31908
15. Harman, D. (1956) *J. Gerontol.* **11,** 298–300
16. Harman, D. (1972) *Am. J. Clin. Nutr.* **25,** 839–843
17. Raha, S., and Robinson, B. H. (2001) *Am. J. Med. Genet.* **106,** 62–70
18. Wallace, D. C. (1999) *Science* **283,** 1482–1488
19. Cadenas, E., and Davies, K. J. (2000) *Free Radic. Biol. Med.* **29,** 222–230
20. Zhang, L., Yu, L., and Yu, C. A. (1998) *J. Biol. Chem.* **273,** 33972–33976
21. Ratner, P. L., Fisher, M., Burkart, D., Cook, J. R., and Kozak, L. P. (1981) *J. Biol. Chem.* **256,** 3576–3579
22. Koza, R. A., Kozak, U. C., Brown, L. J., Leiter, E. H., MacDonald, M. J., and Kozak, L. P. (1996) *Arch. Biochem. Biophys.* **336,** 97–104
23. Drahota, Z., Chowdhury, S. K., Floryk, D., Mrácek, T., Wilhelm, J., Rauchová, H., Lenaz, G., and Houstek, J. (2002) *J. Bioenerg. Biomembr.* **34,** 105–113
24. Miwa, S., and Brand, M. D. (2005) *Biochim. Biophys. Acta.* **1709,** 214–219
25. Miwa, S., St-Pierre, J., Partridge, L., and Brand, M. D. (2003) *Free Radic. Biol. Med.* **35,** 938–948
26. Echtay, K. S., Roussel, D., St-Pierre, J., Jekabsons, M. B., Cadenas, S., Stuart, J. A., Harper, J. A., Roebuck, S. J., Morrison, A., Pickering, S., Clapham, J. C., and Brand, M. D. (2002) *Nature* **415,** 96–99
27. Echtay, K. S., Esteves, T. C., Pakay, J. L., Jekabsons, M. B., Lambert, A. J., Portero-Otín, M., Pamplona, R., Vidal-Puig, A. J., Wang, S., Roebuck, S. J., and Brand, M. D. (2003) *EMBO J.* **22,** 4103–4110
28. Couplan, E., del Mar Gonzalez-Barroso, M., Alves-Guerra, M. C., Ricquier, D., Goubern, M., and Bouillaud, F. (2002) *J. Biol. Chem.* **277,** 26268–26275
29. Shabalina, I. G., Petrovic, N., Kramarova, T. V., Hoeks, J., Cannon, B., and Nedergaard, J. (2006) *J. Biol. Chem.* **281,** 13882–13893
30. Silva, J. P., Shabalina, I. G., Dufour, E., Petrovic, N., Backlund, E. C., Hultenby, K., Wibom, R., Nedergaard, J., Cannon, B., and Larsson, N. G. (2005) *EMBO J.* **24,** 4061–4070
31. Klingenspor, M., Ivemeyer, M., Wiesinger, H., Haas, K., Heldmaier, G., and Wiesner, R. J. (1996) *Biochem. J.* **316,** 607–613
32. Mzilikazi, N., Jastroch, M., Meyer, C. W., and Klingenspor, M. (2007) *Am. J. Physiol. Regul. Integr. Comp. Physiol.* **293,** R2120–R2127
33. Bradford, M. M. (1976) *Anal. Biochem.* **72,** 248–254
34. Reynafarje, B., Costa, L. E., and Lehninger, A. L. (1985) *Anal. Biochem.* **145,** 406–418
35. Lambert, A. J., Buckingham, J. A., and Brand, M. D. (2008) *FEBS Lett.* **582,** 1711–1714
36. Locke, R. M., Rial, E., Scott, I. D., and Nicholls, D. G. (1982) *Eur. J. Biochem.* **129,** 373–380
37. Lambert, A. J., and Brand, M. D. (2004) *J. Biol. Chem.* **279,** 39414–39420
38. Lambert, A. J., and Brand, M. D. (2004) *Biochem. J.* **382,** 511–517
39. Brand, M. D., Pakay, J. L., Ocloo, A., Kokoszka, J., Wallace, D. C., Brookes, P. S., and Cornwall, E. J. (2005) *Biochem. J.* **392,** 353–362
40. Andreyev, AYu, Bondareva, T. O., Dedukhova, V. I., Mokhova, E. N., Skulachev, V. P., and Volkov, N. I. (1988) *FEBS Lett.* **226,** 265–269
41. Andreyev, AYu, Bondareva, T. O., Dedukhova, V. I., Mokhova, E. N., Skulachev, V. P., Tsofina, L. M., Volkov, N. I., and Vygodina, T. V. (1989) *Eur. J. Biochem.* **182,** 585–592
42. Khailova, L. S., Prikhodko, E. A., Dedukhova, V. I., Mokhova, E. N., Popov, V. N., and Skulachev, V. P. (2006) *Biochim. Biophys. Acta.* **1757,** 1324–1329
43. Hittelman, K. J., Lindberg, O., and Cannon, B. (1969) *Eur. J. Biochem.* **11,** 183–192
44. Richieri, G. V., Anel, A., and Kleinfeld, A. M. (1993) *Biochemistry* **32,** 7574–7580
45. Murphy, M. P. (2009) *Biochem. J.* **417,** 1–13
46. St-Pierre, J., Drori, S., Uldry, M., Silvaggi, J. M., Rhee, J., Jäger, S., Handschin, C., Zheng, K., Lin, J., Yang, W., Simon, D. K., Bachoo, R., and Spiegelman, B. M. (2006) *Cell* **127,** 397–408
47. Melov, S., Coskun, P., Patel, M., Tuinstra, R., Cottrell, B., Jun, A. S., Zastawny, T. H., Dizdaroglu, M., Goodman, S. I., Huang, T. T., Miziorko, H., Epstein, C. J., and Wallace, D. C. (1999) *Proc. Natl. Acad. Sci. U.S.A.* **96,** 846–851
48. Jastroch, M., Wuertz, S., Kloas, W., and Klingenspor, M. (2005) *Physiol. Genomics* **22,** 150–156

SEASONAL CHANGES IN THERMOGENESIS OF A FREE-RANGING AFROTHERIAN SMALL MAMMAL, THE WESTERN ROCK ELEPHANT SHREW (*ELEPHANTULUS RUPESTRIS*)

R. OELKRUG ∞ C.W. MEYER ∞ G. HELDMAIER
N. MZILIKAZI

J Comp Physiol B
DOI 10.1007/s00360-012-0647-x

ORIGINAL PAPER

Seasonal changes in thermogenesis of a free-ranging afrotherian small mammal, the Western rock elephant shrew (*Elephantulus rupestris*)

Rebecca Oelkrug · Carola W. Meyer · Gerhard Heldmaier · Nomakwezi Mzilikazi

Received: 7 August 2011 / Revised: 15 January 2012 / Accepted: 26 January 2012

Abstract We report on the seasonal metabolic adjustments of a small-sized member of the phylogenetically ancient Afrotheria, the Western rock elephant shrew (*Elephantulus rupestris*). We recorded body temperature (T_b) patterns and compared the capacity for adrenergically induced nonshivering thermogenesis (NST) in *E. rupestris* captured in the wild in summer and winter. Noradrenaline (NA) treatment (0.4–0.5 mg/kg, s.c.) induced a pronounced elevation in oxygen consumption compared to controls (saline), and the increase in oxygen consumption following injection of NA was 1.8-fold higher in winter compared to summer. This suggests that the smaller members of Afrotheria possess functional brown adipose tissue, which changes in thermogenic capacity depending on the season. Torpor was recorded in both seasons, but in winter the incidence of torpor was higher ($n = 205$ out of 448 observations) and minimal T_b during torpor was lower ($T_b$min: 11.9°C) than in summer ($n = 24$ out of 674 observations; $T_b$min: 26°C). In addition to cold, high air humidity emerged as a likely predictor for torpor entry. Overall, *E. rupestris* showed a high degree of thermoregulatory plasticity, which was mainly reflected in a variable timing of torpor entry and arousal. We conclude that *E. rupestris* exhibits seasonal metabolic adjustments comparable to what has been long known for many Holarctic rodents.

Keywords Adaptive thermogenesis · Afrotheria · *Elephantulus* · Relative air humidity · Torpor · UCP1

Abbreviations

BAT	Brown adipose tissue
BMR	Basal metabolic rate
NA	Noradrenaline
NST	Nonshivering thermogenesis
T_a	Ambient temperature
T_b	Body temperature
RH	Relative air humidity
RMR	Resting metabolic rate
TNZ	Thermoneutral zone
UCP1	Uncoupling protein 1

Introduction

Nonshivering thermogenesis (NST) is a facultative, adaptive form of thermogenesis under control of the sympathetic nervous system. In mammals, the main physiological roles of NST are the maintenance of a constant body temperature (T_b) during cold exposure and the production of endogenous heat during arousal from controlled hypometabolic states, such as hibernation and daily torpor (Himms-Hagen 1984). The molecular mechanism of NST has been intensively studied, and the mitochondrial uncoupling protein 1 (UCP1) in brown adipose tissue (BAT) has been identified as the main mediator of endogenous heat production (reviewed by Cannon and Nedergaard 2004, 2011). Prolonged cold exposure leads to a recruitment of brown adipocytes, which is accompanied by an increased

Communicated by H.V. Carey.

R. Oelkrug (✉) · C. W. Meyer · G. Heldmaier
Department of Animal Physiology, Philipps Universität Marburg, Karl-von-Frisch Straße 8, 35043 Marburg, Germany
e-mail: rebecca.oelkrug@biologie.uni-marburg.de

N. Mzilikazi
Department of Zoology, Centre for African Conservation Ecology, Nelson Mandela Metropolitan University, Port Elizabeth, South Africa

Published online: 16 February 2012

mitochondriogenesis and a higher expression of UCP1 (Jacobsson et al. 1994; Klingenspor 2003). Facultative thermogenic capacity is thereby augmented, a process which is referred to as adaptive thermogenesis (Lowell and Spiegelman 2000; Golozoubova et al. 2001, 2006).

Much of our understanding of NST and UCP1-mediated thermogenesis has been derived from studying rodents such as rats, mice and hamsters, in which NST significantly contributes (>65%) to maximal cold-induced thermogenesis (Foster and Frydman 1978; Heldmaier et al. 1982). Indeed, NST seems to be most efficient in small eutherian mammals and hibernators, particularly those which inhabit environments with long cold seasons (Böckler et al. 1982; Feist and Rosenmann 1975; Hayes 1989; Heldmaier 1971; Heldmaier et al. 1981, 1990; Lynch 1973; Sundin et al. 1987). This conclusion, however, may be biased by the fact that the majority of studies have focused on thermoregulation in mammals of the northern hemisphere. In addition, several species of the southern hemisphere from different mammalian orders have already been shown to display torpor and hibernation (Bozinovic et al. 2004; Dausmann et al. 2004; Geiser 2007; Geiser and Körtner 2010; Lovegrove and Genin 2008; Mzilikazi and Lovegrove 2004; Stawski et al. 2009), suggesting that they may also benefit from NST for arousal. In order to fully understand the plasticity of NST and its significance in the evolution of thermoregulatory patterns in mammals, it is therefore important to study the magnitude by which cold-induced adaptive NST from BAT is recruited in species from different mammalian subgroups and geographical regions.

The orders Macroscelidea and Afrosoricida are endemic to the African continent (Springer et al. 1997; Robinson and Seiffert 2004) and comprise a number of small-sized species, some of which have been observed to display daily torpor, e.g. *Elephantulus rupestris* (Boyles et al. 2012), *Elephantulus edwardii* (Geiser and Mzilikazi 2011), *Elephantulus myurus* (Mzilikazi and Lovegrove 2004), *Macroscelides proboscideus* (Lovegrove et al. 1999), *Eremitalpa granti namibensis* (Fielden et al. 1990), *Amblysomus hottentottus longiceps* (Scantlebury et al. 2008) and *Echinops telfairi* (Lovegrove and Genin 2008; Poppitt et al. 1994; Scholl 1974). Out of these, seasonal adaptive thermogenesis has only been observed in the Hottentot golden mole, which lives in subterranean burrow systems that are thermally buffered from ambient temperature (T_a) fluctuations and thus require endogenous heat production for arousal from torpor (Scantlebury et al. 2008).

Recently, we demonstrated the presence of functional BAT in the Eastern rock elephant shrew (*Elephantulus myurus*, Mzilikazi et al. 2007). This species inhabits semi-arid, rocky formations, experiencing hot summers and dry cold winters (T_a <5°C; Skinner and Chimimba 2005). Interestingly, warm- and cold-acclimated *E. myurus* had similar thermogenic characteristics. These observations were consistent at all levels of organization (UCP1 mRNA, UCP1 concentration in BAT, UCP1 concentration in BAT mitochondria, cytochrome-c oxidase activity and metabolic response to adrenergic stimulation), suggesting that the thermogenic capacity of BAT in *E. myurus* was not recruited by low T_a.

Given that the Afrotheria are phylogenetically "basal" eutherian mammals (Springer et al. 1997), the question arises as to whether the thermogenic characteristics observed in captive *E. myurus* are representative of the small-sized terrestrial members of this clade. Absence of an increased NST response following cold acclimation could be a plesiomorphic feature, as the African endemic species were not exposed to highly seasonal cold climates during the Late Cenozoic (Lovegrove 2011). Alternatively, a fixed/constitutive NST capacity could be associated with adaptive heterothermy, which is often associated with unpredictable environments (Lyman et al. 1982). Finally, a laboratory study may not be sufficient to trigger the seasonal changes that *E. myurus* exhibit in the wild.

To elucidate if the BAT of terrestrial-living afrotherian species is seasonally regulated, we investigated the capacity for nonshivering thermogenesis in Western rock elephant shrews (*Elephantulus rupestris*) captured in the wild. Similar to other soft-furred elephant shrews, *E. rupestris* feeds predominantly on small invertebrates, especially ants and termites as well as beetles and grasshoppers. Sometimes, this diet is supplemented (often seasonally) with fruits, seeds and green plant tissue (reviewed by Rathbun 2009; Skinner and Chimimba 2005). *E. rupestris* lives in a highly seasonal environment and inhabits winter rainfall areas, which reduces access to sun basking. We hypothesized that these climatic constraints favored seasonal thermoregulatory adaptations, which should be mirrored by increased torpor frequency and adaptive thermogenesis.

Materials and methods

Study site

This study was conducted during one summer (17 November 2009–4 March 2010) and one winter season (1 May 2010–16 July 2010). Adult *E. rupestris* were captured from the Gamkaberg Nature Reserve (S 33°40.245; E 21°53.164, altitude: 378 m) 30 km from Oudtshoorn in the Western Cape Province, South Africa. The reserve is located between the winter and summer rainfall regions with gentle soaking rain in winter and thundershowers in summer. The annual rainfall averages 500 mm at the summits and 200 mm on the lower slopes of the mountain where the study was conducted (T. Barry, Cape Nature, pers. comm).

Gamka Mountain is an isolated mountain range in the Little Karoo, located between the Swartberg and Outeniqua mountains, where light snow occasionally falls during winter (T_a: summer >40°C and winter <5°C). The photoperiod in the study area varies from 14.5 h of light in summer to 10 h of light in winter. The Gamkaberg region has four main vegetation types, namely mountain fynbos, arid fynbos, succulent karoo and riverine vegetation. The habitat of *E. rupestris* is mainly characterized by the presence of spekbooms (*Portulacaria afra*) growing on sandy/rocky grounds.

Study animals

E. rupestris were caught using walk-in live Sherman traps baited with a mixture of peanut butter rolled in oats. Traps were set up during the early evening hours and checked at sunrise. Captured animals were housed for up to 7 days in small mammal cages (*l*:54 cm; *h*:19 cm; *w*:32 cm) provided with sawdust bedding and cardboard nest boxes. Individuals were maintained under natural photoperiod and T_a conditions and fed daily with water, dog food and proNutro (a commercial high protein cereal, 22% protein, 59% carbohydrate and 6% fat) mixed with water. This diet was supplemented with fresh lettuce and live mealworms. The capture location of all animals was recorded using a GPS, which enabled the release of the animals at the capture site. All animal experiments were approved by the NMMU animal ethics committee (animal ethics clearance no. A08-SCI-ZOO-005) and complied with the American Physiology Society's "Guiding Principles for Research Involving Animals and Human Being" and the "Code of ethics for animal experimentation" manual adopted by the Nelson Mandela Metropolitan University. Animals were captured under permit no AAA004-00150-0035, issued by the Western Cape Nature Conservation board.

Body temperature measurements

Twelve animals were captured during each season and implanted with temperature-sensitive pre-calibrated Thermocron iButtons (Dallas Semiconductor, DS1922L) for T_b measurement. The dataloggers (3 g) were covered in biologically inert wax and programmed to record the T_b in 30 min intervals at a resolution of 0.0625°C, resulting in 4096 data points over a time span of 85 days. For the intraperitoneal implantation of the iButtons, the animals were anesthetized by inhalation anaesthesia using isoflurane (3%, in normal air). In addition, the analgetic carprofen (Rimadyl, Pfizer GmbH, 4 mg/kg i.p.) was administered. Following surgery, animals were maintained in captivity for up to 12 h and released at the point of capture. After 9–10 weeks, a second trapping session was conducted and iButtons were removed using the same procedures as described above. For later identification of implanted animals from non-implanted animals, they were injected with ID-transponders (Trovan, Euro I.D.). Each transponder had an individual code, which could be read out on living animals. T_a was recorded using three iButtons placed at different locations in the field: One iButton was placed under a stone, its T_a representing resting microclimates experienced by *E. rupestris* (Skinner and Chimimba 2005), and another one was placed directly in the sun. The third iButton was trapped in a ventilated steel tube (to protect the iButton from rain) and placed in a bush to record T_a in the semi-shade. This iButton had an integrated air humidity sensor (RH in %, DS1923). Unless otherwise stated, T_a data from the iButton placed in the semi-shade was used for the analysis. Sunrise and sunset times were obtained from Internet page (http://www.srrb.noaa.gov/highlights/sunrise/sunrise.html).

Rewarming rates from torpor

Rewarming rates were calculated from individual torpor bouts. An animal was considered torpid if its T_b decreased below 32°C (Mzilikazi and Lovegrove 2004). For the calculation of rewarming rates (°C min^{-1}) from each bout of torpor, the difference between minimal T_b ($T_b$min) in torpor and peak T_b ($T_b$peak) after arousal was obtained and divided by the time required for rewarming (($T_b$peak− $T_b$min)/Δt).

We also sought to distinguish between endogenous rewarming at a stable T_a and rewarming that could have been assisted by an increase in T_a. We assumed T_a to be stable when the measured T_a of the iButton in the sun (i.e. the first location in the field site exposed to the sun in the morning) and the iButton placed under the stone increased by less than 2°C during the arousal process.

Metabolic rate measurements

Metabolic rate measurements were based on the principle of indirect calorimetry using an open flow-through respirometry set up with one reference and one measurement channel. Measurements were conducted on recaptured individuals during the second trapping session of each season. For the measurements, individuals were kept in modified small mammal perspex chambers (Sable Systems, 2.8ℓ), which were placed in a temperature cabinet. During the measurements, no food or water was available to the animals. The temperature inside the temperature cabinet was maintained using a water bath which pumped water through copper pipes inside the chamber, thereby ensuring a stable air temperature looks like a different style of lettering (±1°C; Smit and McKechnie 2010). The T_a inside the cooling box could be monitored with a thermometer which was inserted into the box; in parallel, the

T_a inside the metabolic chamber was recorded with an iButton. To analyse the oxygen consumption (VO_2) of the animals, air was continuously withdrawn from the chambers and analysed using a portable oxygen analyser (FoxBox, Sable Systems International, USA). Silica gel scrubbers dried incoming air and filters prevented the blockage of the FoxBox or flow pumps with dirt or dust from the animal cages. Carbon dioxide was scrubbed prior to analysis of oxygen consumption using soda lime, and an additional silica gel scrubber ensured the removal of any residual water vapour in the air, prior to analysis for oxygen. The measurement air was drawn through the respirometer at a flow rate of 500 ml/min chosen to maintain <1% oxygen depletion between the incurrent and excurrent air. Changes between channels were carried out manually. We connected additional flow pumps (MFS2, Sable Systems) to channels when they were not connected to the FoxBox to ensure that no accumulation of carbon dioxide or depletion of oxygen occurred in the chambers. On each day of measurement, animals were transferred to the metabolic cage inside the temperature cabinet at least 1 h before data collection commenced. VO_2 was calculated using the data acquisition program Expedata (Sable Systems International, USA) and the equation by Withers 1977.

Determination of basal metabolic rate at thermoneutrality (BMR)

We determined the basal metabolic rate at thermoneutrality (BMR) and the resting metabolic rate (RMR) below thermoneutrality in *E. rupestris* by exposing animals to different T_as while simultaneously measuring their oxygen consumption. Measurements started in the early morning (1 h after sunrise) and lasted until the late afternoon (1 h before sunset), the resting period of the animals (R. Oelkrug, personal observation). Each T_a was maintained for at least 1 h (summer: 32, 30, 28, 25, 22, 20°C; winter: 20, 22, 25, 28, 30, 32°C). Alternately, the oxygen content of the air drawn from the animal chamber was measured for 10 min and then the reference channel was measured for 5–10 min, at a sampling interval of 1 sample per second. For each T_a, resting metabolic rate (RMR) was calculated from the lowest mean oxygen consumption over a period of 5 min in a non-moving animal.

Metabolic responses to noradrenaline (NA)

The metabolic responses to NA were examined at T_a = 25°C to prevent the animals from experiencing heat stress. Individual *E. rupestris* (n = 11 winter; n = 13 summer) were subcutaneously injected with either saline (as an internal control injection) or arterenol (Sanofi Aventis; 85% of dose Wunder and Gettinger (1996), 2.53 × $M^{-0.4}$ NA (mg/kg) according to Mzilikazi and Lovegrove 2006) and quickly returned to the metabolic chamber. During the subsequent 1.5 h, the behaviour of the animal was observed and oxygen consumption was recorded at a resolution of 1 Hz. The VO_2 readings were averaged over time periods of 1 min (60 subsequent VO_2 readings), and maximum oxygen consumption (VO_2 max) was obtained from the highest 1 min VO_2 mean in a resting (non-moving) animal. For each animal, the coefficient of variation for VO_2 max was <0.5%. BMR was subtracted from VO_2 max to obtain the magnitude of the NA-induced metabolic response (NST capacity). All animals received both injections, first saline and on the following day NA.

Statistical analysis

We used the Student's t tests to compare body weight recordings and the Mann–Whitney rank sum test to analyse means of T_b recordings, torpor duration and rewarming rates in summer and winter. The frequency distribution of the time difference (min) between torpor bout entry and sunset was tested for deviation of normality using the Kolmogorov–Smirnov test. The effect of season on changes in RMR with T_a was investigated using the Student′s t test (BMR, RMR at 20 and 22°C) and a linear mixed-effects model (library nIme, Pinheiro et al. 2006) using the statistical package R (R Development Core Team 2006), with individual as the random factor. For the analyses, the RMR data between 28 and 20°C T_a (=below thermoneurality) were included. To compare individual responses to saline versus NA, a one-way repeated measurement ANOVA and Student′s t test was used. These analyses were performed using SigmaStat (Jandel Scientific, San Rafael, California). All mean values were reported ± standard deviation (SD) and the 0.05 level of probability was accepted as indicating statistical significance.

Results

Ambient temperature and relative air humidity

The average daily T_a in summer was 23.6 ± 5.2°C (ranging from 10.7 to 48.6°C) and 13.6 ± 5.2°C in winter (ranging from 0.6 to 36.2°C; Table 1 semi-shade iButton). Average RH was 51.6 ± 15.2% in summer and 67.7 ± 19.4% in winter, showing more humid conditions in winter especially during the night. The total rainfall measured in the reserve was 39 mm in summer and 76 mm in winter during the period of data collection (T. Barry, Cape Nature, pers. comm.).

Table 1 Ambient temperature (T_a) and relative air humidity (RH) recordings during summer (17 November 2009–4 March 2010) and winter (1 May 2010–16 August 2010)

Both parameters were recorded with a Thermocron iButton, which was placed in the semi-shade inside a bush (mean values ± SD)

	T_a(°C)		RH (%)	
	Summer	Winter	Summer	Winter
Average daily minimum	16.4 ± 2.5	6.9 ± 3.9	33.5 ± 16.8	45.4 ± 22.9
Range daily minimum	10.7–24.7	0.6–21.1	4.0–64.4	9.1–100.0
Average daily maximum	29.5 ± 7.2	20.1 ± 7.6	76.9 ± 10.2	92.3 ± 15.2
Range daily maximum	17.2–48.6	5.2–36.2	33.1–100.0	26.9–100.0
Average daily mean	23.6 ± 5.2	13.6 ± 5.2	51.6 ± 15.2	67.7 ± 19.4
Range daily mean	14.0–37.2	3.7–26.2	18.3–89.0	20.2–100.0

Trapping success and body mass

In summer, eight (7♂; 1♀) implanted *E. rupestris* were recaptured and the iButtons were removed. In winter, T_b data were available for seven animals (4♂; 3♀). The number of individuals investigated with respect to their metabolic rates was increased by including non-implanted animals which were trapped at the end of each season, resulting in $n = 17$ individuals in summer (12♂; 5♀) and $n = 15$ individuals in winter (8♂; 7♀). Body mass of *E. rupestris* ranged between 45.0 and 70.0 g in both sexes. In summer, body mass tended to be lower (in females: 57.6 ± 7.6 g vs. 63.0 ± 4.2 g; males: 57.6 ± 5.0 g vs. 61.4 ± 5.5 g), but the difference in body mass with season was only statistically significant in males ($P = 0.022$). When body mass data were combined for the sexes, winter animals were significantly heavier than summer animals ($P = 0.018$).

Seasonal fluctuations in body temperature

The T_b of recaptured *E. rupestris* showed distinct daily fluctuations with minimum values predominantly reached during the night (lowest recorded T_b: 11.9°C) and maximum values reached during the day (highest recorded T_b: 39.75°C). Peaks and nadirs in T_b corresponded with the daily fluctuations in Ta, irrespective of the season (Fig. 1). Mean T_b was equal during the summer (36.9 ± 0.3°C) and winter months (36.9 ± 0.3°C, Table 2) if animals stayed normothermic ($T_b > 32$°C), whereas the use of torpor resulted in a significantly reduced mean T_b during winter (34.4 ± 2.5; summer: 36.0 ± 2.0; $P < 0.001$). Both daily T_b peaks and T_b troughs of normothermic animals were markedly different between seasons, reaching slightly higher peak values in summer (38.5 ± 0.3°C; winter: 38.4 ± 0.4°C; $P = 0.007$) and lower minimum T_bs ($T_b$min) in winter (34.5 ± 1.2°C; summer: 35.2 ± 0.7; $P < 0.001$). Maximum T_bs on days where the animals showed torpor were the same, but the minimum T_b was significantly reduced in winter (23.6 ± 6.6°C; summer: 30.3 ± 2.0; $P < 0.001$). These differences in maximum and minimum T_b resulted in a greater circadian amplitude of T_b during winter (9.0 ± 7.0°C) than during summer (2.8 ± 0.9°C; $P < 0.001$).

E. rupestris showed clear bouts of daily torpor during both seasons, i.e. in summer and winter (Figs. 1, 2). The incidence of torpor was higher during winter ($N = 7$, $n = 205$ bouts out of 448 observations) than during summer ($N = 7$, $n = 24$ bouts out of 674 observations), with females more frequently torpid than males (47 vs. 34%). Mean torpor depth and duration differed with season, and torpor episodes were significantly deeper and longer in winter ($T_b$min: 23.8 ± 6.7°C, torpor bout duration: 301 ± 198 min; summer: $T_b$min: 30.5 ± 2.0°C, torpor bout duration: 65 ± 55 min; $P < 0.001$; Fig. 3a). $T_b$min during torpor was negatively correlated with torpor duration in both seasons (adj$R^2 = 0.79$, $P < 0.001$ for each season).

E. rupestris entered torpor most commonly around 3:00–7:30 a.m. during summer and between 22:00 p.m. and 6:00 a.m. during winter (Fig. 3b), but they also entered torpor during the early morning or the late afternoon hours. The frequency distribution of the daily time interval between sunset and entry into torpor differed significantly from a normal distribution ($P > 0.001$). In winter, there was a negative correlation between timing of torpor entry and the duration of torpor, i.e. torpor bouts that started early during the night tended to be longer (adjR^2: 0.632, $P < 0.001$).

To compare the degree of heterothermy exhibited by *E. rupestris* with season, we plotted the daily $T_b$min of each animal against the daily minimum T_a ($T_a$min) (Fig. 4a). In summer, torpor was only observed when the T_a fell below 17°C. In winter, bouts of torpor were mainly recorded when daily minimum T_a was below 8°C. Notably, not all animals were torpid on cold days. Next, we explored if RH affected the incidence of torpor and the minimal T_b in *E. rupestris*. T_a and RH were correlated in winter ($P < 0.001$, $R^2 = 0.6715$; summer: $P = 0.0265$, $R^2 = 0.0573$), confounding possible independent effects of RH on $T_b$min. Therefore, in the absence of a linear relationship of daily minimum T_a and RH (Fig. 4b), we transformed the minimal T_a and RH into distinct categories and derived the incidence of torpor for each category (Fig. 4 inset graph, only winter

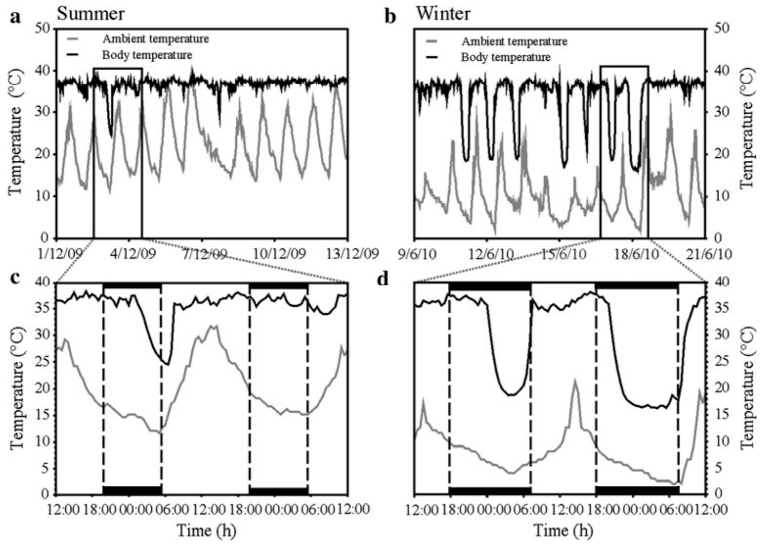

Fig. 1 Ambient temperature (T_a) and body temperature recordings (T_b) in free-ranging *E. rupestris* during summer and winter. **a** and **b** T_b (*black line*) from one male in summer and one male in winter over a period of 12 days and 2 days (**c**, **d**), respectively. *Dark bars* represent night

Table 2 Daily mean, maximum and minimum body temperatures (T_b) of *E. rupestris* during summer and winter on days with or without torpor (mean values ± SD)

Torpor was defined by a periodic decrease in T_b below 32°C during 24 h. The Mann–Whitney *U* test was used for all statistical analysis

	Normothermic	P	Days with torpor	P
Mean Tb (°C)				
Summer (N=8)	36.9±0.3	0.474	36.0±2.0	<0.001
Winter (N=7)	36.9±0.3		34.4±2.5	
Max Tb (°C)				
Summer (N=8)	38.5±0.3	0.007	38.4±0.4	0.166
Winter (N=7)	38.4±0.4		38.2±0.5	
Min Tb (°C)				
Summer (N=8)	35.2±0.7	<0.001	30.3±2.0	<0.001
Winter (N=7)	34.5±1.2		23.6±6.6	
Circadian Tb amplitude (°C)	Summer: 2.8±0.9		Winter: 9.0±7.0	<0.001

season). The analysis revealed that torpor only occurred on cold and wet days (RH ≥ 50%). At a $T_b$min below 8°C, the RH had an additive effect on the degree of hypothermia exhibited by *E. rupestris* (compare the percentage of animals torpid at $T_b$min 5–7°C at RH 50–80% with RH >80% in Fig. 4 inset graph).

Rewarming rates from torpor

The rewarming rates from torpor in *E. rupestris* were higher in winter (0.091 ± 0.042°C min^{-1}; n = 205) than in summer (0.077 ± 0.04°C min^{-1}; n = 24, Fig. 5e, f), but this difference was on the borderline of significance (P = 0.097). Overall rewarming rates, however, do not take into account assisted rewarming by increasing T_a or access to sun basking. Therefore, we also calculated the rewarming rates from summer (n = 8 out of 24) and winter torpor events (n = 147 out of 205) that occurred before sunrise and were therefore not assumed to be coupled to an increase in environmental temperature (Fig. 5c, d). In winter, the rewarming rates at stable T_as were lower than those recorded at increasing T_as (0.087 ± 0.042 vs. 0.102 ± 0.041°C min^{-1}; P = 0.007). There was no difference between rewarming at stable T_a compared to rewarming at increasing T_a in summer

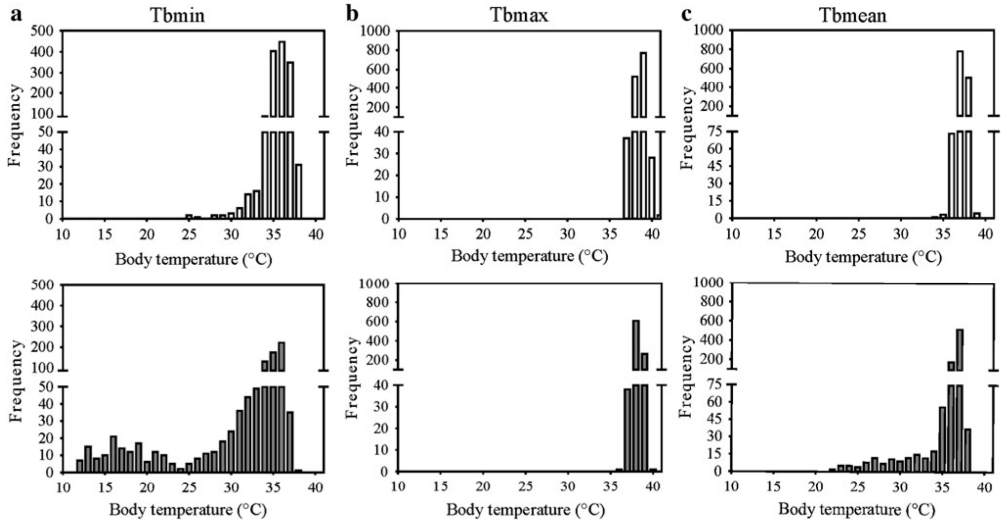

Fig. 2 Frequency distribution of minimum (**a**), maximum (**b**) and mean (**c**) body temperature (T_b) of free-ranging *E. rupestris* during summer (*white bars*, *upper panel*) and winter (*grey bars*, *lower panel*; bin width = 1°C)

(0.069 ± 0.016 vs. 0.082 ± 0.048°C min^{-1}) and no significant difference between the seasons.

Resting metabolic rates of *Elephantulus rupestris* in winter and summer

Resting metabolic rates of *E. rupestris* were lowest at T_as between 28 and 32°C (Fig. 6a). Although we did not measure at higher T_as, we assume that the mean RMR values obtained during this temperature range represent BMR which was 0.89 ± 0.10 $mlO_2\ h^{-1}\ g^{-1}$ (53.17 ± 6.10 $mlO_2\ h^{-1}$) in winter and 1.11 ± 0.07 $mlO_2\ h^{-1}\ g^{-1}$ (60.85 ± 3.39 $mlO_2\ h^{-1}$) in summer ($P = 0.005$ for $mlO_2\ h^{-1}\ g^{-1}$, $P = 0.152$ for $mlO_2\ h^{-1}$). Below 28°C, the resting metabolic rate increased with lowering T_a (Fig. 6a). All RMRs measured below 28°C were lower in winter, and the slope for the linear increase in RMR with decreasing T_a was significantly higher in summer (RMR = 253.99–3.93 T_a) than in winter (RMR = 167.95–6.97 T_a; $P = 0.003$). This may indicate an improvement of fur insulation or a lowered T_b, which leads to a lowered thermal conductance and, consequently, a decrease in thermoregulatory costs.

Nonshivering thermogenesis capacity of *Elephantulus rupestris*

Adrenergic stimulation of thermogenesis is an established method to quantify the magnitude of nonshivering thermogenic capacity in vivo. As shown in Fig. 6, both summer and winter animals showed an increase in their metabolic rate following an injection of noradrenaline. In contrast, saline did not substantially increase VO_2 (Fig. 6c). Maximum VO_2 following NA injection was reached faster in winter than in summer animals (17 ± 5 vs. 26 ± 7 min), and VO_2 remained elevated for a prolonged time in the former. The maximal increase in VO_2 over BMR was 1.45 ± 0.5 $mlO_2\ h^{-1}\ g^{-1}$ (81.19 ± 32.61 $mlO_2\ h^{-1}\ g^{-1}$) in summer and 2.52 ± 0.57 $mlO_2\ h^{-1}\ g^{-1}$ (142.19 ± 42.39 $mlO_2\ h^{-1}$, Fig. 6b, c), in winter, equivalent to a 1.8-fold increase in NST capacity induced by winter acclimation. The significant increase in NST capacity between summer- and winter-acclimatized animals ($P < 0.05$) clearly demonstrates the presence of adaptive NST in *E. rupestris*.

Discussion

Our study demonstrates that the elephant shrew species *E. rupestris* exhibits seasonal changes in NA-mediated NST, which we interpret as a seasonal increase of UCP1-mediated thermogenesis in brown adipose tissue. In winter, the capacity for NST increased by 1.8-fold relative to summer-acclimatized animals. We also provide the first record of resting metabolic rate and T_b patterns of *E. rupestris* captured in the wild during summer and winter. Males and females entered daily torpor during both seasons. In winter,

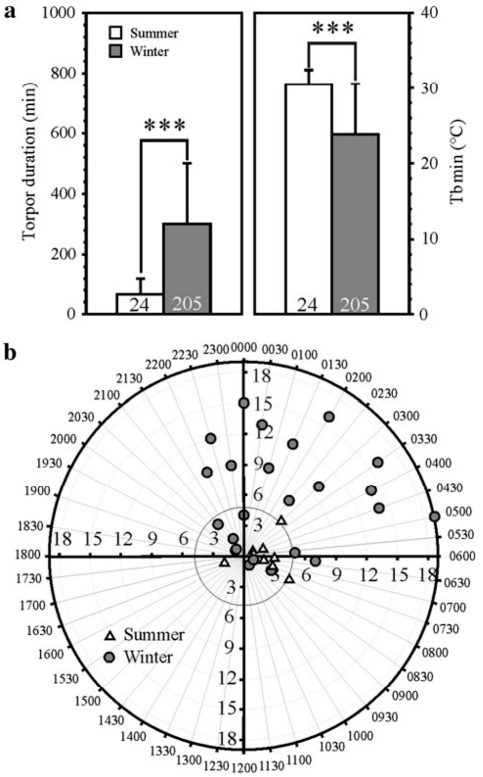

Fig. 3 Torpor variables in summer- and winter-acclimatized *E. rupestris* ($N = 7$ individuals per season). **a** Torpor duration was assessed from the time spent at T_b below 32°C (***$P < 0.001$, Mann–Whitney *U* Test). **b** Polar plot showing the incidence of torpor entry relative to the time of day in $n = 229$ torpor bouts ($n = 24$ summer; $n = 205$ winter). The frequency distribution of the time interval between e.g. sunset and torpor entry differed significantly from a normal distribution ($P < 0.001$). The sun rose between 5:15 and 6:15 a.m. in summer and between 7:20 and 7:40 a.m. during winter, and set between 19:10 and 19:45 p.m. in summer and between 17:30 and 17:50 p.m. in winter

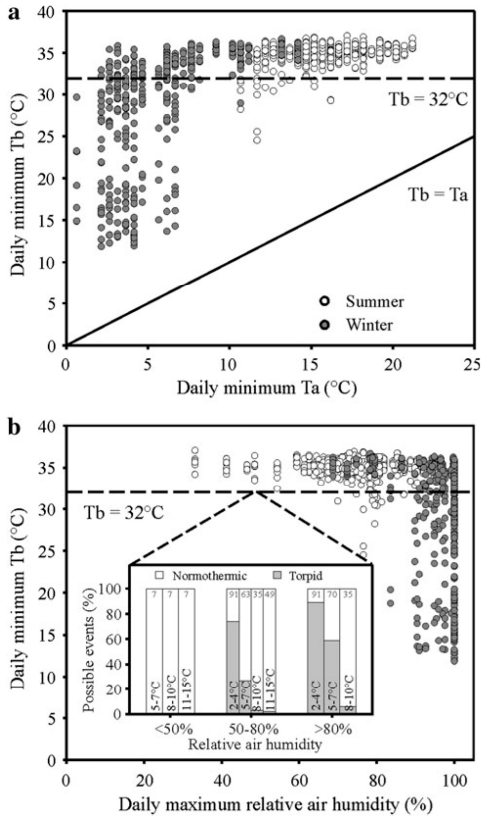

Fig. 4 Ambient temperature (T_a) and relative air humidity (RH) affected the degree of hypothermia in summer- and winter-acclimatized *E. rupestris* ($N = 7$ individuals per season). In **a** and **b** the daily minimum T_b of each animal is plotted against the daily minimum T_a or RH, respectively. The *inset graph* in **b** shows the frequency of animals torpid or normothermic in relation to the mean minimum T_a and RH categories (winter only). In *each bar*, the number of possible events (animal × day) for each category is indicated

the frequency of torpor was higher and torpor episodes were longer and deeper. Low T_a and high RH emerged as the most likely predictors of torpor use in *E. rupestris*. Based on our RMR measurements, we further conclude that thermal conductance was reduced in winter-acclimated animals, possibly through an improved fur insulation or a reduced T_b. In addition, an increase in winter body mass may contribute to a decreased thermal conductance. Taken together *E. rupestris*, a small sized member of the phylogenetically ancient afrotherian clade, exhibits seasonal metabolic adjustments comparable to what has been long known for many Holarctic rodents.

So far, most studies on thermoregulation in elephant shrews have been conducted under laboratory or semi-natural conditions (Downs and Perrin 1995; Lovegrove et al. 1999; Lovegrove et al. 2001a, b). None of these authors previously investigated the seasonal changes in NST capacities, and the degree by which these species used torpor was unclear. The first member of the genus *Elephantulus* to be investigated in the field was *E. myurus*, the Eastern rock elephant shrew, a close relative of *E. rupestris*, which shows torpor throughout the year but mainly during winter and spring (Mzilikazi and Lovegrove 2004). Interestingly, a laboratory-based study on *E. myurus* revealed no differences

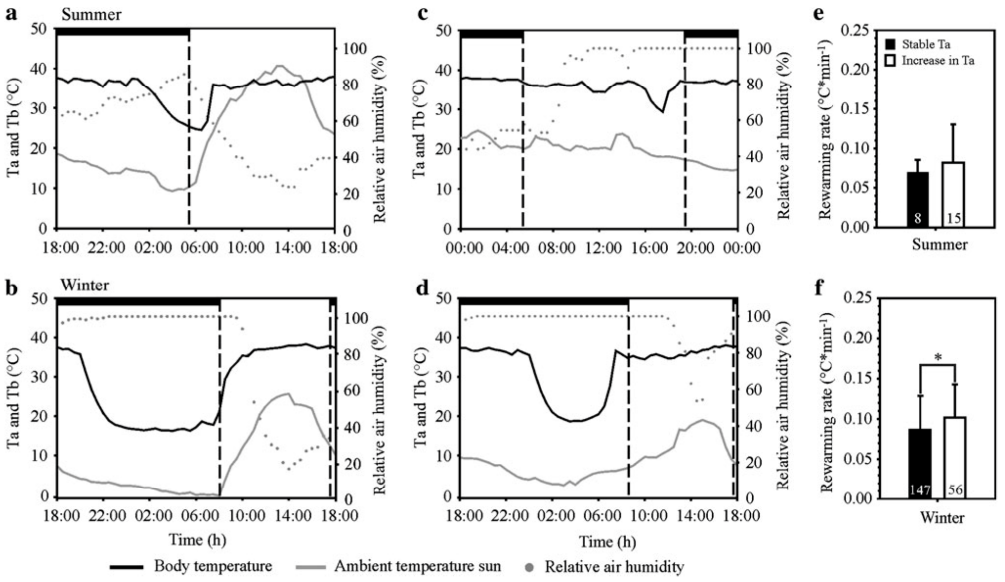

Fig. 5 Rewarming rates from torpor in summer and winter. **a**, **b** Individual summer and winter torpor bouts (T_b: *black line*) where rewarming from torpor was paralleled by an increase in T_a (*grey line*). **c**, **d** Torpor bouts of the same individuals as in a/b, but this time arousal occurred independent of T_a changes. In each panel, the *dotted line* represents the RH. **e**, **f** Mean arousal at a stable T_a and an increasing T_a ($P = 0.007$, Student's t test)

in NST capacities and brown fat characteristics between warm- (28°C) and cold (18°C) -acclimated individuals (Mzilikazi et al. 2007). A laboratory-based approach, however, excludes environmental factors such as a changing photoperiod or rain, and in free-ranging individuals these parameters may enforce the development of a higher NST capacity during harsher seasons (Haim 1982; Kronfeld-Schor et al. 2000). The only member of the Afrotheria in which adaptive NST (measured as a response to NA) with season has previously been demonstrated in the field is the Hottentot golden mole (*Amblysomus hottentottus longiceps*, Scantlebury et al. 2008). The NST capacity of winter-acclimatized animals was 2.8-fold higher compared to summer animals. Hottentot golden moles live in underground burrows with no access to warm microclimates and they may thus be particularly reliant on the contribution of NST for thermoregulation and arousal from torpor (Scantlebury et al. 2008). Therefore, the thermoregulatory capacities of Hottentot golden moles may not be representative for the small members of the Afrotheria.

In contrast to the Hottentot golden mole, the species investigated here *E. rupestris* lives in a seasonal terrestrial environment. *E. rupestris* showed a clear seasonal difference in thermogenic capacity, which was 1.8-fold higher in winter, indicating the presence of adaptive thermogenesis. On the basis of an allometric relationship between body mass and NST of modern eutherians from cold climates (Heldmaier 1971), the maximum (winter) VO_2 of *E. rupestris* after noradrenaline injection is 36% lower than expected. This finding is in accordance with other studies on the NST capacities of species from more unpredictable tropical and subtropical regions, where the maximum VO_2 was more than 50% lower than predicted (Saarela and Hissa 1993; Kronfeld-Schor et al. 2000). Using the regression established by Mzilikazi and Lovegrove 2006 (log NST = 0.442 log Mb + 1.124), which includes 19 species from the southern hemisphere and accounts for phylogeny, however, the NST capacity for *E. rupestris* is only slightly (−14%) below the expected value for a 60 g body mass mammal.

Classical brown fat-mediated adaptive NST is triggered by cold acclimation, but in some species decreasing photoperiod during late summer or autumn allows for an anticipatory recruitment of thermogenic capacity prior to the onset of the cold season (reviewed by Heldmaier et al. 1989). An example is *Phodopus sungorus*, in which exposure to short day photoperiod accounts for roughly 50% of the seasonal increase in thermogenic capacity (Heldmaier et al. 1981). Considering the relatively low mean daily temperatures at the field site where we caught *E. rupestris*, with daily temperatures often well below thermoneutrality even

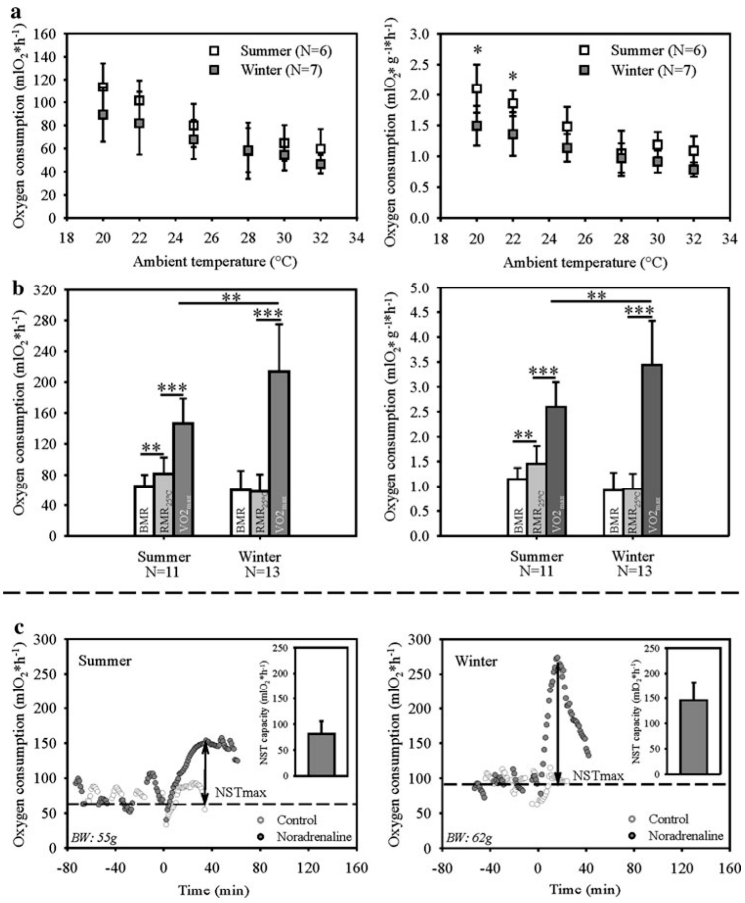

Fig. 6 Resting metabolic rates and maximal NA induced VO_2 in free-ranging *E. rupestris* during summer and winter. **a** RMRs (+SD) of normothermic animals at an T_a of 22 and 20°C were only significantly different when calculated per gram animal ($P = 0.005$ and $P = 0.009$, Student's *t* test). **b** VO_2 max following an NA injection was significantly higher as RMR 25°C and BMR (at T_a: 30°C) in summer and winter animals. **c** Representative tracings of oxygen consumption before and after injection of saline or noradrenaline, (NA) in a summer (male, *left graph*) and a winter (female, *right graph*) -acclimatized *E. rupestris*. At 1.5 h before injection of NA or saline, the T_a was decreased from 30°C (tracing not shown) to 25°C. *Inset graphs* show the maximum NST capacity reached by summer ($N = 11$) and winter ($N = 13$) -acclimatized animals. *Bars* indicate mean values ± SD (**<0.05, Student's *t* test between summer and winter animals; $^{**}P < 0.05$, $^{***}P < 0.001$, one-way RM ANOVA for within group comparisons)

during the summer season, we speculate that photoperiod may be a major additional cue for the recruitment of NST capacity of *E. rupestris* in winter.

As judged from the T_b recordings, *E. rupestris* entered torpor during the winter and the summer season. Even though heterothermy is a physiological response which is usually associated with cold conditions that coincide with short photoperiod, decreased food availability and food quality, summer torpor is not an unusual behaviour in mammals (reviewed by McKechnie and Mzilikazi 2011). It has been suggested that summer torpor could be advantageous during uncharacteristically dry summers or at low food availability. *E. rupestris* feeds mainly on insects, but sometimes also on seeds and grass (reviewed by Rathbun 2009; Skinner and Chimimba 2005). We have no records about prey abundance during the study year, but from personal observations we know that a high number of invertebrates were available during the summer season, which makes it unlikely that torpor was a response to local energetic shortfalls. From the average rainfall, we can further exclude the possibility that summer torpor was the consequence of a drought year. Occasional summer torpor in *E. rupestris* may thus reflect a flexible metabolic strategy, but the daily predictors are presently unclear. It is even possible that the frequency of summer torpor in *E. rupestris* was underestimated, because at high T_as depression of metabolic rate (torpor) may not be accompanied by substantial reductions in T_b (Ehrhardt et al. 2005; Levy et al. 2011). To resolve this issue, measurements of field metabolic rate in conjunction with T_b recordings will be necessary.

In winter, the degree of heterothermy of *E. rupestris* was more pronounced, but daily torpor was not obligatory.

Furthermore, torpor entry in *E. rupestris* was not strongly coupled to a specific time of day, e.g. the onset of the circadian resting phase (R. Oelkrug, personal observations). Indeed, the frequency distribution of the time interval between e.g. sunset and torpor entry differed significantly from a normal distribution ($P > 0.001$). Therefore, *E. rupestris* differs from many mammals including *E. myurus*, in which torpor entry has a strong temporal relation to the circadian day.

E. myurus predominantly enters torpor around 5 h after sunset and rewarming is observed within 2 h after sunrise (Mzilikazi and Lovegrove 2004). This strategy is assumed to reduce arousal costs by passive exogenous heating using increasing daily T_as (Lovegrove et al. 1999; Mzilikazi et al. 2002, 2008; Mzilikazi and Lovegrove 2005; Warnecke et al. 2008; Warnecke and Geiser 2010). Compared with *E. myurus*, rewarming in *E. rupestris* was not necessarily related to T_a cycles. Of note, 147 out of 203 rewarming events in winter occurred at relatively stable T_as and before sunrise, i.e. clearly without access to solar radiation. This shows that *E. rupestris* can rewarm from torpor exclusively by means of endogenous heat production. In winter, an increased NST capacity may specifically support rewarming in the absence of passive heating opportunities (Scantlebury et al. 2008).

On the other hand, *E. rupestris* may also take advantage of increasing T_a to support arousal from torpor. This conclusion is substantiated by the observation that a number of arousal events appear to be coupled to increasing daily T_a. We did not make any behavioural observations and thus cannot make any definite statements on whether *E. rupestris* used sun basking for rewarming from torpor on these occasions. Numerically, however, the rate of rewarming at increasing daily T_a was ~0.02°C higher in winter, suggesting that arousal was supported by exogenous heat (Fig. 5). Taken together, *E. rupestris* appears flexible to choose between endogenous heat production and assisted endogenous heating where internal heat sources are augmented by exogenous means. This enables flexible timing of torpor entry and arousal, allowing more opportunistic behavioural traits independent of daytime and season, such as foraging, mating behaviour or territoriality.

Although the torpor frequency was higher and minimal T_b in torpor was lower in winter, the incidence and depth of torpor in *E. rupestris* was not only related to low T_a, but also to high RH. This is of interest, since the natural habitat of *E. rupestris* lies between a summer and winter rainfall area, and the animals might therefore particularly benefit from endogenous arousal capacity through NST on cold and rainy occasions. To our knowledge, only one study previously found a correlation between the occurrence of rain and torpor (*Petaurus breviceps*, Körtner and Geiser 2000). This is surprising since air humidity is an environmental factor, which could moisten the fur and thereby increase thermal conductance. It will be important to further assess the impact of air humidity on life history traits and metabolic adjustments in future studies.

Recently, the heterothermy index has been put forward as a comparative measure for the degree of heterothermy in different animal species (Boyles et al. 2011). In our study, the HI is 2.50 ± 2.84°C for males and 3.96 ± 4.08°C for females. Boyles et al. 2012 also reported on winter torpor in *E. rupestris* captured in the Namaqualand region of western South Africa. While the minimal T_bs recorded were similar (8.9°C vs. 11.9°C in our study), the HI values were considerably higher (5.13 ± 4.9 and 6.16 ± 5.3°C for the males and females, respectively). Unfortunately, Boyles et al. did not provide minimum T_a values of the field site, and they did not record the amount of rain or measure air humidity during their study period. The reason for the site-specific difference in HI values from the same species is therefore not clear. However, it also raises the question of whether an index like the HI can give a valuable statement about the heterothermic capacity of a species in comparison to other species when the measurements are not performed under the same environmental/experimental conditions (Brigham et al. 2011).

Taken together, *E. rupestris* shows adaptive thermogenesis with season and a high degree of plasticity in thermoregulatory ability. This suggests that the metabolic strategies and the seasonal thermogenic capacities of southern small mammals are not generally different from their northern counterparts. It will nevertheless be of interest to compare the molecular basis of nonshivering thermogenesis (expression of UCP1, its sequence and coupling activity) between different afrotherian species and in relation to the more basal (marsupial) and more modern (rodent) members of the mammalian lineage, to uncover the evolution of BAT-NST and UCP1 thermogenic function.

Acknowledgments This work was supported by the German Research Foundation (DFG, grant #HE-990 to GH and CWM) and the South African National Research Foundation (NRF, grant # 70703 to NM). Any opinions, findings and conclusions or recommendations expressed in this material are those of the authors and therefore the NRF does not accept any liability in regard thereto. We would like to thank Tom Barry from Cape Nature for the comfortable housing in the reserve and for supporting this study, Graham Kerley for lending us the Sherman traps and Aneri Vlok, Gareth Mann and Stacey Hallam for helpful field assistance.

References

Böckler H, Steinlechner S, Heldmaier G (1982) Complete cold substitution of noradrenaline-induced thermogenesis in the Djungarian hamster, *Phodopus sungorus*. Experientia 38:261–262

Boyles JG, Smit B, McKechnie AE (2011) A new comparative metric for estimating heterothermy in endotherms. Physiol Biochem Zool 84:115–123

Boyles JG, Smit B, Sole CL, McKechnie AE (2012) Body temperature patterns in two syntopic elephant shrew species during winter. Comp Biochem Physiol A 161:89–94

Bozinovic F, Ruiz G, Rosenmann M (2004) Energetics and torpor of a South American 'living fossil', the microbiotheriid *Dromiciops gliroides*. J Comp Physiol B 174:293–297

Brigham RM, Willis CKR, Geiser F, Mzilikazi N (2011) Baby in the bathwater: should we abandon the use of body temperature thresholds to quantify expression of torpor? J Therm Biol 36:376–379

Cannon B, Nedergaard J (2004) Brown adipose tissue: function and physiological significance. Physiol Rev 84:277–359

Cannon B, Nedergaard J (2011) Nonshivering thermogenesis and its adequate measurement in metabolic studies. J Exp Biol 214:242–253

Dausmann KH, Glos J, Ganzhorn JU, Heldmaier G (2004) Physiology: hibernation in a tropical primate. Nature 429:825–826

Downs CT, Perrin MR (1995) The thermal biology of the white-tailed rat *Mystromys albicaudatus*, a cricetine relic in southern temperate African grassland. Comp Biochem Physiol A 110:65–69

Ehrhardt N, Heldmaier G, Exner C (2005) Adaptive mechanisms during food restriction in *Acomys russatus*: the use of torpor for desert survival. J Comp Physiol B 175:193–200

Feist DD, Rosenmann M (1975) Seasonal sympatho-adrenal and metabolic responses to cold in the Alaskan snowshoe hare (*Lepus americanus*, Macfarlani). Comp Biochem Physiol A 51:449–455

Fielden LJ, Perrin MR, Hickman GC (1990) Water metabolism in the Namib Desert golden mole, *Eremitalpa granti namibensis* (Chrysochloridae). Comp Biochem Physiol A 96:227–234

Foster DO, Frydman ML (1978) Brown adipose tissue: the dominant site of nonshivering thermogenesis in the rat. Exp Suppl 32:147–151

Geiser F (2007) Yearlong hibernation in a marsupial mammals. Naturwissenschaften 94:941–944

Geiser F, Körtner G (2010) Hibernation and daily torpor in Australian mammals. In: Beard L, Lunney D, McCallum H, Franklin C (eds) Theme edition of Australian Zoologist "Ecology meets Physiology", a Gordon Grigg Festschrift. Australian Zoologist vol 35. pp 204–215

Geiser F, Mzilikazi N (2011) Does torpor of elephant shrews differ from that of other heterothermic mammals? J Mammal 92:444–451

Golozoubova V, Hohtola E, Matthias A, Jacobsson A, Cannon B, Nedergaard J (2001) Only UCP1 can mediate adaptive nonshivering thermogenesis in the cold. FASEB J 15:2048–2050

Golozoubova V, Cannon B, Nedergaard J (2006) UCP1 is essential for adaptive adrenergic nonshivering thermogenesis. Am J Physiol Endocrinol Metab 291:E350–E357

Haim A (1982) Effects of long scotophase and cold acclimation on heat production in two diurnal rodents. J Comp Physiol B 148:77–81

Hayes JP (1989) Altitudinal and seasonal effects on aerobic metabolism of deer mice. J Comp Physiol B 159:453–459

Heldmaier G (1971) Zitterfreie Wärmebildung und Körpergröße bei Säugetieren. Z Vergl Physiol 73:222–248

Heldmaier G, Steinlechner S, Rafael J, Vsiansky P (1981) Photoperiodic control and effects of melatonin on nonshivering thermogenesis and brown adipose tissue. Science 212:917–919

Heldmaier G, Steinlechner S, Rafael J, Latteier B (1982) Photoperiod and ambient temperature as environmental cues for seasonal thermogenic adaptation in the Djungarian hamster, *Phodopus sungorus*. Int J Biometeorol 26:339–345

Heldmaier G, Steinlechner S, Ruf T, Wiesinger H, Klingenspor M (1989) Photoperiod and thermoregulation in vertebrates: body temperature rhythms and thermogenic acclimation. J Biol Rhythms 4:251–265

Heldmaier G, Klaus S, Wiesinger H (1990) Seasonal adaptation of thermoregulatory heat production in small mammals. Springer, Berlin, pp 235–243

Himms-Hagen J (1984) Nonshivering thermogenesis. Brain Res Bull 12:151–160

Jacobsson A, Muhleisen M, Cannon B, Nedergaard J (1994) The uncoupling protein thermogenin during acclimation: indications for pretranslational control. Am J Physiol 267:R999–R1007

Klingenspor M (2003) Cold-induced recruitment of brown adipose tissue thermogenesis. Exp Physiol 88:141–148

Körtner G, Geiser F (2000) Torpor and activity patterns in free-ranging sugar gliders *Petaurus breviceps* (Marsupialia). Oecologia 123:350–357

Kronfeld-Schor N, Haim A, Dayan T, Zisapel N, Klingenspor M, Heldmaier G (2000) Seasonal thermogenic acclimation of diurnally and nocturnally active desert spiny mice. Physiol Biochem Zool 73:37–44

Levy O, Dayan T, Kronfeld-Schor N (2011) Adaptive thermoregulation in golden spiny mice: the influence of season and food availability on body temperature. Physiol Biochem Zool 84:175–184

Lovegrove BG (2011) The evolution of endothermy in Cenozoic mammals: a plesiomorphic–apomorphic continuum. Biol Rev Camb Philos Soc. doi:10.1111/j.1469-185X.2011.00188.x

Lovegrove BG, Genin F (2008) Torpor and hibernation in a basal placental mammal, the Lesser Hedgehog Tenrec *Echinops telfairi*. J Comp Physiol B 178:691–698

Lovegrove BG, Lawes MJ, Roxburgh L (1999) Confirmation of pleisiomorphic daily torpor in mammals: the round-eared elephant shrew *Macroscelides proboscideus* (Macroscelidea). J Comp Physiol B 169:453–460

Lovegrove BG, Raman J, Perrin MR (2001a) Heterothermy in elephant shrews, *Elephantulus* spp. (Macroscelidea): daily torpor or hibernation? J Comp Physiol B 171:1–10

Lovegrove BG, Raman J, Perrin MR (2001b) Daily torpor in elephant shrews (Macroscelidea: *Elephantulus* spp.) in response to food deprivation. J Comp Physiol B 171:11–21

Lowell BB, Spiegelman BM (2000) Towards a molecular understanding of adaptive thermogenesis. Nature 404:652–660

Lyman C, Willis J, Malan A, Wang LCH (1982) Hibernation and torpor in mammals and birds. Academic Press, New York

Lynch G (1973) Seasonal changes in thermogenesis, organ weights, and body composition in the white-footed mouse, *Peromyscus leucopus*. Oecologia 13:363–376

McKechnie AE, Mzilikazi N (2011) Heterothermy in afrotropical mammals and birds: a review. Integr Comp Biol 51:R349–R363

Mzilikazi N, Lovegrove BG (2004) Daily torpor in free-ranging rock elephant shrews, *Elephantulus myurus*: a year-long study. Physiol Biochem Zool 77:285–296

Mzilikazi N, Lovegrove BG (2005) Daily torpor during the active phase in free-ranging rock elephant shrews (*Elephantulus myurus*). J Zool Lond 267:103–111

Mzilikazi N, Lovegrove BG (2006) Noradrenalin induces thermogenesis in a phylogenetically ancient eutherian mammal, the rock elephant shrew, *Elephantulus myurus*. J Comp Physiol B 176:75–84

Mzilikazi N, Lovegrove B, Ribble DO (2002) Exogenous passive heating during torpor arousal in free-ranging rock elephant shrews, *Elephantulus myurus*. Oecologia 133:307–314

Mzilikazi N, Jastroch M, Meyer CW, Klingenspor M (2007) The molecular and biochemical basis of nonshivering thermogenesis in an African endemic mammal, *Elephantulus myurus*. Am J Physiol 293:R2120–R2127

Mzilikazi N, Meyer C, Klingenspor M (2008) Towards ecological relevance: a comparison of physiological and molecular evidence for the presence of adaptive, UCP1-mediated non-shivering thermogenesis in mammals. In: Lovegrove BG, McKechnie AE (eds) Hypometabolism in animals. University of KwaZulu-Natal, Pietermauritzburg, pp 209–214

Pinheiro J, Bates D, DebRoy S, Sarkar D (2006) nlme: Linear and nonlinear mixed effect models. R package version 3:1–77

Poppitt SD, Speakman JR, Racey PA (1994) Energetics of reproduction in the lesser Hedgehog Tenrec, *Echinops telfairi*. Physiol Zool 67:976–994

R Development Core Team (2006) R: A language and environment for statistical computing. R Foundation for Statistical Computing, Vienna, ISBN 3-900051-07-0, http://www.R-project.org

Rathbun GB (2009) Why is there discordant diversity in sengi (Mammalia: Afrotheria: Macroscelidea) taxonomy and ecology? Afr J Eco 47:1–13

Robinson TJ, Seiffert ER (2004) Afrotherian origins and interrelationships: new views and future prospects. Curr Top Dev Biol 63:37–60

Saarela S, Hissa R (1993) Metabolism, thermogenesis and daily rhythm of body temperature in the wood lemming, *Myopus schisticolor*. J Comp Physiol B 163:546–555

Scantlebury M, Lovegrove BG, Jackson CR, Bennett NC, Lutermann H (2008) Hibernation and non-shivering thermogenesis in the Hottentot golden mole (*Amblysomus hottentottus longiceps*). J Comp Physiol B 178:887–897

Scholl P (1974) Temperaturregulation beim madegassischen Igeltanrek *Echinops telfairi*. J Comp Physiol 89:175–195

Skinner J, Chimimba C (2005) The mammals of the Southern African subregion. Cambridge University Press, Cape Town

Smit B, McKechnie AE (2010) Avian seasonal metabolic variation in a subtropical desert: basal metabolic rates are lower in winter than in summer. Funct Ecol 24:330–339

Springer MS, Cleven GC, Madsen O, de Jong WW, Waddell VG, Amrine HM, Stanhope MJ (1997) Endemic African mammals shake the phylogenetic tree. Nature 388:61–64

Stawski C, Turbill C, Geiser F (2009) Hibernation by a free-ranging subtropical bat (*Nyctophilus bifax*). J Comp Physiol B 179:433–441

Sundin U, Moore G, Nedergaard J, Cannon B (1987) Thermogenin amount and activity in hamster brown fat mitochondria: effect of cold acclimation. Am J Physiol 252:R822–R832

Warnecke L, Geiser F (2010) The energetics of basking behaviour and torpor in a small marsupial exposed to simulated natural conditions. J Comp Physiol B 180:437–445

Warnecke L, Turner JM, Geiser F (2008) Torpor and basking in a small arid zone marsupial. Naturwissenschaften 95:73–88

Withers PC (1977) Measurement of VO2, VCO2, and evaporative water loss with a flow-through mask. J Appl Physiol 42:120–123

Wunder BA, Gettinger RD (1996) Effects of body mass and temperature acclimation on the non-shivering thermogenic response of small mammals. In: Geiser F, Hulbert AJ, Nicol SC (eds) Adaptations to the cold: tenth international hibernation symposium. University of New England Press, Armidale, pp 131–139

BROWN FAT IN A ´PROTOENDOTHERMIC´ MAMMAL FUELS THE PARENTAL CARE MODEL OF MAMMALIAN EVOLUTION

R. OELKRUG ∞ N. GOETZE ∞ C. EXNER ∞ L. YANG ∞ G.K. GANJAM ∞ M. KUTSCHKE ∞ S. MÜLLER ∞ S. STÖHR ∞ M.H. TSCHÖP P.G. CRICHTON ∞ G. HELDMAIER ∞ M. JASTROCH ∞ C.W. MEYER

BROWN FAT IN A ´PROTOENDOTHERMIC´ MAMMAL FUELS THE PARENTAL CARE MODEL OF MAMMALIAN EVOLUTION

Rebecca Oelkrug[1], Nadja Goetze[1], Cornelia Exner[1], Yang Lee[3], Goutham K. Ganjam[1†], Maria Kutschke[2], Saskia Müller[2], Sigrid Stöhr[1], Matthias H. Tschöp[2], Paul G. Crichton[3], Gerhard Heldmaier[1], Carola W. Meyer[1, 2] and Martin Jastroch[2]

Endothermy has facilitated mammalian species radiation and led to multiple evolutionary models of its origin. Yet, to date, these models lack molecular evidence. Here, we studied the Lesser hedgehog tenrec (*Echinops telfairi*), a phylogenetically ancient, extant 'protoendothermic' mammal, in which constantly high body temperatures were reported only during pregnancy and parental care. Evidence for nonshivering thermogenesis (NST) was found *in vivo* during periodic ectothermic-endothermic transitions. Anatomical studies revealed large brown fat-like structures in the proximity of the reproductive organs. Biochemical analysis demonstrated cold-induced recruitment of oxidative capacity and a high mitochondrial proton leak catalyzed by an uncoupling protein 1 (UCP1) ortholog. Strikingly, bioenergetic profiling of tenrec UCP1 revealed similar thermogenic potency as modern mouse UCP1, despite the large phylogenetic distance. The inevitable use of NST during reproduction and the unusual anatomic location of brown adipose tissue (BAT) support the parental care model, linking BAT directly to the evolutionary onset of sustained Eutherian endothermy.

[1]Department of Animal Physiology, Faculty of Biology, Philipps-Universität, Karl-von-Frisch Strasse 8, 35043 Marburg, German, [2]Institute for Diabetes and Obesity, Helmholtz Zentrum München, German Research Center for Environmental Health (GmbH), Munich, Germany, [3]Medical Research Council, Mitochondrial Biology Unit, Hills Road, Cambridge CB2 0XY, UK, [†]Current address: Institute of Pharmacology and Clinical Pharmacy, Faculty of Pharmacy, Philipps-Universität, Karl-von-Frisch Strasse 1, 35043 Marburg, Germany. Correspondence and requests for materials should be addressed to C. W. Meyer (carola.meyer@helmholtz-muenchen.de) or M. Jastroch (martin.jastroch@helmholtz-muenchen.de).

The discovery of evolutionary events that allowed mammals to generate and sustain high body temperatures (Tb) is one of the most intriguing, and still unresolved, questions in the evolutionary physiology of vertebrates[1-3]. A variety of evolutionary models promote high Tb as a facilitator of higher resting metabolic rate (RMR), which may represent selection benefits[4-6]. Other models, however, favour the idea that high metabolic rates are instead a secondary consequence of increased exercise, increased brain size and high aerobic capacity, arguing that the advantages of high Tb *per se* are insufficient to compensate for the energetic costs[7]. Evolutionary ecologists agree that decreasing juvenile mortality and accelerating growth to maturity are among the most effective ways of increasing species fitness[8], leading to the hypothesis that the benefits of parental care are key in the undestanding of endothermic convergence between mammals and birds[2, 5].

During mammalian evolution, there is increasing archaeological evidence that early mammals were rather small, and, though not having to cope with extreme cold climates, endothermy at unfavourable body surface-to-volume ratios possibly required insulation and regulatory heating abilities[6]. Recent Eutherian mammals regulate and maintain high Tbs by various physiological processes, including both shivering and nonshivering thermogenesis (NST, ref. 9). In many modern Eutherian mammals the major source of NST is brown adipose tissue (BAT), which is characterized by high mitochondrial content and the expression of uncoupling protein 1 (UCP1)[10]. UCP1 transports protons directly across the mitochondrial inner membrane, bypassing ATP production, thereby dissipating proton motive force as heat. For small sized mammalian species, the significance of BAT for the maintenance of high Tbs in the cold and for the arousal from torpid or hibernating states is well established[9, 11]. Yet an ultimate cause favouring the evolution of distinct anatomical depots with specific thermogenic properties has to be revealed. This is particularly intriguing as the evolutionary history of UCP1 dates back to the origin of teleost fishes about 420 million years ago[12].

To gain insight into the origins of NST and its role in the evolution of endothermy, we studied the Lesser hedgehog tenrec, *Echinops telfairi*, a member of the phylogenetically ancient Afrotherian clade of Eutherian mammals. The tenrec is considered 'protoendothermic' as Tb tracks closely to ambient temperature (Ta) in reptilian-like patterns, with only a few hours of endothermic periods[13]. Although having primitive thermoregulation, tenrec females maintain constantly high Tbs (~33°C) during pregnancy and periods of parental care[14].

Results

Similar to observations in the wild[13] all tenrecs in captivity showed pronounced Tb fluctuation even when kept at a relatively constant Ta (Fig. 1a, ref. 15). Tb nadirs decreased in the cold and were paralleled by a corresponding expansion of daily Tb amplitudes (Fig. 1b). As judged from the Tb distribution patterns, tenrecs were colder than 30°C for most of the time (Fig.1c). On average, minimal Tb was always 0.4-1.6°C higher than Ta. Tb maximized at 32°C, irrespective of Ta, reflecting the lowest Tbs of Eutherians among egg-laying monotremes and

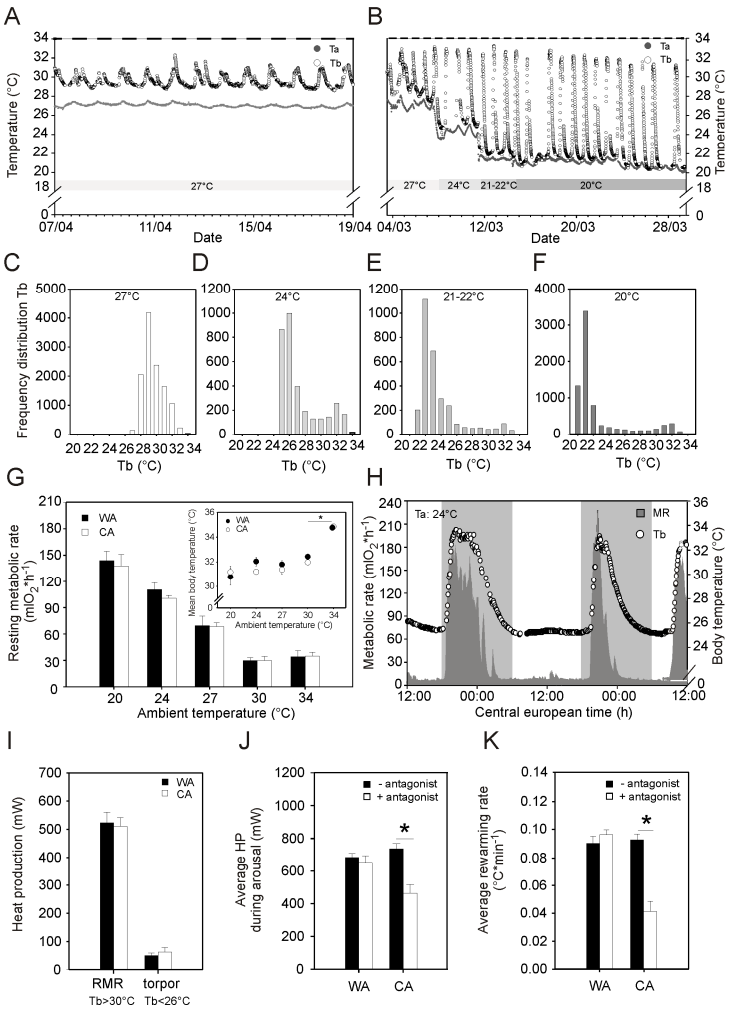

Figure 1: Thermoregulatory behavior of *E. telfairi*. a-b) Representative Tb traces of a WA (a, WA, Ta =27°C) and a successively CA acclimated (b, 27°C to 20°C) tenrec. c-f) Tb histograms at different Tas (N=6 per chart). g) Mean RMR and Tb ± SD (inset graph) over a range of Tas, determining the TNZ (WA: N=5-6; CA: N=6; *P=0.001, Students t-test). h) Temporal-resolved thermogenic profile, including heating events from hypothermia. i) Heat production (HP) during euthermia and hypometabolism. j-k) Average HP and average rewarming rates during arousal, calculated over the same temperature range of 25.5-29.75°C, with or without injection of the β3-adrenergic antagonist SR 59230A (see also Supplemental fig. 1) (N=5 per group; P< 0.05 paired t-test).

"poikilothermic" Naked mole-rats (*Heterocephalus glaber*)[16]. The brief daily episodes of high Tb were regularly observed during the dark phase of the light/dark cycle, but tenrecs never remained homeothermic at this level for more than 6 hours. Notably, all tenrecs were capable of rewarming from hypothermia in the absence of exogenous sources of heat. We frequently observed animals feeding while still at low Tb, and then rewarming to >30°C, which was always accompanied by visible shivering.

Using combined indirect calorimetry and Tb telemetry the thermoneutral zone of warm (WA) and cold acclimated (CA) *E. telfairi* was determined for the first time, revealing a thermal window of 30 to <34°C in both groups (Fig. 1g). The RMRs at thermoneutrality were exceptionally low as compared to similar sized members of higher mammalian orders (e.g. *Glis glis*, ref. 17). Below 30°C, cold induced regulatory thermogenesis was evident by an increase in RMRs with decreasing Ta. In contrast, at 34°C, cessation of active thermoregulation was evident by a diminished Tb – Ta gradient (Fig. 1g insert), with animals obviously suffering from heat stress.

The heat production patterns of *E. telfairi* were recorded for at least two episodes of arousal from hypometabolism for each individual (Fig. 1h). The minimal metabolic rate prior to arousal was about 9 ml O_2*h^{-1} (~ 50mW), equivalent to an almost 10-fold reduction compared to resting heat production levels for each group (Figure 1i).

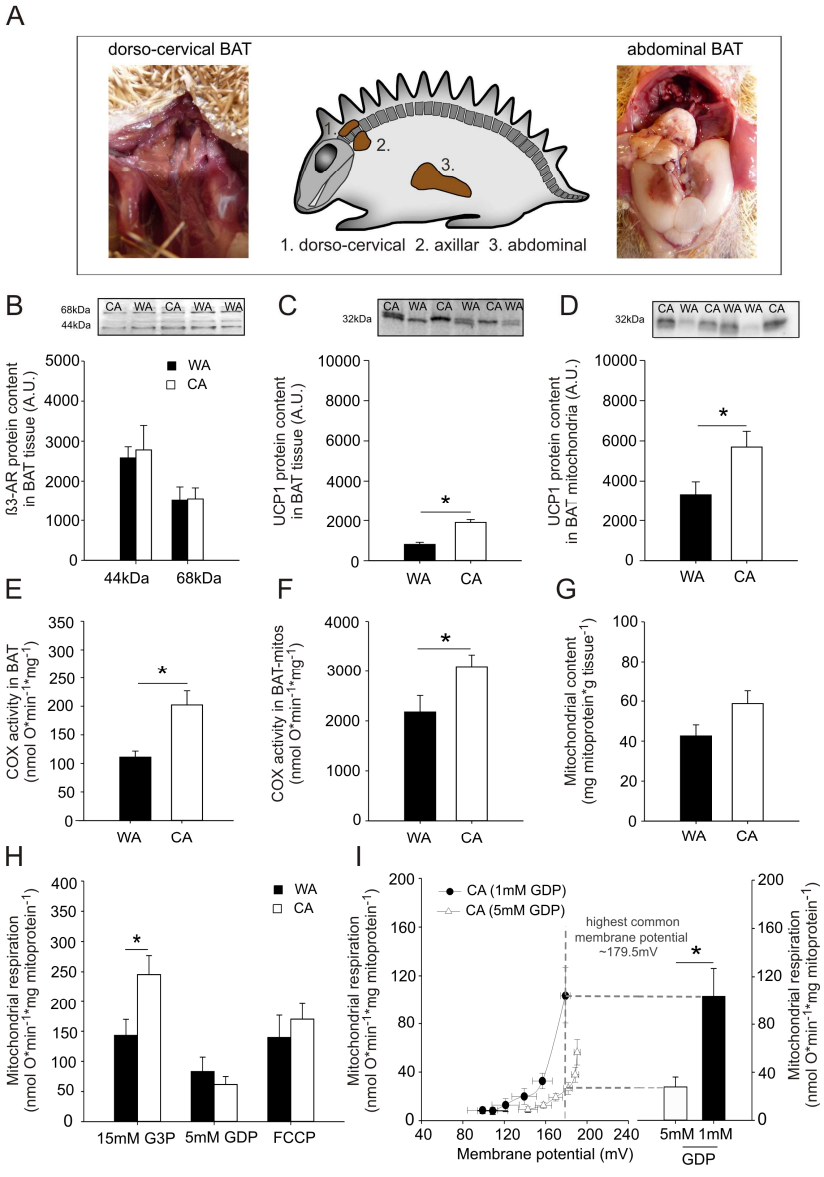

Figure 2: Morphological, molecular and biochemical evidence for BAT, adaptive NST and functional UCP1. a) Anatomical location of tenrec BAT. b-d) Immunological detection of b) β3-adrenoreceptor protein subunits in tissue homogenates, c) UCP1 in tissue homogenates and d) in isolated mitochondria, revealing cold-induction. e-f) Cytochrome C oxidase (COX) activity in BAT homogenates and isolated mitochondria, demonstrating increased oxidative capacity in the cold. g) Mitochondrial content, estimated from the ratio of tissue to mitochondrial COX activity. (* P<0.05 Students t-test (c-e), Rank sum test (b)). h-i) Mitochondria respiration rates and proton leak kinetics of isolated BAT mitochondria in response to GDP, FCCP and 5 mM GDP (N=4-5; P<0.05 paired t-test).

In modern Eutherian mammals, classical NST is mediated via beta 3- adrenergic receptor signalling in BAT[9]. In CA tenrecs, treatment with the β3-adrenergic antagonist SR 59230A at the onset of arousal from hypometabolism significantly reduced heat production (Fig.1j, P=0.008) and rewarming rates (Fig. 1k, P=0.021), supporting inhibition of adaptive NST that classically replaces shivering thermogenesis in the cold.

Anatomical inspection post mortem identified small brown fat patches in the typical dorso-cervical and axillar region while, surprisingly, a large depot of brown fat-like tissue was located in the abdominal region, adjacent to the reproductive organs (~ 60-70% of total BAT, Fig. 2a). The presence of β3-adrenoreceptors was corroborated by immunological detection in brown fat homogenates. While β3-adrenoreceptor content was unchanged in response to cold acclimation (Fig. 2b), differential recruitment of NST was reflected in increased oxidative capacity of tissue and mitochondria of CA tenrecs (measured as cytochrome c oxidase (COX) activity, Fig. 2e-g). Further immunological analysis of this tissue suggested cold-induced expression of UCP1 (Fig. 2c, d), and this detection was confirmed using an anti-hamster UCP1 antibody and cloning of the tenrec UCP1 cDNA.

Intact BAT mitochondria, energized with glycerol-3-phosphate (G3P) in a temperature-controlled chamber at 32°C,

showed significantly higher respiration rates in CA tenrecs (Fig. 2h). This difference was most likely caused by UCP1 proton leak activity as addition of guanosine diphosphate (GDP), an UCP1 inhibitor, decreased the respiration rate by 40% and 76% in WA and CA animals, respectively. Next, we assessed mitochondrial proton conductance by measuring proton leak kinetics as flux-force curves of

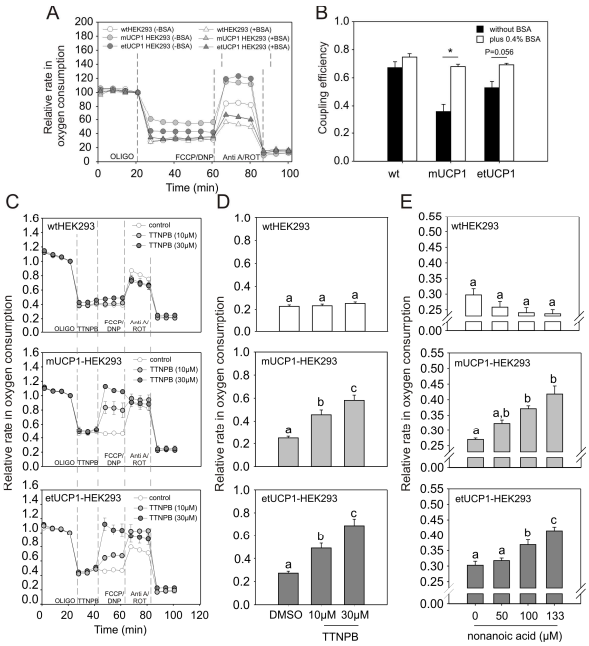

Figure 3: Comparative bioenergetic profiling of tenrec (et) and mouse (m)UCP1 in HEK293 cells. a) Representative traces of normalized plate-based respirometry, showing basal respiration, proton leak respiration (after oligomycin treatment), maximal substrate oxidation (FCCP or DNP) and non-mitochondrial respiration (antimycin A/rotenone). b) BSA-sensitive coupling efficiency (white bars) of mUCP1 and etUCP1 containing HEK293 cells (N=5 per group and condition; *P<0.05, Students t-test). c-e) Specific activation of stably expressed mUCP1) and etUCP1, in comparison to wild-type wtHEK293 (N=5-6; P<0.001, One Way ANOVA).

mitochondrial respiration and membrane potential (Fig. 2i). As mitochondria were fully uncoupled under basal conditions, measurement of proton motive force (membrane potential in the presence of nigericin) required the addition of 1mM GDP. Increasing the concentration to 5 mM GDP fully recoupled the mitochondria, shifting proton leak kinetics significantly downwards, demonstrating that UCP1 catalyzes the major proportion of proton conductance. For further comparative bioenergetic characterization tenrec etUCP1 and mouse mUCP1 orthologs were stably transfected in HEK293 cells and functionally analyzed using plate-based respirometry of intact cells. Comparing the respiration profiles and coupling efficiencies of HEK293 cells in the presence and absence of bovine serum albumin (BSA) confirmed that residual fatty acids induced proton leak respiration (oligomycin-insensitive) selectively in UCP1-containing cells (Fig. 3a, b). Residual fatty acids in the absence of BSA, however, were also oxidized and contributed to mitochondrial substrate oxidation as judged by increased FCCP-induced respiration (Fig 3a). Specific activation of UCP1 was confirmed using the retinoic acid analogue TTNPB, which activates UCP1 but is not metabolized (Fig. 3c, d)[18]. Furthermore, we activated UCP1 in the intact cell with nonanoic acids that do not require conjugation to BSA and readily diffuse into the HEK293 cells. The bioenergetic profile of tenrec and mouse UCP1 revealed a similar dose-dependency for these small molecular activators (Fig. 3d, e). Notably, there was no activator effect on wild-type HEK293 cells.

Despite demonstrating similar molecular activators of etUCP1 and mUCP1 the question remained whether these orthologs differ in their specific activities as a result of their distant phylogenetic relationship. For comparative molecular characterization of etUCP1, we isolated mitochondria from HEK293 cells and measured proton leak kinetics of wild-type, mouse and tenrec UCP1-containing HEK293 cell mitochondria (Fig. 4a, c). Basal, palmitate-induced and GDP-inhibited UCP1 activity was similar to that of native BAT mitochondria. The decrease of proton leak to wild-type levels by addition of GDP demonstrated full inhibition of both mUCP1 and etUCP1. For quantitative functional comparison of etUCP1 and mUCP1, we normalized the proton leak curves to UCP1 content using overexpressed and purified UCP1 orthologs as mass standards. Next, we subtracted the GDP-insensitive basal proton leak from the UCP1 leak under control conditions. The resulting specific UCP1 catalytic activity did not differ between mouse and tenrec UCP1 (Fig. 4d), suggesting the full functional potential of UCP1 was present at the evolutionary stage of Afrotherian divergence, prior to mammalian migration to the cold.

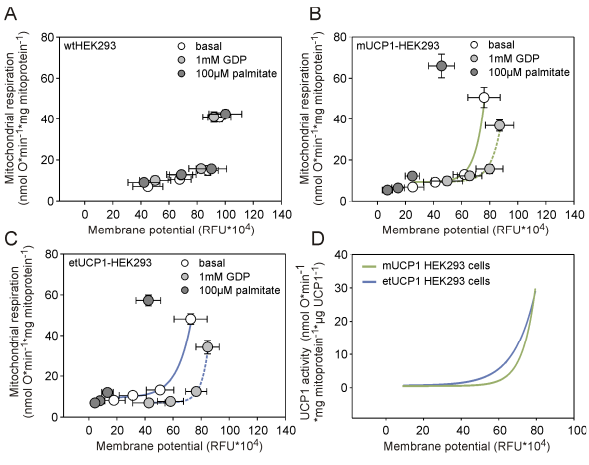

Figure 4: Determination of catalytic center activities of tenrec and mouse UCP1 in isolated HEK293 cell mitochondria. a-c) Proton leak kinetics of wildtype (wt), mUCP1 and etUCP1 HEK293 cells, under basal conditions and after activation with 100µM palmitate and after inhibition with 1mM GDP (N=6 per group and condition) d) Specific UCP1 activity curves reveal similar catalytic power of tenrec and mouse UCP1 (derived from 4b/c).

Obligatory thermogenesis in mammals conveys energetic costs that need to be outweighed by fitness gain, a tenet that has provoked controversial discussions on the events leading to the evolution of endothermy[1-8]. The protoendothermic tenrec provides molecular and functional evidence that NST by brown adipose tissue facilitates periodic endothermy during intermittent episodes of homoeothermy. As judged from the anatomical distribution of BAT, NST is likely to be particularly relevant during periods of gamete and offspring incubation. Our study therefore supports a direct link between BAT and parental care as the driving force for endothermy at the evolutionary roots of mammalian thermogenesis.

Methods summary

Further detailed experimental procedures are described in the supplementary materials[15].

Animal experiments - Experiments were performed on laboratory bred, adult Lesser hedgehog tenrecs (*Echinops telfairi*; N=8 females and N=4 males) during their annual activity period. Tenrecs were surgically implanted with temperature sensitive transmitters (Minimitter, Model X, Sunriver, OR, USA, accuracy 0.1°C) for monitoring abdominal core Tb. Metabolic rate (MR) measurements were based on the principle of indirect calorimetry using a 2-channel, open circuit respiratory system as described previously[19]. We calculated arousal and rewarming rates where arousal occurred spontaneously or arousal was induced by disturbing the animals[11]. For determination of BAT-derived non-shivering thermogenesis, each tenrec received a single subcutaneous injection of the ß3-adrenergic antagonist SR 59230A (3-(2-Ethylphenoxy)-1-[[(1S)-1,2,3,4-tetrahydronaphth-1-yl]amino]-(2S)-2-propanol oxalate salt, Sigma)[20] at a dosage of 1 mg*kg^{-1}. Animal experimental procedures were approved by the German Animal Welfare Authorities.

Molecular experiments - We dissected animals to identify and locate BAT depots. Tissue samples were collected and used to confirm the expression of UCP1 mRNA and protein, perform COX activity and proton leak measurements similar to ref. 21. Analysis of UCP1 in HEK293 cells, the tenrec UCP1 cds (BankIt1580920) was transcribed to cDNA and cloned into a pcDNA3 vector and analysis performed as established in ref. 22.

Statistical analysis - The paired t-test was used to test for effects of the β3-adrenergic antagonist within the CA and WA group, the Students t tests was used to test for differences between the acclimation groups. Differences in proton leak respiration rates of UCP1-containing cells activated with various concentrations of TTNPB or nonanoic acids were determined with a One Way Anova analysis. We calculated the UCP1 centre activity of mouse and tenrec UCP1 with a dynamic fitting exponential growth curve (Single, 3 Parameter, f=y0+a*exp(b*x)). These analyses were performed using SigmaStat (Jandel ScientiWc, San Rafael, California). All mean values were reported ± Standard Error (SE) and the 0.05 level of probability was accepted as indicating statistical significance.

Acknowledgements

This work was supported by the German Research Foundation (DFG, grant #HE-990 to GH and CWM). We would like to thank Gabor Szerencsi and Mechthild Zissel for helpful assistance. The authors declare no conflict of interest.

Literature

1. Crompton, A. W., Taylor, C. R. & Jagger, J. A. Evolution of homeothermy in mammals. Nature **272**, 333-336 (1978).
2. Koteja, P. Energy assimilation, parental care and the evolution of endothermy. *Proc. Biol. Sci.* **267**, 479-84 (2000).
3. Lovegrove, B. G. The evolution of endothermy in Cenozoic mammals: a plesiomorphic- apomorphic continuum. *Biol. Rev. Camb. Philos. Soc.* **87**, 128-162 (2012).
4. McNab, B. K. The evolution of homeothermy in the phylogeny of mammals. *Amer. Nat.* **112**, 1-21 (1978).
5. Farmer, C. G. Parental care: the key to understanding endothermy and other convergent features in birds and mammals. *Am. Nat.* **155**, 326-334 (2000).
6. Clarke, A. & Portner, H. Temperature, metabolic power and the evolution of endothermy. *Biol. Rev. Camb. Philos. Soc.* **85**, 703-727 (2010).
7. Bennett, A. F. & Ruben, J. A. Endothermy and activity in vertebrates. *Science* **206**, 649-654 (1979).
8. Kozlowski, J. Optimal allocation of resources to growth and reproduction: implications for age and size at maturity. *Trends. Ecol. Evol.* **7**, 15-19 (1992).
9. Cannon, B. & J. Nedergaard, J. Brown adipose tissue: function and physiological significance. *Physiol. Rev.* **84**, 277-359 (2004).
10. Nicholls, D. G. & Locke, R. M. Thermogenic mechanisms in brown fat. *Physiol. Rev.* **64**, 1-64 (1984).
11. Oelkrug, R., Heldmaier, G. & Meyer, C. W. Torpor patterns, arousal rates, and temporal organization of torpor entry in wildtype and UCP1-ablated mice. *J. Comp. Physiol. B* **181**, 137-145 (2011).
12. Jastroch, M., Wuertz, S., Kloas, W. & Klingenspor, M. Uncoupling protein 1 in fish uncovers an ancient evolutionary history of mammalian nonshivering thermogenesis. *Physiol. Genomics* **22**, 150-156 (2005).
13. Lovegrove, B. G. & Genin, F. Torpor and hibernation in a basal placental mammal, the Lesser hedgehog tenrec *Echinops telfairi*. *J. Comp. Physiol. B* **178**, 691-698 (2008).
14. Poppitt, S. D., Speakman, J. R. & Racey, P. A. Energetics of Reproduction in the Lesser hedgehog tenrec, *Echinops telfairi* (Martin). *Physiol. Zool.* **67**, 976-994 (1994).
15. Materials and methods are available as supplementary materials on *Nature* online.
16. Urison, N. T. & Buffenstein, R. Shifts in thermoregulatory patterns with pregnancy in the poikilothermic mammal-the Naked mole-rat (*Heterocephalus glaber*). *J. of Therm. Biol.* **19**, 395-371 (1994).
17. Elvert, R. & Heldmaier, G. Cardiorespiratory and

metabolic reactions during entrance into torpor in dormice, *Glis glis*. *J. Exp. Biol.* **208**, 1373-1383 (2005).
18. Rial, E. *et al.*, Retinoids activate proton transport by the uncoupling proteins UCP1 and UCP2. *EMBO J.* **18**, 5827-5833 (1999).
19. Heldmaier, G. & Ruf, T. Body temperature and metabolic rate during natural hypothermia in endotherms. *J. Comp. Physiol. B* **162**, 696-706 (1992).
20. Swoap S.J. & Weinshenker D. Norepinephrine controls both torpor initiation and emergence via distinct mechanisms in the mouse. *PLoS One* **3**, e4038 (2008).
21. Mzilikazi, N., Jastroch, M., Meyer, C. W. & Klingenspor, M. The molecular and biochemical basis of nonshivering thermogenesis in an African endemic mammal, *Elephantulus myurus*. *Am. J. Physiol. Regul. Integr. Comp. Physiol.* **293**, 2120-2127 (2007).
22. Jastroch M., Hirschberg V. & Klingenspor M. Functional characterization of UCP1 in mammalian HEK293 cells excludes mitochondrial uncoupling artefacts and reveals no contribution to basal proton leak. *Biochim. Biophys. Acta*, **1817**, 1660-70 (2012).

SUPPLEMENTS

SUPPLEMENTAL MATERIAL FOR CHAPTER II:

UNCOUPLING PROTEIN 1 DECREASES SUPEROXIDE PRODUCTION IN BROWN ADIPOSE TISSUE MITOCHONDRIA

S1 Titration of mitochondrial respiration with GDP and glycerol-3-phosphate

a) Brown adipose tissue mitochondria possess low contents of ATP-synthase preventing the use of conventional determination of respiratory control as a ratio of state3/state4 respiration. Therefore we tested mitochondrial integrity by re-coupling respiration by successive addition (1-5mM) of GDP which inhibits UCP1 activity. Oxygen consumption was measured using a Clark-type oxygen electrode maintained at 37°C and calibrated with air-saturated medium which was assumed to contain 406 nmol O ml^{-1}. Prior to GDP addition, mitochondria of cold acclimated animals were incubated in a medium containing 2µM oligomycin and 4.8µM rotenone. Mitochondria were then energized with 4 mM succinate.

b) Stepwise addition of glycerol-3-phosphate (4, 7, 10, 13 and 16 mM) was used to determine the dose-response of mitochondrial respiration, similar to the GDP titration.

c) To measure superoxide production glycerol-3-phosphate was added at different concentration (5, 10, 15 mM) to wildtype and UCP1-ablated mitochondria which were previously incubated in a medium containing oligomycin (2µM), SOD (30U/ml), HRP (6 U/ml) and the reagent Amplex Red (50µM) which fluorescent was measured at 37°C in a microplate reader. Glycerol-3-phosphate experiments were performed from brown adipose tissue mitochondria of individual animals kept at 30°C.

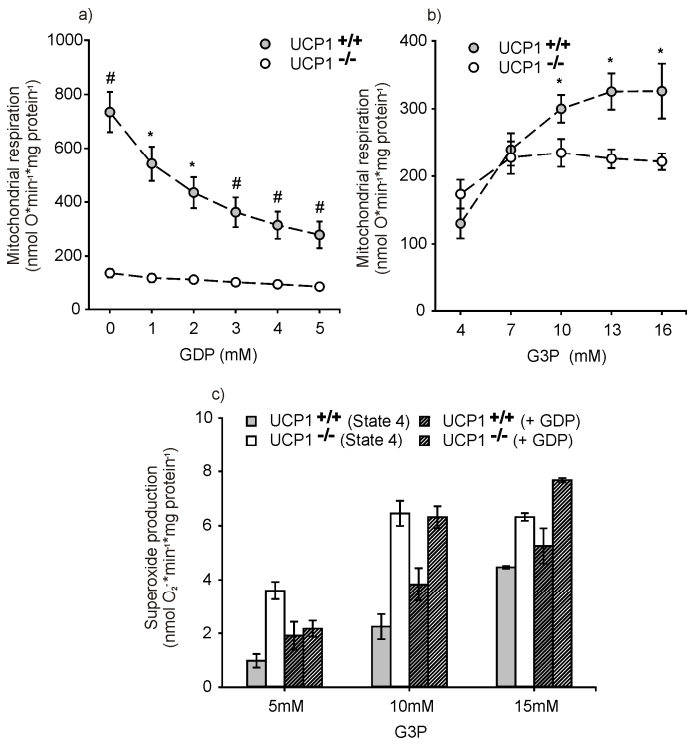

S. 1: Mitochondrial respiration and superoxide production in response to different concentrations of GDP and glycerol-3-phosphate in brown adipose tissue mitochondria. a) State 4 respiration of brown adipose tissue mitochondria from cold acclimated wildtype (n=5) and UCP1-ablated (n=7) mice was titrated by successive addition of GDP. Generally, 5mM GDP was sufficient to nearly fully re-couple mitochondria (60% reduction of respiration in wildtype mitochondria) and was used in further experiments (*$p<0.05$ and Student's t-test). Respiratory control of UCP1-wildtype mitochondria was calculated to be about 3. b) Titration was performed using mitochondria of warm acclimated wildtype (n=7) and UCP1-ablated (n=7) mice. Mitochondrial respiration rate of wildtype and UCP1-ablated mitochondria diverged above 7 mM G3P and further increased in wildtype mitochondria. c) Superoxide production was dependent on G3P substrate concentration. State 4 superoxide production as well as superoxide production after inhibition of UCP1 with GDP (5mM) was measured. Importantly, the GDP effect on superoxide production altered in response to substrate availability (b; *$p<0.05$ Student's t-test).

S2 Role of the ANT in ROS production of brown adipose tissue mitochondria

Superoxide production rate was measured in wildtype and UCP1-ablated mitochondria which were incubated in a medium containing oligomycin (2µM), SOD (30U/ml), HRP (6 U/ml), Amplex Red (50µM) and carboxyatractylate (CAT; 2.5 nM) to distinguish from adenine-nucleotide transporter-dependent effects. We used GDP (5mM) to inhibit UCP1 and rotenone (2µM) to evaluate the complex I dependent superoxide production. Experiments were performed from brown adipose tissue mitochondria of individual animals kept at 5°C.

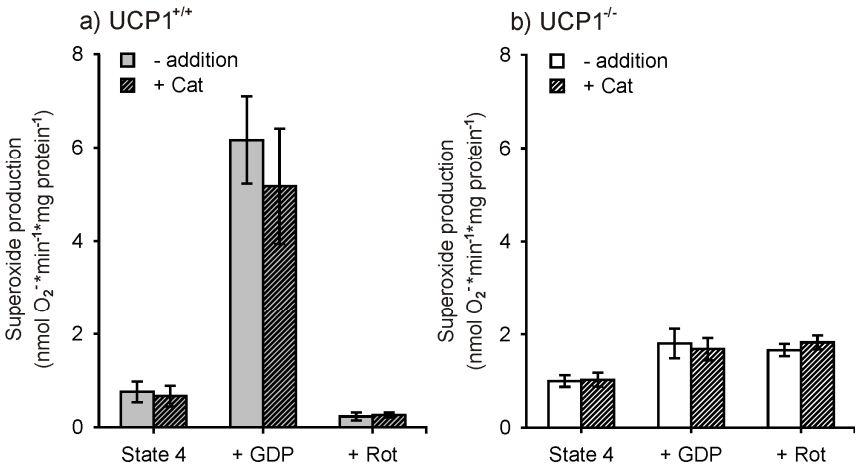

S. 2: Superoxide production of cold acclimated wildtype (UCP1$^{+/+}$) and UCP1-ablated (UCP1$^{-/-}$) brown adipose tissue mitochondria in the absence of ANT uncoupling activity. Superoxide production was measured after energizing mitochondria with succinate (5mM) and either with or without carboxyatractylate (CAT) (2.5µM). We could observe no effect of ANT-Inhibition on superoxide production of wildtype (n=5) and UCP1-ablated (n=7) mice in every treatment, indicating that the ANT has no function in prevention of oxidative stress.

S3 NAD(P)H-autofluorescence

NAD(P)H autofluorescence was determined at 365 nm excitation and 450 nm emission wavelengths, respectively. Conditions were identical to those used during the measurement of Amplex red fluorescence. Fluorescence units were corrected by subtraction of values without substrate. Fluorescence was measured in response to malate (3mM), pyruvate (5mM), pyruvate/malate (3mM/5mM), palmitate (20µM), or palmitate/malate (20µM/ 3mM). 100% reduction of NAD(P)H was induced by addition of rotenone (4.8µM). This value served to calculate the proportion of NAD(P)H reduction during substrate oxidation.

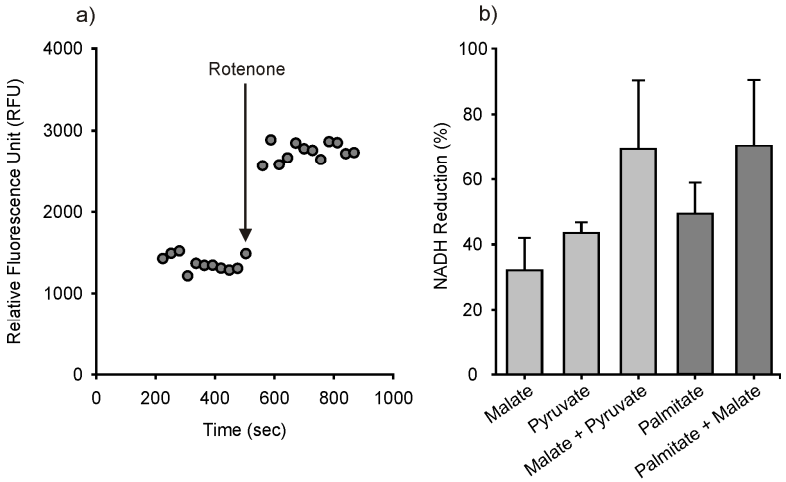

S. 3: NAD(P)H reduction in isolated mitochondria respiring on different substrates. To determine the substrate dependent NAD(P)H reduction, the reaction used for superoxide production measurements was used, but emission (450 nm) and excitation (365 nm) wavelength changed to measure NAD(P)H autofluorescence. a) Representative trace of NADH-autofluorescence is shown (palmitate+malate) expressed in relative fluorescence units (RFU). b) Percentage of NAD(P)H reduction determined after maximal reduction induced by addition of 4.8µM rotenone (complex I inhibitor).

EFFECTS OF LONG TERM COLD EXPOSURE ON SKELETAL MUSCLE MITOCHONDRIA FROM UCP1-DEFICIENT MICE

BACKGROUND

Heat produced by UCP1 activity in brown adipose tissue mitochondria is widely accepted as a major contributor to nonshivering thermogenesis in small mammals (Nicholls and Locke 1984). Nevertheless the contribution of alternative mechanisms to this form of endogenous heat production has been questioned frequently in the past (Block 1994, Lowell and Spiegelman 2000). Even though UCP1-deficient mice are cold sensitive, they can maintain their body temperature at an ambient temperature of 4°C for several weeks, provided that they were acclimated to 18°C initially (Golozobouva et al. 2001). Somehow they can compensate for the loss of functional brown adipose tissue by the recruitment of other sources of endogenous heat production. However, Golozobouva et al. (2001) postulated that no alternative mechanisms of heat production exist, as animals did not decrease their shivering intensity during the cold acclimation process. From their point of view the initial acclimation to 18°C was "a sufficient muscle training period to allow for the subsequent survival at 4°C" and therefore can be rated as a weak form of "adaptive (shivering) thermogenesis". This assumption has been further verified by Shabalina et al. in 2010. Moreover, muscle shivering thermogenesis (Aydin et al. 2008, Monemdjou et al. 2000) and accelerated metabolic flux in white adipose tissue (Anunciado-Koza et al. 2008, Granneman et al. 2003, Meyer et al. 2010, Ukropec et al. 2006) have been suggested as alternative heating pathways. The mechanism itself appears less efficient and disadvantageous as the median survival rate of UCP1-ablated mice decreases from 24 to 13 weeks in the cold (compared to wild-type mice).

The results of chapter II clearly demonstrated that UCP1 ablation negatively influences the production of superoxide in brown adipocytes, a physiological condition that could possibly affect the life span of an animal ("uncoupling to survive", Brand 2000). However, it seems unlikely that the elevated reactive oxygen species production (ROS) in brown adipose tissue mitochondria alone causes such a dramatic decrease of the survival rates of UCP1-ablated mice in the cold. The likelihood is higher, that endurance shivering led to an accumulation of ROS in skeletal muscle mitochondria, thereby increasing the probability of serious cell damage and decreasing the ability for sustained shivering thermogenesis. Shivering involves contractile activity of skeletal muscles and can therefore be interpreted as a form of exercise. Exercise is discussed as a condition increasing the risk for oxidative damage (Cooper et al. 2002, Parker et al. 2008). Cold exposed UCP1-ablated mice shiver without interruption, an intensity that should result in robust effects of skeletal muscle mitochondria.

The uncoupling protein 3 (UCP3) is a UCP1 paralogue that is predominantly expressed in skeletal muscle mitochondria (Boss et al. 1998). While a thermogenic function of UCP1 has been well-established in the last years (Nicholls and Rial 1999, Cannon and Nedergaard 2004), the main function of UCP3 is rather vague. However, mild uncoupling of the electron transport chain is currently the most compelling candidate (Brand and Esteves 2005). Talbot and Brand (2005) recently confirmed that UCP3 mildly uncouples skeletal muscle mitochondria when superoxide levels increase, similar to the uncoupling function of UCP1. Aconitase is a mitochondrial enzyme responsible for the convertion of citrate to isocitrate in the tricarboxylic acid cycle. ROS inactivates aconitase in the mitochondrial matrix (Janero and Hreniuk 1996) and conclusively the enzyme activity can be used as a marker for oxidative stress (Gardner 2002, Hausladen and Fridovich 1996). Mitochondria isolated from UCP3 deficient mice have higher oxidative stress and accordingly have decreased aconitase activity and increased markers of oxidative damage than wild-type mice (Vidal-Puig et al. 2000, Brand et al. 2002). Additionally it has been suggested that UCP3 contributes to the basal proton leak of skeletal muscle mitochondria of UCP1-deficient mice, thereby contributing to alternative mechanisms of heat production (Monemdjou et al. 2000). However, this evidence has been refuted in other studies (Meyer et al. 2010, Shabalina et al. 2010).

It might be possible that the premature death of UCP1 deficient mice exposed to 4°C occurs at a time point when the damage in shivering muscles becomes severe and shivering-induced thermogenesis can no longer be used for body temperature defense. This study aimed to further evaluate if cold exposure leads to an accumulation of ROS in the skeletal muscle of UCP1 deficient mice.

EXPERIMENTAL SETUP

Animals - We examined isolated skeletal muscle mitochondria of UCP1 deficient and wild-type mice acclimated to 30°C (thermoneutral) and 5°C (cold) according to the acclimation protocol of Oelkrug et al.

2010. The mice were fed ad libitum (Sniff 1534) with free access to water and kept on a 12 h of light/12 h of dark cycle. For experiments, the animals were kept in single cages. Wild type and UCP1-ablated mice were provided by Dr. Leslie Kozak (Pennington Medical Research Center), and littermates (genetic background C57Bl/6J) were derived from heterozygous breeding pairs in the animal facility of the Philipps-Universität of Marburg. In these mice the UCP1 gene has been disrupted by homologues recombination of a neomycin gene in exon 2 and parts of exon 3. Genotypes were identified using a PCR-based strategy which was validated post mortem on the protein level using western blot analysis (Oelkrug et al. 2010); female and male wild-type and UCP1-KO mice were included in this study. All experimental procedures were approved by the German Animal Welfare Authorities and were performed by Maria Kutschke and Dr. Martin Jastroch.

Mitochondrial Isolation - Mice were sacrificed and the pectoral muscle as well as all hindlimb muscles were removed and rapidly placed in ice cold buffer, mitochondria were isolated at 4°C as previously described (Keipert et al. 2010). In a few preparations the digestion step had to be slightly modified, instead of using a polytron for homogenization, the tissue samples were digested for 9 minutes on ice without an additional homogenization step. The protocol change had no effect on mitochondria quality and integrity. Mitochondrial protein concentrations were determined using the Biuret method.

Measurements of Mitochondrial Aconitase Activity - Mitochondrial aconitase activity was determined by a coupled assay: 1) The conversion of citrate to isocitrate by aconitase and 2) the decarboxylation of isocitrate to α-ketoglutarate by isocitrate dehydrogenase (ICDH). The second step includes the reduction of $NADP^+$ to NADPH, the absorbance of NADPH was measured at 340 nm in a 96-well microplate reader (BMG labtech, FLUOstar Optima) based on Gardner (2002). 20 µg of freshly isolated mitochondria were added to a well of a 96 well plate together with 200 µL of assay buffer (50 mM Tris-HCl, pH 7.4; 0.6 mM sodium citrate, pH 7.0; 0.2 mM $NADP^+$; 0.1% Triton X-100, 0.4 U/ml ICDH) pre-equilibrated to 37°C. The absorbance was measured at 340 nm over at least 20 min (or 70 cycles à 18 sec with shaking for 3 s after each cycle) at 37°C. To determine the background rate NADPH production was measured in the presence of the competitive aconitase inhibitor fluocitrate (95 µM; Stock 2 mM in 50 mM Tris-HCl).

Measurements of Mitochondrial Hydrogen Peroxide Release - Measurements of hydrogen peroxide production of isolated mitochondria were performed similarly to the procedures of Oelkrug et al. (2010). 35 µg of skeletal muscle mitochondria were incubated in 200 µl of pre-equilibrated assay buffer (50 mM KCl, 5 mM TES, 2 mM $MgCl_2$ $6H_2O$, 1 mM EGTA, bovine serum albumin 0.4% (w/v), pH 7.2 at room temperature) containing a mixture of the fluorescent probe Amplex Red (50 µM; Invitrogen), 30 units ml^{-1} superoxide dismutase (to convert superoxide to hydrogen peroxide), 6 units ml^{-1} horseradish peroxidase (catalyzing the reaction of hydrogen peroxide with Amplex Red resulting in fluorescent resorufin), and 2 µM oligomycin (to inhibit ATP synthase). Amplex Red reacts with H_2O_2 at a 1:1 stoichiometry, whereas the stoichiometry of conversion from superoxide to H_2O_2 is assumed to be 1:2. H_2O_2 formation was initiated by the addition of succinate (5 mM). Fluorescence was detected at 37°C in a microplate reader (BMG Labtech, FLUOstar Optima) in 96-well microplates (Greiner 96-Well, clear, F-Bottom, black). The excitation wavelength was set to 560-10nm, and the fluorescence emission was detected at 590 nm. Fluorescence was calibrated using known amounts of H_2O_2 at each experimental day. Optionally, superoxide production was measured in the presence of rotenone (2 µM, inhibiting complex I-derived reactive oxygen species production) and carboxyatractylate (2.5 nM) to distinguish from adenine nucleotide transporter-dependent effects.

RESULTS AND DISCUSSION

Superoxide production rates in isolated skeletal muscle mitochondria – Under thermoneutral conditions (30°C) skeletal muscle mitochondria of wild-type and UCP1-ablated mice had similar superoxide production rates in state 4 (basal or leak respiration, Fig. 9A). Cold acclimation caused an increase of mitochondrial hydrogen peroxide releasing rates of UCP1-ablated mice, resulting in a significant difference between genotypes ($P<0.05$, Two Way Anova). Superoxide production rates from reverse electron transfer tended to be higher in mitochondria from UCP1-deficient mice and were unaltered by the acclimation temperature (Fig. 9B). Interestingly, cold acclimation led to a decrease of superoxide production rates mediated by the andenosine translocase (ANT) in wild-type mice, while levels found in UCP1-ablated mice mitochondria remained unchanged (Fig. 9C).

Aconitase enzyme activity - At thermoneutrality we could not detect a difference in aconitase activity of skeletal muscle mitochondria isolated from wild-type and UCP1-ablated mice (Fig. 10). Whereas, cold acclimation led to an elevation of aconitase enzyme activity in both groups but had greater effects on skeletal muscle mitochondria of UCP1-ablated mice. The non-intermittent shivering of UCP1-deficient mice increased aconitase enzyme activity significantly by 104% ($P<0.05$ Two Way Anova). This was an

unexpected result, as an increase of aconitase activity reflects a decreased ROS production. Furthermore, previously reported for skeletal muscle mitochondria under exercise conditions (Zhang et al. 2007). The

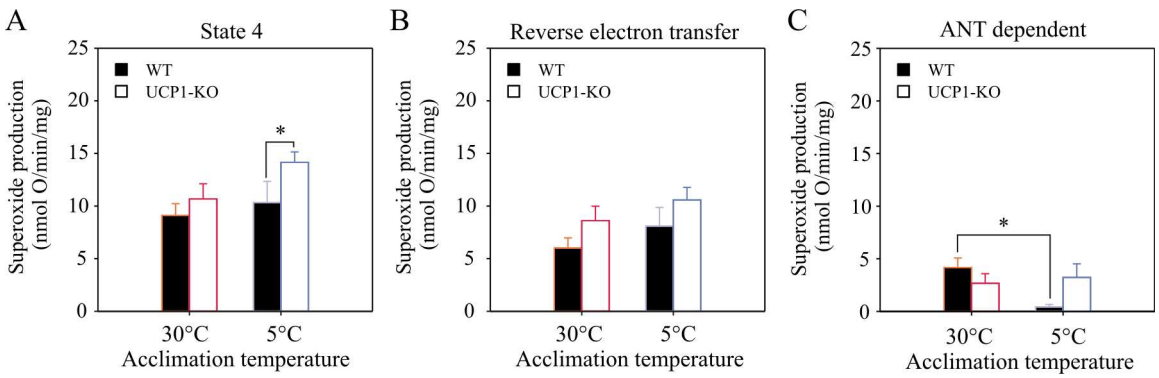

Figure 9: Superoxide production rates of skeletal muscle mitochondria isolated from wild-type (WT) and UCP-ablated (UCP1-KO) mice. A) Cold acclimation caused a significant difference in basal superoxide production between wild-type and UCP1-KO mice in state 4. B) Complex I dependent superoxide production rates tended to be higher in UCP1-ablated animals. C-D) Following cold exposure the ANT mediated superoxide production was significantly lower in mitochondria isolated from wild-type animals, the same accounted for UCP3 dependent superoxide production rates of both genotypes. (*P<0.05 Two Way Anova, n=4-8).

exercise has been argued as a main producer of cellular ROS in skeletal muscle, accordingly aconitase activity should be lower in UCP1-ablated than in wild-type mice and not the other way round.

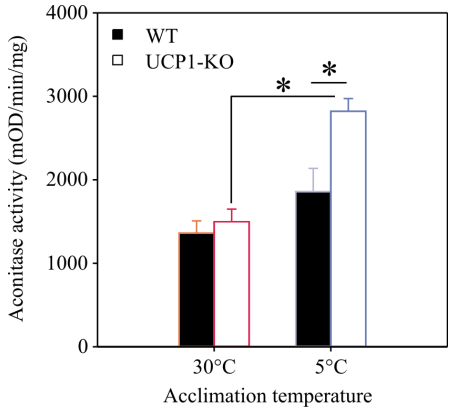

Fig. 10: Aconitase enzyme activity measured as the absorbance of NADPH (340nm). Prolonged cold exposue (>3 weeks) increased aconitase activity significantly in UCP1-ablated (UCP1-KO) compared to wild-type mice (*P<0.05, Two Way Anova, n=4-7).

Even though this result did not meet our expectations, an increased aconitase activity has been authors concluded that two mechanisms of aconitase activity exist, oxidation/reduction by ROS and a phosphorylation/dephosphorylation process. It is possible that ROS-mediated inactivation of aconitase compromises aerobic ATP production during exercise (Anderson et al. 1998, Sadek et al 2002, Tokheim and Martin 2006). Additionally dephosphorylation of aconitase alters the enzyme activity (Duchen 2004, Tokheim and Martin 2006). Conclusively the authors argued that during exercise the ROS mediated inactivation of aconitase can be overcome, "possibly by a dephosphorylaytion to maintain aerobic ATP production during muscle contraction" (Zhang et al. 2007). In our case this could mean, that the sustained shivering of UCP1-ablated mice was a sufficient training period to alter ATP production mechanisms (higher aconitase) and to survive the cold. Subsequent experiments will be necessary to verify if the slight increase in ROS-production rates of UCP1-ablated mice caused any cell damage *in vivo*, that led to a severe impairment of shivering muscles in the course of cold exposure. From another point of view, it could be also possible that UCP1-ablated mice had increased levels of antioxidant enzymes that counteracted an accumulation of cellular ROS and thereby prevented the inhibition of aconitase.

REFERENCES

Andersson U., Leighton B., Young M.E., Blomstrand E. and Newsholme E.A. (1998) *Inactivation of aconitase and oxoglutarate dehydrogenase in skeletal muscle in vitro by superoxide anions and/or nitric oxide.* Biochem Bioph Res Co 249: 512-516.

Anunciado-Koza R., Ukropec J., Koza R.A. and Kozak L.P. (2008) *Inactivation of UCP1 and the glycerol phosphate cycle synergistically increases energy expenditure to resist diet-induced obesity.* J Biol Chem 283: 27688-27697.

Aydin J., Shabalina I.G., Place N., Reiken S., Zhang S. et al. (2008) *Nonshivering thermogenesis protects against*

defective calcium handling in muscle. FASEB J 22: 3919-39124.

Block B.A. (1994) *Thermogenesis in muscle.* An Rev Physiol 56: 535-577.

Boss O., Samec S., Kuhne F., Bijlenga P., Assimacopoulos-Jeannet F. et al. (1998) *Uncoupling protein-3 expression in rodent skeletal muscle is modulated by food intake but not by changes in environmental temperature.* J Biol Chem 273: 5-8.

Brand M.D. (2000) *Uncoupling to survive? The role of mitochondrial inefficiency in ageing*. Exp Gerontol 35: 811-820.

Brand M.D., Pamplona R., Portero-Otin M., Requena J.R., Roebuck S.J., et al. (2002) *Oxidative damage and phospholipid fatty acyl composition in skeletal muscle mitochondria from mice underexpressing or overexpressing uncoupling protein 3.* Biochem J 368: 597-603.

Brand M.D. and Esteves T.C. (2005) *Physiological functions of the mitochondrial uncoupling proteins UCP2 and UCP3*. Cell Metab 2: 85-93.

Cannon B. and Nedergaard J. (2004) *Brown adipose tissue: function and physiological significance.* Physiol Rev 84: 277-359.

Cooper C.E., Vollaard N.B., Choueiri T. and Wilson M.T. (2002) *Exercise, free radicals and oxidative stress.* Biochem Soc T 30: 280-285.

Duchen M.R. (2004) *Roles of mitochondria in health and disease.* Diabetes 53: 96-102.

Gardner P.R. (2002) *Aconitase: sensitive target and measure of superoxide.* Method Enzym 349: 9-23.

Golozoubova V., Hohtola E., Matthias A., Jacobsson A., Cannon B. et al. (2001) *Only UCP1 can mediate adaptive nonshivering thermogenesis in the cold.* FASEB J 15: 2048-2050.

Granneman J.G., Burnazi M., Zhu Z. and Schwamb L.A. (2003) *White adipose tissue contributes to UCP1-independent thermogenesis.* Am J Physiol Endocrinol Metab 285: E1230-1236.

Hausladen A. and Fridovich I. (1996) *Measuring nitric oxide and superoxide: rate constants for aconitase reactivity*. Method Enzymol 269: 37-41.

Janero D.R. and Hreniuk D. (1996) *Suppression of TCA cycle activity in the cardiac muscle cell by hydroperoxide-induced oxidant stress.* Amer J Physiol 270: C1735-1742.

Keipert S., Klaus S., Heldmaier G. and Jastroch M. (2010) *UCP1 ectopically expressed in murine muscle displays native function and mitigates mitochondrial superoxide production.* Biochim Biophysica Acta 1797: 324-330.

Lowell B.B. and Spiegelman B.M. (2000) *Towards a molecular understanding of adaptive thermogenesis.* Nature 404: 652-660.

Meyer C.W., Willershauser M., Jastroch M., Rourke B.C., Fromme T., Oelkrug R. et al. (2010) *Adaptive thermogenesis and thermal conductance in wild-type and UCP1-KO mice.* Amer J Physiol 299: R1396-1406.

Monemdjou S., Hofmann W.E., Kozak L.P. and Harper M.E. (2000) *Increased mitochondrial proton leak in skeletal muscle mitochondria of UCP1-deficient mice.* Amer J Physiol 279: E941-946.

Nicholls D.G. and Locke R.M. (1984) *Thermogenic mechanisms in brown fat*. Physiol Rev 64: 1-64.

Nicholls D.G. and Rial E. (1999) *A history of the first uncoupling protein, UCP1*. J Bioenerg Biomembr 31: 399-406.

Oelkrug R., Kutschke M., Meyer C.W., Heldmaier G. and Jastroch M. (2010a) *Uncoupling protein 1 decreases superoxide production in brown adipose tissue mitochondria*. J Biol Chem 285: 21961-21968.

Parker N., Affourtit C., Vidal-Puig A. and Brand M.D. (2008) *Energization-dependent endogenous activation of proton conductance in skeletal muscle mitochondria.* Biochem J 412: 131-139.

Sadek H.A., Humphries K.M., Szweda P.A. and Szweda L.I. (2002) *Selective inactivation of redox-sensitive mitochondrial enzymes during cardiac reperfusion.* Arch Biochem Biophys 406: 222-228.

Shabalina I.G., Hoeks J., Kramarova T.V., Schrauwen .P, Cannon B. et al. (2010) *Cold tolerance of UCP1-ablated mice: a skeletal muscle mitochondria switch toward lipid oxidation with marked UCP3 up-regulation not associated with increased basal, fatty acid- or ROS-induced uncoupling or enhanced GDP effects.* Biochim Biophys Acta 1797: 968-980.

Talbot D.A. and Brand M.D. (2005) *Uncoupling protein 3 protects aconitase against inactivation in isolated skeletal muscle mitochondria*. Biochim Biophys Acta 1709: 150-156.

Tokheim A.M. and Martin B.L. (2006) *Association of calcineurin with mitochondrial proteins.* Proteins 64: 28-33.

Ukropec J., Anunciado R.P., Ravussin Y., Hulver M.W. and Kozak L.P. (2006) *UCP1-independent thermogenesis in white adipose tissue of cold-acclimated Ucp1-/- mice.* J Biol Chem 281: 31894-318908.

Vidal-Puig A.J., Grujic D., Zhang C.Y., Hagen T., Boss O. et al. (2000) *Energy metabolism in uncoupling protein 3 gene knockout mice.* J Biol Chem 275: 16258-66.

Zhang S., Sandstrom M.E., Lanner J.T., Thorell A., Westerblad H. et al. (2007) *Activation of aconitase in mouse fast-twitch skeletal muscle during contraction mediated oxidative stress.* American journal of physiology. Cell Physiol 293: C1154-1159.

SUPPLEMENTAL MATERIAL FOR CHAPTER IV

BROWN FAT IN A ´PROTOENDOTHERMIC´ MAMMAL FUELS THE PARENTAL CARE MODEL OF MAMMALIAN EVOLUTION

Study animals - Experiments were performed on laboratory bred, adult Lesser hedgehog tenrecs (*Echinops telfairi*; N=8 females and N=4 males) during their annual activity period. Tenrecs were kept in Makrolon Type IV cages (1800 cm^2) equipped with sawdust bedding and plastic nest boxes, at an Ta of 27°C on a 12:12 hrs light:dark cycle throughout the experimental procedure. They were fed alternately with canned cat food (Kitekat), cockroaches, fruits and seeds every second day at 2-5 pm and had ad libitum access to water. All study animals were weighed at least once per week. All experimental procedures were approved by the German Animal Welfare Authorities.

Tb recording - Tenrecs were surgically implanted with temperature sensitive transmitters (Minimitter, Model X, Sunriver, OR, USA, accuracy 0.1°C) for monitoring abdominal core Tb. Animals were anaesthetized via a subcutaneous injection of the α2-agonist Medetomidine ($2mg*kg^{-1}$), the benzodiazepine Midazolam ($3mg*kg^{-1}$) and the dissociative Ketamine ($20mg*kg^{-1}$) (MKK-anaesthesia, ref. 1). Optionally, the inhalation anaesthesia Isoflurane (0.6-1.5 Vol %) was co-administered over a breathing mask. During surgery the tenrecs were placed on a heating pad with a constant temperature of 30°C. To induce post-surgical recovery from anaesthesia the antidotes Atipamezole ($1mg*kg^{-1}$) and Flumazenile ($0.2mg*kg^{-1}$) were administered. Following surgery tenrecs were maintained at 27°C for at least 3 weeks, Hereafter, six animals were randomly selected for the CA group (N = 5♀ and N = 1♂) and stepwise acclimated to 20°C (4d at 24°C, 3d at 21-22°C). The other six animals remained at 27°C (WA group; WA; N = 3♀ and N = 3♂). The average body mass of the animals was 133.3 ± 29.1g for the WA group (93.4g-166.4g) and 162.5 ± 27.1g (122.8g-196.5g) for the CA group (P=0.102, Students t-test) and remained constant throughout the entire study. During long term Tb recordings, Tb readings were obtained every 6 mins for 7-12 days at a Ta of 27°C, 3-4d at 24°C, 2-3d at 21-22°C and 3-6 d at 20°C (only CA group).

Measurements of RMR - Metabolic rate (MR) measurements were based on the principle of indirect calorimetry using a 2- channel, open circuit respiratory system as described previously[2]. Tenrecs were transferred to metabolic cages (~5 l) equipped with bedding material. The cages were placed inside a climated chamber. Air was drawn from the cages at a flow rate of 42 l/h chosen to maintain <1% oxygen depletion between the incurrent and excurrent air. On each measurement day, tenrecs were exposed for 4-5 hours to only one of the following temperatures: 34°C, 30°C, 27°C, 24°C, 20°C, at random order. In between each measurement tenrecs were allowed to recover for at least 2 days in their home cage. On each occasion, readings of MR (O_2 consumption) and, Tb were taken at 3-5min intervals. Animals became hypometabolic and hypothermic in every measurement at ambient temperatures below 30°C, and introduction of food as used to induce arousal. Following arousal, we obtained stable metabolic readings of resting animals at high Tbs (not post-absorptive).

Suppression of NST - To quantify sensitivity to pharmacological suppression of nonshivering thermogenesis we used a multi-day protocol. During the experiment, tenrecs were single housed in modified Makrolon III cages suitable for measurements of metabolic rate and Tb. Cages were equipped with bedding material a plastic nest box as well as water ad libitum. The light-dark photoperiod was set to 12:12 (lights on at 6:00 CET). In total, N=5 WA and N=6 CA tenrecs were measured at a Ta of 24°C for three consecutive days. MR and Tb were recorded in parallel at 3-5 min intervals. Measurements were started at approximately 17:00 CET and for the following 42-46 hours the animals were only disturbed when fed, at around 16:00 CET. We calculated arousal and rewarming rates where arousal occurred spontaneously or arousal was induced by disturbing the animals. On the third day, each tenrec received a single subcutaneous injection of the β3-adrenergic antagonist SR 59230A (3-(2-Ethylphenoxy)-1-[[(1S)-1,2,3,4-tetrahydronaphth-1-yl]amino]-(2S)-2-propanol oxalate salt, Sigma) at a dosage of 1 $mg*kg^{-1}$. For subcutaneous injection of the antagonist, the spines were lifted in the neck region using forceps. The timing of the injection corresponded to the onset of arousal. Tenrecs were immediately returned to the metabolic cages and recordings were continued until the next day. A tenrec was considered in steady state (torpid) when its oxygen consumption had stably attained <30 ml O_2*h^{-1} (~30 % of RMR) for more than 2 hours. In order to compare the efficiency of rewarming, we calculated average rewarming and heat production rates from the Tb time course during a spontaneous and an induced arousal with or without prior treatment with the antagonist (Supplemental fig. 1).

Confirmation of BAT and UCP1 expression - We dissected animals to identify and locate BAT depots. Tissue samples were collected and used to confirm the expression of UCP1 on the mRNA and protein level. Therefore we first amplified UCP1 cDNA using a

reverse transcriptase (Invitrogen, Super Script III, First Strand cDNA Synthesis Super Mix for qRT PCR) and tenrec UCP1 specific primers (forward: 5`-GAC TAT GGG GGT GAA GAT CTT C-3´; reverse: 5´-AAA GGC CGG CAG CCC TTC CTT G-3´), followed by a PCR using the same primer pair and a gel electrophoresis to validate UCP1 expression. The presence or absence of UCP1 protein was confirmed post mortem by immunological detection in BAT and BAT mitochondria. The membranes were probed with a rabbit anti-UCP1 polyclonal antibody (1: 10 000; 3046; Chemicon), followed by the relevant fluorescence-conjugated secondary antibody. The expression of the β3-adrenergic receptor was confirmed using a goat polyclonal β3-Adrenoreceptor primary antibody (1:200, Santa Cruz).

Mitochondria isolation - Mitochondria were prepared by homogenization and differential centrifugation as described previously[3]. BAT depots were removed (dorso-cervical, axillar and abdominal) and immediately placed in ice-cold isolation medium. Protein concentration was determined photometrically using the Biuret method.

Mitochondria respiration - Mitochondrial oxygen consumption was measured using a Clark-type oxygen electrode (Rank Brothers Ltd.) maintained at 32°C and calibrated with air-saturated medium (BAT-KHE: 50 mM KCl, 5 mM TES, 2 mM MgCl2 – 6xH_2O, 4 mM KH_2PO_4, 1 mM EGTA, 0.4% bovine serum albumin (BSA; w/v), pH 7.2 at RT) that was assumed to contain 406 nmol of O ml^{-1} at 37°C[4]. BAT mitochondria respiration was measured in 500 µl of medium at a concentration of 0.5 mg/ml. BAT mitochondria possess a small amount of ATP synthase and were previously incubated with 4.8 µM rotenone and 2 µM oligomycin. Mitochondria were energized by the addition of glycerol-3-phosphate (G3P; titrating up to 15 mM). Subsequently GDP was titrated to a final concentration of 5 mM. The ability of GDP to establish respiratory control also confirmed the integrity of the mitochondria after the isolation process. At the end of each respiration measurement, the artificial uncoupler FCCP (carbonyl cyanide p-trifluoromethoxyphenylhydrazone) was titrated in 1 µM steps to estimate the maximal substrate oxidation rate of both mitochondria types.

Proton leak kinetics - The kinetics of mitochondrial proton leak were measured by determining the respiration rate required to drive the proton leak. Measurements were performed with the same protein concentrations as mentioned above and always contained 2 µM oligomycin, 100 nM nigericin (which dissipates the pH gradient, ref. 5), 4.8 µM rotenone and 2.5 µM carboxyatractylate (which inhibits the adenine nucleotide translocase). The mitochondrial membrane potential was measured simultaneously with mitochondrial respiration by using an electrode sensitive to the potential-sensitive probe, TPMP+ (triphenylmethylphosphonium), in 2ml of BAT-KHE (32°C). The TPMP+-sensitive electrode was calibrated with sequential additions of TPMP+ up to 2.5 µM, and succinate (4 mM) was added to initiate mitochondrial respiration. Membrane potential and respiration were progressively inhibited through successive steady states with the complex II inhibitor, malonate, up to 5 mM (BAT). Finally FCCP (0.3 µM) was added to dissipate the membrane potential and release all the TPMP+ from the mitochondria, allowing for correction of baseline drift. Respiration at each steady state was plotted against the corresponding membrane potential to verify the dependence of proton leak rate on the membrane potential. To account for UCP1 dependent proton leak we performed measurements in the presence of 1-5 mM GDP.

COX-measurements - COX activity was measured polarographically[6] with a Clark-type oxygen electrode maintained at 25°C and calibrated with 350 µl of air-saturated measuring buffer (79 mM K_2HPO_4, 20.1 mM KH_2PO_4, 5 mM EDTA, 3 mM horse cytochrome C (Sigma) and 250 mM ascorbate; pH 7.4) which was assumed to contain 479 nmol O ml^{-1} (*37*). 20-70 mg of BAT were weighed and then homogenized in tissue buffer containing 33.9 mM KH2PO4 , 66.1 mM K2HPO4 x 3 H_2O, 2 mM EDTA and 10 mM glutathione (pH 7.5). Protein extracts were quantified using the BCA assay. The tissue homogenate was diluted 1:8 for BAT and 1:2 for liver with tissue buffer containing 0.1% (w/v) of the detergent n-Dodecyl-ß-D-Maltoside (Sigma). COX activity of BAT and liver mitochondria was performed with the same experimental setup.

Stable expression of etUCP1 in mammalian HEK293 cells - Human embryo kidney cells (HEK293) were cultured in Dulbecco's modified eagle medium (DMEM; GIBCO, 4. 5g/L glucose, + L-glutamine, - pyruvate), supplemented with 10% FBS (S0115, BIOCHROM) and 5% nonessential amino acids (PAA). Wild-type HEK293 were grown in the presence of 1% Penicillin/Streptomycin (GIBCO) and mouse (mUCP1 HEK293) or tenrec UCP1 (etUCP1 HEK293) expressing cells in the presence of 50 µg/mL geneticin (GIBCO). For passaging, the cell medium was removed and the cells washed with PBS, trypsinised (0.2% trypsin) and centrifuged (500 g; 3 min). After resuspending the cells in growth medium they could be seeded onto new plates.

The coding sequence of tenrec UCP1 (BankIt1580920) was transcribed from mRNA to cDNA and cloned into a pcDNA3 vector (Invitrogen, containing neomycin/geneticin resistance genes). For stable transfection of HEK293 cells with tenrec UCP1 we followed the protocol established in ref. 7. Cells were grown up to a confluency of 60-70% on 10 cm dishes and transfected with 15 µg of plasmid which was precipitated by mixing it with calcium chloride and Hepes buffered saline. In parallel we transfected cells with a pcDNA3 vector containing GFP (green fluorescent protein) for transfection control. After 24 hr cells were washed and new medium was added. On the third day after transfection, the cells were split,

seeded on new plates at a confluency of 20-30% and the selection process was started by adding 400 µg/ml geneticin to the medium. Positive clones were picked, separately cultured and the UCP1 expression was validated by immunological detection using the same protocol as mentioned above. Several aliquots of a clonal cell line were stored in liquid nitrogen to control for passaging effects (90% DMEM, 10% DMSO).

Cell culture procedure for cell respiration measurements - Cells were seeded (20 000 per well) using the two-step seeding method on 24XF V7 PS tissue culture plates (Seahorse Bioscience), which have been previously coated with PEI (Polyethylenimine, 1:15,000 dilution, 35 µl per well). DMEM (4.5 g/L glucose, +L-Glutamine, -Pyruvate, pH 7.6 at RT) supplemented with 10% heat inactivated FBS (Gibco) and 1% Penicillin/Streptomycin (Pen/Strep, wtHEK293) or 50 µg/mL geneticin (mUCP1 HEK293, etUCP1 HEK293) was used for cell culturing. On the day of assay (48 hr after seeding), cells were washed twice with assay medium (EB 1:2 with NaCl + 10 mM glucose, + 10 mmol pyruvate, +/- 0.4% BSA (w/v)) and afterwards they were incubated in 700 µl of assay medium in an air incubator without CO_2 at 37 °C.

The XF24 plate was then transferred to a temperature-controlled (37 °C) Seahorse analyzer (XF24 Extracellular Flux analyser) and subjected to a 10-min equilibration period and 4 assay cycles, comprising a 1-min mix, 2-min wait, and 3-min measure period each to determine basal respiration, then oligomycin (4 µM) was added by automatic pneumatic injection (3 assay cycles). Oligomycin inhibits the ATP synthase and thus approximate the proportion of respiration used to drive ATP synthesis (coupling efficiency). Then different concentrations of TTNBP (15 µM, 30 µM diluted in DMSO; DMSO was used as control injection) or nonanoic acid (30 µM, 50 µM, 100 µM and 133 µM) were injected, followed by an injection of FCCP (0.5 µM) or DNP (100 µM) to completely uncouple mitochondria. Each experimental trace was ended by addition of a rotenone (4 µM) and antimycin A (2 µM) mixture to determine the non-mitochondrial respiratory rate, which was subtracted from all other rates. Coupling efficiency was calculated as the oligomycin-sensitive fraction of glucose/pyruvate-stimulated mitochondrial respiratory activity.

Mitochondria isolation of HEK293 cells - For the isolation of mitochondria from HEK293 cells an aliquot of wtHEK293 cells, mUCP1 HEK293 cells and etUCP1 HEK293 was seeded on a 10cm cell culture dish. Cells were grown in DMEM (4.5 g/L glucose, +L-Glutamine, -Pyruvate) supplemented with 10% heat inactivated FBS (Gibco) and 1% Pen/Strep (wtHEK293) or 50 µg/ml geneticin (mUCP1 HEK293, etUCP1 HEK293). After reaching 85% of confluency (day 5) they were transferred to a 175 T_7 Flask and after approximately 3 days (85% of confluency) to two 500 cm^2 dishes per cell line. All 500 cm^2 dishes were coated with PEI (Polyethylenimine, dilution 1:15.000, 50 ml per plate). The day before mitochondria isolation, the medium was changed to medium without antibiotics and FBS.

After 5 days of cultivating the cells they were harvested, and the mitochondria were isolated by homogenisation and subsequent differential centrifugation[7]. The cell pellet was transferred to a dounce homogenizer (WHEATON, 40 ml) and cells were disrupted by seven strokes with a sanded-loose fitting plunger. The final mitochondrial pellet was carefully resuspended in a minimal volume of buffer and the mitochondrial protein concentration was quantified using the Biuret method.

Proton leak measurements of HEK293 cells mitochondria - Mitochondrial respiration and proton leak rate were measured in parallel in 2ml KHE buffer (120 mM KCl, 5 mM KH_2PO_4, 3 mM HEPES, 1mM EGTA, 0.3% BSA (w/v); pH 7.2 at RT) at a protein concentration of 0.8 mg/ml. We used the dye safranin O for the measurement of mitochondrial membrane potential. Safranin O changes fluorescence in a manner linearly proportional to the mitochondrial membrane potential[8]. The excitation and emission wavelengths were set to 533 nm and 576 nm, respectively, and measurements were performed in a 96 well plate at a gain of 500 and a focal height of 7.1 nm in a high-throughput-screening microplate reader (Pherastar FS, BMG Labtech). 40 µg of mitochondrial protein were measured in 200 µl of KHE in the presence of 5µM Safranin O, 4µM rotenone, 1 µg/µl oligomycin and 100nM nigericin, GDP (1 mM) and palimtat (100 µm) were added in trials were indicated. After incubation time, succinate (5 mM) was added to energize mitochondria. The induced membrane potential and respiration were subsequently inhibited by 2 mM titration steps with malonate (up to 6 mM). At the end of each run, the membrane potential was dissipated by addition of 0.3 µM FCCP. The relative changes in fluorescent signal are proportional to the membrane potential, larger changes in relative fluorescence units (RFU) indicating higher membrane potentials after mitochondria energetization. Comparison of the safranin O signal before energetization and after dissipation of the membrane potential with FCCP allowed correction for drifts in the baseline fluorescent signal. Additionally, background wells without mitochondria were measured for each condition to correct for fluorescence quenching effects.

Recombinant UCP1 standard - The coding sequence of tenrec UCP1 was amplified by PCR from the pcDNA3 vector and ligated into the *Nde*I and *Eco*RI restriction sites of the pMW172 vector using conventional molecular biology methods. Mouse UCP1 and tenrec UCP1 were expressed in *E. coli* (strain C41 (DE3)) and inclusion bodies were isolated as described previously[9]. Total protein content of isolated inclusion bodies was determined using the

BCA Method. Protein concentration and purity of the UCP1 standard were verified by separation on a 12% SDS polyacrylamide gel and subsequent Coomassie staining (Gelcode, Pierce). The Coomassie staining was quantified densitometrically using the program Image J (NIH, http://rsbweb.nih.gov/ij/). The purity of the UCP1 standard was calculated by dividing the UCP1 band intensity by the total signal intensity of the gel lane[10]. 10-40 ng of the respective UCP1 proteins were loaded on a 12% SDS gel to calculate the exact UCP1 amount in the mUCP1 and etUCP1 cell line. UCP1 was detected with the same antibody and protocol as mentioned above.

Statistical analysis - We used the paired t-test to test for effects of the β3-adrenergic antagonist within the CA and WA group, the Students t tests was used to test for differences between the acclimation groups. Differences in proton leak respiration rates of UCP1-containing cells activated with various concentrations of TTNPB or nonanoic acids were determined with a One Way Anova analysis. We calculated the UCP1 centre activity of mouse and tenrec UCP1 with a dynamic fitting exponential growth curve (Single, 3 Parameter, f=y0+a*exp(b*x)). These analyses were performed using SigmaStat (Jandel ScientiWc, San Rafael, California). All mean values were reported ± Standard Error (SE) and the 0.05 level of probability was accepted as indicating statistical significance.

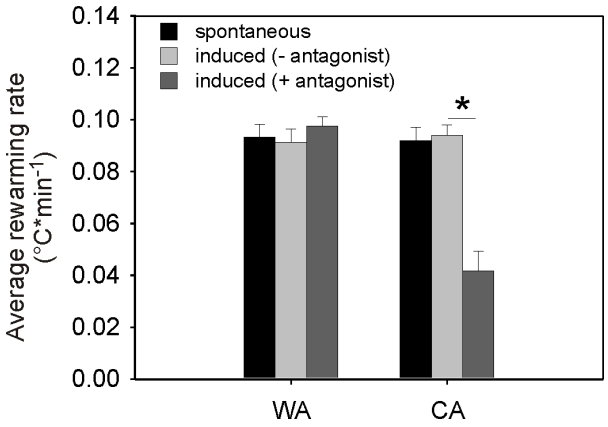

Supplemental figure 1: Average rewarming rates during spontaneous and induced arousals. Rewarming rates were similar when animals were woken up spontaneously or arousal was induced. In a second trial this induced arousal was accompanied with an injection of the ß3 Antagonist SR 59230A. Animals were injected with the ß-3 Antagonist at the onset of arousal. In CA animals blockade of ß3-adrenergic signalling caused a significant decrease in average rewarming rates (N=5 per group, P<0.05 paired t-test)**.**

Literature

1. Henke, J., Reinert, J., Preissel, A. K. & Radtke-Schuller, S. Partially antagonisable anaesthesia of the Small hedgehog tenrec (*Echinops telfairi*) with medetomidine, midazolam and ketamine. *J. Anim. Sci.* **43**, 255-264 (2007).
2. Heldmaier, G. & Ruf, T. Body temperature and metabolic rate during natural hypothermia in endotherms. *J. Comp. Physiol. B* **162**, 696-706 (1992).
3. Mzilikazi, N., Jastroch, M., Meyer, C. W. & Klingenspor, M. The molecular and biochemical basis of nonshivering thermogenesis in an African endemic mammal, *Elephantulus myurus*. *Am. J. Physiol. Regul. Integr. Comp. Physiol.* **293**, 2120-2127 (2007).
4. Reynafarje, B., Costa, L. E. & Lehninger, A. L. O2 solubility in aqueos media determined by a kinetic method. Anal. Biochem. 145. 406-418 (1985).
5. Cadenas, S. & Brand, M. D. Effects of magnesium and nucleotides on the proton conductance of rat skeletal-muscle mitochondria. *Biochem. J.* **348**, 209-213 (2000).
6. Smith, L. &. Camerino, P. W Comparison of polarographic and spectrometric assays for cytochrome C oxidase activity. *Biochemistry* **2**, 1428-1432 (1963).
7. Jastroch, M. Expression of uncoupling proteins in a mammalian cell culture system (HEK293) and assessment of their protein function. *Methods Mol. Biol.* **810**, 153-164 (2012).
8. Akerman, K. E. & Wikstrom, M. K. Safranine as a probe of the mitochondrial membrane potential. *FEBS Lett.* **68**, 191-197 (1976).
9. Echtay, K. S. *et al.*, Regulation of UCP3 by nucleotides is different from regulation of UCP1, *FEBS Lett.* **450**, 1-2 (1990).
10. Stuart, J. A., Harper, J. A., Brindle, K. M., Jekabsons, M. B & Brand, M. D. A mitochondrial uncoupling artifact can be caused by expression of uncoupling protein 1 in yeast, *Biochem. J.* **356**, 779-789 (2001).

SUPEROXIDE PRODUCTION IN BROWN ADIPOSE TISSUE OF LESSER HEDGEHOG TENRECS IS SENSITIVE TO UCP1 EXPRESSION

BACKGROUND

In chapter II I confirmed a role of modern Eutherian UCP1 in mild uncoupling brown adipose tissue mitochondria during thermogenesis. I concluded that mitochondrial mild uncoupling could have been the regulatory function of UCP1 orthologues in ectotherms and that during mammalian evolution UCP1 developed a dual function in heat production and ROS prevention. Here I used mitochondria isolated from brown adipose tissue of a more ancient Afrotherian mammal, Lesser hedgehog tenrec (*Echinops telfairi*), to further approve this hypothesis.

EXPERIMENTAL SETUP

Animals - I examined isolated brown adipose tissue mitochondria of warm (WA, 27°C) and cold acclimated tenrecs (CA, 20°C) according to the acclimation protocol of chapter IV. Tenrecs were kept in Makrolon Type IV cages (1800 cm^2) equipped with sawdust bedding and plastic nest boxes, on a 12:12 h light:dark cycle before the experimental procedure. They were fed alternately with canned cat food (Kitekat), cockroaches, fruits and seeds every second day at 2-5 pm (CET) and had ad libitum access to water. All experimental procedures were approved by the German Animal Welfare Authorities.

Mitochondrial Isolation – Tenrecs were sacrificed and all brown adipose tissue depots were removed and rapidly placed in ice cold buffer, mitochondria were isolated at 4°C as previously described (Mzilikazi et al. 2007). Mitochondrial protein concentrations were determined using the Biuret method.

Measurements of Mitochondrial Respiration and UCP1 content – Data were obtained from chapter IV, review this chapter for further information about the experimental procedure.

Measurements of Mitochondrial Hydrogen Peroxide Release - Measurements of hydrogen peroxide production of isolated mitochondria were performed similarly to the procedures of Oelkrug et al. (2010). 20 µg of brown adipose tissue mitochondria were incubated in 200 µl of pre-equilibrated assay buffer (50m MKCl, 5 mM TES, 2 mM $MgCl_2$ $6H_2O$, 4 mM KH_2PO_4, 1 mM EGTA, bovine serum albumin 0.4% (w/v), pH 7.2 at room temperature). This assay contained the fluorescent probe Amplex Red (50 µM; Invitrogen), 30 units ml^{-1} superoxide dismutase, 6 units ml^{-1} horseradish peroxidase and 2 µM oligomycin. Furthermore superoxide production was also measured in the presence of rotenone (2 µM, inhibiting complex I-derived reactive oxygen species production), GDP (5 mM, to inhibit UCP1), and carboxyatractylate (2.5 nM) to distinguish from adenine nucleotide transporter-dependent effects. The stoichiometry of the reaction between Amplex Red and H_2O_2 is 1:1, whereas the conversion from superoxide to H_2O_2 is assumed to be 1:2. H_2O_2 formation was initiated by the addition of succinate (5 mM) or glycerol-3-phosphate (15 mM). Fluorescence was detected at 37 °C in a microplate reader (BMG Labtech, FLUOstar Optima) in 96 well microplates (Greiner 96-Well, clear, F-Bottom, black), at an excitation wavelength of 560–10nm and an emission wavelength of 590 nm. Fluorescence was calibrated using known amounts of H_2O_2 at each experimental day.

RESULTS AND DISCUSSION

Initially I measured superoxide production rates of mitochondria respiring on succinate (5 mM) or glycerol-3-phosphate (15 mM) under thermoneutral conditions (30°C). At state 4 (basal or leak) respiration, superoxide production rates of warm (WA, 27°C) and cold (CA, 20°C) acclimated tenrecs were similar (Fig. 12) but glycerol-3-phosphate caused significantly elevated hydrogen peroxide releasing rates compared to succinate ($P<0.05$, Two Way Repeated Measurement Anova). Similar to my results in chapter II, inhibition of UCP1 with GDP strongly recoupled mitochondria, leading to an increase in superoxide production rates (Fig 12A, C). This increase was most pronounced in cold acclimated animals respiring on succinate; glycerol-3-phosphate abolished genotype difference. The GDP-sensitive superoxide production rate was attributable to UCP1 as the additional inhibition of the adenosine translocase (ANT) with carboxyatractylate did not alter superoxide production rates (Fig 12B, D). The administration of rotenone allowed determination of the superoxide production at the I_Q site of complex I, interestingly superoxide production of tenrec brown

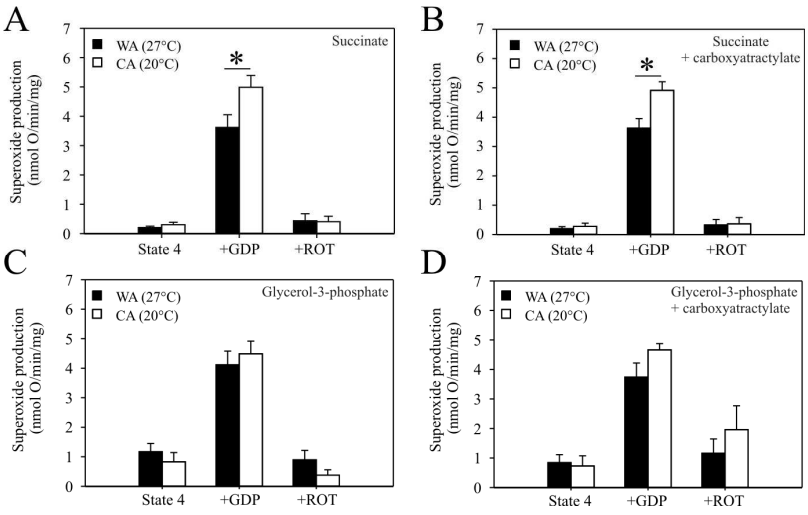

Figure 12: Superoxide production rates of tenrec brown adipose tissue mitochondria respiring either on succinate (5 mM, A-B) or glycerol-3-phosphate (15 mM, C-D). GDP (5 mM) was used as a potent inhibitor of UCP1, rotenone (ROT 2 µM) of Complex I and carboxyatractylate (2.5 nM) of the ANT. Mitochondria respiring on succinate showed significant differences in superoxide production rates after inhibition of UCP1 (*P<0.05, Students t-test).

adipose tissue mitochondria was only slightly sensitive to rotenone.

Conclusively, cold acclimation of Lesser hedgehog tenrecs significantly increased superoxide production rates under coupled conditions (+GDP), whereas uncoupled (state 4) superoxide production rates remained unchanged. It is well established that there is a strong positive correlation between membrane potential and ROS production (Hansford et al. 1997, Boveris et al. 1976, Nohl et al. 1996, Herrero et al. 1998). A small increase in membrane potential (-10 mV) is able to inhibit H_2O_2 production by approximately 70% (Hansford et al. 1997, Votyakova et al. 2001). I could not measure the membrane potential of tenrec brown adipose tissue mitochondria in state 4, as mitochondria were fully uncoupled after the isolation process (see chapter IV Fig. 2I). Nevertheless, under recoupled conditions the membrane potential of warm acclimated animals was 2.4 mV higher, resulting in 32% lower superoxide production rates compared to cold acclimated animals. Cold acclimation caused an increase in UCP1 protein levels (mg mitochondrial protein) and oxidative capacity of brown adipose tissue mitochondria (see chapter IV Fig 2c). There was no correlation between UCP1 protein content and ROS production rates in state 4 (Fig. 13A). After inhibition of UCP1 with GDP I observed a strong correlation between UCP1 content and superoxide production rates (Fig. 13B). In the cold acclimated group this effect was caused by a UCP1 dependent decrease in respiration rates that affected ROS production rates (Fig 13C-D). Conclusively, inhibition of UCP1 couples brown adipose tissue mitochondria, leading to a higher membrane potential that lowers respiration rates and in turn elevates ROS production rates.

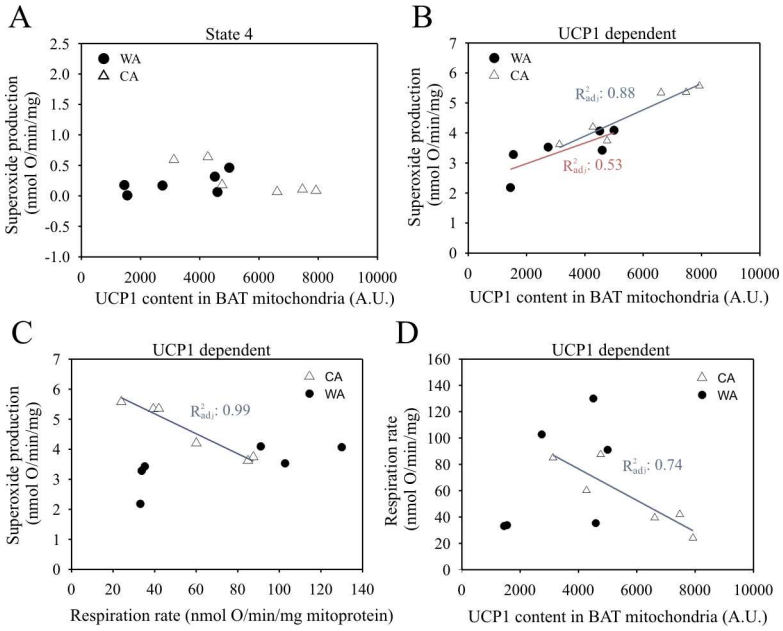

Figure 13: Correlation between superoxide production rates, respiration rates (using 5 mM succinate as substrate) and the content of UCP1 (mg mitochondrial protein) in brown adipose tissue (BAT) mitochondria. A) There was no correlation between superoxide production rates and the UCP1 content in state 4 (uncoupled), whereas recoupling of mitochondria induced a strong correlation between superoxide production rates and the UCP1 content of mitochondria isolated from cold acclimated animals (B). This result was caused by a negative correlation between superoxide production rates and respiration rates (C), which dependent on the UCP1 content (D).

Taken together, the expression of UCP1 in brown adipose tissue mitochondria may enable Lesser hedgehog tenrecs to maintain high respiration rates in the absence of deleterious superoxide production rates. Furthermore, tenrec UCP1 seems to be as potent as Eutherian UCP1 in mildly uncoupling the mitochondria. The presented data additionally report on a strong negative correlation between respiration and ROS production rates, dependent on the mitochondrial membrane potential.

REFERENCES

Boveris A., Cadenas E. and Stoppani A.O. (1976) *Role of ubiquinone in the mitochondrial generation of hydrogen peroxide.* Biochem J 156: 435-444.

Hansford R.G., Hogue B.A. and Mildaziene V. (1997) *Dependence of H2O2 formation by rat heart mitochondria on substrate availability and donor age.* J Bioenerg Biomembr 29: 89-95.

Herrero A. and Barja G. (1998) *H2O2 production of heart mitochondria and aging rate are slower in canaries and parakeets than in mice: sites of free radical generation and mechanisms involved.* Mech Ageing Dev 103: 133-146.

Mzilikazi N., Jastroch M., Meyer C.W. and Klingenspor M. (2007) *The molecular and biochemical basis of nonshivering thermogenesis in an African endemic mammal, Elephantulus myurus.* Amer J Physiol 293: R2120-2227.

Nohl H., Gille L., Schonheit K. and Liu Y. (1996) *Conditions allowing redox-cycling ubisemiquinone in mitochondria to establish a direct redox couple with molecular oxygen.* Free Radical Biol Med 20: 207-213.

Oelkrug R., Kutschke M., Meyer C.W., Heldmaier G. and Jastroch M. (2010a) *Uncoupling protein 1 decreases superoxide production in brown adipose tissue mitochondria.* J Biol Chem 285: 21961-21968.

Votyakova T.V. and Reynolds I.J. (2001) *DeltaPsi(m)-Dependent and -independent production of reactive oxygen species by rat brain mitochondria.* J Neurochem 79: 266-77.

PHYLOGENETIC TREE OF UCP1

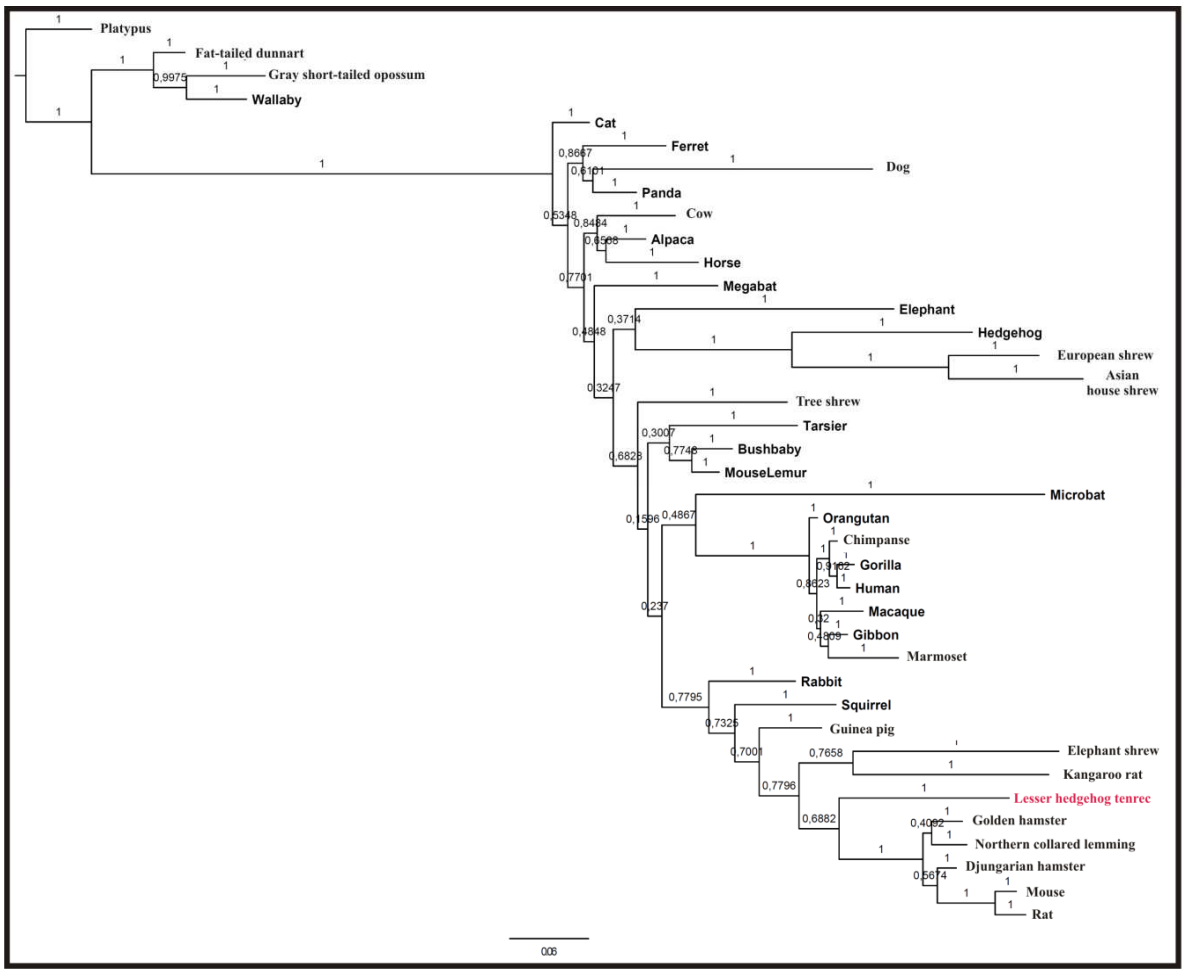

Figure 11: Phylogenetic tree of UCP1. A comprehensive search for UCP1 sequences was performed in public databases using keywords and by BLAST (GenBank/EMBL). A multiple sequence alignment was generated by MAFFT (http://mafft.cbrc.jp/alignment/software/). A Bayesian phylogenetic tree was inferred using the program MrBayes 3.1, assuming the JTT model of protein evolution and a gamma distribution of rates. Metropolis-coupled Markov chain Monte Carlo (MCMCMC) sampling was performed with one cold and three heated chains. Two independent runs were performed in parallel for 10 million generations and trees were sampled every 1000 generation. Posterior probabilities were estimated on the final 5,000 trees (burnin = 5,000; designed in a cooperation project with Prof. Dr. Thorsten Burmester, Universität Hamburg, Germany).

ADAPTIVE THERMOGENESIS AND THERMAL CONDUCTANCE IN WILD-TYPE AND UCP1-KO MICE

C.W. MEYER ∞ M. WILLERSHÄUSER ∞ M. JASTROCH
B. ROURKE ∞ T. FROMME ∞ R. OELKRUG
G. HELDMAIER ∞ M. KLINGENSPOR

Am J Physiol Regul Integr Comp Physiol 299: R1396–R1406, 2010.
First published September 8, 2010; doi:10.1152/ajpregu.00021.2009.

Adaptive thermogenesis and thermal conductance in wild-type and UCP1-KO mice

Carola W. Meyer,[1] Monja Willershäuser,[2] Martin Jastroch,[3] Bryan C. Rourke,[4] Tobias Fromme,[5] Rebecca Oelkrug,[1] Gerhard Heldmaier,[1] and Martin Klingenspor[5]

[1]*Department of Animal Physiology, Faculty of Biology, Philipps-Universität, Marburg, Germany;* [2]*Institute of Experimental Genetics, Helmholtz Center Munich, Neuherberg, Germany;* [3]*Buck Institute for Age Research, Novato California;* [4]*Department of Biological Sciences, California State University, Long Beach, California; and* [5]*Molecular Nutritional Medicine, Technische Universität München, Else Kröner Fresenius Center, Freising, Germany*

Submitted 14 January 2009; accepted in final form 17 August 2010

Meyer CW, Willershäuser M, Jastroch M, Rourke BC, Fromme T, Oelkrug R, Heldmaier G, Klingenspor M. Adaptive thermogenesis and thermal conductance in wild-type and UCP1-KO mice. *Am J Physiol Regul Integr Comp Physiol* 299: R1396–R1406, 2010. First published September 8, 2010; doi:10.1152/ajpregu.00021.2009.—We compared maximal cold-induced heat production (HPmax) and cold limits between warm (WA; 27°C), moderate cold (MCA; 18°C), or cold acclimated (CA; 5°C) wild-type and uncoupling-protein 1 knockout (UCP1-KO) mice. In wild-type mice, HPmax was successively increased after MCA and CA, and the cold limit was lowered to −8.3°C and −18.0°C, respectively. UCP1-KO mice also increased HPmax in response to MCA and CA, although to a lesser extent. Direct comparison revealed a maximal cold-induced recruitment of heat production by +473 mW and +227 mW in wild-type and UCP1-KO mice, respectively. The increase in cold tolerance of UCP1-KO mice from −0.9°C in MCA to −10.1°C in CA could not be directly related to changes in HPmax, indicating that UCP1-KO mice used the dissipated heat more efficiently than wild-type mice. As judged from respiratory quotients, acutely cold-challenged UCP1-KO mice showed a delayed transition toward lipid oxidation, and 5-h cold exposure revealed diminished physical activity and less variability in the control of metabolic rate. We conclude that BAT is required for maximal adaptive thermogenesis but also allows metabolic flexibility and a rapid switch toward sustained lipid-fuelled thermogenesis as an acute response to cold. In both CA groups, expression of contractile proteins (myosin heavy-chain isoforms) showed minor training effects in skeletal muscles, while cardiac muscle of UCP1-KO mice had novel expression of beta cardiac isoform. Neither respiration nor basal proton conductance of skeletal muscle mitochondria were different between genotypes. In subcutaneous white adipose tissue of UCP1-KO mice, cold exposure increased cytochrome-*c* oxidase activity and expression of the cell death-inducing DFFA-like effector A by 3.6-fold and 15-fold, respectively, indicating the recruitment of mitochondria-rich brown adipocyte-like cells. Absence of functional BAT leads to remodeling of white adipose tissue, which may significantly contribute to adaptive thermogenesis during cold acclimation.

nonshivering thermogenesis; cold limit; mitochondrial proton leak; respiratory quotient; myosin heavy chain isoforms

IN MAMMALS TWO FORMS OF FACULTATIVE heat production exist: shivering and nonshivering thermogenesis. While the former releases heat from involuntary contractions of skeletal muscle fibers, a large proportion of the latter is derived from brown adipose tissue (BAT) and its thermogenic uncoupling protein, UCP1 (5). The ability to produce heat through UCP1-mediated adaptive nonshivering thermogenesis is considered to be a critical evolutionary development that promoted the radiation of eutherian mammals in cold environments (5). Comparative physiological studies of endothermic vertebrates, however, also suggest the presence of UCP1-independent mechanisms of adaptive thermogenesis. Marsupials exhibit increased HPmax in response to cold acclimation, and some species cope with cold winter seasons in their natural habitat (9, 41). Although in these ancient mammals, a gene encoding the UCP1 ortholog is found, the functional significance of marsupial UCP1 for thermogenesis is questionable (21, 22, 31). In birds, despite the lack of UCP1 and BAT, many avian species, even of small body size, inhabit regions where ambient temperatures may decrease below −20°C for prolonged periods of time and are known to exhibit pronounced seasonal changes in HPmax (40). In rats and hamsters, measurements of BAT metabolic activity in vivo suggested that a significant proportion of the cold-induced increase in nonshivering thermogenesis does not originate in BAT (8, 35).

As such, mice with a targeted inactivation of the UCP1 gene (UCP1-KO) provide a mammalian model organism for studying (adaptive) metabolic responses in the absence of functional BAT. UCP1-KO mice cannot replace shivering with nonshivering thermogenesis and exhibit a cold-sensitive phenotype when tested at 4°C (7). However, UCP-1 KO mice are able to survive in the cold (4°C) for prolonged periods when previously acclimated to 18°C (moderate cold). Whereas shivering thermogenesis may be the sole contributor to this increased heat production and cold tolerance in UCP1-KO mice (11), elevated proton leak in skeletal muscle mitochondria (28) and metabolic alterations in white adipose tissue (WAT), including futile ion and substrate cycling and the emergence of brown-like adipocytes, have been suggested (1, 12, 45).

To judge the physiological relevance of any specific biochemical mechanism for adaptive thermogenesis, the magnitude of the cold-induced thermogenic capacity increase must be in accordance with the improvement of the cold limit. Maximal cold-induced thermogenesis and corresponding cold limits have been previously studied in laboratory mice and other small mammals and birds (e.g., Refs. 9, 13, 15, 19, 20, 39), but they have never been determined in genetically modified mouse models with metabolic or thermogenic deficiencies. To further characterize the thermophysiology of UCP1-KO mice, we first studied their metabolic responses to acute cold exposure (5 h at 5°C) in more detail, by simultaneously recording body temperature (T_b), physical activity, metabolic rate (MR), and respiratory quotient (RQ). To assess

Address for reprint requests and other correspondence: C. W. Meyer, Dept. of Animal Physiology, Faculty of Biology, Philipps-Universität, Karl-von-Frisch Strasse 8, 35032 Marburg, Germany (e-mail: meyerc@staff.uni-marburg.de).

the maximal thermogenic capacity, we exposed mice to stepwise decreasing ambient temperatures (T_a) in the range of 30°C to −20°C. This protocol enabled us to calculate cold limits, i.e., the threshold ambient temperature at which euthermia could be sustained by maximal heat production at rest (HPmax). The comparison of HPmax and cold limit in warm- (27°C, WA), moderate cold- (18°C, MCA), and cold- (5°C, CA) acclimated mice revealed the extent to which adaptive thermogenesis occurs in the presence and absence of functional BAT. The parallel recordings of T_b and MR enabled us to calculate the thermal conductance and to compare heat production and heat loss of warm- and cold-acclimated wild-type and UCP1-KO mice. By injection of norepinephrine, we determined the fraction of cold-induced HPmax due to nonshivering thermogenesis regulated by the sympathetic nervous system.

In the search for structural or functional adaptations of cold-acclimated UCP1-KO mice outside of BAT, we sampled skeletal muscles, heart muscle, and white adipose tissues. We analyzed the expression of myosin heavy chain (MyHC) isoforms in different skeletal muscles and measured proton leak kinetics in isolated mitochondria from the hind limb skeletal muscles. In white adipose tissues, we measured cytochrome-*c* oxidase (COX) activity as a surrogate for respiratory capacity and expression of the cell death-inducing DFFA (DNA fragmentation factor alpha)-like effector A (CideA) as a marker for the recruitment of brown adipocyte-like cells. Thereby, we aimed to provide further insights into metabolic alterations and thermoregulatory adjustments, which facilitate cold acclimation in the absence of functional BAT.

MATERIALS AND METHODS

Mice and maintenance. Wild-type and UCP1-KO littermates (genetic background C57BL/6J) were derived from heterozygous breeding pairs in our colony. The founder mice for establishing our colony were originally provided by Dr. Leslie Kozak (Pennington Medical Research Center). Mice were born at 27°C and weaned to 24°C at 3–4 wk of age. They were fed Altromin 1314 standard breeding chow (Lage, Germany), had free access to water, and were kept on a 12:12-h light-dark cycle. Mice were genotyped by amplifying a 201-bp (wild-type) and 409 bp (KO) fragment from the UCP1 gene, using the primers 8265–5F: GGT AGT ATG CAA GAG AGG TGT and E2Rev: CCT AAT GGT ACT GGA AGC CTG and NeoRev: CCT ACC CGC TTG CAT TGC TCA, according to a protocol kindly provided by L. Kozak. After genotyping, the WT and UCP1-KO mice included in our experiments were housed singly throughout the entire study period. Each cage was equipped with sawdust and two to three slices of tissue paper. Except for white adipose tissue sampling, only female mice were used. In all experimental mice, the presence or absence of UCP1 protein was also confirmed post mortem by immunological detection in BAT [as published previously (23)].

Experimental schedules. At the age of 2–4 mo, female mice were intraperitoneally implanted with temperature-sensitive transmitters (series 3000; model XM-FH; Mini Mitter, Bend, OR, USA). These transmitters weigh 1.5–1.6 g and are able to register body temperature at ±0.1°C. In addition, they provide a relative measure of gross activity over time, i.e., if the animal is moving relative to a receiver antenna. After 1 wk of recovery from surgery, mice were randomly assigned to warm (WA, 27°C) or to moderate cold (MCA, 18°C) acclimation. Following 3 wk at the respective acclimation temperature, acute cold tolerance to 5°C was investigated, and cold limits were determined 1 wk later. A third group of mice was maintained at 18°C for 3–4 wk, after which ambient temperature was lowered to 5°C for another 3–4 wk (CA, 5°C), until cold limits were determined.

On the molecular level, we determined the expression of MyHC isoforms in various skeletal muscle groups and the heart and measured basal proton leak kinetics in isolated mitochondria from the hind limb skeletal muscles. In white adipose tissues, we measured cytochrome-*c* oxidase activity as a surrogate for respiratory capacity and CideA expression as a marker for the recruitment of brown adipocyte-like cells. Mitochondrial proton leak kinetics of skeletal muscles, as well as COX activity and CideA expression in white adipose tissues were investigated in separate groups of wild-type and UCP1-KO mice (males and females) acclimated to either 27°C (WA) or 5°C (CA) for 3–4 wk. For CA experiments, mice were kept in climate chambers controlling ambient temperature at a precision of ±0.5°C. Only the mice cold acclimated for mitochondrial studies were kept in a cooling cabinet in which the ambient temperature at the cage level was 10°C during the light phase due to heat production from illumination, while it was 5°C during the dark phase. All experiments and procedures were approved by the German animal welfare authorities (RP Giessen, approval no. MR 17/1–32/2005 and MR 17/1–14/2009).

Indirect calorimetry and body temperature telemetry setup. Mice were transferred to metabolic cages (1.8 l) placed on telemetry receivers (TR 3000, Mini Mitter) in a temperature-controlled (± 0.5°C) climate chamber. Body temperature and physical activity were recorded in 1-min epochs using the VitalView software (Mini Mitter). The principal setup of the respirometric system has been published previously (19). In brief, volumes of oxygen consumed ($\Delta vol\%O_2$) and volumes of carbon dioxide ($\Delta Vol\%CO_2$) produced by each mouse were measured during 60 s every 2 to 4 min using an electrochemical O_2 analyzer (S-3AII, Ametek, Pittsburgh, PA) and a CO_2 analyzer (UNOR 6N; Sick-Maihak, Hamburg, Germany and Uras 14; Hartmann & Braun, Skyva, Switzerland). The coordination of the different peripheral measuring devices was governed via customized Visual Basic modules developed by G. Heldmaier. Oxygen readings were converted to MR, according to the following equation: MR [ml O_2/h] = $\Delta vol\%O_2$·flow [l/h]·10. The flow rate was set ~35 l/h. To adjust for differences in flow rates in air leaving and entering the metabolic cages, RQ (volumes of CO_2 produced/volumes of O_2 consumed) was used. Effective heat production [HP, mW] and thermal conductance C [mW/°C] were calculated according to (17) as *Eq. 1*: $HP = (4.44+1.43 \cdot RQ) \cdot MR$ and *Eq. 2*: $C = HP \cdot (T_b - T_a)^{-1}$, where MR is metabolic rate (ml/h), T_b is body temperature (°C), and T_a is ambient temperature (°C).

Cold endurance test. Mice were maintained in cages of 1.8 l with no food or water provided. Following 3–4 h of thermoneutral conditions (30°C; e.g., Refs 16, 27, and 42), ambient temperature (T_a) was maintained at 5°C for up to 5 h. In each trial, up to 3 mice and one obligate reference channel were recorded in parallel, yielding a 2–4-min resolution of metabolic readings (i.e., 1 mouse = 2-min resolution, 2 mice = 3-min resolution, 3 mice = 4-min resolution per individual reading). A mouse was immediately rescued from the chamber and classified as cold sensitive if its body temperature dropped below 31°C. All measurements commenced at 0800 CET, and the genotype was blinded to the experimenter. Resting metabolic rates (RMRs) were determined from the lowest mean of three consecutive O_2 readings, equivalent to 9–12 min in the climate chamber, which yielded lowest variability (assessed by CV, coefficient of variation).

HPmax and cold limit. For determination of maximal cold-induced heat production (HPmax) at rest and calculation of cold limits, single animals (plus one reference channel) were measured (genotype blinded), which yielded a 2 min resolution of O_2 readings. After 2 3 h at 30°C, a mouse was exposed to a series of decreasing T_as for determination of RMRs. In MCA and CA mice, T_a was lowered stepwise from 30, 24, 15, 10, 5, 0°C to −20°C. In WA mice, we were unable to determine RMRs at any $T_a \leq 15$°C (mice were continuously active). In this experimental group T_a was lowered stepwise from 30,

27, 24, 20, 18, to −20°C. With the exception of −20°C, each temperature was sustained for at least 20 min and up to 90 min, i.e., until stable readings could be observed over a period of 6–10 min (see Supplemental Fig. S1 in the online version of this article). A mouse was removed from the metabolic chamber when its body temperature clearly dropped despite an increase in heat production (oxygen consumption). During the experiment, none of the animals suffered from frostbite or any other adverse side effects resulting from cold exposure. A whole measurement day lasted up to 8 h, during which time, no food or water was supplied to the mouse.

Maximal resting metabolic rate (RMRmax; ml/h) was defined as the highest MR observed in a nonexercising mouse. These highest values were usually exhibited around the time when mice became hypothermic (see Supplemental Fig. S1 in the online version of this article). RMRmax was converted to maximal resting heat production (HPmax, mW) using *Eq. 1*. The point of intersection of HPmax with the regression of resting HP with T_a was used to calculate the effective cold limit (see Supplemental Fig. S2 in the online version of this article).

Norepinephrine-stimulated thermogenesis. For determination of maximal norepinephrine-stimulated heat production (NEmax), single mice were maintained in the calorimetry system for 2–3 h at 30°C. Mice were briefly removed from the system and received a subcutaneous injection of norepinephrine (1 mg/kg). The changes in oxygen consumption and carbon dioxide production before and after NA stimulation were measured as outlined above, except that the resolution of readings was set to 20 s. NEmax was calculated from the highest mean, resting metabolic rate at 30°C [= resting metabolic rate at thermoneutrality (RMRt)] and was calculated from the lowest mean of three consecutive O_2 readings, equivalent to 1 min in the climate chamber. Data were converted to HP according to *Eq*. 1.

SDS-PAGE electrophoresis of myosin heavy-chain isoforms. Selected skeletal muscle biopsies (M. gastrocnemius, M. tibialis anterior, and M. masseter*)* were quickly dissected and shock frozen in liquid nitrogen. In addition, heart muscle was obtained from the mice kept at 5°C. Muscle samples from 5 to 20 mg were homogenized on ice in 19 or 38 vol of buffer (in mM): 250 sucrose, 100 KCl, and 5 EDTA, for protein analyses. Electrophoretic separation of murine MyHC isoforms was adapted from a method used in rats and applicable to other rodents (44). SDS-PAGE was run on <1 μg total protein and identified four skeletal muscle isoforms, types MyHC 1, 2a, 2x, and 2b. Although heart-specific isoforms can be separated with native conformation gels, our technique also resolved cardiac isoforms clearly, types MyHC alpha and beta (identical to MyHC 1). Bands were visualized with silver-stain (Bio-Rad), photographed on a digital camera (Nikon, Tokyo, Japan), and analyzed with densitometry software (ImageQuant).

Isolation of skeletal muscle mitochondria. Hindlimb skeletal muscle tissue was quickly dissected and immediately placed in ice-cold isolation CP1-medium containing 100 mM KCl, 50 mM Tris-HCl and 2 mM EGTA, pH 7.4, at 4°C. Muscle tissue was cleaned of adipose tissue patches, minced with scissors, and repeatedly rinsed with CP-1 medium, stirred for 3 min in CP-2 medium [CP-1 plus 1 mM ATP, 5 mM $MgCl_2$, 0.5% (wt/vol) fatty acid free BSA (Sigma no. A3803), 2.1 U/ml protease (Subtilisin A, Sigma-Aldrich), pH 7.4, at 4°C] and homogenized in CP-2 medium using a polytron tissue homogenizer (Kinetica, Franklin, OH). The homogenate was stirred in CP-2 for 3 min, and then, mitochondria were isolated using differential centrifugation and resuspended in CP-1 medium. Protein concentration was determined using the Biuret method with fatty acid-free BSA as a standard.

Measurement of mitochondrial oxygen consumption and proton conductance in skeletal muscle. Oxygen consumption was measured using a Clark-type oxygen electrode (Rank Brothers, Cambridge, UK) maintained at 37°C and calibrated with air-saturated medium [120 mM KCl, 5 mM KH_2PO_4, 3 mM HEPES, 1 mM EGTA, and 0.3% (wt/vol) defatted BSA, pH 7.2], which was assumed to contain 406 nmol O_2/ml (37). Skeletal muscle mitochondria were suspended at 0.35 mg/ml in 2.5 ml medium and incubated with 8 μM rotenone (to inhibit complex I) and energized with 6 mM succinate. State 3 respiration was established by addition of 600 μM ADP and shifted to state 4 by the addition of 1 μM oligomycin to inhibit the ATP synthase. Finally, carbonyl cyanide 4-(trifluoromethoxy)phenylhydrazone (FCCP) was titrated in 0.3-μM steps to completely uncouple the mitochondria and stimulate maximum respiratory activity. For the measurement of mitochondrial proton leak, mitochondria were incubated with oligomycin, rotenone, and 150 nM nigericin (to convert the pH gradient to membrane potential). The respiration rate of mitochondria, in the presence of oligomycin (state 4), is proportional to the rate at which protons leak across the inner membrane. The kinetic response of the proton conductance to its driving force (proton motive force) can, therefore, be measured as the relationship between respiration rate and membrane potential when the potential is varied by titration with electron transport chain inhibitors (3, 30). Respiration rate and membrane potential were determined simultaneously using electrodes sensitive to oxygen and to the potential-dependent probe methyltriphenylphosphonium (TPMP+) (4). The TPMP+ electrode was calibrated with sequential additions of up to 2.5 μM TPMP+. Then 6 mM succinate was added to start the reaction, and the respiratory chain was progressively inhibited with up to 1.2 mM malonate. Finally, 0.3 μM FCCP was added to release all TPMP+ from the mitochondrial matrix to correct for the drift of the electrodes. TPMP+ correction factor was assumed to be 0.35 for skeletal muscle, as described previously (38).

Cytochrome-c oxidase activity assay in white adipose tissues. Mice were killed by means of a CO_2 overdose. Snap-frozen white adipose tissue was grinded in liquid nitrogen and further homogenized in tissue buffer [10 mM HEPES, 40 mM KCl, 2 mM EGTA, 1% (vol/vol) Tween 20, 2 μM PMSF, 2 μM oligomycin, 10 mM KF] with a Potter-type homogenizer. The homogenate was sonicated with several short bursts, centrifuged (16,000 *g*, 2 min), and the supernatant was employed for protein quantification by the Biuret method. Activity assays were performed with cleared homogenate equivalent to 300 μg protein in assay buffer [50 mM KH_2PO_4, 2 mM EGTA, 1% (vol/vol) Tween 20, 20 mM ascorbic acid, 5 mM ADP, 2 μM oligomycin] and started by the addition of cytochrome *c* (40 μM final concentration). COX activity was determined by recording oxygen consumption with a Clark-type electrode (model no. 10; Rank Brothers, Cambridge, UK). For every sample, we calculated the mean of two independent measurements on different days.

Quantitative PCR. Flash-frozen white adipose tissue depots were grinded in liquid nitrogen. A portion of the resulting powder was homogenized with a turrax-type instrument. Total RNA was isolated with a column-based kit (SV Total RNA Isolation System; Promega, Madison, WI) and quantified photometrically. We retrotranscribed 500 ng total RNA into cDNA (QuantiTect reverse transcription kit; Qiagen, Germantown, MD). For quantitative PCR, the SensiMix SYBR reagent (Bioline) was employed with an Eppendorf MasterCycler instrument. For all primer pairs, template dilution series were included to determine and correct for PCR efficiency. Every sample was measured in technical triplicates. CideA expression was normalized to the mRNA abundance of the housekeeping gene Hsp90. Primer sequences: Hsp90 forward: AGGAGGGTCAAGGAAGTGGT, Hsp90 reverse: TTTTTCTTGTCTTTGCCGCT, CideA forward: TGCTCTTCTGTATCGCCCAGT, and CideA reverse: GCCGTGTTAAGGAATCTGCTG.

Statistical analysis. Unless otherwise indicated, data in figures, tables, and text are expressed as means ± SD. To assess the statistical significance of differences between mean values, a two way ANOVA (factors genotype, acclimation temperature, and their interaction) was performed. Because of heterogeneity of variances, significant differences in the response to NE injection were assessed using Kruskal-Wallis ANOVA on ranks (H-test), followed by multiple comparisons. Summed activity counts before and after lowering T_a to 5°C (cold

endurance test) were compared using Wilcoxon test. RQ and conductance time courses at 5°C were analyzed by repeated-measures ANOVA. For these statistical analyses, SigmaStat 3.5 (Systat Software, Chicago, IL) was used. A linear mixed-effects model fit by maximum likelihood (random factor: individual mouse, fixed factors: body mass × T_a × genotype) using the statistical software package R (36) was employed to reveal significant differences between slopes for HP vs. T_a between experimental groups. A threshold of $P < 0.05$ was considered statistically significant.

RESULTS

To compare the cold-induced changes in metabolic rate, body temperature, RQ, and thermal conductance, we challenged wild-type and UCP1-KO mice with two paradigms of acute cold exposure: a cold endurance test (5 h at 5°C) and a cold limit test (determination of HPmax).

In the cold endurance test, the metabolic responses in the WA and MCA mice of both genotypes were compared. Body temperatures at 30°C were similar in the four groups of mice, with minimal values observed within the last hour before ambient temperature (T_a) was lowered to 5°C (Fig. 1*A*). Upon cold exposure, body temperature in all groups dropped by 1–2°C within 30 min. Whereas mice from the WA groups were unable to sustain normal body temperature at 5°C ($T_b > 31$°C), the MCA mice of both genotypes were able to maintain euthermia throughout the entire 5-h cold period, albeit at a reduced body temperature set-point compared with 30°C T_a. These results confirmed previous published findings that a 3-wk acclimation period to 18°C was sufficient to increase cold tolerance in wild-type and UCP1-KO mice (11).

The MCA mice were heavier than the WA mice, and RMRs were significantly higher. Within WA and MCA acclimation groups, however, body mass and RMRs were not different between genotypes (Table 1), which enabled us to directly compare the metabolic rates of wild-type and UCP1-KO mice. In response to the lowering of ambient temperature from 30 to 5°C (Fig. 1*B*), all mice increased their metabolic rate. In the WA mice of both genotypes, the metabolic rate at 5°C was almost constantly maintained between 90 and 100 ml O_2/h without pronounced fluctuations (Figs. 1*B* and 2). In contrast, metabolic rates of the MCA mice were consistently higher. Furthermore, we observed a distinct phenotypic difference in the temporal pattern of thermoregulatory heat dissipation between genotypes: MCA wild-type mice displayed intermittent thrusts of oxygen consumption, resulting in a large range of readings, whereas metabolic rates of the MCA UCP1-KO mice appeared much more constant (Fig. 1*B*). The ability to display metabolic excursions was mirrored in behavior at 5°C (Fig. 2): 5 out of 6 of the MCA wild-type mice showed highly variable metabolic rates and displayed clear bouts of activity every 1.5–2.0 h, as assessed by autoregression analysis and sine curve fitting. In contrast, the MCA KO and also the WA mice of either genotype were much less active during the 5-h period at 5°C and did not display rhythmicity in either MR or T_b. A comparison of summed activity counts from the initial 3 h (at 30°C) with the first 3 h in the cold (5°C) revealed that despite substantial interindividual variation in activity levels, all MCA wild-type mice had increased their activity upon cold exposure ($P = 0.028$), while all MCA KO individuals had decreased activity ($P = 0.018$).

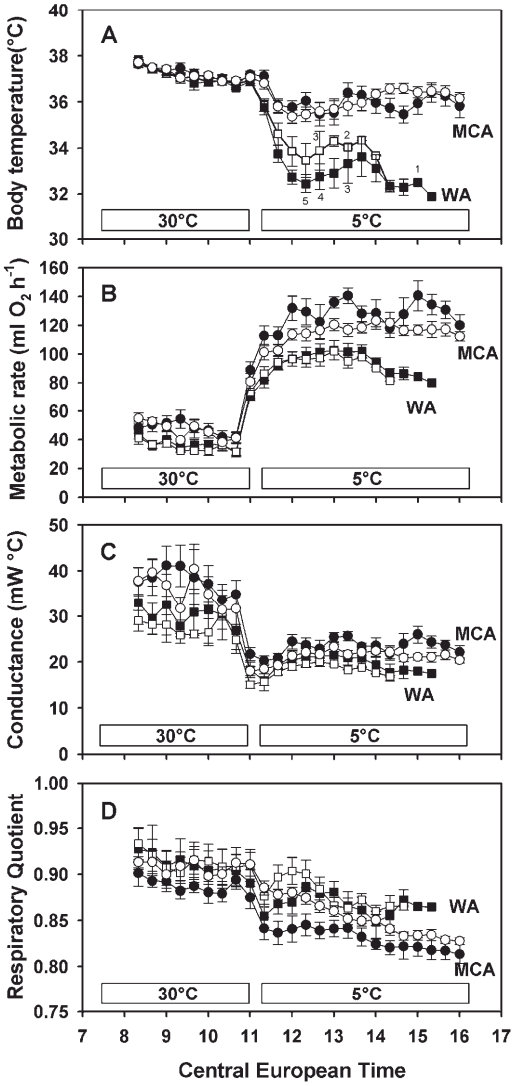

Fig. 1. Body temperature (*A*), metabolic rate (*B*), thermal conductance (*C*), and respiratory quotient (RQ) (*D*) of warm (WA; 27°C) and moderate cold (MCA; 18°C) acclimated wild-type (solid symbols) and uncoupling protein 1-knockout (UCP1-KO) mice (open symbols) maintained at 30°C and 5°C (cold endurance test). Each data point represents the means ± SE of 10–15 readings collected during 30 min in the metabolic cage. Mice ($n = 5$) in each group initially entered the experiment, but numbers in the WA groups progressively decreased (*A*) because mice became hypothermic and had to be removed from the metabolic cage.

Table 1. *Metabolic characteristics of resting warm acclimated (27°C) and moderately cold acclimated (18°C) wild-type and UCP1-KO mice measured at 30°C and 5°C*

	At 30°C				At 5°C			
	Wild-Type		UCP1-KO		Wild-Type		UCP1-KO	
	WA	MCA	WA	MCA	WA	MCA	WA	MCA
Body mass, g	22.6[a] ± 1.0	24.8[b] ± 1.0	23.0[a] ± 1.0	24.1[b] ± 1.3				
RMR, ml O_2/h	29.6[a] ± 4.6	36.9[b] ± 4.1	27.8[a] ± 3.8	37.3[b] ± 2.9	99.4[a] ± 10.7	109.7[b] ± 8.1	95.3[a] ± 12.9	108.7[b] ± 11.6
T_b, °C	36.8[a] ± 0.6	36.9[a] ± 0.2	36.7[a] ± 0.4	37.0[a] ± 0.3	33.0[a] ± 0.8	34.7[b] ± 0.7	33.7[a] ± 1.5	35.5[b] ± 1.0
Conductance, mW/°C	24.8[a] ± 2.4	30.3[b] ± 4.0	23.3[a] ± 3.1	29.6[b] ± 5.5	20.8[a] ± 2.1	20.9[a] ± 1.7	19.0[a] ± 1.9	20.3[a] ± 2.5

Data are expressed as means ± SD from n = 5–7 individuals per group. In each parameter, there was a significant effect of acclimation temperature ($P < 0.05$) but not of genotype. WA, warm acclimated; MCA, moderately cold acclimated; UCP1, uncoupling protein 1; KO, knockout; RMR, resting metabolic rate; T_b, body temperature. [a,b]Differences between mean values at 30°C and 5°C, respectively, are indicated by superscripted letters that differ.

In the thermoneutral environment, thermal conductance was higher in MCA compared with WA mice, irrespective of genotype (Fig. 1*C*, Table 1). Upon cold exposure thermal conductance was immediately reduced in all acclimation groups. On average, thermal conductance at 5°C was not significantly different between genotypes (genotype: $P = 0.07$; time: $P < 0.001$; genotype × time: $P = 0.43$). Mirroring the larger range of metabolic rates seen at 5°C, however, the thermal conductance in the MCA wild-type mice was more variable than in the MCA KO mice.

Throughout the entire experimental period, RQs of the MCA wild-type mice were distinctly lower than in the other three groups (Fig. 1*D*). In all groups of mice, exposure to 5°C induced a lowering of RQ, reflecting increased lipid oxidation in the cold. This cold-induced decrease in RQ was most pronounced in the MCA wild-type mice. In contrast, it took >2 h until RQs of the MCA KO mice had attained wild-type levels (time: $P < 0.001$; genotype: $P = 0.033$, time × genotype: $P < 0.001$).

The cold limit test was performed to compare the metabolic responses of WA, MCA, and CA mice exposed to stepwise decreasing ambient temperatures, and to determine HPmax from which we could calculate the cold limit for each group. This experiment did not reveal any consistent genotype differences in mean RMRs, body temperature, and, hence, thermal conductance, either within WA or MCA mice (Fig. 3). In contrast, in the CA state, RMRs of the UCP1-KO mice (and also their heat production, graph not shown) were lower compared with wild-type mice. This lowered heat production was frequently accompanied by reduced body temperature and consistently lower thermal conductance.

HPmax progressively increased with cold acclimation (WA < MCA < CA), attaining a maximal recruitment of 473 mW adaptive thermogenic capacity in CA wild-type mice (Table 2). In UCP1-KO mice, a similar recruitment of adaptive thermogenic capacity, though to a lesser extent (227 mW), was also found in MCA and CA. Effective cold limits were obtained by intersecting mean HPmax from each group with the respective linear regressions of mean HP vs. T_a (see Supplemental Fig. S2 in the online version of this article). We did not analyze the WA mice because of the comparatively narrow T_a range available. Comparison of wild-type mice in the MCA and CA state revealed that the improvement of the cold limit by ~10°C

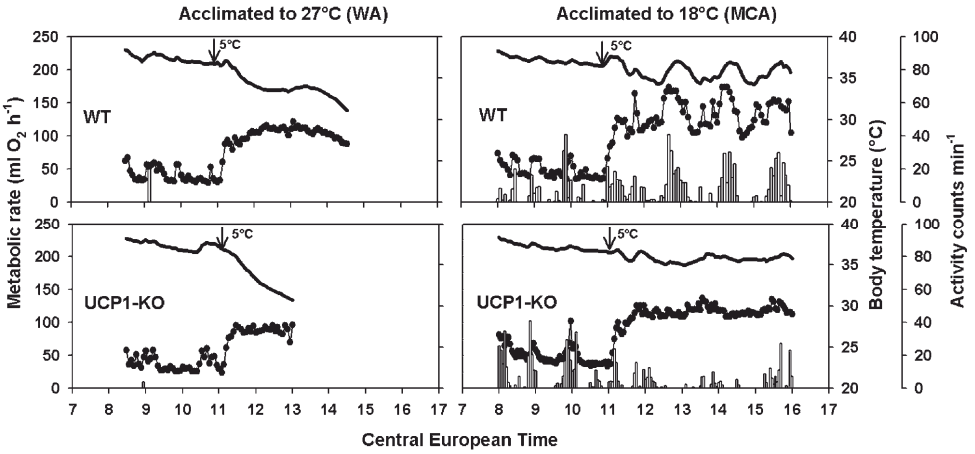

Fig. 2. Representative original tracings of activity readings (bars), metabolic rate (line and scatterplot) and body temperature (line plot) in individual wild-type and UCP1-KO mice during a cold endurance test (~4 h at 30°C, up to 5 h at 5°C, temperature switch indicated with an arrow). Previously WA mice of either genotype had to be removed from the experiment because of hypothermia (final body temperature <31°C). In contrast, the mice acclimated to MCA (18°C) remained normothermic. Note the reduced activity and the less variable metabolic rates of the WA wild-type (WT) mouse and the two UCP1-KO mice.

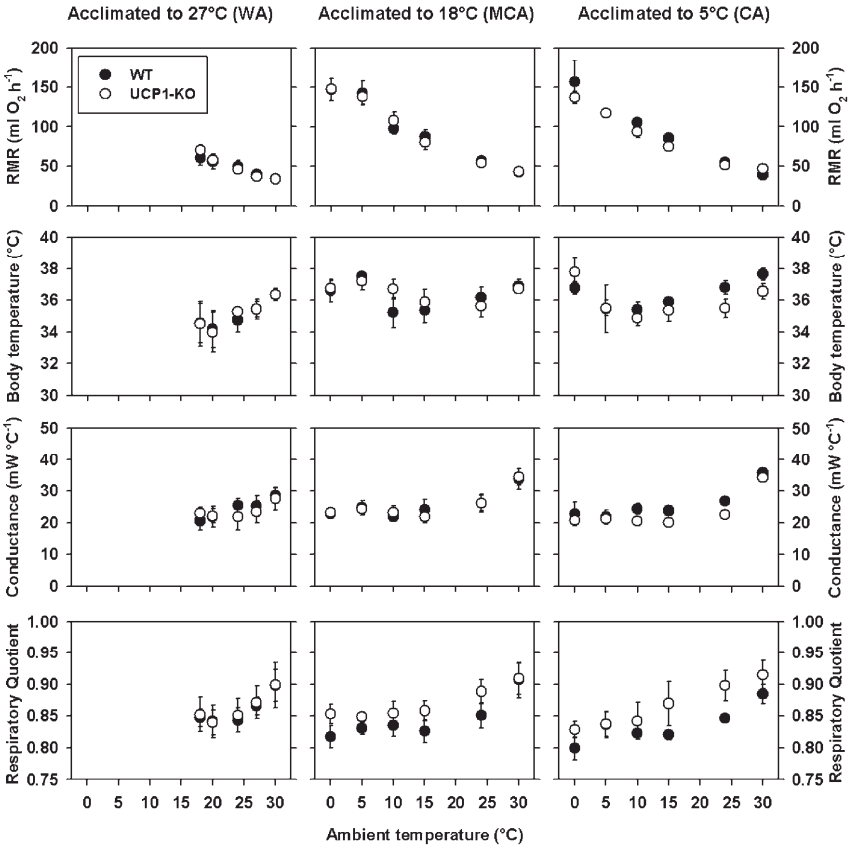

Fig. 3. Means ± SD resting metabolic rate (RMR), body temperature (T_b), thermal conductance, and RQ of wild-type and UCP1-KO mice (n = 5–7 mice per group) acutely exposed to stepwise decreasing ambient temperatures. The mice had been previously acclimated to either 27°C (warm, WA), 18°C (moderate cold; MCA), or 5°C (cold, CA) for at least 3 wk.

in CA mice was well in accord with a further increase in HPmax (+216 mW). Notably, MCA KO mice significantly increased HPmax relative to WA, while the further marginal elevation of HPmax in CA KO mice was not significant. The slope for the regression of HPmax vs. T_a in the CA KO mice was significantly lower than in the other three groups ($P <$ 0.014). Our calculations, therefore, predict an improved cold limit of CA KO mice by about the same magnitude as in the wild-type mice (~9°C), even though HPmax had only increased by 69 mW (8%).

In cold-acclimated wild-type mice (MCA and CA), NE produced pronounced elevations in heat production, whereas only minor increases in NE-stimulated heat production were observed in the UCP1-KO mice, which did not attain statistical significance. Subtraction of NE-stimulated maximal thermogenesis (NEmax) and RMRt from HPmax revealed the major components of heat production and their relative contribution to maximal cold-induced heat production within each genotype and acclimation group (Fig. 4).

Finally, we dissected distinct skeletal muscle groups, heart muscle, and white adipose tissue depots to identify structural and functional adaptations in CA UCP1-KO mice. MyHC skeletal muscle isoforms (see Supplemental Fig. S3 in the online version of this article) showed relatively minor but significant alterations in the masseter (increase in type 2x with CA, $P = 0.022$, decrease in type 2b, $P = 0.015$) but no genotype differences. Furthermore, CA mice demonstrated prominent shifts toward slower MyHC 2a and 2x isoforms via reductions of MyHC 2b in the gastrocnemius ($P < 0.001$ for each). The minor changes in tibialis anterior did not reach statistical significance (all $P > 0.05$). In cardiac tissues, UCP1-KO mice (CA) displayed novel expression of the MyHC beta isoform, but without a significant overall decrease in MyHC alpha.

In isolated skeletal muscle mitochondria, mitochondrial oxygen consumption in state 2 (succinate respiration), state 3 (ADP-induced), state 4 (oligomycin-inhibited leak respiration), and FCCP-induced oxygen consumption showed no differ-

Table 2. *Maximal cold induced resting metabolic rate (RMRmax) and maximal heat production of WA (27°C), MCA (18°C), and cold acclimated (5°C) wild-type and UCP1-KO mice*

	Wild-Type			UCP1-KO			ANOVA (all $P < 0.001$)
	WA ($n = 5$)	MCA ($n = 6$)	CA ($n = 4$)	WA ($n = 6$)	MCA ($n = 7$)	CA ($n = 7$)	
Body mass, g	22.7 ± 0.9	24.5 ± 1.3	26.8 ± 0.7	23.0 ± 0.8	24.1 ± 1.2	25.7 ± 1.2	$P_{geno} = 0.680$ $P_{accl} < 0.001$ $P_{gxa} = 0.360$
RMRmax, ml O_2/h	133.5 ± 11.0	180.2 ± 21.5	218.3 ± 11.4	125.6 ± 12.2	154.4 ± 10.0	167.5 ± 18.1	$P_{geno} < 0.001$ $P_{accl} < 0.001$ $P_{gxa} = 0.010$
HPmax, mW	756.5 ± 65.0	1012.9 ± 121.1	1229.5 ± 61.3	714.0 ± 73.0	872.8 ± 56.0	941.0 ± 109.1	$P_{geno} < 0.001$ $P_{accl} = 0.425$ $P_{gxa} = 0.010$
Cold limit, °C	>5°C	−8.3	−18.0	>5°C	−0.9	−10.1	

Data are expressed as means ± SD. For the MCA and CA groups, mean maximal heat production (HPmax) was converted into cold limit numbers (°C) from the point of intersection of HPmax with the respective regression equation for heat production (HP) vs. ambient temperature (T_a; Supplemental Fig. S2). RMRmax, maximum resting metabolic rate; CA, cold acclimated; P_{geno}, probability among genotypes; P_{accl}, probability among acclimation groups; P_{gxa}, probability among genotype × acclimated groups. For clarity, superscripted letters indicating significant differences between groups (derived from multiple pairwise comparisons by Tukey post hoc test) have been omitted.

ences between acclimation temperatures (here: WA and CA) and genotypes. The state 2–4 values of CA animals, however, tended to be higher than in WA mice (see Supplemental Fig. S4 in the online version of this article). We next compared the full kinetic response of the basal proton leak (monitored as oxygen consumption rate) at 37°C to stepwise changes in its driving force, membrane potential, in skeletal muscle mitochondria of CA and WA mice (Fig. 5). There was no apparent difference in the proton leak curves between WA and CA groups, as well as wild-type and UCP1-KO mitochondria.

We determined the specific activity of COX as a surrogate marker for maximal mitochondrial respiratory capacity in several WAT depots of wild-type and KO mice, both WA and CA (Fig. 6, *A* and *B*). In wild-type mice, COX activity was not influenced by ambient temperature in epididymal WAT (eWAT) or inguinal WAT (iWAT). In CA KO mice, however, COX activity was significantly increased compared with WA

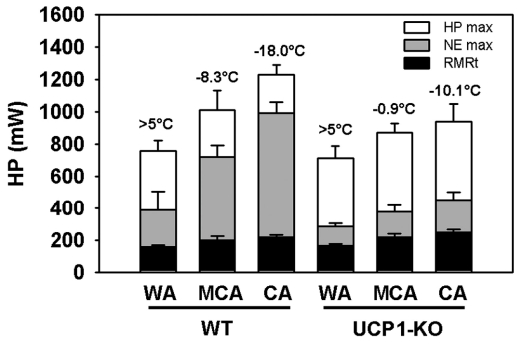

Fig. 4. Summarizing figure depicting RMRt (resting metabolic rate at thermoneutrality) and maximal norepinephrine-induced heat production (NEmax) of WT and UCP1-KO mice acclimated to different ambient temperatures: WA: 27°C, MCA: 18°C; cold acclimated (CA): 5°C, and in relation to maximal cold-induced heat production (HPmax). The corresponding cold limits for each group of mice are indicated. Data are indicated as means ± SD; $n = 4–7$ individuals per group. Note that HPmax and NEmax were determined in two different sets of mice for each genotype. RMRt was obtained prior to the injection of norepinephrine (for details, see text).

KO mice in eWAT and in iWAT ($P < 0.001$), as well as in periovarian WAT of a further group of female mice (data not shown). The cold-induced difference was greatest in iWAT with an approximate 3.6-fold increase (Fig. 6*B*). CideA expression was assessed as a marker for the emergence of brown adipocyte-like cells in white adipose tissue. In the CA state, CideA mRNA levels were ~15-fold increased in UCP1-KO compared with wild-type mice, whereas in the WA state CideA expression was low and not affected by genotype ($P < 0.001$, Fig. 6*C*).

DISCUSSION

During cold acclimation, the recruitment of thermogenic capacity in BAT contributes to an overall increase of cold-induced HPmax and improved cold tolerance. In wild-type mice, the increased thermogenic capacity in BAT is represented by a corresponding rise in norepinephrine-stimulated nonshivering thermogenesis capacity (5). In our study, CA wild-type mice showed the expected increase in norepinephrine-stimulated nonshivering thermogenesis relative to WA, and accordingly, an increase in HPmax in the cold by +473 mW. So far, it was known that UCP1 KO mice, lacking functional BAT, can also survive in the cold, but their maximal capacity for adaptive thermogenesis had not been determined. We, here, demonstrate that cold acclimation of UCP1-KO mice increases HPmax by +227mW. The comparison of the adaptive increase in HPmax demonstrates that in the absence of UCP1-mediated nonshivering thermogenesis, the UCP1-KO mice are still capable of exhibiting almost 50% of the wild-type increase in maximal cold-induced heat production, i.e., 227/473 mW.

There is a therapeutic interest in identifying thermogenic mechanisms in mammals, which may be exploited to combat dysregulations in body composition in humans (6). As the UCP1-KO mice cannot recruit BAT thermogenesis for adaptive heat production in the cold, they may provide models to identify other principal thermogenic processes. In our study UCP1-KO mice in the CA state showed a 2–4-fold increase in COX activity in several WAT depots. This strong recruitment of respiratory capacity was not observed in wild-type mice. CideA, which is highly expressed in murine BAT compared

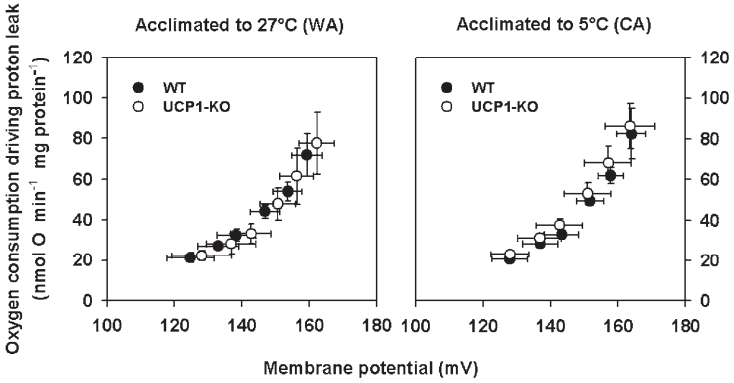

Fig. 5. Dependence of proton leak rate (measured as the respiration rate driving proton leak) on membrane potential of isolated skeletal muscle mitochondria of WA (27°C), CA (5°C), WT, and UCP1-KO mice. Duplicate measurements were performed on each mitochondrial preparation and averaged. Values are expressed as means ± SD from 5 independent preparations.

with WAT (49), was also strongly up-regulated in inguinal WAT of CA UCP1-KO mice. These observations provide evidence that a remodeling of WAT occurs, which could contribute adaptive thermogenesis in UCP1-KO mice.

It has been previously demonstrated that multilocular mitochondria-rich adipocytes expressing UCP1 emerge in different WAT depots of mice following cold acclimation or chronic β-adrenergic stimulation (29, 48), which is mediated by a cyclooxygenase-dependent mechanism (25, 46). In UCP1-KO mice histologically identical brown adipocyte-like cells, which do not express UCP1, can be induced at even higher abundance (1, 12). Expression profiling and respiration of inguinal WAT tissue explants suggest that the mitochondrial content and respiratory activity is increased in WAT of cold-acclimated UCP1-KO mice (45). As the mitochondria in these brown adipocyte-like cells are UCP1 deficient, an alternative futile mechanism must exist that utilizes the increased COX activity per mass unit of inguinal WAT for heat dissipation. Futile cycling of Ca^{2+} between the endoplasmic reticulum and cytosolic compartments could serve as such an ATP sink (45). According to our results, CA UCP1-KO mice recruited 227 mW adaptive thermogenic capacity, of which 30% (80 mW) were attributable to increased RMRt occurring in both genotypes, although the underlying mechanism is not understood. The remaining increase of ~150 mW could be contributed by the UCP1-KO-specific increases in WAT oxidative capacity. The contribution of WAT to total metabolic rate has been estimated to be ~2.6% or 0.89 ml $O_2 \cdot g^{-1} \cdot h^{-1}$ (= 4.9 mW/g; Ref. 26), making up to a total heat dissipation of ~10 mW in a mouse of 20 g with 2 g total fat mass. In the light of the observed ~2–4-fold increase in respiratory capacity, WAT could, therefore, contribute significantly to adaptive thermogenesis in UCP1-KO mice.

One straightforward conclusion is that mice without functional BAT predominantly depend on sustained shivering thermogenesis to maintain normothermia. UCP1-KO mice can only recruit thermogenic capacity when successively transferred to the cold, and it has been suggested that sustained shivering should have a training effect in skeletal muscle leading to enhanced endurance and capacity for shivering thermogenesis (11). The latter may be related to improved oxidative phosphorylation capacities of skeletal muscle mitochondria on fatty acid-derived substrates in UCP1-KO mice (43). In vivo, the proportion of NE-insensitive thermogenesis is often equated with shivering thermogenesis (18), but we could not observe major alterations in the thermogenic capacity of this component (white areas in stacked bars; see Fig. 4). Furthermore, the fiber composition of the gastrocnemius, masseter, and tibialis muscle did not mirror structural changes that might be anticipated from improved lipid-fuelled oxidation capacities. In contrast, we observed modest increases in slower MyHC isoforms in the gastrocnemius and masseter muscle of both the wild-type and the UCP1-ablated mice during CA (5°C). The detectable changes in the gastrocnemius are most similar to exercise-training responses, which might predict transitions toward slower 2a and 2x isoforms. Our results, therefore, generally support a specific "training" adaptation mirrored in skeletal muscle fiber composition of CA mice irrespective of genotype, but the response is muscle specific, as we observed no major changes in tibialis. The novel expression of slower MyHC beta cardiac isoforms is intriguing, as this is more typically seen in response to hypoxia, fasting, or thyroid disease but not during exercise (14).

We determined the possible contribution of skeletal muscle basal proton leak to enhanced heat production, for which conflicting evidence has been reported (compare Ref. 28 with Ref. 43). In skeletal muscle mitochondria isolated from wild-type and UCP1-KO mice, we neither found alterations in mitochondrial respiration rates (states 2–4) nor in the basal proton leak using succinate as a complex II substrate. To assess basal proton leak in isolated mitochondria, the control for the concentration of free fatty acids is of particular importance, as fatty acids increase proton leakage either by a flip-flop mechanism or by activation of mitochondrial transporter proteins, e.g., UCP3 or ANT1. In mitochondrial preparations from skeletal muscle of wild-type and UCP1-KO mice, the concentration of free fatty acids may vary either due to different carryover of fatty acids during the isolation procedure or due to systematic genotype differences in the fatty acid level. To measure basal proton leak, it is, therefore, essential to buffer fatty acid at comparably low levels by the addition of albumin. Previously published genotype differences in basal proton leak kinetics between skeletal muscle mitochondria from wild-type and UCP1-KO mice (28) may have been caused by differences

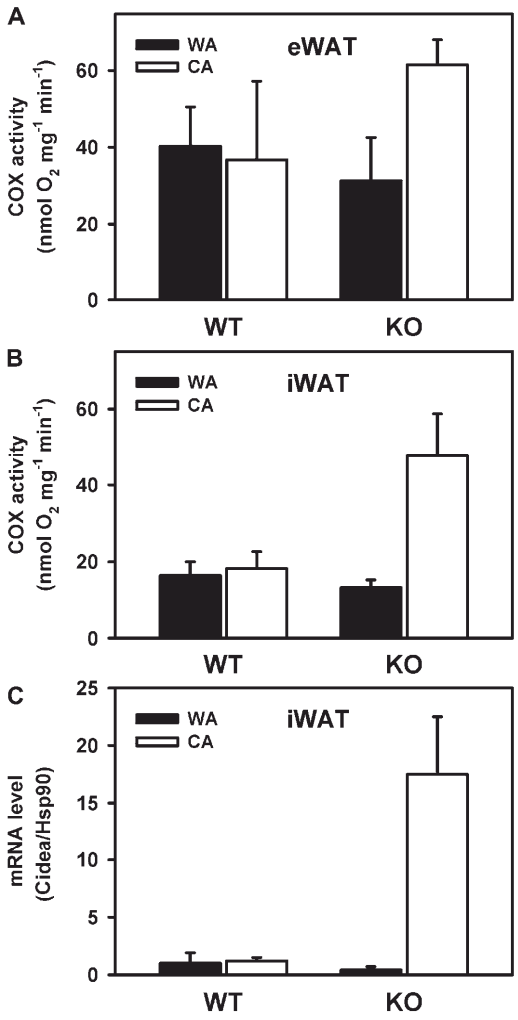

Fig. 6. Cytochrome *c* oxidase acitivity (*A* and *B*) and Cidea expression (*C*) in white adipose tissues (eWAT, epididymal white adipose tissue; iWAT, inguinal white adipose tissue) of WT and UCP1-KO mice either acclimated to 27°C (WA) or 5°C (CA). Values are expressed as means ± SD; $n = 4$, except $n = 3$ for the WA KO group.

in free fatty acid levels in mitochondrial preparations and thus may reflect an increased fatty acid-sensitive proton leak.

In wild-type mice, increased cold tolerance with cold acclimation corresponded to the pronounced recruitment of adrenergically stimulated nonshivering thermogenesis capacity. In contrast, the increase in cold tolerance of KO mice could not be directly related to major changes in HPmax (Fig. 4). This is particularly evident from the comparison of cold limits in the CA UCP1-KO knockout mice with the MCA wild-type mice displaying similar values for HPmax. As judged from our metabolic readings, an increase in acute cold tolerance of UCP1-KO mice may also be supported by lowered body temperature and metabolic rates leading to lower thermal conductance (reduced heat loss) in the cold (Fig. 3). This conclusion is in line with a previous report by Wang et al. (47), who demonstrated that UCP1-KO mice use sustained vasoconstriction in response to acute changes of ambient temperature to reduce heat loss. We recently demonstrated that loss of recruitable thermogenic power from BAT increases the arousal duration from torpor in UCP1-KO mice and renders this process energetically more costly (32). Thus, in the cold, UCP1-KO mice are forced to use the dissipated heat more efficiently than wild-type mice.

Challenging mice with a stepwise reduction of ambient temperature revealed consistently higher RQs in MCA and CA KO as opposed to MCA and CA wild-type mice. In MCA mice, this difference is definitely maintained for several hours in the cold (Fig. 1*D*). To our best knowledge, our study is the first demonstration of clear differences in RQ between wild-type and UCP1-KO mice (compare Refs. 24 and 1). At first sight, higher RQs in UCP1-KO mice in vivo may contradict the finding that oxidative phosphorylation capacities of skeletal muscle mitochondria on fatty acid-derived substrates are improved (43). The delayed or diminished lowering of RQs in acutely cold exposed UCP1-KO mice may, however, be interpreted as a lag in the activation of lipid oxidation for thermogenesis in the cold. Most likely, the inability of UCP1-KO mice to recruit uncoupled respiration upon cold-induced norepinephrine release in BAT provokes the activation of thermogenic pathways, which can less readily switch to lipid utilization.

Despite significant alterations in the thermophysiology of the UCP1-KO mice leading to elevated HPmax, the underlying mechanism(s) must be detrimental to the animal's well being, as the life span of UCP1-KO mice in the cold is markedly reduced (10). As shown from our cold endurance test, acute cold exposure abolished thermoregulatory flexibility in the UCP1-KO mice, as well as in the WA mice (Fig. 2). WA mice and MCA KO mice, furthermore, displayed significantly lower physical activity in the cold. Periodic BAT activity has been associated with rhythmic elevations in brain temperature, and low or diminished levels of UCP1 may interfere with the ability to fully express normal ultradian rhythmicity of thermogenesis (34). Sustained cold-induced shivering thermogenesis in UCP1-KO mice was further associated with severe dysfunction of (red) soleus muscle (2), and recruitment of other tissues for heat production with less mitochondrial uncoupling capacity might also increase systemic radical damage affecting lifespan (33).

In summary, CA UCP1-deficient mice can exhibit a substantial increase in thermogenesis and an improved cold tolerance as low as −10°C. Absence of functional BAT leads to remodeling of white adipose tissue, which could significantly contribute to adaptive thermogenesis with cold acclimation. It is, however, likely that the adaptive increase in HPmax of UCP1-KO mice is not due to enhanced oxidative capacity from a single thermogenic tissue but reflects multiple thermogenic pathways by which the lack of functional BAT can be compensated, provided heat loss does not exceed the rate of heat production (i.e., acclimation to the cold occurs successively). In vivo, heat loss may further be substantially reduced by

vasoconstriction and decreased thermal conductance, thereby facilitating body temperature set-point maintenance. We further conclude that small mammals may not only benefit from net increase in heat production supported by BAT nonshivering thermogenesis but also UCP1-mediated uncoupling allows metabolic flexibility (short-term thermoregulation and physical activity) and a rapid switch toward sustained lipid-fuelled thermogenesis in response to acute cold stress. In their natural environment, small dwelling mammals are frequently exposed to immediate changes in ambient temperature when leaving or entering their nest or burrow and will thus profit from the instantaneous availability of BAT nonshivering thermogenesis to maintain constant body temperature and alertness.

Perspectives and Significance

Exploring the metabolic consequences of BAT ablation is of interest since this tissue has been associated with the evolution of endothermy, but it is absent in birds and in adult marsupials and monotremes. Furthermore, the significance of BAT in adult body weight regulation is currently under investigation. The UCP1-knockout mouse line provides a mammalian model to directly compare endogenous heat production independent of UCP-1-mediated nonshivering thermogenesis. Any search exploring thermogenic mechanisms in mammals will benefit from knowledge on the magnitude of thermogenic capacity recruitment in the presence and absence of functional BAT and the metabolic characterization of any UCP1-independent thermogenesis. Reminescent of classical studies measuring tissue-specific metabolic rates in rats and hamsters, modern less-invasive functional magnetic resonance imaging technologies, e.g., PET/CT of 18-fluor-deoxyglucose uptake, need to be applied to directly assess the contribution of selected tissues to the total heat production of the body in vivo.

ACKNOWLEDGMENTS

The authors would like to thank Gábor Szerencsi, Sigrid Stöhr, Ingrid Fischer, and Nicole Choi for excellent technical assistance.

GRANTS

This work was funded by grants to M. Klingenspor from the German National Genome Research Network NGFN*plus* (01GS0822) and the Deutsche Forschungsgemeinschaft (KL 973/8). B. Rourke was funded by National Institutes of Health Minority Biomedical Research Support SCORE 2 (S06 GM063119).

DISCLOSURES

No conflicts of interest, financial or otherwise, are declared by the authors.

REFERENCES

1. **Anunciado-Koza R, Ukropec J, Koza RA, Kozak LP.** Inactivation of UCP1 and the glycerol phosphate cycle synergistically increases energy expenditure to resist diet-induced obesity. *J Biol Chem* 283: 27688–27697, 2008.
2. **Aydin J, Shabalina IG, Place N, Reiken S, Zhang SJ, Bellinger AM, Nedergaard J, Cannon B, Marks AR, Bruton JD, Westerblad H.** Nonshivering thermogenesis protects against defective calcium handling in muscle. *FASEB J* 22: 3919–2924, 2008.
3. **Brand MD.** The proton leak across the mitochondrial inner membrane. *Biochim Biophys Acta* 1018: 128–133, 1990.
4. **Brand MD, Kesseler A.** Control analysis of energy metabolism in mitochondria. *Biochem Soc Trans* 23: 371–376, 1995.
5. **Cannon B, Nedergaard J.** Brown adipose tissue: function and physiological significance. *Physiol Rev* 84: 277–359, 2004.
6. **Enerback S.** Human brown adipose tissue. *Cell Metab* 11: 248–252, 2010.
7. **Enerback S, Jacobsson A, Simpson EM, Guerra C, Yamashita H, Harper ME, Kozak LP.** Mice lacking mitochondrial uncoupling protein are cold-sensitive but not obese. *Nature* 387: 90–94, 1997.
8. **Foster DO, Frydman ML.** Brown adipose tissue: the dominant site of nonshivering thermogenesis in the rat. *Experientia Suppl* 32: 147–151, 1978.
9. **Geiser F, Drury RL, McAllan BM, Wang DH.** Effects of temperature acclimation on maximum heat production, thermal tolerance, and torpor in a marsupial. *J Comp Physiol* 173: 437–442, 2003.
10. **Golozoubova V, Cannon B, Nedergaard J.** UCP1 is essential for adaptive adrenergic nonshivering thermogenesis. *Am J Physiol Endocrinol Metab* 291: E350–E357, 2006.
11. **Golozoubova V, Hohtola E, Matthias A, Jacobsson A, Cannon B, Nedergaard J.** Only UCP1 can mediate adaptive nonshivering thermogenesis in the cold. *FASEB J* 15: 2048–2050, 2001.
12. **Granneman JG, Burnazi M, Zhu Z, Schwamb LA.** White adipose tissue contributes to UCP1-independent thermogenesis. *Am J Physiol Endocrinol Metab* 285: E1230–E1236, 2003.
13. **Grodzinski W, Heldmaier G.** Basal and cold induced metabolic rates in the harvest mouse (*Micromys minutus*). *Acta Theriol* 33: 283–291, 1988.
14. **Gupta MP.** Factors controlling cardiac myosin-isoform shift during hypertrophy and heart failure. *J Mol Cell Cardiol* 43: 388–403, 2007.
15. **Hart JS.** The relation between thermal history and cold resistance in certain species of rodents. *Can J Zool* 31: 80–91, 1952.
16. **Heldmaier G.** Temperature adaptation and brown adipose tissue in hairless and albino mice. *J Comp Physiol* 92: 281–292, 1974.
17. **Heldmaier G.** Metabolic and thermoregulatory responses to heat and cold in the Djungarian hamster, *Phodopus sungorus*. *J Comp Physiol* 102: 115–122, 1975.
18. **Heldmaier G, Böckler H, Buchberger A, Lynch GR, Puchalski W, Steinlechner S, Wiesinger H.** Seasonal acclimation and thermogenesis. *Circulation, Respiration, and Metabolism,* edited by R Gilles, Heidelberg, Germany: Springer Verlag, 1985.
19. **Heldmaier G, Ruf T.** Body temperature and metabolic rate during natural hypothermia in endotherms. *J Comp Physiol* 162: 696–706, 1992.
20. **Heldmaier G, Steinlechner S, Rafael J.** Nonshivering thermogenesis and cold resistance during seasonal acclimatization in the Djungarian hamster. *J Comp Physiol* 149: 1–9, 1982.
21. **Jastroch M, Withers KW, Taudien S, Frappell PB, Helwig M, Fromme T, Hirschberg V, Heldmaier G, McAllan BM, Firth BT, Burmester T, Platzer M, Klingenspor M.** Marsupial uncoupling protein 1 sheds light on the evolution of mammalian nonshivering thermogenesis. *Physiol Genomics* 32: 161–169, 2008.
22. **Johnston DW.** The absence of brown adipose tissue in birds. *Comp Biochem Physiol A Comp Physiol* 40: 1107–1108, 1971.
23. **Klingenspor M, Ebbinghaus C, Hulshorst G, Stohr S, Spiegelhalter F, Haas K, Heldmaier G.** Multiple regulatory steps are involved in the control of lipoprotein lipase activity in brown adipose tissue. *J Lipid Res* 37: 1685–1695, 1996.
24. **Liu X, Rossmeisl M, McClaine J, Riachi M, Harper ME, Kozak LP.** Paradoxical resistance to diet-induced obesity in UCP1-deficient mice. *J Clin Invest* 111: 399–407, 2003.
25. **Madsen L, Pedersen LM, Lillefosse HH, Fjaere E, Bronstad I, Hao Q, Petersen RK, Hallenborg P, Ma T, De Matteis R, Araujo P, Mercader J, Bonet ML, Hansen JB, Cannon B, Nedergaard J, Wang J, Cinti S, Voshol P, Doskeland SO, Kristiansen K.** UCP1 induction during recruitment of brown adipocytes in white adipose tissue is dependent on cyclooxygenase activity. *PLoS One* 5: e11391, 2010.
26. **Martin AW, Fuhrmann FA.** The relationship between summated tissue respiration and metabolic rate in the mouse and dog. *Physiol Zool* 28: 18–34, 1955.
27. **Meyer CW, Klingenspor M, Rozman J, Heldmaier G.** Gene or size: metabolic rate and body temperature in obese growth hormone-deficient dwarf mice. *Obes Res* 12: 1509–1518, 2004.
28. **Monemdjou S, Hofmann WE, Kozak LP, Harper ME.** Increased mitochondrial proton leak in skeletal muscle mitochondria of UCP1-deficient mice. *Am J Physiol Endocrinol Metab* 279: E941–E946, 2000.
29. **Nagase I, Yoshida T, Kumamoto K, Umekawa T, Sakane N, Nikami H, Kawada T, Saito M.** Expression of uncoupling protein in skeletal muscle and white fat of obese mice treated with thermogenic beta 3-adrenergic agonist. *J Clin Invest* 97: 2898–2904, 1996.
30. **Nicholls DG.** The influence of respiration and ATP hydrolysis on the proton-electrochemical gradient across the inner membrane of rat-liver

mitochondria as determined by ion distribution. *Eur J Biochem* 50: 305–315, 1974.
31. **Nicol SC, Andersen NA.** Rewarming rates and thermogenesis in hibernating echidnas. *Comp Biochem Physiol A Mol Integr Physiol* 150: 189–195, 2008.
32. **Oelkrug R, Heldmaier G, Meyer CW.** Torpor patterns, arousal rates, and temporal organization of torpor entry in wild-type and UCP1-ablated mice. *J Comp Physiol B*. In press.
33. **Oelkrug R, Kutschke M, Meyer CW, Heldmaier G, Jastroch M.** Uncoupling protein 1 decreases superoxide production in brown adipose tissue mitochondria. *J Biol Chem* 285: 21961–21968, 2010.
34. **Ootsuka Y, de Menezes RC, Zaretsky DV, Alimoradian A, Hunt J, Stefanidis A, Oldfield BJ, Blessing WW.** Brown adipose tissue thermogenesis heats brain and body as part of the brain-coordinated ultradian basic rest-activity cycle. *Neuroscience* 164: 849–861, 2009.
35. **Puchalski W, Bockler H, Heldmaier G, Langefeld M.** Organ blood flow and brown adipose tissue oxygen consumption during noradrenaline-induced nonshivering thermogenesis in the Djungarian hamster. *J Exp Zool* 242: 263–271, 1987.
36. **R Development Core Team.** *R: A Language and Environment for Statistical Computing*. *R* Vienna, Austria: Foundation for Statistical Computing.
37. **Reynafarje B, Costa LE, Lehninger AL.** O_2 solubility in aqueous media determined by a kinetic method. *Anal Biochem* 145: 406–418, 1985.
38. **Rolfe DF, Hulbert AJ, Brand MD.** Characteristics of mitochondrial proton leak and control of oxidative phosphorylation in the major oxygen-consuming tissues of the rat. *Biochim Biophys Acta* 1188: 405–416, 1994.
39. **Saarela S, Klapper B, Heldmaier G.** Daily rhythm of oxygen consumption and thermoregulatory responses in some european winter-or summer-acclimatized finches at different ambient temperatures. *J Comp Physiol* 165: 366–376, 1995.
40. **Saarela S, Heldmaier G.** Effect of photoperiod and melatonin on cold resistance, thermoregulation and shivering/nonshivering thermogenesis in Japanese quail. *J Comp Physiol* 157: 625–633, 1987.
41. **Schaeffer PJ, Villarin JJ, Lindstedt SL.** Chronic cold exposure increases skeletal muscle oxidative structure and function in *Monodelphis domestica*, a marsupial lacking brown adipose tissue. *Physiol Biochem Zool* 76: 877–887, 2003.
42. **Selman C, Korhonen TK, Bunger L, Hill WG, Speakman JR.** hermoregulatory responses of two mouse *Mus musculus* strains selectively bred for high and low food intake. *J Comp Physiol* 171: 661–668, 2001.
43. **Shabalina IG, Hoeks J, Kramarova TV, Schrauwen P, Cannon B, Nedergaard J.** Cold tolerance of UCP1-ablated mice: A skeletal muscle mitochondria switch toward lipid oxidation with marked UCP3 up-regulation not associated with increased basal, fatty acid- or ROS-induced uncoupling or enhanced GDP effects. *Biochim Biophys Acta* 1797: 968–980, 2010.
44. **Talmadge RJ, Roy RR.** Electrophoretic separation of rat skeletal muscle myosin heavy-chain isoforms. *J Appl Physiol* 75: 2337–2340, 1993.
45. **Ukropec J, Anunciado RP, Ravussin Y, Hulver MW, Kozak LP.** UCP1-independent thermogenesis in white adipose tissue of cold-acclimated $Ucp1^{-/-}$ mice. *J Biol Chem* 281: 31894–31908, 2006.
46. **Vegiopoulos A, Muller-Decker K, Strzoda D, Schmitt I, Chichelnitskiy E, Ostertag A, Berriel DM, Rozman J, Hrabe dA, Nusing RM, Meyer CW, Wahli W, Klingenspor M, Herzig S.** Cyclooxygenase-2 controls energy homeostasis in mice by de novo recruitment of brown adipocytes. *Science* 328: 1158–1161, 2010.
47. **Wang Y, Kimura K, Inokuma K, Saito M, Kontani Y, Kobayashi Y, Mori N, Yamashita H.** Potential contribution of vasoconstriction to suppression of heat loss and homeothermic regulation in UCP1-deficient mice. *Pflügers Arch* 452: 363–369, 2006.
48. **Young P, Arch JR, Ashwell M.** Brown adipose tissue in the parametrial fat pad of the mouse. *FEBS Lett* 167: 10–14, 1984.
49. **Zhou Z, Yon TS, Chen Z, Guo K, Ng CP, Ponniah S, Lin SC, Hong W, Li P.** Cidea-deficient mice have lean phenotype and are resistant to obesity. *Nat Genet* 35: 49–56, 2003.

HIBERNATION IN FREE RANGING AFRICAN WOODLAND DORMICE, *GRAPHIURUS MURINUS*

N. MZILIKAZI ∞ Z. MADIKIZA ∞ R. OELKRUG
R. BAXTER

Chapter 4
Hibernation in Free-Ranging African Woodland Dormice, *Graphiurus murinus*

Nomakwezi Mzilikazi, Zimkitha Madikiza, Rebecca Oelkrug and Roderick M. Baxter

Abstract Although daily torpor is common in African animals, hibernation seems to be uncommon. In this study we investigated the use of hibernation in free-ranging African woodland dormice, *Graphiurus murinus*, during winter. We also investigated if this species made any seasonal adjustments to basal metabolic rates. *G. murinus* were heterothermic on a 100% of the measurement days. The minimum body temperature recorded was 1.5°C and the longest torpor bout without arousal was 8 days. There were no significant differences in basal metabolic rates between seasons and the measured values were similar to those previously reported in laboratory studies. We conclude that hibernation is the main adjustment that *G. murinus* utilise to deal with challenging winter conditions.

N. Mzilikazi (✉)
Centre for African Conservation Ecology, Department of Zoology,
Nelson Mandela Metropolitan University, PO Box 77000,
Port Elizabeth 6031, South Africa
e-mail: nomakwezi.mzilikazi@nmmu.ac.za

Z. Madikiza
Department of Zoology and Entomology, University of Fort Hare,
P/Bag X1314, Alice 5700, South Africa

R. Oelkrug
Department of Animal Physiology, Phillips Universitaet Marburg,
Marburg, Germany

R. M. Baxter
Department of Geology and Resource Management,
School of Environmental Sciences, University of Venda,
P/Bag X5050, Thohoyandou 0950, South Africa

T. Ruf et al. (eds.), *Living in a Seasonal World*,
DOI: 10.1007/978-3-642-28678-0_4,

4.1 Introduction

Heterothermy has been observed in many African mainland small mammal species, with representatives from bats (Cory Toussaint et al. 2010), elephant shrews (Lovegrove et al. 1999; Mzilikazi et al. 2002), golden moles (Jackson et al. 2009), hedgehogs (Hallam and Mzilikazi 2011), rodents (Webb and Skinner 1996), shrews (Baxter 1996) and primates (Nowack et al. 2010). With the exception of the elephant shrews and the golden moles whose heterothermic profiles straddle the line between daily torpor and hibernation, the majority of species tend to display daily torpor and true hibernation has not been widely documented in the mainland (McKechnie and Mzilikazi 2011). One laboratory study found that the spectacled dormouse, *Graphiurus ocularis,* enters hibernation of up to 13 days (Ridgard and Perrin 1999), and another recent study found that semi-captive hedgehogs were also capable of hibernation (Hallam and Mzilikazi 2011). As yet, no study has found hibernation in unrestrained, African mainland animals.

Although laboratory studies provide insights into potentially important physiological mechanisms that enable organisms to live in their environments, the results obtained achieve ecological and evolutionary meaning only if patterns correlate with attributes of organisms in their natural environments (Williams and Tieleman 2002). Furthermore, in order to understand the association between patterns of time allocation to various behaviours, their cost in terms of energy expenditure, their influence on life history parameters, information about variation of allotments of time and energy over the annual cycle is crucial (Stearns 1992). In this regard, data on animals' energy expenditure during different seasons and preferably different years should be obtained.

Several aspects of the woodland dormouse (*Graphiurus murinus*) ecology, behaviour and physiology make this an ideal species in which to investigate energy balance and use of hibernation by small mammals in their natural habitats. *G. murinus* has a wide distribution across South Africa excluding the arid west. They occur in a range of habitats ranging from grassland and rocky areas to woodland and forest (Skinner and Chimimba 2005). Within the Eastern Cape of South Africa, it is found only in forested areas. It is often found in areas where winter temperatures regularly fall below 0°C. Its small size, ca. 30 g (Skinner and Chimimba 2005) means it has high thermoregulatory costs. Furthermore, its diet consists largely of arthropods whose availability is greatly reduced during winter months. Although lone foragers, woodland dormice are known to aggregate during winter, with as many as eleven individuals known to huddle together. In addition, food caches are often observed in artificial nest boxes that they use (Madikiza 2010). Data obtained from a mark-capture-recapture study over a 4-year period reveal that *G. murinus* also show seasonal increases of up to 20% in body mass before the onset of winter in the Eastern Cape (Baxter, unpublished data).

Given the thermoregulatory and energetic challenges faced by this species, especially during the winter time, the aim of this study was to investigate the use of hibernation in free-ranging *G. murinus* as well as to establish whether any

seasonal adjustments are made in other parameters associated with expenditure, such as body mass and basal metabolic rate (BMR).

4.2 Materials and Methods

The study was carried out at the Great Fish River Reserve (33°04′–33°09′S and 26°37′–26°49′E) about 40 km northeast of Grahamstown in the Eastern Cape, South Africa from April 2008 to June 2009. The study site is described in detail by Madikiza et al. (2010). The site is dominated by African bushwillows, *Combretum caffrum*, which are prone to rotting and provide numerous nest sites for *G. murinus*. In addition, as part of a long-term project, 70 nest boxes were deployed in the study site and these were regularly used by the dormice.

4.3 Body Temperature Measurements

Nine female *G. murinus* were captured using Sherman traps baited with oats and sunflower oil in April 2008. They were implanted with pre-calibrated, temperature sensitive, data loggers (iBBat—Alpha Mach Inc—Canada, mass ca. 1.3 g, resolution = 0.5°C) for body temperature (T_b) measurement. The mass of the data loggers did not exceed 5% of the animals' body mass. The data loggers were covered in biologically inert wax and programmed to record the body temperature in 15 min intervals, starting on 15 May–27 June 2008, resulting in data obtained over a 42-day period. For the intraperitoneal implantation of the data loggers the animals were anesthetized by inhalation anaesthesia using isoflurane (3% for induction and maintenance) in medical oxygen. Animals usually recovered within 24 h of implantation and were released at their point of capture. After 9–10 weeks a second trapping session was conducted and recaptured animals were explanted using the same procedure detailed above. Each animal was tagged with a subcutaneous transponder (Trovan, Euro I.D.) ensuring that no single animal would be subjected to repeated surgery other than that necessary for implantation and removal of data loggers.

Ambient temperature (T_a) was recorded using three iButtons placed at different locations in the field: one iButton was placed inside a nest box and another was placed in the shade. The third iButton was placed in a black tin, which was exposed to the sun so as to get an idea of passive heating, if any occurred.

4.4 Metabolic Rate Measurements

Metabolic rate measurements were based on the principle of the indirect calorimetry using open flow-through respirometry. Measurements were conducted during February ($N = 9$, summer) 2009 and July ($N = 7$, winter) 2009. None of

the animals used in winter had been captured previously. In winter, no animals were captured in traps, and all the individuals were found torpid in nest boxes and hand captured. All animals were allowed to become normothermic and fully capable of coordinated movements before metabolic rate measurements were made. All measurements were carried out at 29 ± 1°C, the thermoneutral zone of this species (Whittington-Jones and Brown 1999). Measurements were conducted at a sampling interval of one sample per second over a 4-h period. BMR was calculated from the lowest mean oxygen consumption over a period of 5 min in a resting animal.

All animal experiments were approved by the Nelson Mandela Metropolitan University (NMMU) animal ethics committee (animal ethics clearance no. A08-SCI-ZOO-002) and complied with the American Physiology Society's "Guiding principles for research involving animals and human being" and the "Code of ethics for animal experimentation" manual adopted by the NMMU.

4.5 Data Analyses

Seasonal changes in mass were assessed using a paired-*t*-test for recaptured individuals equipped with a data logger. Animals were considered torpid if their body temperature decreased below 32°C. This is 3.4°C below published normothermic T_b (Whittington-Jones and Brown 1999). The torpor bout length was therefore taken as the total time during which T_b was maintained below 32°C. The minimum T_b (T_b min) was taken as the lowest T_b measured during a 24 h period. Torpor frequency was calculated for individual animals as the proportion of days during which the animals displayed torpor. The relationship between various torpor variables (T_b min, bout length) with T_a was described using regression equations. Unless otherwise stated, T_a refers to that measured in the nest boxes. All values are represented as mean ± SE.

4.6 Results

4.6.1 Seasonal Changes in Body Mass and Basal Metabolic Rate

Of the nine originally implanted animals only three were recaptured (33% recapture rate). The average body mass in April 2008 (implanted animals) was 33.1 ± 1.7 g ($N = 9$) and had decreased to 22.3 ± 1.5 g ($N = 3$), upon recapture (September) representing a significant mass loss of 32.6% in body mass over winter period ($t = 2.92$, $P < 0.05$). For the non-implanted animals (used in BMR measurements) the mean body mass in summer was 27.6 ± 0.8 g ($N = 9$) and 28.8 ± 1.5 g in winter ($N = 7$). There were no significant differences between these values ($P > 0.05$, $F_{1,16} = 0.365$). The mean BMR during summer was

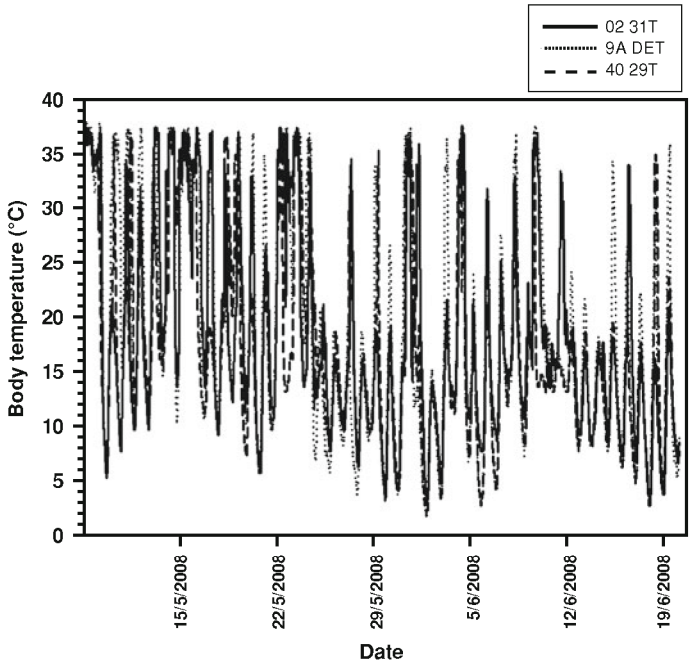

Fig. 4.1 The body temperature profiles of three free-ranging female *G. murinus* in winter 2008

1.160 ± 0.08 ml O_2 g^{-1} h^{-1} and that during the winter was 1.376 ± 0.112 ml O_2 g^{-1} h^{-1}.

4.6.2 Prevalence of Heterothermy and Torpor Parameters

The lowest T_a measured in a nest box during the study period was 2.1°C, and the mean minimum T_a was 11.1 ± 0.6°C and 7.3 ± 0.6°C in May and June, respectively. The mean maximum T_a in the nest boxes was 21.8 ± 0.7°C and 17.7° ± 0.4°C in May and June, respectively.

All animals entered torpor on all measurement days (Fig. 4.1). The mean torpor T_b min was 9.5 ± 0.5°C and the range of torpor T_b minima was 1.5–29.5°C (Fig. 4.2). The mean daily T_b maximum was 30.9 ± 0.7°C and daily T_b maxima ranged between 13.5 and 38.0°C (Fig. 4.2 inset). The T_b maxima below 32°C corresponds with data where the animals did not arouse from torpor within a 24 h period (00h00–00h00).

The lowest T_b measured was 1.5°C at $T_a = 2.1$°C. In fact, there were a number of data points that appeared below the $T_b = T_a$ line, implying that the T_b was lower than the measured T_a. Body temperatures lower than T_a are only possible if the

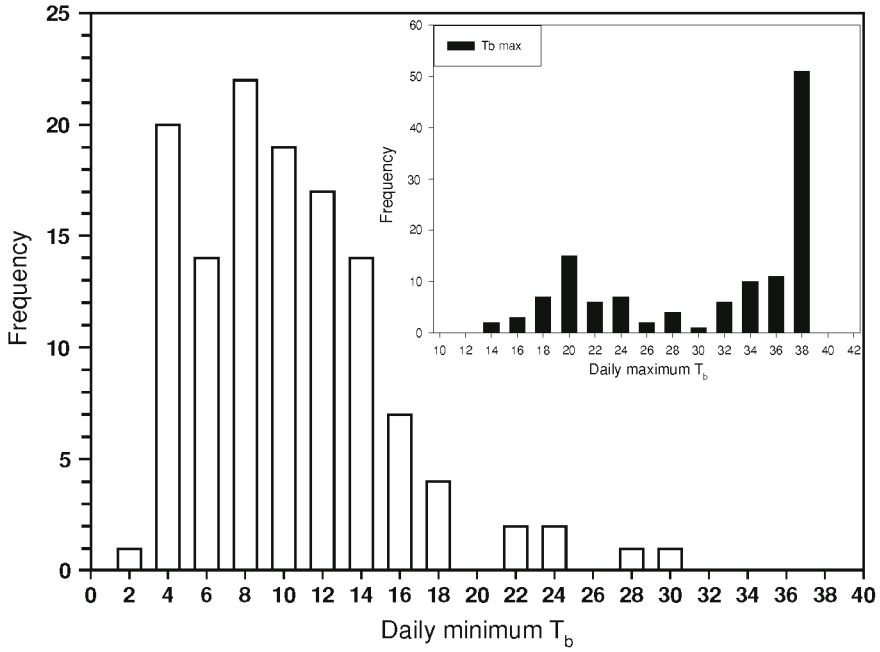

Fig. 4.2 The frequency distribution of minimum T_b measured in free-ranging *G. murinus* during winter 2008. The *inset* graph shows the frequency distribution of maximum T_b

animals were utilising evaporative water loss, a situation that is highly unlikely during winter time. Since we measured T_a in a single nest box, it is possible that at the time that the T_a was measured, the animals may have been in a different nest box or even a tree hole. The largest discrepancy between T_b and T_a (that is, T_b lower than T_a) was 3.1°C. However, the mean $T_b - T_a$ (ΔT) was 0.2°C showing that T_b min was closely coupled to T_a min on any day. The correlation between T_b min and T_a was significant and was described by the equation: T_b min $= 1.25$ (T_a)$-$ 2.05; $R^2 = 0.77$, $P < 0.05$). There was a significant negative correlation between Julian day and T_b min ($R^2 = 0.106$; $P < 0.05$), showing that as winter progressed (and nights became colder) the animals displayed significantly lower T_b minima.

Mean torpor bout length was 32.5 ± 4.7 h. The longest continuous torpor bout was 8 days (Fig. 4.3) and the shortest torpor bout lasted 2.5 h. Even when the animal did not arouse during the longest bout, T_b fluctuated with T_a, although it never increased above 20°C. Although this species is nocturnal, the animals entered torpor during the night on the majority of the days. There was evidence of passive heating in so far as T_b fluctuated with T_a, but a return to normothermic T_bs was presumably achieved through heat production via non-shivering thermogenesis or shivering because most arousals were completed during the night, and full arousal seldom coincided with the increase in T_a.

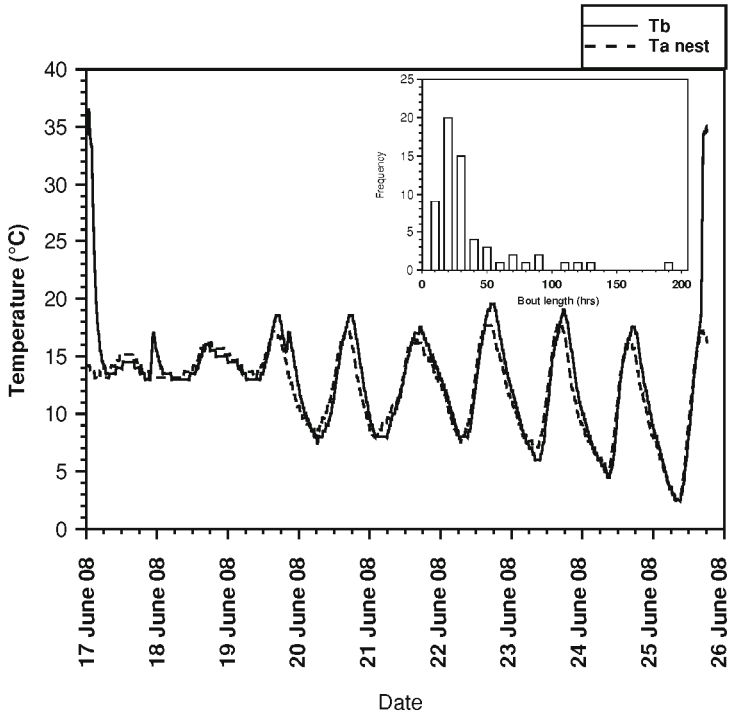

Fig. 4.3 The body temperature trace of the longest torpor bout measured in hibernating *G. murinus*. The *inset* graph shows the frequency distribution of torpor bout lengths

4.7 Discussion

Among non-volant Afrotropical mammals, true hibernation has been described in only in six species, four of them are Malagasy lemur species (McKechnie and Mzilikazi 2011). On the mainland the prevalence of hibernation seems to be uncommon, being so far recorded in *Graphiurus ocularis* (Ridgard and Perrin 1999) and *Atelerix frontalis* (Hallam and Mzilikazi 2011). The heterothermic patterns observed in golden moles, *Amblysomus hottentotus longiceps* (Scantlebury et al. 2008) and tenrecs, *Echinops telfairi* (Lovegrove and Genin 2008) are difficult to characterise as either daily torpor or hibernation and at present are probably best described as prolonged torpor. The T_b data presented here add to the body of literature documenting hibernation in mainland Africa and with a T_b min of 1.5°C represent some of the lowest body temperatures measured in the Afrotropics. This is very similar to that measured in *A. frontalis* recently.

Excluding the bats (Cory Toussaint et al. 2010), the woodland dormouse is currently the smallest known non-volant African mainland hibernator. The body mass of hibernators ranges from 10 to 80,000 g although most hibernators are in the body mass range of 10–1,000 g, with a median of 85 g (Geiser and Ruf 1995).

Consistent with other hibernators which increase body mass by 10–30% at the onset of the hibernation season (Geiser 2001), *G. murinus* increased their body mass from an average of 24.9 g (Webb and Skinner 1996) to 33.1 g (this study) representing an increase of 33% at the end of autumn. This mass gain is enough to sustain the animals through the hibernation season because BMR reduction in small hibernators may be down to 1% of normothermic values (Geiser 2001), allowing them to survive on modest fat stores for extended periods of time.

The longest torpor bout in this study was 8 days. It is unfortunate that we obtained data for only 6 weeks, as longer bouts may have been recorded in July and August, the coldest winter months. Indeed we did observe that the torpor bouts became significantly longer with the progression of winter. Although in this study we did not capture *G. murinus* in traps during winter, Madikiza et al. (2010) have trapped this species throughout the year in our study site, providing evidence of some foraging activity during winter time. It has been noted that there tends to be higher capture success of the late-breeding season offspring during winter. This observation suggests that late season offspring do not gain enough mass to sustain long torpor bouts. Furthermore, it is well known that in some hibernators forage during the hibernation season so as to supplement internal energy stores (Geiser 2001). We suggest that maximum torpor bout length in this species is a trade-off between the need to balance energy savings through extended bout lengths with maintenance of body condition through foraging.

G. murinus has been shown to utilise summer torpor in the laboratory (Webb and Skinner 1996). It would be interesting to investigate whether this species utilises summer torpor in the wild especially in light of the observation that for most rodents, reproductive activity and use of heterothermy are mutually exclusive (Goldman et al. 1986; Lovegrove and Raman 1998). Incidental observations reveal that *G. murinus* do indeed utilise daily torpor in the field during summer (Madikiza 2010) with torpid individuals being found in nest boxes throughout the year. It therefore appears that *G. murinus* is fairly flexible and opportunistic in its use of heretothermy throughout the year, exhibiting daily torpor, hibernation and summer torpor. This is similar to observations made in the edible dormouse, *Glis glis* (Wilz and Heldmaier 2000). Another factor that may potentially influence patterns of heterothermy in *G. murinus* is huddling with conspecifics. Unfortunately we did not obtain behavioural data and cannot comment on whether any of our individuals did huddle with conspecifics.

G. murinus captured in the Drakensburg reached a body mass of 70 g and hibernated continuously without arousal for 3 months (unpublished data). However, it has long been "common" knowledge the *G. murinus* is a complex of medium-sized glirid species awaiting revision. More recently, Kryštifek et al. (2004) have found significant morphometric differences between two Eastern Cape populations occurring 80 km apart. Subsequent genetic analyses have indicated that the Eastern Cape has at least two species of the *G. murinus* complex and that there are considerably more species in the rest of South Africa. Until this problem is resolved, data obtained from *G. murinus* from different localities should be

treated cautiously, at least with regards to conclusions on differences in heterothermic responses in different populations.

Seasonal adjustments other than heterothermy are utilised by many small mammals and these include changes in body mass, basal metabolic rates and conductance (Heldmaier 1989; Lovegrove 2005). In this study, the winter and summer BMR were not significantly different and were quite similar to values previously published from laboratory studies (Webb and Skinner 1996; Whittington-Jones and Brown 1999). In this species, the greatest changes in winter energy requirements were presumably met through use of heterothermy (Heldmaier 1989). The animals used in this study were never in the laboratory for more than 12 h and we take our values to be a fair representation of BMR in free-ranging woodland dormice.

Acknowledgments This study was supported by a Thuthuka grant from the National Research Foundation (NRF) of South Africa. Any opinions, findings and conclusions expressed in this material are those of the authors and therefore the NRF does not accept any liability in regard thereto. Mr Brad Fike graciously hosted us and assisted with logistics at the Great Fish River Reserve (GFRR). The Eastern Cape Parks Board granted permission to work at GFRR.

References

Baxter RM (1996) Evidence for spontaneous torpor in *Crocidura flavescens*. Acta Theriol 41:327–330

Cory Toussaint D, McKechnie AE, Van der Merwe M (2010) Heterothermy in free-ranging male Egyptian free-tailed bats (*Tadarida aegyptiaca*) in a subtropical climate. Mamm Biol 75: 466–470

Geiser F (2001) Hibernation: endotherms. In: Encyclopedia of life sciences. Macmillan Publishers, New York

Geiser F, Ruf T (1995) Hibernation versus daily torpor in mammals and birds: physiological variables and classification of torpor patterns. Phys Zoo 68:935–966

Goldman BD, Darrow JM, Duncan MJ, Yogev L (1986) Photoperiod, reproductive hormones, and winter torpor in three hamster species. In: Heller HC, Musacchia XJ, Wang LCH (eds) Living in the cold: physiological and biochemical adaptations. Elsevier, New York, pp 341–351

Hallam SL, Mzilikazi N (2011) Heterothermy in the southern African hedgehog, *Atelerix frontalis*. J Comp Physiol B 181:437–445

Heldmaier G (1989) Seasonal acclimatization of energy requirements in mammals: functional significance of body weight control, hypothermia, torpor and hibernation. In: Wieser W, Gnaiger E (eds) Energy transformations in cells and organisms. Georg Thieme Verlag, Stuttgart, pp 130–139

Jackson C, Setsaas T, Robertson M, Scantlebury M, Bennett N (2009) Insights into torpor and behavioural thermoreguation of the endangered Juliana's golden mole. J Zool 278:299–307

Kryštifek B, Haberl W, Baxter RM, Zima J (2004) Morphology and karyology of two populations of the woodland dormouse, *Graphiurus murinus* in the Eastern Cape, South Africa. Folia Zool 53:339–350

Lovegrove BG (2005) Seasonal thermoregulatory responses in mammals. J Comp Physiol B 175:231–247

Lovegrove BG, Génin F (2008) Torpor and hibernation in a basal placental mammal, the lesser hedgehog tenrec, *Echinops telfairi*. J Comp Physiol B 178:691–698

Lovegrove BG, Lawes MJ, Roxburgh L (1999) Confirmation of pleisiomorphic daily torpor in mammals: the round-eared elephant shrew *Maroscelides proboscideus* (Macroscelidea). J Comp Physiol B 169:453–460

Lovegrove BG, Raman J (1998) Torpor patterns in the pouched mouse (*Saccostomus camprestris*; Rodentia): a model animal for unpredictable environments. J Comp Physiol B 168:303–312

Madikiza ZKJ (2010) Population Biology and aspects of socio-spatial organisation of the woodland dormouse, *Graphiurus murinus* (Desmaret 1822) in the Great Fish River Reserve, South Africa. MSc dissertation, University of Fort Hare

Madikiza ZKJ, Bertolino S, Baxter RM, Do Linh San E (2010) Seasonal, sexual and age related variations in the live trapping success of woodland dormice, *Graphiurus murinus*. Zool Stud 49:797–805

McKechnie AE, Mzilikazi N (2011) Heterothermy in Afrotropical mammals and birds: a review. Integr Comp Biol. doi:10.1093/icb/icr035:1-15

Mzilikazi N, Lovegrove BG, Ribble DO (2002) Exogenous passive heating during torportorpor arousal in free-ranging rock elephant shrews, *Elephantulus myurus*. Oecologia 133:307–314

Nowack J, Mzilikazi N, Dausmann K (2010) Torpor on demand: heterothermy in the non-lemur primate *Galago moholi*. PLoS One 5:e10797

Ridgard BW, Perrin MR (1999) Thermoregulation and patterns of torpor in the spectacled dormouse *Graphiurus ocularis* (Smith 1829):Gliridae. Trop Zool 12:253–266

Scantlebury M, Lovegrove BG, Jackson C, Bennett N, Lutermann H (2008) Hibernation and non-shivering thermogenesis in the Hottentot golden mole *(Amblysomus hottentotus longiceps*). J Comp Physiol B 178:887–897

Skinner J, Chimimba C (2005) The mammals of the southern African subregion, 3rd edn. Cambridge University Press, Cambridge

Stearns SC (1992) The evolution of life histories. Oxford University Press, Oxford

Webb PI, Skinner JD (1996) Summer torpor in African woodland dormice *Graphiurus murinus* (Myoxidae: Graphiurinae). J Comp Physiol B 166:325–330

Whittington-Jones CA, Brown CR (1999) Thermoregulatory capabilities of the woodland dormouse, *Graphiurus murinus*. S Afr J Zool 34:34–38

Williams JB, Tieleman BI (2002) Ecological and evolutionary physiology of desert birds: a progress report. Intergr Comp Biol 42:68–75

Wilz M, Heldmaier G (2000) Comparison of hibernation, estivation and daily torpor in the edible dormouse, *Glis glis*. J Comp Physiol B 170:511–521

HYPOTHALAMIC GLYCOGEN SYNTHASE KINASE 3B HAS A CENTRAL ROLE IN THE REGULATION OF FOOD INTAKE AND GLUCOSE METABOLISM

J. BENZLER ∞ G.K. GANJAM ∞ M. KRÜGER
O. PINKENBURG ∞ M. KUTSCHKE ∞ S. STÖHR ∞ J. STEGER
C.E. KOCH ∞ R. OELKRUG ∞ M.W. SCHARTZ P.R. SHEPERD
A. TUPS

BJ Metabolism

Biochem. J. (2012) **447**, 175–184 (Printed in Great Britain) doi:10.1042/BJ20120834

ACCELERATED PUBLICATION

Hypothalamic glycogen synthase kinase 3β has a central role in the regulation of food intake and glucose metabolism

Jonas BENZLER*[1], Goutham K. GANJAM*[1], Manon KRÜGER*, Olaf PINKENBURG†, Maria KUTSCHKE‡, Sigrid STÖHR*, Juliane STEGER*, Christiane E. KOCH*, Rebecca ÖLKRUG*, Michael W. SCHWARTZ§, Peter R. SHEPHERD‖, David R. GRATTAN¶ and Alexander TUPS*[2]

*Department of Animal Physiology, Faculty of Biology, Philipps University Marburg, Marburg, Germany, †Department of Immunology, Faculty of Medicine, Philipps University Marburg, Marburg, Germany, ‡Institute for Diabetes and Obesity, Helmholtz Centre, Munich, Germany, §Diabetes and Obesity Center of Excellence, Department of Medicine, University of Washington, Seattle, WA, U.S.A., ‖Maurice Wilkins Centre for Molecular Biodiscovery and Department of Molecular Medicine and Pathology, University of Auckland, Auckland, New Zealand, and ¶Centre for Neuroendocrinology and Department of Anatomy and Structural Biology, University of Otago, Dunedin, New Zealand

GSK3β (glycogen synthase kinase 3β) is a ubiquitous kinase that plays a key role in multiple intracellular signalling pathways, and increased GSK3β activity is implicated in disorders ranging from cancer to Alzheimer's disease. In the present study, we provide the first evidence of increased hypothalamic signalling via GSK3β in leptin-deficient $Lep^{ob/ob}$ mice and show that intracerebroventricular injection of a GSK3β inhibitor acutely improves glucose tolerance in these mice. The beneficial effect of the GSK3β inhibitor was dependent on hypothalamic signalling via PI3K (phosphoinositide 3-kinase), a key intracellular mediator of both leptin and insulin action. Conversely, neuron-specific overexpression of GSK3β in the mediobasal hypothalamus exacerbated the hyperphagia, obesity and impairment of glucose tolerance induced by a high-fat diet, while having little effect in controls fed standard chow. These results demonstrate that increased hypothalamic GSK3β signalling contributes to deleterious effects of leptin deficiency and exacerbates high-fat diet-induced weight gain and glucose intolerance.

Key words: adeno-associated virus, arcuate nucleus, Dickkopf 1, food intake, high-fat diet, obesity, synapsin, Type II diabetes.

INTRODUCTION

Type II diabetes affects more than 165 million individuals and is increasing at an alarming rate [1]. Although a large number of papers has implicated the brain as a critical target for insulin regulation of systemic glucose metabolism [2–7], mechanisms underlying such insulin effects remain incompletely understood. Even less is known about the importance of altered neuronal insulin signalling in the pathogenesis of Type II diabetes. Studies focused on hypothalamic insulin signal transduction via the IRS (insulin receptor substrate)–PI3K (phosphoinositide 3-kinase) pathway suggest that it plays a critical role in CNS (central nervous system) regulation of peripheral glucose homoeostasis [5,8,9]. Leptin action in the brain similarly depends on intact IRS–PI3K signalling [9–11], but key neuronal mediators downstream of this pathway remain to be identified.

GSK3β (glycogen synthase kinase 3β) is a serine-threonine kinase that is phosphorylated and inhibited by protein kinase B (AKT) [12], a principal target of PI3K signalling. In addition to inhibiting cellular responses to insulin (for example, inhibition of GSK3β is required for insulin stimulation of glycogen synthesis), this enzyme also influences cell division, growth and development [13] as an endogenous inhibitor of canonical WNT signalling. The finding that systemic inhibition of GSK3β improves whole-body glucose homoeostasis [14-16] implies that GSK3β exerts a tonic inhibitory effect on glucose metabolism, but neither the mechanism(s) nor the specific tissue(s) involved in this effect are known. Some evidence points to GSK3β in skeletal muscle as a mediator of impaired glucose metabolism in diabetic mouse models [17,18], but activities of both AKT and GSK3β are also regulated in mouse brain in response to physiological changes of glucose [19]. In the present study we investigated whether an action in the brain might explain the deleterious effects of GSK3β signalling on peripheral glucose homoeostasis.

MATERIALS AND METHODS

Animals

All experiments used male mice that were purchased from Janvier. The animals were between 2- and 4-months-old and housed individually under standard conditions with a light/dark cycle of 12 h. All procedures were performed in accordance with the guidelines of the German Council of Animal Care. The ambient temperature for mice was 26 °C. Apart from the dark phase before the experiments, all animals had access to standard rodent diet, low-fat diet or HFD (high-fat diet) (containing 45 % fat) and water *ad libitum*. For the central administration of drugs, cannulae were

Abbreviations used: AAV, adeno-associated virus; aCSF, artificial cerebral spinal fluid; ARC, arcuate nucleus; CNS, central nervous system; DEXA, dual-emission X-ray absorptiometry; DKK-1, dickkopf 1; EGFP, enhanced green fluorescent protein; GSK3β, glycogen synthase kinase 3β; HA, haemagglutinin; HEK, human embryonic kidney; HFD, high-fat diet; ICV, intracerebroventricular; ipGTT, intraperitoneal glucose tolerance test; IRS, insulin receptor substrate; PEPCK, phosphoenolpyruvate carboxykinase 2; PI3K, phosphoinositide 3-kinase; SOCS-3, suppressor of cytokine signalling 3; WPRE, WHV (Woodchuck hepatitis virus) post-transcriptional regulatory element.

[1] These authors contributed equally to this work.
[2] To whom correspondence should be addressed (email alexander.tups@staff.uni-marburg.de).

stereotaxically implanted into the left lateral ventricle as described previously [9].

In situ hybridization

To determine the central expression of DKK-1 (dickkopf 1 homologue) and SOCS-3 (suppressor of cytokine signalling 3) we performed *in situ* hybridization on coronal brain sections. As previously described [20], forebrain sections (16 μm) were collected throughout the extent of the ARC (arcuate nucleus) on to a set of twelve slides, with twelve sections mounted on each slide. Accordingly, the slides spanned the hypothalamic region approximating from -2.8 to -1.22 mm relative to Bregma according to the atlas of the mouse brain [21]. *In situ* hybridizations and analysis was performed as described previously [20].

Glucose tolerance tests

We determined whether activation of GSK3β might impair glucose tolerance in lean mice. Therefore the WNT antagonist DKK-1 [1 μg in 1 μl of aCSF (artificial cerebral spinal fluid); R&D Systems, 5897-DK/CF] was administered ICV (intracerebroventricular) to one group ($n = 4$) of $Lep^{+/+}$ mice, whereas a second group ($n = 6$) received an ICV vehicle injection (aCSF). At 15 min later an ipGTT (intraperitoneal glucose tolerance test; 1 g of glucose/kg of body mass) was performed. To determine the blood glucose levels, the vena facialis was punctured and the glucose concentration was measured using a commercially available glucometer (Accu-Check Performa, Roche).

We next determined whether inhibition of GSK3β might improve glucose homoeostasis. Therefore the mice received a specifically designed inhibitor for GSK3β (AR-A014418, Calbiochem). To test whether central GSK3β inhibition affects hypothalamic PI3K, four groups of $Lep^{ob/ob}$ mice received two ICV injections (0.5 μl each), 30 min apart. The first group received vehicle (5% DMSO/aCSF) followed by GSK3β inhibitor (0.5 nmol in 5% DMSO/aCSF). The second group received isoform-specific PI3K inhibitors (0.1 nmol in 5% DMSO/aCSF, PIK-75/TGX-221), since both isoforms are required for insulin signalling in the hypothalamus [22], followed by vehicle (5% DMSO/aCSF). A third group received isoform-specific PI3K inhibitors, followed by GSK3β inhibitor, and the last group received two vehicle injections ($n = 4$–7). At 15 min after the second injection, an ipGTT was performed (1 g of glucose/kg of body mass) as described above.

To measure glucose tolerance after virus administration we performed two ipGTTs. The first one was performed on day 58 on chow diet (1 g of glucose/kg of body mass), whereas the second ipGTT was conducted at day 18 of the HFD (0.75 g of glucose/kg of body mass) as described above.

Food intake experiment

To test whether inhibition of central GSK3β affects food intake, we administered a GSK3β inhibitor (AR-A014418, Calbiochem) ICV in a separate group of 8-week-old $Lep^{ob/ob}$ mice. The mice were fasted for 16 h and weight matched. Mice received either a GSK3β inhibitor (0.5 nmol in 0.5 μl of aCSF/5% DMSO) or vehicle injection (aCSF/5% DMSO) 1 h before the beginning of the dark phase. Food intake was measured at 4 h and 24 h after administration ($n = 8$/group).

Immunohistochemistry

First we investigated the phosphorylation of GSK3β (Ser^{9}, catalogue number 9323) in the ARC of 8-week-old wild-type mice fed a HFD (containing 45% fat) for 3 weeks. In addition, we also compared phosphorylation of GSK3β (Ser^{9}) in wild-type and $Lep^{ob/ob}$ mice. To do this the animals were fasted for 16 h and transcardial perfusion was performed. To determine any possible cross-talk between GSK3β and the IRS–PI3K pathway, we measured the effect of ICV GSK3β inhibitor on IRS-1 phosphorylation (Ser^{612}) and phospho-AKT (Ser^{473}) in the hypothalamic ARC. Accordingly, $Lep^{ob/ob}$ mice ($n = 10$/group) received either GSK3β inhibitor (AR-A014418, 0.5 nmol in 0.5 μl aCSF/5% DMSO) or vehicle (aCSF/5% DMSO) ICV 15 min before transcardial perfusion. Immunohistochemistry was performed using anti-(phospho-IRS-1 Ser^{612}) (catalogue number 3203) and anti-(phospho-AKT Ser^{473}) antibodies (catalogue number 4058). Immunohistochemistry was carried out on mouse brain coronal cryosections as described previously [9,22]. All antibodies were purchased from Cell Signaling Technology.

Recombinant adeno-associated viral vector generation and virus production

The human cDNA for *GSK3β* was subcloned from the eukaryotic expression vector pcDNA3-GSK3β HA (Addgene, 14753) into an AAV2-hSyn-EGFP-WPRE vector [23]. *GSK3β* cDNA along with an HA (haemagglutinin) tag coding sequence was amplified from the pcDNA3-GSK3*β*-HA plasmid by PCR (phusion DNA polymerase) using the forward, 5′-GCTAGCTAATACGACTCACTATAGG-3′ and reverse, 5′-TGTACACAATTTAGGTGACACTATCG-3′ primers. These primers contain suitable Nhe1 and BsrG1 restriction sites for cloning into the AAV (adeno-associated virus) construct. Amplified PCR product was first cloned into the pGemT easy cloning vector. The *GSK3β* cDNA fragment from pGemT easy vector was subcloned into Nhe1 and BsrG1 sites of AAV2-hSyn-EGFP-WPRE by replacing EGFP (enhanced green fluorescent protein) cDNA to obtain AAV2-hSyn-GSK3*β*-HA-WPRE. In this vector system the expression of GSK3β is under the control of the human synapsin-1 promoter to restrict the expression to neurons and WPRE [WHV (Woodchuck hepatitis virus) post-transcriptional regulatory element] facilitates long-term expression of the transgene. All molecular cloning procedures were performed in SURE2 bacterial cells to minimize the recombination events.

Recombinant AAV vectors of serotype 2 were produced by transfecting AAV *cis* plasmids encoding the gene of interest and a viral helper plasmid pDG [24] encoding *rep-2* (replication protein 2) and *cap-2* (capsid protein 2) genes into HEK (human embryonic kidney)-293 cells. Total cell lysates were collected after 48 h of transfection in AAV lysis buffer (50 mM Hepes with 150 mM NaCl, pH 7.6) by repeated freezing in liquid nitrogen and thawing at 37 °C. The cell lysates were cleared by centrifugation for 15 min at 4600 ***g*** at 4 °C to remove the cell debris. Unencapsulated nucleic acids were degraded by treating the cleared cell lysates with 250 units of benzonase (Sigma) for 90 min at 37 °C. AAV particles were purified in three step CsCl density gradient ultracentrifugation (rotor type SW41 at 15 °C), desalting and concentration by Amicon® Ultra Centrifugal filters (30 K MWCO UFC903008). The viral genome isolated by the Qiagen mini prep plasmid isolation kit was titrated by quantitative real-time PCR using the forward, 5′-CCTCAATCCAGCGGACCTTC-3′ and reverse, 5′-ACAGTGGGAGTGGCACCTTC-3′ primers.

Protein expression verification in primary cortical neuronal cells

Freshly isolated primary rat cortical neurons were plated at a density of 0.3 million cells on polyethyleneimine pre-coated plates and cultured in MEM$^{\oplus}$ medium as described previously [25]. After 4 h the cells were replenished with neurobasal medium [25] and were infected with 10^{10} vector genomes of purified AAV particles for 5 days. Total protein lysate (20 μg) from the cortical cells was used to verify the expression of GSK3β by Western blotting with an anti-HA tag antibody (catalogue number 2367, Cell Signaling Technology). The same cell lysates were used to analyse the phosphorylation of Tau protein with an anti-(phospho-Tau Ser^{396}) antibody (catalogue number 9632, Cell Signaling Technology) and total Tau with an anti-Tau antibody (catalogue number 4019, Cell Signaling Technology). The expression of EGFP control virus was verified by fluorescence light microscopy. To prove that the expression of human synapsin promoter controlled GSK3β is limited to neurons, we infected HEK-293 cells with 10^{10} vector genomes of EGFP and GSK3β viral particles. As a positive control we transfected HEK-293 cells with 5 μg of pcDNA3-GSK3β-HA plasmid [26]. After 3 days the total cell lysates were collected as described previously [27]. Total cell lysates (20 μg) were Western blotted with an anti-HA tag antibody.

Stereotaxic injections

Intracerebral injections were performed under isoflurane anaesthesia as described previously [9]. Stereotaxic co-ordinates to reach the ARC of hypothalamus are 1.5 mm posterior, $\pm$0.3 mm lateral and 6.1 mm ventral relative to Bregma. AAV2 particles, containing 4×10^{10} vector genomes, were injected into the ARC using a 0.5 μl Hamilton glass syringe for 2 min. The injection needle remained in place at each injection site for an additional 5 min to allow for diffusion and prevent backflow. The incision was sutured and the animals were placed under a heating lamp to recover from the surgery.

Body composition

To analyse their body composition, mice were anaesthetized with isoflurane (CP-Pharma) and were analysed via DEXA (dual-emission X-ray absorptiometry)-scan (Lunar PIXImus Densitometer; GE Medical Systems).

Metabolic measurement

We measured the effect on metabolic rate of regular chow and the HFD. Accordingly, carbon dioxide production (VCO_2) and oxygen consumption (VO_2) were measured in metabolic cages ($\sim$5 l vol.). Measurements were taken continuously for 2 days with a constant ambient temperature of 23 °C. The air flow in the cage was adjusted to $\sim$42 l/h and continuously monitored. The procedure has been described in detail previously [28].

Plasma insulin levels

We investigated whether blood insulin levels were affected by GSK3β overexpression. Accordingly, blood was collected by decapitation and plasma insulin was measured via a Rat/Mouse insulin ELISA kit (Millipore EZRMI-13K) according to the manufacturer's instructions.

Central inhibition of GSK3β decreased hepatic glucose production

To test whether inhibition of GSK3β in the brain affects gluconeogenesis, we performed pyruvate tolerance tests. Lep$^{ob/ob}$ mice received a single ICV injection of either GSK3β inhibitor (AR-A014418, Calbiochem, 0.5 nmol in 0.5 μl of aCSF/5 % DMSO, $n=5$) or vehicle (0.5 μl of aCSF/5 % DMSO, $n=11$). At 60 min before pyruvate was administered, blood glucose levels were measured as described above. To analyse the protein level of PEPCK (phosphoenolpyruvate carboxykinase 2) in the liver, three groups of Lep$^{ob/ob}$ mice ($n=4$–5/group) underwent the treatment regimen shown above with the exception that livers were removed 90 min after ICV treatment. Immunoblotting with 5 μg of total liver protein lysate was performed as described elsewhere [27] and normalized to β-actin.

Statistics

The data were analysed by one- or two-way ANOVA followed by a Holm–Sidak comparison test, as appropriate, using SigmaStat statistical software (Jandel). Where the data failed equal variance or normality tests, they were analysed by one-way ANOVA on ranks followed by Dunn's multiple comparison test. The results are presented as means $\pm$ S.E.M. and differences were considered significant if $P<0.05$.

RESULTS AND DISCUSSION

As a first step, we investigated whether activity of GSK3β is increased in the ARC, a key brain region for neuronal control of energy and glucose homoeostasis, during diet-induced obesity and leptin deficiency. It has been comprehensively established that activity of GSK3β is mediated via phosphorylation at Ser^{9}, a post-translational modification that is critical to inactivate the enzyme [12,29–32]. Furthermore, intact insulin signalling appears to involve inhibition of GSK3β phosphorylation at Ser^{9} in the muscle [12,33]. Using an antibody specific against Ser^{9} phosphorylation, we found that the number of phospho-GSK3β immunoreactive cells in this brain area was reduced in both models of impaired glucose homoeostasis (mice fed an HFD and Lep$^{ob/ob}$ mice) compared with their respective controls, suggesting that local GSK3β activity is increased in these animals (Figures 1a and 1b, $n=5$–6/group, $P=0.007$ and $P=0.026$ respectively). For a proof of concept, in extremely glucose intolerant Lep$^{ob/ob}$ mice we investigated whether central inhibition of GSK3β affects glucose homoeostasis. Consistent with this hypothesis, glucose tolerance in these animals was markedly improved following a single ICV injection of a GSK3β inhibitor (AR-A014418) relative to the ICV vehicle (Figure 1c, $n=4$–7/group, $P=0.016$). This effect cannot be attributed to changes of food intake or energy balance, since ICV injections were performed 15 min before ipGTT and the animals were not provided food during this time.

Since central insulin action is required for whole-body glucose homoeostasis [2–4,8,9,34] via a hypothalamic mechanism involving signal transduction via the PI3K pathway, we next asked whether pharmacological inhibition of central GSK3β restores impaired PI3K signalling in the ARC of Lep$^{ob/ob}$ mice. This was accomplished by histochemical analysis of the effect of ICV administration of a GSK3β inhibitor (AR-A014418) on the phosphorylation of IRS-1 (Ser^{612}) and AKT (Ser^{473}) in the ARC of Lep$^{ob/ob}$ mice. These markers were selected because serine phosphorylation of IRS-1 impairs signalling via PI3K, whereas phospho-AKT (Ser^{473}) is a marker of PI3K activation [9]. Following ICV injection, the GSK3β inhibitor acutely (within 15 min) decreased the number of phospho-IRS-1 (Ser^{612}) immunoreactive cells within the ARC of Lep$^{ob/ob}$ mice by

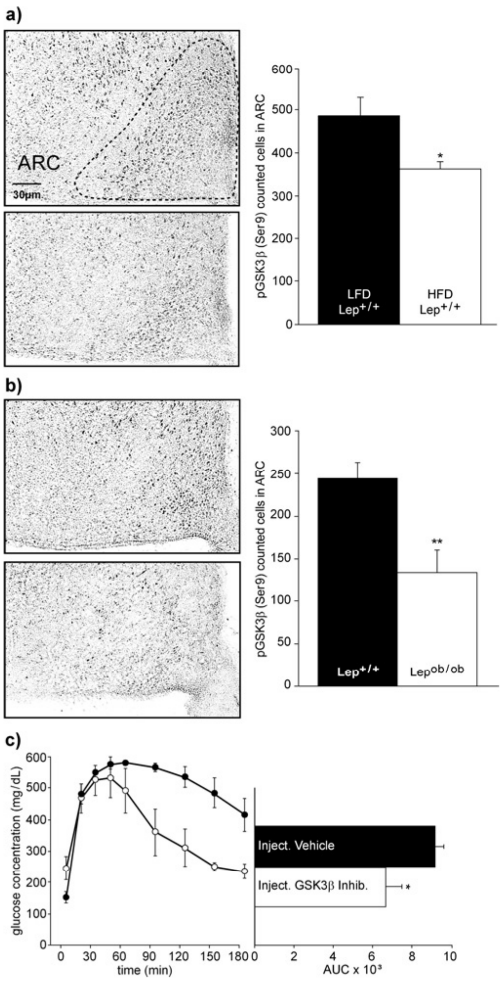

Figure 1 Phospho-GSK3β in the ARC during obesity and pharmacological inhibition of this enzyme

(**a**) Immunohistochemistry was performed on brain sections of mice fed an HFD compared with low-fat diet (LFD) mice. Inserts depict representative images of phospho-GSK3β (Ser^9) immunoreactivity in the ARC (phosphorylation at Ser^9 inactivates the enzyme). The histogram shows the counted phospho-GSK3β (Ser^9) cells in the ARC ($n = 5$–6/ group). (**b**) The same experiment, mentioned above, was performed on brain sections of wild-type and $Lep^{ob/ob}$ mice. The histogram shows the counted phospho-GSK3β (Ser^9) cells in the ARC ($n = 5$–6/ group). (**c**) A central injection of a GSK3β inhibitor improves glucose tolerance in $Lep^{ob/ob}$ mice. ipGTT was performed 15 min after administration of GSK3β inhibitor (○) or vehicle (●) into the lateral ventricle ($n = 4$–7 each group). Results are means ± S.E.M., $^*P \leqslant 0.05$ and $^{**}P \leqslant 0.01$. AUC, area under curve.

~20 % relative to vehicle-treated mice (Figure 2a, $P = 0.028$, $n = 10$/group), while increasing the number of phospho-AKT (Ser^{473}) immunoreactive cells in the ARC by ~3-fold, compared with the ICV vehicle (Figure 2b, $P \leqslant 0.001$, $n = 10$/group). Thus the glucose-lowering effects of central GSK3β are associated with increased hypothalamic IRS–PI3K signalling.

To determine whether the beneficial effect of central GSK3β inhibition depends on intact PI3K signalling, we determined if its effect on glucose tolerance is blocked by pharmacological inhibition of PI3K. Animals received an ICV injection of selective inhibitors of the PI3K catalytic subunits, p110α and p110β (PIK75 and TGX221) [22] with and without the GSK3β inhibitor, which was given 30 min later, followed by an ipGTT. Our findings that the metabolic improvement induced by the GSK3β inhibitor was fully blocked by co-administration of the PI3K p110α- and β-selective inhibitors (Figure 2c, $n = 4$–7/group) implicate increased PI3K signalling as a mediator of this beneficial effect.

We next investigated the effects of central inhibition of GSK3β on food intake in $Lep^{ob/ob}$ mice. Relative to the vehicle, ICV injection of the GSK3β inhibitor 30 min before the beginning of the dark phase induced a modest, but significant, reduction of 24 h food intake in these animals (− 15 % compared with the vehicle, $n = 8$/group, $P = 0.032$) (Figure 2d). These observations are consistent with published evidence that leptin administration increases hypothalamic IRS–PI3K signalling, and that leptin's ability to reduce food intake is prevented by central blockade of PI3K [10].

The above data collectively suggest that GSK3β is overactive in the hypothalamus of leptin-deficient mice, contributing to the diabetic state of these animals. Given the known role of the WNT pathway to inactivate GSK3β, we next investigated whether expression of DKK-1, a potent antagonist of the WNT pathway that activates GSK3β in neurons [35], might be up-regulated in the ARC of diabetic $Lep^{ob/ob}$ mice. As predicted, *DKK1* mRNA, as measured by *in situ* hybridization using an antisense riboprobe specific for DKK-1, was increased 3-fold in the ARC of diabetic $Lep^{ob/ob}$ mice (Figure 2e, $P = 0.008$) compared with wild-type controls. This observation suggests that increased hypothalamic GSK3β activity may be a consequence of increased DKK-1 in these animals. If this hypothesis is correct, interventions that increase neuronal DKK-1 signalling in normal animals should impair glucose homoeostasis. To test this hypothesis, we administered DKK-1 as an acute ICV injection to wild-type mice 15 min before an ipGTT was performed. Remarkably, the marked impairment of glucose homoeostasis induced by ICV injection of DKK-1 ($n = 4$–6, $P < 0.001$ compared with the controls) was comparable with that observed in $Lep^{ob/ob}$ mice (Figure 2f). On the basis of these findings, we infer that hypothalamic GSK3β activity in leptin-deficient mice: (i) arises at least in part from increased DKK-1 signalling and (ii) contributes to their impaired glucose metabolism. Further, metabolic benefit arising from reduced hypothalamic GSK3β action depends upon intact hypothalamic PI3K signalling, and increased brain signalling via either DKK-1 or GSK3β impairs systemic glucose homoeostasis.

As local inhibition of GSK3β in the brain improved glucose homoeostasis, the neuroanatomical identity of the underlying phenomenon remained limited due to ICV administration of the GSK3β inhibitor. Therefore we generated a viral construct enabling neuron-specific overexpression of functional GSK3β in the ARC, a key brain region for neuronal control of energy and glucose homoeostasis. This approach furthermore enables GSK3β overexpression in adult healthy mice, thereby circumventing potential defects in embryogenesis due to the ontogenic capacity of this enzyme. This was accomplished by cloning human *GSK3β* cDNA into the AAV2 vector. In contrast with adenoviruses, AAV2s do not cause adverse local immune responses and they have a higher transfection rate in the brain than lentiviruses [36,37]. To direct GSK3β expression selectively to neurons, transcription was directed by the human synapsin-1 promoter (Figure 3a). The ability of AAV2 vectors to drive selective neuronal expression of a transgene was

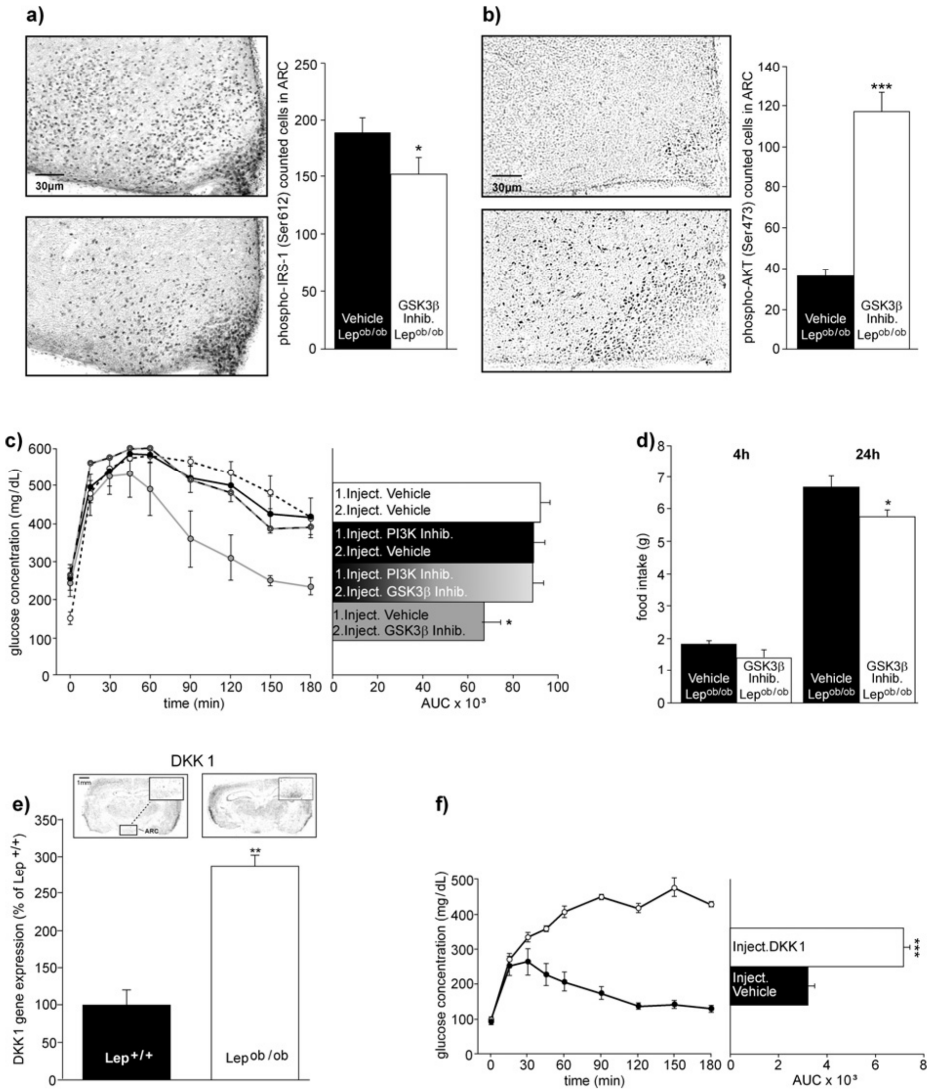

Figure 2 Pharmacological manipulation of GSK3β in the brain: effects on food intake and interaction with hypothalamic insulin signalling

(**a**) Immunohistochemistry was performed on brain sections of Lep$^{ob/ob}$ mice after central administration of a GSK3β inhibitor (Inhib.) or vehicle, 15 min before transcardial perfusion. Images are representative of phospho-IRS-1 (Ser^{612}) immunoreactivity in the ARC. The histogram shows the counted cells in the ARC that were immunoreactive for phospho-IRS-1 and were down-regulated after ICV injection of the GSK3β inhibitor ($n = 10$/group). (**b**) An additional set of brain sections of the experiment presented in (**e**) was analysed for phospho-AKT (Ser^{473}) immunoreactive cells in the ARC. The number of phospho-AKT (Ser^{473}) immunoreactive cells was increased after ICV injection of the GSK3β inhibitor. (**c**) Central improvement of glucose homoeostasis by the GSK3β inhibitor in Lep$^{ob/ob}$ mice was blocked by pre-treatment with isoform-specific PI3K inhibitors. The PI3K-inhibitor was injected ICV 30 min before GSK3β inhibitor injection (ICV) ($n = 4$–7 each group). (**d**) A single central injection of a GSK3β inhibitor decreased food intake in Lep$^{ob/ob}$ mice within 24 h by approximately 15 %. Lep$^{ob/ob}$ mice received a GSK3β inhibitor or vehicle injection ($n = 8$ each group) into the lateral ventricle and food intake was analysed after 4 h and 24 h. (**e**) Autoradiographs of mouse brain sections after *in situ* hybridization to an antisense ^{35}S-labelled riboprobe binding to the WNT antagonist DKK-1. Within the ARC gene expression was up-regulated in Lep$^{ob/ob}$ mice compared with the Lep$^{+/+}$ mice. The upper panels depict autoradiographs of the respective genes, whereas the lower panels show a histogram generated from quantification of the signal in the ARC ($n = 5$–6 animals in each group). (**f**) ICV administration of DKK-1 protein impairs glucose tolerance in wild-type mice (Lep$^{+/+}$ mice). DKK-1 protein (○, $n = 4$) or aCSF (●, $n = 6$) was administered 15 min before the ipGTT. Results are means ± S.E.M., $^{*}P \leqslant 0.05$, $^{**}P \leqslant 0.01$ and $^{***}P \leqslant 0.001$. AUC, area under curve.

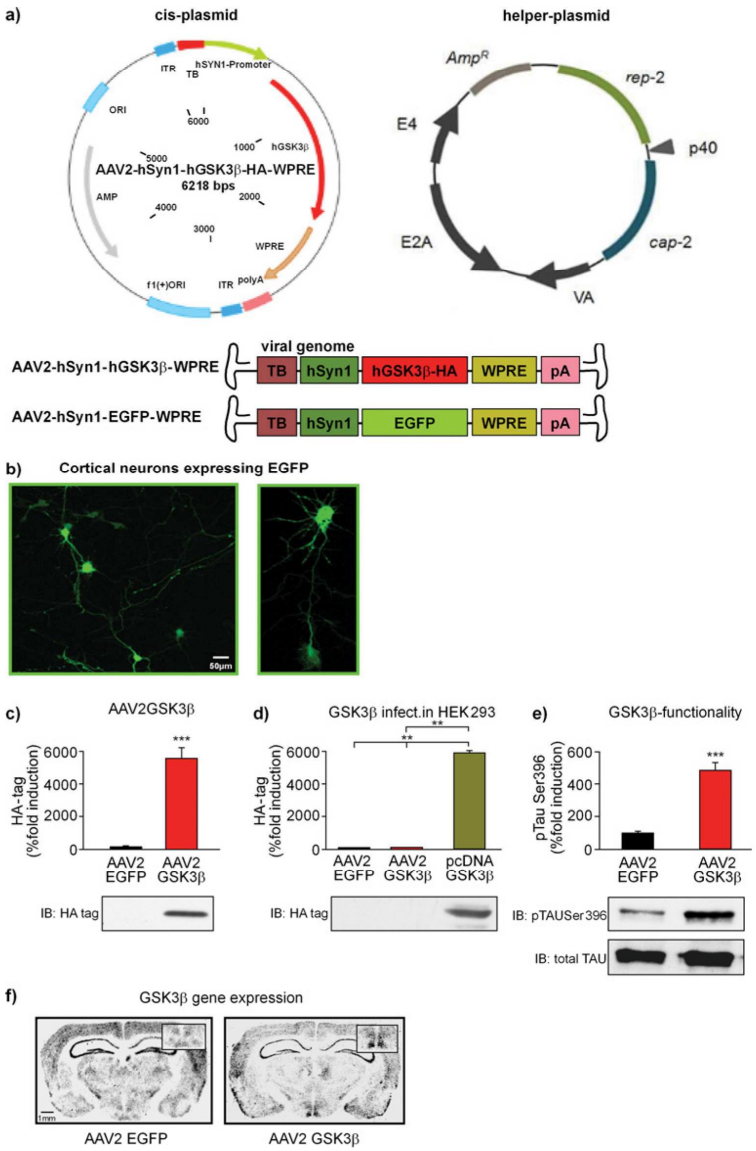

Figure 3 Neuron-specific AAV2-mediated overexpression of GSK3β in the ARC

(**a**) Schematic representation of *cis* and helper plasmid maps transfected into HEK-293 cells to produce AAV2–GSK3β (upper panels). Important elements of the viral genome are depicted in the lower panel. GSK3β transcription was controlled by the neuron-specific synapsin promoter. (**b**) Confocal image showing primary cortical neurons expressing EGFP after 5 days of AAV2–EGFP infection. (**c**) Confirmation of AAV2–GSK3β over-expression by immunoblotting of viral HA tag specific to AAV2–GSK3β in primary cortical neurons 5 days after infection. (**d**) In immunoblots of peripheral HEK-293 cells infection with neuron-specific AAV2–GSK3β was absent. Only cells transfected with pcDNA3-GSK3β led to an increase in the HA tag protein. (**e**) Immunoblot showing increased phospho-Tau (Ser^{396})/total Tau protein ratio in cortical neurons infected with AAV2–GSK3β. (**f**) Overexpression of AAV2–GSK3β *in vivo* was confirmed by *in situ* hybridizations. Shown are representative autoradiographs of mouse brain sections after *in situ* hybridization to an antisense ^{35}S-labelled riboprobe binding to GSK3β of AAV2–EFGP and AAV2–GSK3β mice. For validation each cell culture experiment was repeated three times and statistical analysis is represented in the histograms. Results are means $\pm$ S.E.M. $^{**}P \leqslant 0.01$ and $^{***}P \leqslant 0.001$. TB, transcriptional blocker; hSyn1, human synapsin1 promoter; hGSK3β, human GSK3β tagged with HA epitope; pA, poly A sequence from bovine growth hormone; ITR, inverted terminal repeat; IB, immunoblot.

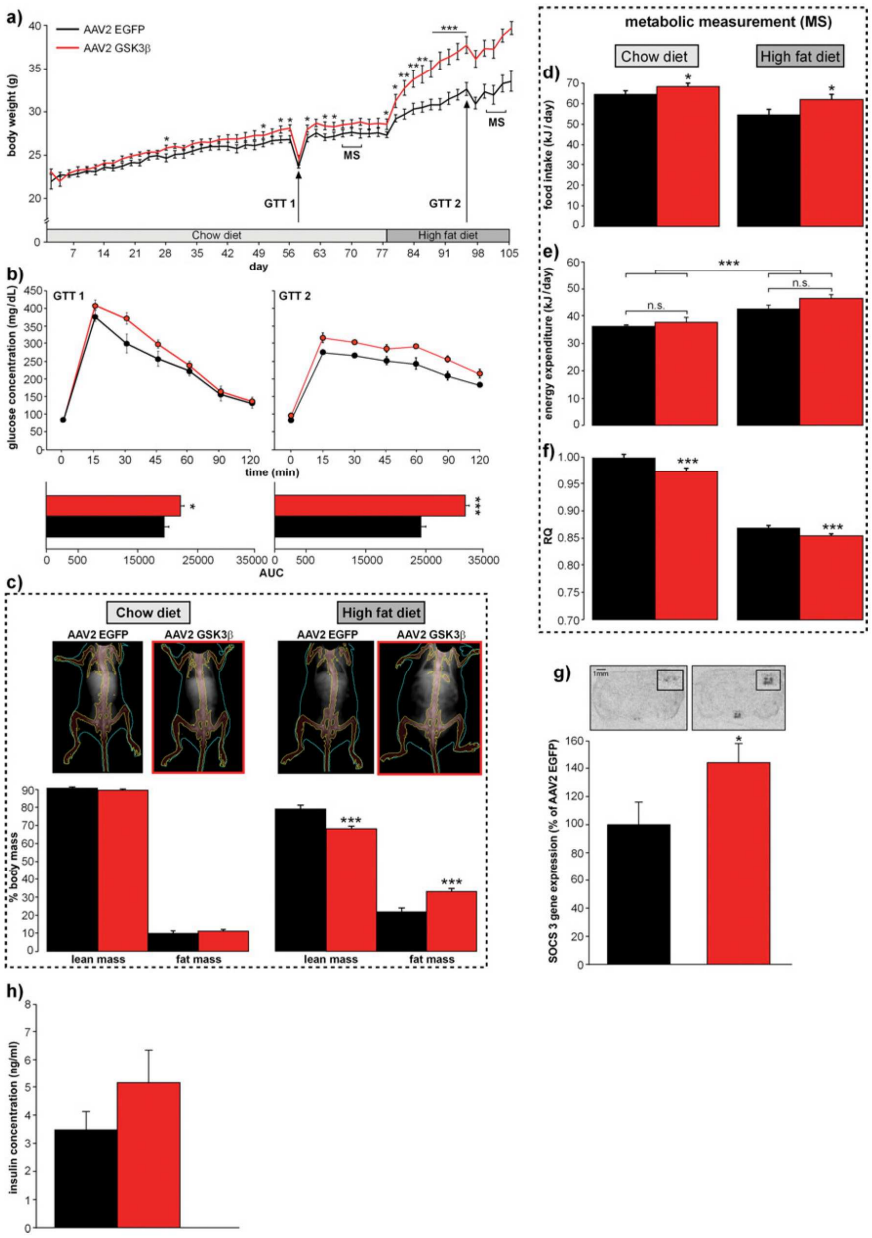

Figure 4 Neuron-specific AAV2-mediated overexpression of GSK3β in the ARC: effects on whole-body energy and glucose metabolism in mice

(**a**) Wild-type mice were stereotaxically injected into the bilateral halves of the ARC with 2×200 nl of AAV2 virus expressing EGFP ($n = 7$) as a control and GSK3β ($n = 8$). Shown are the body masses of EGFP- and GSK3β-overexpressing animals maintained on a chow diet (*ad libitum*) for 11 weeks followed by 18 days on an HFD (*ad libitum*). (**b**) Glucose tolerance tests 1 (GTT1) and 2 (GTT2) (upper panel) and associated area under the curve (AUC; lower panel). GTT1, performed on day 58 on chow diet after surgery, revealed impaired glucose tolerance in AAV2–GSK3β mice compared with AAV2–EGFP mice. After mice were switched to an HFD for 18 days GTT2 revealed exacerbated enhanced glucose intolerance in mice treated with AAV2–GSK3β compared with HFD-induced glucose

validated by infecting both primary cortical neurons (Figure 3c) and a peripheral cell line (HEK-293; Figure 3d) with AAV2 vectors expressing the fluorescent reporter EGFP (Figure 3b). As expected, viral-induced GSK3β overexpression occurred in neurons, but not HEK-293 cells. Following intraparenchymal injection of the AAV2–GSK3β vector into the ARC of wild-type mice, local overexpression of GSK3β was confirmed by *in situ* hybridization (Figure 3f), and increased GSK3β kinase activity was verified by measuring phospho-Tau content, a target of GSK3β in the brain [38]. In cultured primary cortical neurons, AAV2-mediated overexpression increased phospho-Tau protein 5-fold (Figure 3e, $P \leqslant 0.001$).

To investigate the effects of ARC-directed GSK3β overexpression on energy metabolism, we injected 10^{10} genomic units of either AAV2–GSK3β or a control AAV2 virus into the ARC of 8-week-old wild-type mice. On a standard chow diet, GSK3β overexpression induced a mild increase in body mass that was only intermittently and transiently significant over a time period of 78 days after injection (Figure 4a). Despite its minor effects on body mass, ARC-directed overexpression of GSK3β impaired glucose tolerance significantly relative to controls injected with AAV2–EGFP, based on an ipGTT performed on day 58 (Figure 4b, $P = 0.04$). After 78 days, both groups of mice were switched to an HFD for 18 days, which led to an increased body mass in both groups. However, the increase of body mass induced by the HFD was strikingly increased in AAV2–GSK3β mice compared with the controls, an effect that became significant within 2 days after the diet switch and reached a value 17% greater than the controls by day 18 (Figure 4a). An ipGTT after 18 days on the HFD revealed that glucose tolerance had deteriorated markedly in the AAV2–GSK3β mice compared with the controls (Figure 4b, $P \leqslant 0.001$). DEXA analyses performed immediately after the ipGTT revealed significant reductions of relative lean mass ($P \leqslant 0.001$) and increases of relative fat mass ($P \leqslant 0.001$) in AAV2–GSK3β mice fed the HFD, but not in mice fed standard chow (Figure 4c). Cumulative food intake (kJ/day) was increased in AAV2–GSK3β mice compared with the AAV2–EGFP controls regardless of the diet (Figure 4d, $P \leqslant 0.05$), whereas energy expenditure was unaltered (Figure 4e). Lastly, the respiratory quotient (an indicator of substrate utilization) was reduced in AAV2–GSK3β mice on both the standard chow diet and HFD (Figure 4f, $P \leqslant 0.001$), suggesting preferential oxidation of lipid as a fuel.

Taken together, these data provide clear evidence that GSK3β signalling potently affects energy and glucose homoeostasis in a diet-sensitive manner via effects in the mediobasal hypothalamus. The striking increase in the body mass differential between AAV2–GSK3β and AAV2–EGFP mice after being fed the HFD probably involves increased food intake, whereas the metabolic rate was unchanged by hypothalamic GSK3β overexpression in the former mice. By comparison, the effects of neuronal GSK3β overexpression on the regular chow diet were modest, a discrepancy that might be explained by redundancy in components of the evolutionarily conserved WNT pathway, which may have partially compensated for the effects of increased GSK3β signalling on the chow diet. Interestingly, growing evidence indicates that consuming an HFD induces pro-inflammatory responses in the hypothalamus [39]. Combined with evidence that mediators of peripheral tissue inflammation [e.g. JNK (c-Jun N-terminal kinase)] also activate GSK3β [40], it is plausible that inflammation triggered by the HFD disrupts compensatory mechanisms that might be functional on the chow diet, thereby revealing potent deleterious effects of increased GSK3β activity.

This interpretation is strengthened by evidence of increased hypothalamic expression of SOCS3, which is induced during inflammation and suppresses leptin and insulin signalling [41,42], in AAV2–GSK3β mice compared with the controls while being fed an HFD (Figure 4g, $P = 0.02$). The possibilities that increased hypothalamic GSK3β signalling exacerbates inflammation and leptin resistance during HFD feeding and/or that hypothalamic inflammation increases local GSK3β activity are each consistent with the results of the present study and warrant additional study.

Our findings show that although activation of central GSK3β exacerbates the deleterious effects of HFD feeding on whole-body energy and glucose metabolism, there was only a trend towards increased serum insulin levels in AAV2–GSK3β mice relative to the controls (Figure 4h). A large number of papers suggest that hypothalamic insulin signalling is required for the inhibition of hepatic glucose production [3,4] and both hypothalamic insulin and leptin signalling appear to improve liver insulin sensitivity via a mechanism involving the vagus nerve [43]. To investigate whether central GSK3β activity opposes these effects and increases hepatic glucose output, we employed a strategy that involves an indirect measurement of hepatic glucose production using pyruvate as a substrate for gluconeogenesis, such that the observed glucose excursion reflects hepatic glucose output. $Lep^{ob/ob}$ mice received either GSK3β inhibitor or vehicle ICV 60 min before pyruvate was injected intraperitoneally and blood glucose levels were measured (Figure 5a). Leptin-deficient mice treated with the GSK3β inhibitor showed a significantly reduced glucose excursion compared with the vehicle ($P \leqslant 0.001$, $n = 5$–11/group). To further analyse the impact of central GSK3β inhibition on liver glucose metabolism, we measured the hepatic levels of PEPCK, which is rate-limiting for gluconeogenesis. $Lep^{ob/ob}$ mice received either GSK3β inhibitor or vehicle (aCSF) ICV 90 min before the liver was removed and immunoblotting was performed (Figure 5b) and normalized to the β-actin content. Central inhibition of GSK3β administration significantly decreased the amount of PEPCK protein in the liver compared with the vehicle-treated group ($P = 0.003$, $n = 4$–5/group), which is consistent with data obtained from hepatoma cells [44]. These results support a model in which GSK3β in the brain tonically favours increased plasma glucose levels via a mechanism that involves increased hepatic gluconeogenesis, a phenomenon that can be induced by local hypothalamic inhibition of PI3K [3] and is also observed in diabetic animals and humans [45,46].

Taken together, our data provide the first evidence that increased GSK3β signalling within the CNS drives hyperglycaemia and exerts deleterious effects on whole-body energy balance and glucose

intolerance in AAV2–EGFP mice. (**c**) DEXA scan images of representative animals with overexpression of AAV2–EGFP or AAV2–GSK3β mice on a chow diet and an HFD (upper panel). Body lean and fat mass did not change after treatment with AAV2–GSK3β virus on the chow diet. On the HFD, body lean mass was significantly reduced and body fat mass was increased accordingly after AAV2–GSK3β overexpression (lower panels). Values are expressed as the percentage of body mass. (**d**) AAV2–GSK3β over-expression in the ARC led to an increase in cumulative food intake in animals fed a chow diet or an HFD. Food intake is shown in kJ/day over the whole period of chow diet or an HFD. HFD led to a significant increase in energy expenditure (**e**), whereas GSK3β overexpression did not alter energy expenditure regardless of diet; respiratory quotient was reduced on both the chow diet and HFD after GSK3β overexpression (**f**). (**g**) GSK3β over-expression led to an increase in *SOCS3* gene expression in the ARC. Representative autoradiographies of coronal brain sections exposed to ^{35}S-labelled riboprobe against SOCS3. Insets depict localization within the ARC of mice treated with AAV2–EGFP (left-hand) or AAV2–GSK3β (right-hand). Semi-quantitative analyses of gene expression of *SOCS3* is represented in the histogram as the percentage of AAV2–EGFPb. (**h**) Plasma insulin levels as measured by ELISA were unaltered regardless of treatment with AAV20–EGFP or AAV20–GSK3β. Results are means $\pm$ S.E.M., $^{*}P \leqslant 0.05$, $^{**}P \leqslant 0.01$ and $^{***}P \leqslant 0.001$.

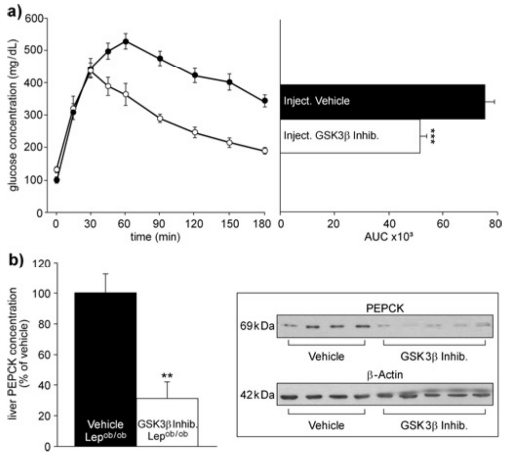

Figure 5 Central GSK3β regulates hepatic glucose production

(**a**) Shown are glucose concentrations (left-hand panel) and associated area under the curve (AUC; right-hand panel) during intraperitoneal pyruvate tolerance tests. A central injection of a GSK3β inhibitor decreased hepatic glucose production in Lep$^{ob/ob}$ mice. Pyruvate tolerance tests were performed 60 min after the administration of GSK3β inhibitor (○) or vehicle (●) into the lateral ventricle ($n = 5$–11/group). (**b**) Hepatic PEPCK levels were semi-quantitatively assessed by immunoblotting using a specific antibody against PEPCK 90 min after the central administration of either GSK3β inhibitor ($n = 5$) or vehicle ($n = 11$) and were normalized by β-actin. Results are means $\pm$ S.E.M., $^{**}P \leqslant 0.01$ and $^{***}P \leqslant 0.001$.

metabolism in the adult mouse, particularly in the setting of an HFD or genetic leptin deficiency. This, together with the notion that this enzyme sensitizes insulin signalling in the hypothalamus, further reinforces the concept that the brain is an essential organ in the maintenance of peripheral glucose homoeostasis. Aberrant GSK3β has also been associated with the pathogenesis of many human diseases, such as osteoporosis [47], atherosclerosis [48], cancer and Alzheimer's disease [49]. The proposed role of GSK3β in the brain in regulating peripheral glucose homoeostasis might constitute an important link between Type II diabetes and the pathogenesis of these other severe diseases.

AUTHOR CONTRIBUTION

Jonas Benzler carried out all of the experiments in Figures 1, 2 and 5, and helped to write the paper and develop the project. Goutham K. Ganjam and Manon Krüger generated the viral construct with technical support from Olaf Pinkenburg and performed the experiments in Figures 3 and 4. Maria Kutschke, Sigrid Stoehr and Juliane Steger provided technical support for all experiments. Christiane Koch helped performing the ipGTTs and Rebecca Oelkrug provided support for performing the metabolic measurements. Michael Schwartz helped to write and revise the paper. Peter R. Shepherd helped to write and revise the paper and gave advice on experiments. David R. Grattan helped to write and revise the paper and gave advice on developing the project. Alexander Tups was the principal investigator developed the project, supervised the research and wrote and revised the paper.

ACKNOWLEDGEMENT

We thank Professor James Woodgett (Samuel Lunenfeld Research Institute, Toronto, Canada) for providing the pcDNA3-GSK3β-HA vector.

FUNDING

This work was supported by the German Ministry of Education and Research [grant number 0315087 (to A.T.)].

REFERENCES

1 Chan, J. C., Malik, V., Jia, W., Kadowaki, T., Yajnik, C. S., Yoon, K. H. and Hu, F. B. (2009) Diabetes in Asia: epidemiology, risk factors, and pathophysiology. JAMA, J. Am. Med. Assoc. **301**, 2129–2140
2 Bruning, J. C., Gautam, D., Burks, D. J., Gillette, J., Schubert, M., Orban, P. C., Klein, R., Krone, W., Muller-Wieland, D. and Kahn, C. R. (2000) Role of brain insulin receptor in control of body weight and reproduction. Science **289**, 2122–2125
3 Obici, S., Zhang, B. B., Karkanias, G. and Rossetti, L. (2002) Hypothalamic insulin signaling is required for inhibition of glucose production. Nat. Med. *8* 1376–1382
4 Obici, S., Feng, Z., Karkanias, G., Baskin, D. G. and Rossetti, L. (2002) Decreasing hypothalamic insulin receptors causes hyperphagia and insulin resistance in rats. Nat. Neurosci. **5**, 566–572
5 Niswender, K. D., Morrison, C. D., Clegg, D. J., Olson, R., Baskin, D. G., Myers, Jr, M. G., Seeley, R. J. and Schwartz, M. W. (2003) Insulin activation of phosphatidylinositol 3-kinase in the hypothalamic arcuate nucleus: a key mediator of insulin-induced anorexia. Diabetes **52**, 227–231
6 Okamoto, H., Nakae, J., Kitamura, T., Park, B. C., Dragatsis, I. and Accili, D. (2004) Transgenic rescue of insulin receptor-deficient mice. J. Clin. Invest. **114**, 214–223
7 Okamoto, H., Obici, S., Accili, D. and Rossetti, L. (2005) Restoration of liver insulin signaling in Insr knockout mice fails to normalize hepatic insulin action. J. Clin. Invest. **115**, 1314–1322
8 Gelling, R. W., Morton, G. J., Morrison, C. D., Niswender, K. D., Myers, Jr, M. G., Rhodes, C. J. and Schwartz, M. W. (2006) Insulin action in the brain contributes to glucose lowering during insulin treatment of diabetes. Cell Metab. **3**, 67–73
9 Koch, C., Augustine, R. A., Steger, J., Ganjam, G. K., Benzler, J., Pracht, C., Lowe, C., Schwartz, M. W., Shepherd, P. R., Anderson, G. M. et al. (2010) Leptin rapidly improves glucose homeostasis in obese mice by increasing hypothalamic insulin sensitivity. J. Neurosci. **30**, 16180–16187
10 Niswender, K. D., Morton, G. J., Stearns, W. H., Rhodes, C. J., Myers, Jr, M. G. and Schwartz, M. W. (2001) Intracellular signalling. Key enzyme in leptin-induced anorexia. Nature **413**, 794–795
11 Zhao, A. Z., Huan, J. N., Gupta, S., Pal, R. and Sahu, A. (2002) A phosphatidylinositol 3-kinase phosphodiesterase 3B-cyclic AMP pathway in hypothalamic action of leptin on feeding. Nat. Neurosci. **5**, 727–728
12 Cross, D. A., Alessi, D. R., Cohen, P., Andjelkovich, M. and Hemmings, B. A. (1995) Inhibition of glycogen synthase kinase-3 by insulin mediated by protein kinase B. Nature **378**, 785–789
13 Hur, E. M. and Zhou, F. Q. (2010) GSK3 signalling in neural development. Nat. Rev. Neurosci. **11**, 539–551
14 Cline, G. W., Johnson, K., Regittnig, W., Perret, P., Tozzo, E., Xiao, L., Damico, C. and Shulman, G. I. (2002) Effects of a novel glycogen synthase kinase-3 inhibitor on insulin-stimulated glucose metabolism in Zucker diabetic fatty (fa/fa) rats. Diabetes **51**, 2903–2910
15 Kaidanovich-Beilin, O. and Eldar-Finkelman, H. (2006) Long-term treatment with novel glycogen synthase kinase-3 inhibitor improves glucose homeostasis in ob/ob mice: molecular characterization in liver and muscle. J. Pharmacol. Exp. Ther. **316**, 17–24
16 Rao, R., Hao, C. M., Redha, R., Wasserman, D. H., McGuinness, O. P. and Breyer, M. D. (2007) Glycogen synthase kinase 3 inhibition improves insulin-stimulated glucose metabolism but not hypertension in high-fat-fed C57BL/6J mice. Diabetologia **50**, 452–460
17 Eldar-Finkelman, H. (2002) Glycogen synthase kinase 3: an emerging therapeutic target. Trends Mol. Med. **8**, 126–132
18 Nikoulina, S. E., Ciaraldi, T. P., Mudaliar, S., Carter, L., Johnson, K. and Henry, R. R. (2002) Inhibition of glycogen synthase kinase 3 improves insulin action and glucose metabolism in human skeletal muscle. Diabetes **51**, 2190–2198
19 Clodfelder-Miller, B., De Sarno, P., Zmijewska, A. A., Song, L. and Jope, R. S. (2005) Physiological and pathological changes in glucose regulate brain Akt and glycogen synthase kinase-3. J. Biol. Chem. **280**, 39723–39731
20 Mercer, J. G., Moar, K. M., Logie, T. J., Findlay, P. A., Adam, C. L. and Morgan, P. J. (2001) Seasonally inappropriate body weight induced by food restriction: effect on hypothalamic gene expression in male Siberian hamsters. Endocrinology **142**, 4173–4181
21 Paxinos, G. and Franklin, K. (2002) The Mouse Brain in Stereotaxic Coordinates, Academics, San Diego
22 Tups, A., Anderson, G. M., Rizwan, M., Augustine, R. A., Chaussade, C., Shepherd, P. R. and Grattan, D. R. (2010) Both p110α and p110β isoforms of phosphatidylinositol 3-OH-kinase are required for insulin signalling in the hypothalamus. J. Neuroendocrinol. **22**, 534–542
23 Kugler, S., Lingor, P., Scholl, U., Zolotukhin, S. and Bahr, M. (2003) Differential transgene expression in brain cells *in vivo* and *in vitro* from AAV-2 vectors with small transcriptional control units. Virology **311**, 89–95

24 Grimm, D., Kay, M. A. and Kleinschmidt, J. A. (2003) Helper virus-free, optically controllable, and two-plasmid-based production of adeno-associated virus vectors of serotypes 1 to 6. Mol. Ther. **7**, 839–850

25 Culmsee, C., Zhu, C., Landshamer, S., Becattini, B., Wagner, E., Pellecchia, M., Blomgren, K. and Plesnila, N. (2005) Apoptosis-inducing factor triggered by poly(ADP-ribose) polymerase and Bid mediates neuronal cell death after oxygen-glucose deprivation and focal cerebral ischemia. J. Neurosci. **25**, 10262–10272

26 He, X., Saint-Jeannet, J. P., Woodgett, J. R., Varmus, H. E. and Dawid, I. B. (1995) Glycogen synthase kinase-3 and dorsoventral patterning in *Xenopus* embryos. Nature **374**, 617–622

27 Ganjam, G. K., Dimova, E. Y., Unterman, T. G. and Kietzmann, T. (2009) FoxO1 and HNF-4 are involved in regulation of hepatic glucokinase gene expression by resveratrol. J. Biol. Chem. **284**, 30783–30797

28 Heldmaier, G. and Ruf, T. (1992) Body temperature and metabolic rate during natural hypothermia in endotherms. J. Comp. Physiol. B **162**, 696–706

29 Sutherland, C., Leighton, I. A. and Cohen, P. (1993) Inactivation of glycogen synthase kinase-3β by phosphorylation: new kinase connections in insulin and growth-factor signalling. Biochem. J. **296**, 15–19

30 Stambolic, V. and Woodgett, J. R. (1994) Mitogen inactivation of glycogen synthase kinase-3β in intact cells via serine 9 phosphorylation. Biochem. J. **303**, 701–704

31 Dajani, R., Fraser, E., Roe, S. M., Young, N., Good, V., Dale, T. C. and Pearl, L. H. (2001) Crystal structure of glycogen synthase kinase 3β: structural basis for phosphate-primed substrate specificity and autoinhibition. Cell **105**, 721–732

32 Woodgett, J. R. (2001) Judging a protein by more than its name: GSK-3. Sci. STKE **2001**, re12

33 Shaw, M., Cohen, P. and Alessi, D. R. (1997) Further evidence that the inhibition of glycogen synthase kinase-3β by IGF-1 is mediated by PDK1/PKB-induced phosphorylation of Ser-9 and not by dephosphorylation of Tyr-216. FEBS Lett. **416**, 307–311

34 Koch, L., Wunderlich, F. T., Seibler, J., Konner, A. C., Hampel, B., Irlenbusch, S., Brabant, G., Kahn, C. R., Schwenk, F. and Bruning, J. C. (2008) Central insulin action regulates peripheral glucose and fat metabolism in mice. J. Clin. Invest **118**, 2132–2147

35 Scali, C., Caraci, F., Gianfriddo, M., Diodato, E., Roncarati, R., Pollio, G., Gaviraghi, G., Copani, A., Nicoletti, F., Terstappen, G. C. et al. (2006) Inhibition of Wnt signaling, modulation of Tau phosphorylation and induction of neuronal cell death by DKK1. Neurobiol. Dis. **24**, 254–265

36 Monahan, P. E. and Samulski, R. J. (2000) AAV vectors: is clinical success on the horizon? Gene Ther. **7**, 24–30

37 de Backer, M. W., Fitzsimons, C. P., Brans, M. A., Luijendijk, M. C., Garner, K. M., Vreugdenhil, E. and Adan, R. A. (2010) An adeno-associated viral vector transduces the rat hypothalamus and amygdala more efficient than a lentiviral vector. BMC Neurosci. **11**, 81

38 Sperber, B. R., Leight, S., Goedert, M. and Lee, V. M. (1995) Glycogen synthase kinase-3β phosphorylates tau protein at multiple sites in intact cells. Neurosci. Lett. **197**, 149–153

39 Posey, K. A., Clegg, D. J., Printz, R. L., Byun, J., Morton, G. J., Vivekanandan-Giri, A., Pennathur, S., Baskin, D. G., Heinecke, J. W., Woods, S. C. et al. (2009) Hypothalamic proinflammatory lipid accumulation, inflammation, and insulin resistance in rats fed a high-fat diet. Am. J. Physiol. Endocrinol. Metab **296**, E1003–E1012

40 Hu, D., Fang, W., Han, A., Gallagher, L., Davis, R. J., Xiong, B. and Yang, W. (2008) c-Jun N-terminal kinase 1 interacts with and negatively regulates Wnt/β-catenin signaling through GSK3β pathway. Carcinogenesis **29**, 2317–2324

41 Bjorbaek, C., Elmquist, J. K., Frantz, J. D., Shoelson, S. E. and Flier, J. S. (1998) Identification of SOCS-3 as a potential mediator of central leptin resistance. Mol. Cell **1**, 619–625

42 Tups, A., Ellis, C., Moar, K. M., Logie, T. J., Adam, C. L., Mercer, J. G. and Klingenspor, M. (2004) Photoperiodic regulation of leptin sensitivity in the Siberian hamster, *Phodopus sungorus*, is reflected in arcuate nucleus SOCS-3 (suppressor of cytokine signaling) gene expression. Endocrinology **145**, 1185–1193

43 German, J., Kim, F., Schwartz, G. J., Havel, P. J., Rhodes, C. J., Schwartz, M. W. and Morton, G. J. (2009) Hypothalamic leptin signaling regulates hepatic insulin sensitivity via a neurocircuit involving the vagus nerve. Endocrinology **150**, 4502–4511

44 Lochhead, P. A., Coghlan, M., Rice, S. Q. and Sutherland, C. (2001) Inhibition of GSK-3 selectively reduces glucose-6-phosphatase and phosphatase and phosphoenolypyruvate carboxykinase gene expression. Diabetes **50**, 937–946

45 Consoli, A., Nurjhan, N., Capani, F. and Gerich, J. (1989) Predominant role of gluconeogenesis in increased hepatic glucose production in NIDDM. Diabetes **38**, 550–557

46 Gerich, J. E. and Nurjhan, N. (1993) Gluconeogenesis in type 2 diabetes. Adv. Exp. Med. Biol. **334**, 253–258

47 Smith, E. and Frenkel, B. (2005) Glucocorticoids inhibit the transcriptional activity of LEF/TCF in differentiating osteoblasts in a glycogen synthase kinase-3β-dependent and -independent manner. J. Biol. Chem. **280**, 2388–2394

48 Robertson, I. A., Kim, A. J. and Werstuck, G. H. (2006) Mechanisms linking diabetes mellitus to the development of atherosclerosis: a role for endoplasmic reticulum stress and glycogen synthase kinase-3. Can. J. Physiol. Pharmacol. **84**, 39–48

49 Jope, R. S. and Johnson, G. V. (2004) The glamour and gloom of glycogen synthase kinase-3. Trends Biochem. Sci. **29**, 950–102

Received 22 May 2012/26 July 2012; accepted 1 August 2012
Published as BJ Immediate Publication 1 August 2012, doi:10.1042/BJ20120834

P62 LINKS BETA-ADRENERGIC INPUT WITH MITOCHONDRIAL FUNCTION

T.D. MUELLER ∞ S.J. LEE ∞ M. JASTROCH ∞ D. KABRA K. STEMMER ∞ M. AICHLER ∞ B. ABPLANALP G.ANANTHAKRISHNAN N.BHARDWAJ ∞ S.COLLINS ∞ S. DIVANOVIC ∞ M. ENDELE ∞ B. FINAN ∞Y. GAO ∞ K.M. HABEGGER ∞ J. HEMBREE ∞ K.M. HEPPNER S. HOFMANN J. HOLLAND ∞ D. KÜCHLER ∞ M. KUTSCHKE R. KRISHNA M. LEHTI ∞ R. OELKRUG ∞ N. OTTAWAY D. PEREZ-TILVE C. RAVER ∞ A.K. WALCH ∞ S.C. SCHRIEVER J. SPEAKMAN Y. ∞ TSENG ∞ M. DIAZ-MECO ∞ P.T. PFLUGER ∞ J. MOSCAT TSCHÖP M.H.

Research article

p62 Links β-adrenergic input to mitochondrial function and thermogenesis

Timo D. Müller,[1] Sang Jun Lee,[2] Martin Jastroch,[1] Dhiraj Kabra,[1] Kerstin Stemmer,[1] Michaela Aichler,[3] Bill Abplanalp,[4] Gayathri Ananthakrishnan,[4] Nakul Bhardwaj,[4] Sheila Collins,[5] Senad Divanovic,[6] Max Endele,[7] Brian Finan,[1] Yuanqing Gao,[4] Kirk M. Habegger,[4] Jazzmin Hembree,[4] Kristy M. Heppner,[4] Susanna Hofmann,[8] Jenna Holland,[4] Daniela Küchler,[1] Maria Kutschke,[1] Radha Krishna,[4] Maarit Lehti,[4] Rebecca Oelkrug,[9] Nickki Ottaway,[4] Diego Perez-Tilve,[4] Christine Raver,[4] Axel K. Walch,[3] Sonja C. Schriever,[1] John Speakman,[10,11] Yu-Hua Tseng,[12] Maria Diaz-Meco,[2] Paul T. Pfluger,[1,4] Jorge Moscat,[2] and Matthias H. Tschöp[1,4]

[1]Institute for Diabetes and Obesity, Helmholtz Zentrum Muenchen and Department of Medicine, Technische Universität München, Munich, Germany. [2]Sanford-Burnham Medical Research Institute, La Jolla, California, USA. [3]Institute of Pathology — Research Unit Analytical Pathology, Helmholtz Centre Munich, Munich, Germany. [4]Metabolic Diseases Institute, Department of Internal Medicine, University of Cincinnati, Cincinnati, Ohio, USA. [5]Diabetes and Obesity Research Center, Sanford-Burnham Medical Research Institute, Orlando, Florida, USA. [6]Division of Molecular Immunology, Cincinnati Children's Hospital Research Foundation, and the University of Cincinnati College of Medicine, Cincinnati, Ohio, USA. [7]Research Unit Stem Cell Dynamics, Helmholtz Center Munich — German Research Center for Environmental Health, Neuherberg, Germany. [8]Institute of Experimental Genetics, Helmholtz Centre Munich, Munich, Germany. [9]Department of Animal Physiology, Philipps Universität Marburg, Marburg, Germany. [10]Institute of Genetics and Developmental Biology, Beijing, China. [11]Institute of Biological and Environmental Sciences, University of Aberdeen, Aberdeen, Scotland, United Kingdom. [12]Joslin Diabetes Center, Harvard Medical School, Boston, Massachusetts, USA.

The scaffold protein p62 (sequestosome 1; SQSTM1) is an emerging key molecular link among the metabolic, immune, and proliferative processes of the cell. Here, we report that adipocyte-specific, but not CNS-, liver-, muscle-, or myeloid-specific *p62*-deficient mice are obese and exhibit a decreased metabolic rate caused by impaired nonshivering thermogenesis. Our results show that p62 regulates energy metabolism via control of mitochondrial function in brown adipose tissue (BAT). Accordingly, adipocyte-specific *p62* deficiency led to impaired mitochondrial function, causing BAT to become unresponsive to β-adrenergic stimuli. Ablation of p62 leads to decreased activation of p38 targets, affecting signaling molecules that control mitochondrial function, such as ATF2, CREB, PGC1α, DIO2, NRF1, CYTC, COX2, ATP5β, and UCP1. *p62* ablation in HIB1B and BAT primary cells demonstrated that p62 controls thermogenesis in a cell-autonomous manner, independently of brown adipocyte development or differentiation. Together, our data identify p62 as a novel regulator of mitochondrial function and brown fat thermogenesis.

Introduction

Obesity and its comorbidities, such as cardiovascular disease and type 2 diabetes, are increasingly challenging health threats in modern societies. Obesity, defined as a pathologically exaggerated accumulation of body fat, is the direct consequence of a prolonged positive energy balance that occurs when energy intake chronically exceeds energy expenditure. So far, pharmacological weight loss therapies, frequently aiming to minimize energy intake, have been hampered by limited efficacy or considerable side effects. Therefore, novel strategies to safely and efficiently combat the obesity and diabetes epidemic are urgently required.

In small mammals and infants, brown adipose tissue (BAT) plays an important role in energy metabolism due to its ability to burn energy by dissipating heat in response to sympathetic nerve activity (1, 2). In adult humans, however, BAT was long believed to play, at most, a minor role in energy metabolism. More recently, this historical view has been called into question by the observations that adult humans possess considerable amounts of BAT (3–6) and that the amount of BAT is decreased in obese compared with lean individuals (3, 5). These observations, in addition to recent advances in understanding the complex processes of brown adipocyte differentiation and function (7–12), have resulted in a rekindled scientific interest in BAT as a therapeutic target for the treatment of obesity.

Scaffold proteins are important mediators ensuring efficient and selective cell signal transduction. Enzymatic signal specificity mediated by scaffold proteins is thereby achieved through specific protein-protein interactions between shared motifs located in both the target enzyme and the scaffold protein. p62 (sequestosome 1; SQSTM1) was originally identified as a signal adaptor for isoforms of the atypical PKC subfamily (aPKCs) (13, 14). p62 is a multimodular adaptor protein involved in a number of signaling pathways affecting important biological processes, such as inflammation, cell differentiation, cell growth, and tumorigenesis (15–17). We have previously shown that global ablation of p62 in mice results in obesity and systemic glucose intolerance and insulin resistance (18, 19). The main goal of the present study was to rigorously establish the in vivo target tissue accounting for the role of p62 in the control of metabolic homeostasis and obesity and also to unravel the mechanistic details of p62 in those processes.

Results

Generation of tissue-specific p62$^{-/-}$ *mice.* To establish the p62 target tissue responsible for its role in whole-body metabolic control and obesity in vivo, we used the Cre-lox system to target key tissues

Conflict of interest: John Speakman holds stock in Swedish Orphan Biovitrum, has received grants from AstraZeneca and Pfizer, and is a founder shareholder in Cambridge Biotechnology. Yu-Hua Tseng receives grant support from Chugai Pharmaceutical Co. D. Perez-Tilve has a collaborative association with F. Hoffmann-La Roche Ltd. pertaining to peptide-based therapeutics in metabolism.

Citation for this article: *J Clin Invest.* doi:10.1172/JCI64209.

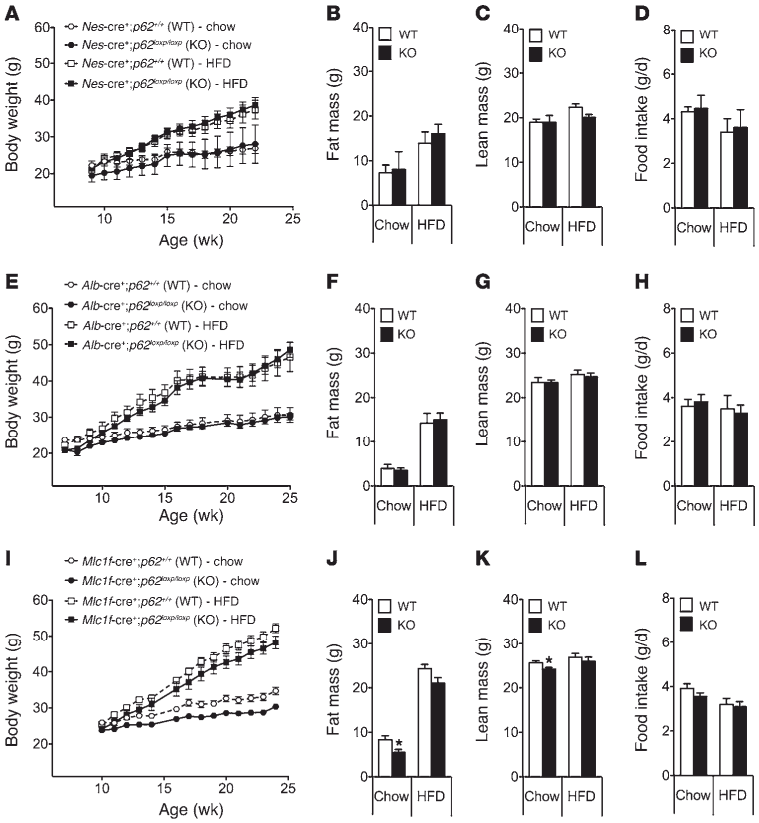

Figure 1
Mice with tissue-specific deletion of p62 in the CNS, liver, or skeletal muscles do not show a metabolically relevant phenotype. Body weight, body composition (fat and lean tissue mass), and food intake of male mice that lack p62 selectively in the CNS (**A–D**), the liver (**E–H**), or the skeletal muscles (**I–L**). Fat and lean tissue mass was measured at an age of 23 weeks (**A**), 22 weeks (**B**), or 24 weeks (**C**). n = 8–10 mice each group. Data represent mean ± SEM. *$P < 0.05$.

implicated in systemic energy metabolism control, namely CNS, liver, skeletal muscle, adipose tissue, and cells of the myeloid lineage. To that end, we generated the tissue-specific $p62^{-/-}$ mouse lines shown in Supplemental Figure 1 (supplemental material available online with this article; doi:10.1172/JCI64209DS1). Briefly, the coding exon 1 of the murine p62 isoform 1 (NM_011018.2) was deleted by mating chimeric p62 floxed mice with mice expressing Cre recombinase (Cre) under the control of the promoter for either nestin (*Nes*, CNS specific) (20), albumin (*Alb*, liver specific) (21), myosin light chain 1f (*Mlc1f*, muscle specific) (22), or adipocyte protein 2 (*aP2* also known as *Fabp4*, adipocyte-specific) (23). As aP2 is also expressed in macrophages (24), we also generated mice that lack p62 in the myeloid lineage using lysozyme M (LysM, also known as Lyz2) cre mice. Validation of tissue-specific p62 deletion was assessed using Western blot analysis (Supplemental Figure 1).

CNS-specific deletion of p62 in mice does not affect systemic metabolism. The metabolic phenotype of mice with exclusive deletion of p62 in the CNS was assessed under 2 different feeding regimes. Some mice were fed a regular standard chow diet (5.6% fat), whereas a parallel cohort was fed a high-fat diet (HFD) (58% fat). Surprisingly, we observed no difference in body weight (Figure 1A), body composition (Figure 1, B and C), or food intake (Figure 1D) in mice that lack p62 selectively in the CNS (*Nes*-cre^{+};$p62^{loxp/loxp}$) as compared with WT controls (*Nes*-cre^{+};$p62^{+/+}$), irrespective of the diet. Accordingly, we concluded that obesity in the global $p62^{-/-}$ mice was mediated by peripheral mechanisms and independent of p62 signaling in the brain.

Hepatic deletion of p62 in mice does not affect systemic metabolism. The phenotypical analysis of mice that lack p62 exclusively in the liver (*Alb*-cre^{+};$p62^{loxp/loxp}$) also failed to reveal any alterations in body weight (Figure 1E), body composition (Figure 1, F and G), or food intake (Figure 1H) when compared with WT controls (*Alb*-cre^{+};$p62^{+/+}$) independently of the diet. In addition, no signs of liver steatosis were observed and no differences in systemic glucose tolerance were observed when comparing liver-specific $p62^{-/-}$ mice and their WT littermate controls (Supplemental Figure 2A). Together, these data do not support a role for hepatic p62 signaling in the regulation of body weight or systemic metabolism.

Deletion of p62 in mouse skeletal muscle does not affect systemic metabolism. We next analyzed the metabolic phenotype of mice lacking p62 exclusively in skeletal muscle (*Mlc1f*-cre^{+};$p62^{loxp/loxp}$). When compared with WT controls (*Mlc1f*-cre^{+};$p62^{+/+}$), these mutant mice did not show any signs of obesity on either regular chow or HFD (Figure 1I). In fact, the body weight of the muscle-specific $p62^{-/-}$

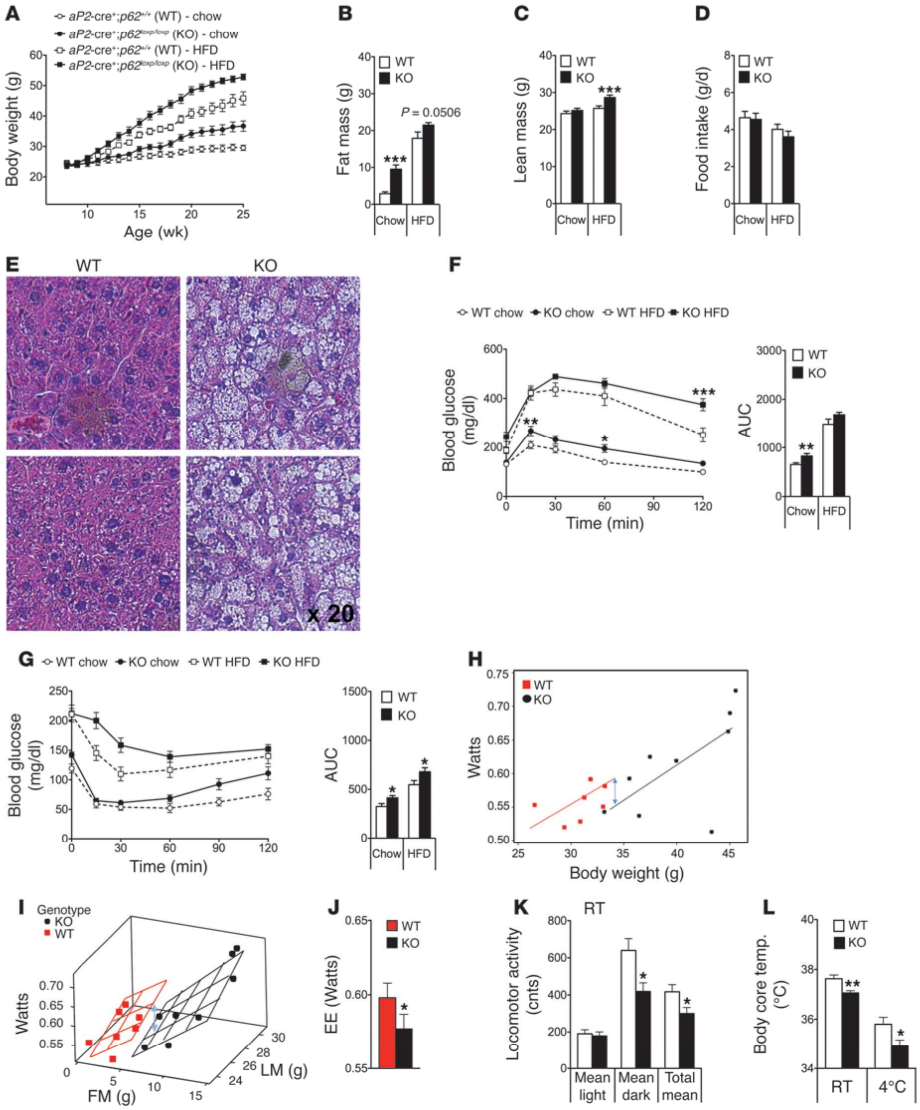

Figure 2
Metabolic phenotype of adipocyte-specific *p62*$^{-/-}$ mice. Body weight (**A**), body composition at an age of 26 weeks (**B** and **C**), and food intake (**D**) of adipocyte-specific *p62*$^{-/-}$ and control mice fed either with a standard chow diet (5.6% fat) or HFD (58% kcal fat). H&E staining of liver samples from 35-week-old chow-fed adipocyte-specific *p62*$^{-/-}$ and WT mice (**E**). Glucose tolerance (**F**) and insulin sensitivity (**G**) of 17-week-old chow-fed adipocyte-specific *p62*$^{-/-}$ and WT mice. Energy expenditure (EE). (**H–J**) and locomotor activity (**K**) of 33-week-old chow-fed adipocyte-specific *p62*$^{-/-}$ and WT mice at room temperature (23 ± 2°C). Body core temperature of 35-week-old chow-fed adipocyte-specific *p62*$^{-/-}$ and WT mice at room temperature and during acute cold exposure (16 hours at 4°C) (**L**). n = 7–11 mice each group. Data represent mean ± SEM. $^{*}P < 0.05$; $^{**}P < 0.01$; $^{***}P < 0.001$.

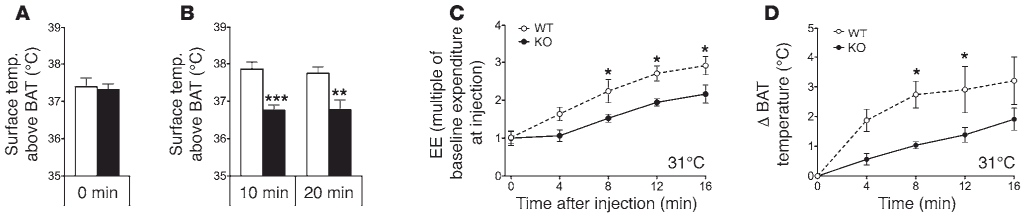

Figure 3
Impaired response to β-adrenergic receptor stimulation in adipocyte-specific *p62*$^{-/-}$ mice. Body surface temperature above the BAT, measured with an IR camera, of obese adipocyte-specific *p62*$^{-/-}$ mice before (**A**) and after (**B**) i.p. treatment with CL-316,243 (0.6 mg/kg). Measurement of energy expenditure (expressed as multiple of baseline expenditure at injection) (**C**) and increase of BAT temperature (measured using implanted temperature sensors) at different time points after s.c. treatment with norepinephrine (1 mg/kg) (**D**). n = 7–11 mice per group (**A** and **B**); n = 4 mice each group (**C** and **D**). Data represent mean ± SEM. *P < 0.05; **P < 0.01; ***P < 0.001.

mice was moderately lower when compared with WT controls fed standard chow diet but not HFD (Figure 1I). The decreased body weight of the chow-fed muscle-specific *p62*$^{-/-}$ mice was accompanied by a decrease in body fat and lean tissue mass (Figure 1, J and K) without notable changes in food intake (Figure 1L) or glucose tolerance (Supplemental Figure 2B). Indirect calorimetry performed at the age of 20 weeks revealed no detectable differences in energy expenditure, locomotor activity, or substrate utilization between the muscle-specific *p62*$^{-/-}$ mice and their WT controls (Supplemental Figure 3, A–D). Also, the energy expenditure response to a norepinephrine challenge (1 mg/kg, single s.c. injection) did not differ between both genotypes (Supplemental Figure 3E). Together, these data indicate that lack of p62 signaling in the skeletal muscles does not explain the role of p62 in the systemic control of body weight and adiposity observed in global *p62*$^{-/-}$ mice.

Adipocyte-specific, but not macrophage-specific, deletion of p62$^{-/-}$ *results in obesity and glucose intolerance.* When mice that lack p62 selectively in the adipose tissue (*aP2*-cre^{+};*p62*$^{loxp/loxp}$) were analyzed, we observed a dramatically enhanced body weight gain as compared with WT controls (*aP2*-cre^{+};*p62*$^{+/+}$) on both standard chow and HFD (Figure 2A). The obese phenotype of the adipocyte-specific *p62*$^{-/-}$ mice was comparable to that observed in the global *p62*$^{-/-}$ mice and was a consequence of increased body fat and lean tissue mass (Figure 2, B and C). Interestingly, as in the case of global *p62*$^{-/-}$ mice, obesity was not paralleled by changes in food intake (Figure 2D). On either diet, adipocyte-specific *p62*$^{-/-}$ mice had liver steatosis (Figure 2E), impaired glucose tolerance, and decreased insulin sensitivity (Figure 2, F and G). aP2cre mice have been reported to potentially cause target gene deletion in cells beyond adipocytes, such as CNS neurons or macrophages. However, we had already shown that deletion of p62 in the CNS did not cause a body weight phenotype and consequently could not explain the phenotype of *aP2*-cre^{+};*p62*$^{loxp/loxp}$ mice. Therefore, we next used lysozyme M (*LysM*) cre mice to selectively knock out p62 in the myeloid cell lineage (*LysM*-cre^{+};*p62*$^{loxp/loxp}$). Careful phenotype analysis of these mutant mice did not reveal any differences in body weight, body composition, or glucose and insulin sensitivity when compared with the corresponding WT control mice (Supplemental Figure 4, A–E). Collectively, these findings indicate that obesity in *aP2*-cre^{+};*p62*$^{loxp/loxp}$ mice is a consequence of p62 deficiency in adipocytes and does not result from the lack of p62 in myeloid cells.

White adipocytes of the obese adipocyte-specific *p62*$^{-/-}$ mice were greatly enlarged (Supplemental Figure 5A) and showed increased basal activity of Mapk1 (also known as ERK) (Supplemental Figure 5B), which is in agreement with previously reported data in total p62-deficient mice (19). Expression of proinflammatory cytokines and chemokines, such as *Il6*, *Tnfa*, chemokine cc motif ligand 2 [*Ccl2*], and integrin α-x [*Itgax*], as well as markers of macrophage infiltration (*Cd68* and Emr1 [also known as F4/80]) were increased as expected, considering the obese phenotype of these mice (Supplemental Figure 5, C and D). Of note, expression of *Pparg* and *Cebpb*, well-known master regulators of adipogenesis and fat cell differentiation (2, 25), was not changed in epididymal white adipose tissue (eWAT) of adipocyte-specific *p62*$^{-/-}$ mice (Supplemental Figure 5E). Gene programs controlling lipoprotein metabolism, lipogenesis, fatty acid transport, or lipolysis were also not affected by adipocyte-specific p62 deficiency (Supplemental Figure 5, F–I). Finally, there was no difference in plasma-free fatty acids and free glycerol between genotypes following a challenge with norepinephrine (1 mg/kg) (Supplemental Figure 5, J and K). We conclude that the obese phenotype of adipocyte-specific *p62*$^{-/-}$ mice does not result from changes in fatty acid mobilization or lipolysis.

Impaired nonshivering thermogenesis in adipocyte-specific p62$^{-/-}$ *mice.* Indirect calorimetry, performed at an age of 33 weeks, revealed that energy expenditure was decreased in adipocyte-specific *p62*$^{-/-}$ mice as compared with WT controls (Figure 2H). Importantly, this finding was confirmed when energy expenditure raw data were analyzed without normalizing for body size using ANCOVA, with body fat and lean tissue mass as covariants, as proposed recently (ref. 26 and Figure 2, I and J). The decrease in energy expenditure was accompanied by a significant reduction in locomotor activity (Figure 2K) and considerably lower body core temperature (Figure 2L). Based on these observations, we hypothesized that the decreased energy metabolism of the adipocyte-specific *p62*$^{-/-}$ mice might be a consequence of impaired nonshivering thermogenesis in BAT. Accordingly, to test whether p62 links β-adrenergic stimulation with mitochondrial uncoupling in vivo, we measured the surface temperature above BAT in response to the selective β-3 adrenergic receptor agonist CL-316,243. In line with our hypothesis, single i.p. treatment with CL-316,243 (0.6 mg/kg) significantly increased the surface temperature above BAT in WT mice, but had no measurable effect in adipocyte-specific *p62*$^{-/-}$ mice (Figure 3, A and B). These findings were corroborated by significantly impaired energy expenditure (Figure 3C) and BAT surface temperature (Figure 3D) responses to systemic norepinephrine (1 mg/kg) challenge in adipocyte-specific *p62*$^{-/-}$ mice compared with WT controls.

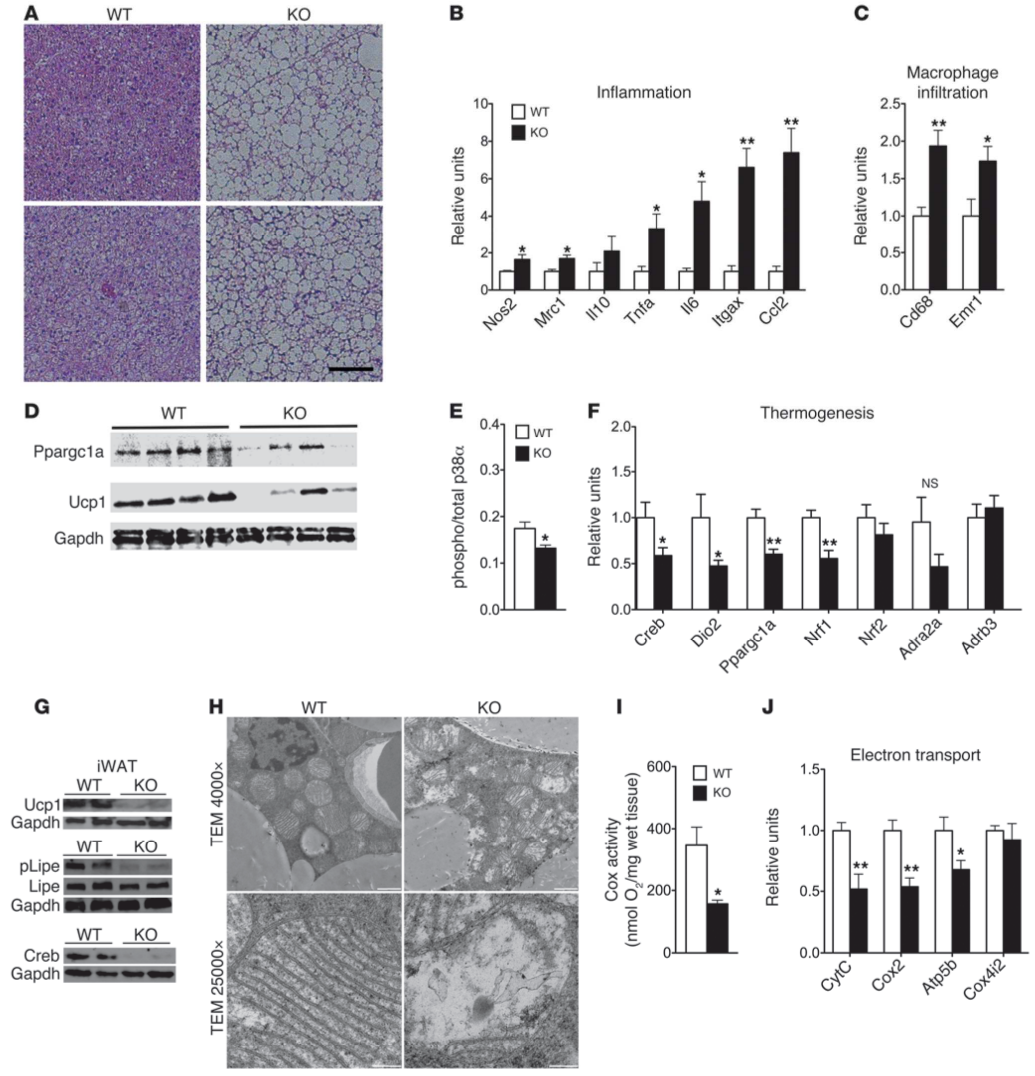

Figure 4
Impaired mitochondrial function in BAT of chow-fed adipocyte-specific *p62*$^{-/-}$ mice. H&E staining of BAT (**A**). Expression of genes related to inflammation (**B**) and macrophage infiltration (**C**) in BAT. Western blot analysis of Ppargc1a and Ucp1 (**D**) and ratio between levels of total and phosphorylated levels of p38α in BAT (**E**). Expression of genes related to thermogenesis (**F**). Western blot analysis of Ucp1, Lipe, and Creb in the inguinal WAT (**G**). Electron micrograph of brown adipocytes (**H**), Cox activity (**I**), and mRNA expression levels of genes related to mitochondrial electron transport (**J**) in BAT of adipocyte-specific *p62*$^{-/-}$ and WT mice. *Cox4i2*, COX subunit 4b. Measurement of gene expression was performed in $n = 7–8$ mice of each genotype. Cox activity and protein levels of p38α were assessed in $n = 4$ mice of each genotype. Scale bars: 25 μm (**A**); 1 μm (**H**, original magnification ×4,000); 200 nm (**H**; original magnification, ×25,000. Data represent mean ± SEM. $^{*}P < 0.05$; $^{**}P < 0.01$.

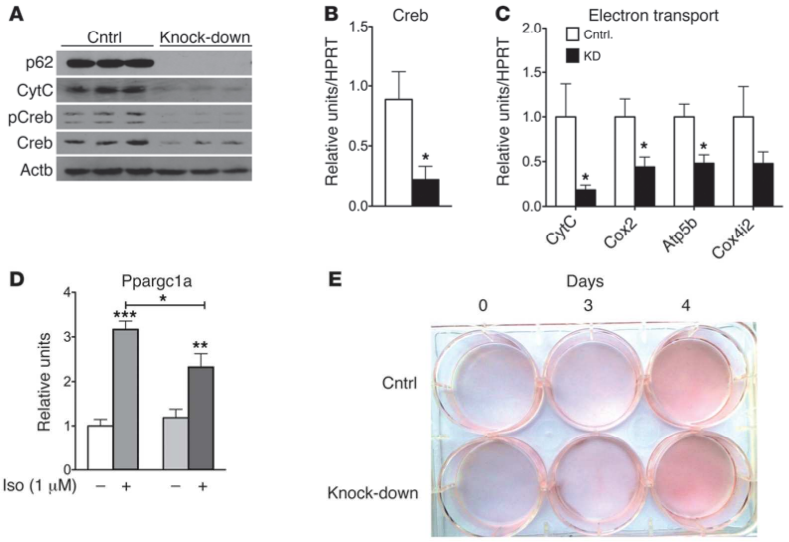

Figure 5
Cell autonomous effect of p62 on mitochondrial function in HIB1B cells. Western blot analysis of p62, CytC,and total and phosphorylated Creb (**A**) and mRNA level of *Creb* (**B**) and genes related to mitochondrial electron transport (**C**) in HIB1B cells lacking p62 and controls. mRNA levels of *Ppargc1a* in p62-deficient HIB1B cells after 6 hours stimulation with isoproterenol (1 μM) (**D**). Oil red O staining in p62-deficient HIB1B cells (**E**). $^{*}P < 0.05$; $^{**}P < 0.01$; $^{***}P < 0.001$.

Impaired mitochondrial function in BAT of adipocyte-specific p62$^{-/-}$ mice. Histological analysis revealed enhanced lipid deposition with increased lipid droplet sizes in BAT of adipocyte-specific *p62*$^{-/-}$ mice (Figure 4A). Accordingly, expression profiles reflecting inflammation (inducible nitric oxide synthase [*Nos2*], mannose receptor C-type 1 [*Mrc1*], *Tnfa*, *Il6*, *Itgax*, *Ccl2*) and macrophage infiltration (*Cd68*, *Emr1*) were increased (Figure 4, B and C). Consistent with our hypothesis that nonshivering thermogenesis is impaired in adipocyte-specific *p62*$^{-/-}$ mice, protein levels of PPARGC1A (also known as PGC1A) and uncoupling protein 1 (UCP1) were decreased in these mice (Figure 4D). Importantly, we discovered that the loss of p62 in adipocytes decreased activation of p38α in BAT (Figure 4E). Consistent with that observation, we found that mRNA expression of p38 downstream targets and key uncoupling regulators was significantly decreased in adipocyte-specific *p62*$^{-/-}$ mice compared with WT controls, including cAMP response element binding protein 1 [*Creb*], diodinase 2 [*Dio2*], *Pgc1a*, and nuclear respiratory factor 1 [*Nrf1*] (Figure 4F). This finding was corroborated by lower protein levels of CREB and UCP1, as well as less phosphorylated LIPE (also known as HSL) in brown adipocyte rich (Brite) inguinal adipose tissue (Figure 4G and ref. 27). Notably, expression of the β-3 adrenergic receptor (*Adrb3*) and the α2A adrenergic receptor (*Adra2a*) was not changed in adipocyte-specific *p62*$^{-/-}$ mice compared with WT controls (Figure 4F), indicating a role for p62 at the molecular interface between β-adrenergic input and intracellular control of uncoupling in BAT.

Electron microscopy analyses revealed considerable differences in mitochondrial structure as a consequence of p62 deficiency in adipocytes (Figure 4H). Brown adipocytes from adipocyte-specific *p62*$^{-/-}$ mice contained mitochondria with fewer cristae, which were also shorter and displaced to the periphery with varying degrees of disorientation (Figure 4H). In line with this observation, we found decreased oxidative capacity, as quantified by measuring cytochrome *c* oxidase (Cox) activity, in BAT of adipocyte-specific *p62*$^{-/-}$ mice (Figure 4I). Moreover, mRNA expression levels of gene programs relevant to electron transport, such as cytochrome C (*CytC*), *Cox2*, and ATP synthase mitochondrial F1 complex subunit β (*Atp5b*), were likewise decreased (Figure 4J). Together, these data indicate that p62 is essential for the structural integrity and proper function of BAT mitochondria.

Cell autonomous role of p62 in mitochondrial function. To assess whether the observed effect on mitochondrial function was mediated by p62 in a cell-autonomous manner, we knocked down p62 in the BAT cell line HIB1B using shRNA against p62 (Figure 5). Consistent with our findings from adipocyte-specific *p62*$^{-/-}$ mice, knockdown of p62 in HIB1B cells led to decreased protein levels of CytC, lower total and phosphorylated levels of Creb, and decreased mRNA levels of the *Creb*, *CytC*, *Cox2*, and *Atp5b* genes (Figure 5, A–C). In line with this observation, the response of PGC1α to isoproterenol (1 μM) was significantly lower in cells lacking p62 (Figure 5D). On an important note, knockdown of p62 did not affect adipocyte development and differentiation (Figure 5E).

To validate the results obtained in both the adipocyte-specific *p62*$^{-/-}$ mice and the HIB1B cells, we assessed the expression profile of the thermogenic genes in BAT primary cells obtained from WT or global *p62*$^{-/-}$ mice over the time course of adipocyte differentiation (Supplemental Figure 6). In line with our previous findings, expression of *Ucp1*, *Ppargc1a*, and *Cox2* was decreased in the p62-deficient cells from day 4 with no notable difference compared with WT controls within the first 3 days of differentiation. Cytochrome *c* expression was decreased from day 3 onwards without any difference between genotypes within the first 2 days of differentiation. No difference at any time point was observed for *Atp5b* and *Cox4* (Supplemental Figure 6, A–F).

Consistent with our findings in HIB1B cells, we likewise did not observe a difference in adipocyte development and differentiation between genotypes in the BAT primary cells (Figure 6A). Aligned with our in vivo data, phosphorylated levels of both p38 and its

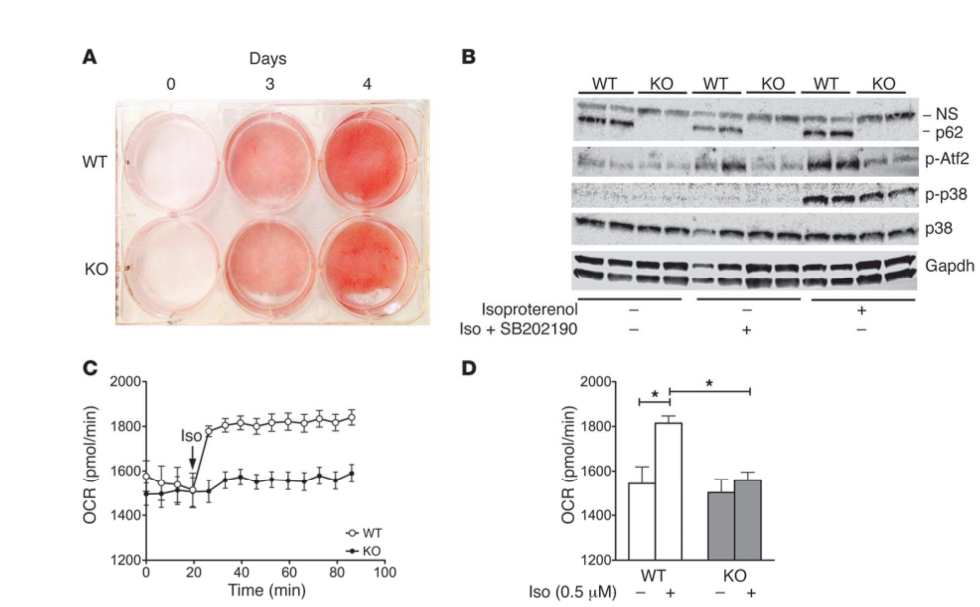

Figure 6
Cell autonomous effect of p62 on mitochondrial function in BAT primary cells. Oil red O staining in p62-deficient BAT primary cells obtained from global *p62*$^{-/-}$ and WT control mice (**A**). Western blot analysis of p62, p38, and phosphorylated levels of p38 and Atf2 in 5-day–differentiated BAT primary cells treated for 30 minutes with isoproterenol (0.5 μM) or pretreated for 30 minutes with the p38 inhibitor SB202190 (10 μM) followed by 30 minutes treatment of isoproterenol (0.5 μM) plus SB202190 (10 μM) (**B**). Measurement of OCR of 2-day–differentiated BAT primary cells obtained from global *p62*$^{-/-}$ mice and WT controls in response to isoproterenol (0.5 μM) (**C** and **D**). *$P < 0.05$.

direct downstream target Atf2 were decreased in p62-deficient cells upon stimulation with isoproterenol (Figure 6B). These observations support our hypothesis that p62 affects thermogenesis through the p38 MAPK pathway.

To functionally validate the results obtained in the HIB1B cells, we measured oxygen consumption in the BAT primary cells, both before and after stimulation with isoproterenol (0.5 μM). Baseline levels of oxygen consumption were comparable between controls and cells lacking p62 (Figure 6, C and D). In primary cells obtained from WT animals, we observed the expected immediate increase in oxygen consumption in response to isoproterenol. However, this effect was completely abrogated in cells lacking p62 (Figure 6, C and D). Based on recent evidence indicating that catecholamines released from macrophages can substantially modulate BAT thermogenesis (28), we next assessed whether the observed changes in mitochondrial function persist after depletion of macrophages from BAT primary cells. We observed a similar lower response to isoproterenol in macrophage-depleted, p62-deficient BAT primary cells (Supplemental Figure 7, B and C). Furthermore, mRNA levels of *Ucp1* and *Ppargc1a* remained decreased in the macrophage-depleted p62-deficient cells both before and after stimulation with isoproterenol (Supplemental Figure 7, D and E). The decreased *Ucp1* mRNA expression translated into decreased protein levels of Ucp1 (Supplemental Figure 7F). Notably, no signs of macrophage infiltration were observed after depletion of Itgam-positive cells (Itgam is also known as Cd11b) (Supplemental Figure 7G), which was confirmed by flow cytometry (Supplemental Figure 7A). No differences regarding markers indicative of inflammation, DNA damage, redox balance, or ER stress were observed between genotypes (Supplemental Figure 7, G–K). Together, these data confirm that p62 directly controls basal mitochondrial function of brown adipocytes as well as their responsiveness to β-adrenergic stimulation in a cell autonomous manner, independently of macrophage infiltration and inflammation.

Discussion

Here we show for what we believe is the first time that the lack of p62 exclusively in adipose tissue is sufficient to recapitulate the metabolic syndrome phenotype of total p62-deficient mice, including obesity, glucose intolerance, and insulin resistance. Our results further identify BAT as the main organ responsible for the impaired energy metabolism observed in the adipose-specific *p62*$^{-/-}$ mice and reveal that p62 controls the mitochondrial function of brown adipocytes in a direct and cell-autonomous manner. The direct effect of p62 deficiency in brown fat thermogenesis includes impaired mitochondrial structure and dysfunction. Interestingly, we observe here that p62 controls activation of p38 in vivo. Several studies have previously shown that p38 MAPK is crucial for sympathetic nervous system–mediated (SNS-mediated) activation of BAT nonshivering thermogenesis and Ucp1 function (7, 29–31). Notably, by screening a HeLa cDNA library, Sudo and colleagues previously identified p62 as a p38-binding protein (32). Following up on that finding, Kawai and colleagues identified 2 p62 binding domains in p38. One domain is located

in the N-terminal p38 interaction (NPI) domain, whereas the other is located in the C-terminal p38 interaction (CPI) domain (33). Consistent with our finding that activated levels of p38 are decreased in p62-deficient cells upon stimulation with isoproterenol, Kawai and colleagues found that genetic inactivation of p62 in HeLa cells led to impaired p38 activation upon stimulation with cytokines (33). Using surface plasmon resonance (SPR) imaging experiments, Saito and colleagues showed that the p62 domain comprising amino acids 164–190 can directly bind to p38 (34). However, whereas several lines of evidence support the interaction of p62 and p38 in vitro, using genetically engineered mice, we here show that this interaction appears to be of physiological relevance in vivo. Accordingly, loss of p62 in adipocytes impairs physiological activation of p38 and its downstream pathways, promoting uncoupling in vivo and in vitro. Such programs governing uncoupling have been either directly or indirectly linked to p38 activity and include *Atf2*, *Creb*, *Ppargc1a*, *Dio2*, *Nrf1*, *Cox2*, *CytC*, *Atp5b*, and *Ucp1*. All of these signals were significantly decreased in adipocyte-specific *p62*$^{-/-}$ mice, suggesting that p62 likely controls mitochondrial function via the p38/Ppargc1a pathway. Notably, this assumption is consistent with reports indicating that p62 binds p38 via its C-terminal domain and that p62 is colocalized with phosphorylated p38 in the nuclei (32–34).

In line with the discovery that p62 controls mitochondrial function of BAT, we found oxidative capacity, measured by Cox activity, to be decreased in BAT of adipocyte-specific *p62*$^{-/-}$ mice. Of appreciable note, no difference in Cox activity was observed in BAT of mice that specifically lack p62 only in skeletal muscle (Supplemental Figure 3F) or the myeloid lineage (Supplemental Figure 4F).

The observation that lipid metabolism is not changed in the adipocyte-specific *p62*$^{-/-}$ mice despite the altered morphology of their adipocytes is intriguing and warrants further investigation. As a matter of fact, previously published data showed that global loss of p62 results in increased adipogenesis in vitro and enhanced expression of adipogenic markers such as Pparg in vivo (19). However, using aP2-conditional KO mice, we have been unable to detect these alterations in WAT but rather changes in BAT. A potential explanation for this discrepancy might be that the loss of p62 in a total KO impairs WAT characteristics early during fat development, revealing the role of p62 in WAT. In the conditional model reported here, p62 is depleted at the time point when aP2 is expressed later during the adipocyte development process. WAT differentiation appears to stay intact, but a clear role for p62 governing BAT function is revealed. We conclude that the alterations in BAT may have secondary consequences on WAT in vivo but do not directly affect Pparg-driven differentiation processes.

The maintenance of mitochondrial integrity is central to numerous cellular processes, especially for those regulating the SNS-mediated activation of brown fat thermogenesis. A number of recent studies using cotransfection and shRNA-mediated knockdown of p62 have suggested that it plays an important role in the disposal of dysfunctional mitochondria by autophagy, also known as mitophagy, which is in accordance with p62's role in the autophagic clearance of polyubiquitinated proteins (35–40). However, the analysis of p62-knockout cells does not support this notion, making this mitophagy function of p62 highly controversial at this moment (40–43). It could be argued that our observation that the mitochondrial structure and function is impaired in the adipocyte-specific *p62*$^{-/-}$ mice is in line with the reports showing that p62 might be implicated in the regulation of mitophagy. However, our observation that loss of p62 affects the genetic program responsible for mitochondrial biogenesis does not support this model. Together, these data strongly suggest that, although decreased mitophagy cannot be completely ruled out, this would not have a great impact on the p62-deficiency phenotype reported here. We favor the notion that p62 is critical in the regulation of transcriptional programs controlling mitochondrial homeostasis, which underlies the phenotype of adipose-specific p62-KO mice.

Collectively, our findings indicate that the adipose-selective inactivation of p62 unveils a new and unexpected function of this important adapter in the direct control of BAT mitochondrial biogenesis and function.

Methods

Animal studies. For analysis of body weight, body composition, and food intake, mice were kept at an ambient temperature of 23 ± 2°C with constant humidity and a 12-hour light/12-hour dark cycle. Mice had free access to water and were fed ad libitum with either a regular standard chow diet (5.6% fat; LM-485, Teklad) or a HFD (58% kcal fat; Research Diets Inc.). Measurements of energy expenditure were performed using a customized indirect calorimetric system (TSE Systems Gmbh.). After adaptation for 24 hours, recordings were collected over the following 118 hours.

Gene expression analysis. Gene expression of tissue samples (n = 7–9 mice per group) was profiled with quantitative PCR–based (qPCR-based) techniques using SYBR green, TaqMan Single Probes, or TaqMan Low Density Arrays (Applied Biosystems). TaqMan Low Density Arrays were performed in n = 4 mice of each genotype. The relative expression of the selected genes was measured using the 7900HT Fast Real-Time PCR System (Applied Biosystems). For low-density arrays, the PCR reactions took place on a 384 well reaction card preloaded with the specific primers and probes by the manufacturer. The sequences of primers and probes were designed and validated by Applied Biosystems and were taken from the Assay-on-Demand mouse library. The relative expression levels of each gene were normalized to the housekeeping gene 18S, HPRT, or RPL32.

Western blotting. Cell extracts for Western blotting were prepared in radioimmunoprecipitation assay buffer (1× PBS, 1% Nonidet P-40, 0.5% sodium deoxycholate, 0.1% sodium dodecyl sulphate, 1 mM phenylmethylsulfonyl fluoride, and protease inhibitors). Lysates were separated by SDS–polyacrylamide gel electrophoresis and transferred to Nitrocellulose-ECL membranes (GE Healthcare), where the immune complex was detected by chemiluminescence (GE Healthcare). Antibodies were purchased from Santa Cruz Biotechnology Inc. (Gapdh, CytC, p38, p-p38, Ppargc1a), Abcam plc (Ucp1), Progen Biotechnik (p62), and Cell Signaling Technology Inc. (Creb, P-Creb, Mapk1, P-Mapk1, Lipe, P-Lipe, P-Atf2).

Cell culturing and analysis of BAT primary cells and HIB1B cells. Culturing of adipocytes was performed according to a protocol provided by C. Ronald Kahn (Joslin Diabetes Center). For isolation of BAT primary cells, the interscapular BAT of 1-day-old global *p62*$^{-/-}$ and WT mice was dissected and digested for 20 minutes in isolation buffer containing 61.5 mM NaCl, 2.5 mM KCL, 0.65 mM $CaCl_2$, 2.5 mM glucose, 50 mM HEPES, 2% BSA Fraction V, and 1.5 mg/ml collagenase A (Roche Diagnostics Gmbh). Cells were cultured for 2 days in DMEM High-Glucose (Fisher Thermo Scientific) containing 20% FBS and 1% penicillin/streptomycin. After reaching confluency, differentiation was induced by switching to DMEM High-Glucose containing 10% FBS, 20 nM insulin, 1 nM T3, 0.125 mM indomethacin, 0.5 mM IBMX, and 5.1 μM dexamethasone. Two days after start of differentiation, medium was switched to DMEM High-Glucose containing 10% FBS, 20 nM insulin, and 1 nM T3 until start of the experiments. The HIB1B cells were provided from Bruce Spiegelman (Department of Cancer Biology, Dana-Farber Cancer Institute and Department of Cell Biology, Harvard Medical School).

Depletion of macrophages from BAT primary cells. Separation of macrophages from BAT primary cells was performed by magnetic immunoaffinity isolation using anti-Cd11b antibodies conjugated to magnetic beads (MACS Cell Separation System; Miltenyi Biotec). Following BAT digestion, Itgam-positive (Cd11b) cells were separated using positive selection columns (LD columns; Miltenyi Biotec) according to the manufacturer's instructions. For validity of cell separation, cell eluates were taken before and after depletion of Cd11b-positive cells as well as from the retained cell fraction. Successful depletion of macrophages was confirmed by flow cytometry and qPCR analysis.

Flow cytometry to determine macrophage frequencies in BAT primary cells. Dissociated BAT primary cells were suspended in PBS/10% FCS and preincubated with 5 μg/ml anti-Cd16/32 (FcγRII/III block, clone 2.4G2; BD Biosciences). Cells were then stained with FITC-conjugated anti-CD45 (clone 30-F11; eBioscience) and APC-conjugated anti-F4/80 (clone BM8; eBioscience) on ice for 20 minutes. Propidium iodide (1 μg/ml) was used to exclude dead cells. Flow cytometry was performed on a FACS Aria III (BD Biosciences), and results were analyzed using FACS Diva software (BD Biosciences).

Bioenergetics of BAT primary cells. Primary cells of litters were pooled and independently differentiated and measured. Measurement of oxygen consumption rate (OCR) was performed using an extracellular flux analyzer (XF24, Seahorse Bioscience; Billerica). After differentiation for 2 days on a XF24 well plate, cells were washed in 1× PBS and incubated in 675 μl of DMEM (no. 5030; Sigma-Aldrich) in a non-CO_2 incubator for 1 hour. Untreated oxygen consumption was recorded for 20 minutes followed by isoproterenol injection (0.5 μM) and subsequent OCR measurement. OCR measurement in macrophage-depleted primary cells was performed after differentiating for 7 days. Untreated oxygen consumption was recorded for 20 minutes followed by measurement of OCR after injection of isoproterenol (0.5 μM, 35 minutes), oligomycin (2 μg/ml, 21 minutes), FCCP (1 μM, 21 minutes), and rotenon/antimycin A (2.5 μM each, 14 minutes).

Cox activity. Cox activity of interscapular BAT was assessed polarographically using a Clark type electrode (RANK Brothers) and a Powerlab for data processing (ADInstruments). Tissue was weighted and homogenized mechanically in tissue buffer (100 mM potassium phosphate, 2 mM EDTA, 10 mM glutathione, pH 7.2, at 37°C) using QIAGEN TissueLyser. Homogenates were treated with detergent (0.1% *n*-dodecyl-β-D-maltoside) and subjected to a temperature-controlled reaction chamber containing 130 μM cytochrome *c* from horse heart (Sigma-Aldrich) and 18 mM ascorbate in measuring buffer (100 mM potassium phosphate, 5 mM EDTA, pH 7.2, at 37°C).

Measurement of p38α. Protein levels of total and phosphorylated p38α were assessed from BAT tissue using an InstantOne ELISA (eBioscience Inc.). BAT samples were disrupted using a TissueLyser (Qiagen) and lysed and analyzed according to the manufacturer's instructions.

Transmission electron microscopy. Tissue samples were fixed in 2.5% electron microscopy grade glutaraldehyde in 0.1 M sodium cacodylate buffer, pH 7.4 (Science Services), postfixed in 2% aqueous osmium tetraoxide, dehydrated in gradual ethanol (30%–100%) and propylene oxide, embedded in Epon (Merck), and cured for 24 hours at 60°C. Semithin sections were cut and stained with toluidine blue. Ultrathin sections of 50 nm were collected onto 200 mesh copper grids and stained with uranyl acetate and lead citrate before examination by transmission electron microscopy (Zeiss Libra 120 Plus; Carl Zeiss NTS GmbH). Pictures were acquired using a Slow Scan CCD-camera and iTEM software (Olympus Soft Imaging Solutions).

Statistics. Statistical analyses were performed using the statistical tools implemented in Graph Pad Prism (GraphPad Software). Differences between treatment groups were assessed by 2-way ANOVA followed by Dunnett's or Bonferroni's post hoc test, 1-way ANOVA, or Student's 2-tailed *t* test. All results are given as mean ± SEM. $P < 0.05$ was considered statistically significant.

Study approval. All procedures were approved by the Institutional Animal Care and Use Committee of the University of Cincinnati and were performed in accordance with the NIH principles of laboratory animal care.

Acknowledgments

The authors would like to thank Bruce Spiegelman and C. Ronald Kahn for their kind support and for providing the BAT cell lines.

Received for publication April 9, 2012, and accepted in revised form November 1, 2012.

Address correspondence to: Matthias Tschöp, Institute for Diabetes and Obesity, Helmholtz Zentrum Muenchen and Department of Medicine, Technische Universität München, 85764 Munich, Germany. Phone: 49.89.3187.2103; Fax: 49.89.3187.2182; E-mail: tschoep@helmholtz-muenchen.de. Or to: Jorge Moscat, Sanford-Burnham Medical Research Institute, 10901 N. Torrey Pines Road, La Jolla, California 92037, USA. Phone: 858.795.5160; Fax: 858.795.5268; E-mail: jmoscat@sanfordburnham.org.

1. Cannon B, Nedergaard J. Brown adipose tissue: function and physiological significance. *Physiol Rev.* 2004;84(1):277–359.
2. Kajimura S, Seale P, Spiegelman BM. Transcriptional control of brown fat development. *Cell Metab.* 2010;11(4):257–262.
3. Cypess AM, et al. Identification and importance of brown adipose tissue in adult humans. *N Engl J Med.* 2009;360(15):1509–1517.
4. Nedergaard J, Bengtsson T, Cannon B. Unexpected evidence for active brown adipose tissue in adult humans. *Am J Physiol Endocrinol Metab.* 2007; 293(2):E444–E452.
5. van Marken Lichtenbelt WD, et al. Cold-activated brown adipose tissue in healthy men. *N Engl J Med.* 2009;360(15):1500–1508.
6. Virtanen KA, et al. Functional brown adipose tissue in healthy adults. *N Engl J Med.* 2009;360(15):1518–1525.
7. Cao W, et al. p38 mitogen-activated protein kinase is the central regulator of cyclic AMP-dependent transcription of the brown fat uncoupling protein 1 gene. *Mol Cell Biol.* 2004;24(7):3057–3067.
8. Kajimura S, et al. Initiation of myoblast to brown fat switch by a PRDM16-C/EBP-beta transcriptional complex. *Nature.* 2009;460(7259):1154–1158.
9. Tseng YH, et al. Prediction of preadipocyte differentiation by gene expression reveals role of insulin receptor substrates and necdin. *Nat Cell Biol.* 2005; 7(6):601–611.
10. Tseng YH, et al. New role of bone morphogenetic protein 7 in brown adipogenesis and energy expenditure. *Nature.* 2008;454(7207):1000–1004.
11. Tseng YH, Kriauciunas KM, Kokkotou E, Kahn CR. Differential roles of insulin receptor substrates in brown adipocyte differentiation. *Mol Cell Biol.* 2004; 24(5):1918–1929.
12. Lowell BB, Spiegelman BM. Towards a molecular understanding of adaptive thermogenesis. *Nature.* 2000;404(6778):652–660.
13. Puls A, Schmidt S, Grawe F, Stabel S. Interaction of protein kinase C zeta with ZIP, a novel protein kinase C-binding protein. *Proc Natl Acad Sci U S A.* 1997;94(12):6191–6196.
14. Sanchez P, De Carcer G, Sandoval IV, Moscat J, Diaz-Meco MT. Localization of atypical protein kinase C isoforms into lysosome-targeted endosomes through interaction with p62. *Mol Cell Biol.* 1998;18(5):3069–3080.
15. Moscat J, Diaz-Meco MT. To aggregate or not to aggregate? A new role for p62. *EMBO Rep.* 2009; 10(8):804.
16. Moscat J, Diaz-Meco MT. p62 at the crossroads of autophagy, apoptosis, and cancer. *Cell.* 2009; 137(6):1001–1004.
17. Moscat J, Diaz-Meco MT. Feedback on fat: p62-mTORC1-autophagy connections. *Cell.* 2011; 147(4):724–727.
18. Lee SJ, et al. A functional role for the p62-ERK1 axis in the control of energy homeostasis and adipogenesis. *EMBO Rep.* 2010;11(3):226–232.
19. Rodriguez A, et al. Mature-onset obesity and insulin resistance in mice deficient in the signaling adapter p62. *Cell Metab.* 2006;3(3):211–222.
20. Tronche F, et al. Disruption of the glucocorticoid receptor gene in the nervous system results in reduced anxiety. *Nat Genet.* 1999;23(1):99–103.
21. Postic C, et al. Dual roles for glucokinase in glucose homeostasis as determined by liver and pancreatic beta cell-specific gene knock-outs using Cre recombinase. *J Biol Chem.* 1999;274(1):305–315.
22. Bothe GW, Haspel JA, Smith CL, Wiener HH, Burden SJ. Selective expression of Cre recombinase in skeletal muscle fibers. *Genesis.* 2000;26(2):165–166.
23. He W, et al. Adipose-specific peroxisome proliferator-activated receptor gamma knockout causes insulin resistance in fat and liver but not in muscle. *Proc Natl Acad Sci U S A.* 2003;100(26):15712–15717.
24. Erbay E, et al. Reducing endoplasmic reticulum stress

through a macrophage lipid chaperone alleviates atherosclerosis. *Nat Med*. 2009;15(12):1383–1391.
25. Farmer SR. Transcriptional control of adipocyte formation. *Cell Metab*. 2006;4(4):263–273.
26. Tschöp MH, et al. A guide to analysis of mouse energy metabolism. *Nat Methods*. 2011;9(1):57–63.
27. Seale P, et al. Prdm16 determines the thermogenic program of subcutaneous white adipose tissue in mice. *J Clin Invest*. 2011;121(1):96–105.
28. Nguyen KD, et al. Alternatively activated macrophages produce catecholamines to sustain adaptive thermogenesis. *Nature*. 2011;480(7375):104–108.
29. Bordicchia M, et al. Cardiac natriuretic peptides act via p38 MAPK to induce the brown fat thermogenic program in mouse and human adipocytes. *J Clin Invest*. 2012;122(3):1022–1036.
30. Cao W, et al. p38 Mitogen-activated protein kinase plays a stimulatory role in hepatic gluconeogenesis. *J Biol Chem*. 2005;280(52):42731–42737.
31. Cao W, Medvedev AV, Daniel KW, Collins S. beta-Adrenergic activation of p38 MAP kinase in adipocytes: cAMP induction of the uncoupling protein 1 (UCP1) gene requires p38 MAP kinase. *J Biol Chem*. 2001;276(29):27077–27082.
32. Sudo T, Maruyama M, Osada H. p62 functions as a p38 MAP kinase regulator. *Biochem Biophys Res Commun*. 2000;269(2):521–525.
33. Kawai K, Saito A, Sudo T, Osada H. Specific regulation of cytokine-dependent p38 MAP kinase activation by p62/SQSTM1. *J Biochem*. 2008; 143(6):765–772.
34. Saito A, Kawai K, Takayama H, Sudo T, Osada H. Improvement of photoaffinity SPR imaging platform and determination of the binding site of p62/SQSTM1 to p38 MAP kinase. *Chem Asian J*. 2008; 3(8–9):1607–1612.
35. Tatsuta T, Langer T. Quality control of mitochondria: protection against neurodegeneration and ageing. *EMBO J*. 2008;27(2):306–314.
36. Bulteau AL, Szweda LI, Friguet B. Mitochondrial protein oxidation and degradation in response to oxidative stress and aging. *Exp Gerontol*. 2006; 41(7):653–657.
37. Tolkovsky AM. Mitophagy. *Biochim Biophys Acta*. 2009;1793(9):1508–1515.
38. Huang C, Andres AM, Ratliff EP, Hernandez G, Lee P, Gottlieb RA. Preconditioning involves selective mitophagy mediated by Parkin and p62/SQSTM1. *PLoS One*. 2011;6(6):e20975.
39. Bjorkoy G, et al. p62/SQSTM1 forms protein aggregates degraded by autophagy and has a protective effect on huntingtin-induced cell death. *J Cell Biol*. 2005;171(4):603–614.
40. Ding WX, et al. Nix is critical to two distinct phases of mitophagy, reactive oxygen species-mediated autophagy induction and Parkin-ubiquitin-p62-mediated mitochondrial priming. *J Biol Chem*. 2010;285(36):27879–27890.
41. Geisler S, et al. PINK1/Parkin-mediated mitophagy is dependent on VDAC1 and p62/SQSTM1. *Nat Cell Biol*. 2010;12(2):119–131.
42. Narendra D, Kane LA, Hauser DN, Fearnley IM, Youle RJ. p62/SQSTM1 is required for Parkin-induced mitochondrial clustering but not mitophagy; VDAC1 is dispensable for both. *Autophagy*. 2010;6(8):1090–1106.
43. Okatsu K, et al. p62/SQSTM1 cooperates with Parkin for perinuclear clustering of depolarized mitochondria. *Genes Cells*. 2010;15(8):887–900.

5P10, doi:10.1016/j.bbabio.2012.06.125, presented as Poster

MOLECULAR CHARACTERIZATION OF BROWN ADIPOSE TISSUE IN A 'PROTO-ENDOTHERMIC' MAMMAL PROVIDES A NOVEL APPROACH TO THE UNDERSTANDING OF UNCOUPLING PROTEIN EVOLUTION

Rebecca Oelkrug[1], Nadja Goetze[1], Cornelia Exner[1], Goutham Ganjam[1], Saskia Müller[2], Maria Kutschke[2], Matthias Tschöp[2], Gerhard Heldmaier[1], Martin Jastroch[2] and Carola W. Meyer[1,2]

[1] Department of Animal Physiology, Faculty of Biology, Philipps-Universität, Karl-von-Frisch Strasse 8, 35043 Marburg, Germany
[2] Institute for Diabetes and Obesity, Helmholtz Zentrum Munich, German Research Center for Environmental Health (GmbH), Munich, Germany

The molecular events that facilitated the evolutionary transition from ecto- to endothermia in vertebrates are still unknown. The 'ancient' Lesser hedgehog tenrec, *Echinops telfairi* is considered a 'protoendothermic' mammal as it shows fluctuating, ectothermic-like body temperature patterns. Interestingly, females maintain constantly high body temperatures (~33°C) during pregnancy and periods of parental care, demonstrating regulatory heat production. Thus, understanding the thermophysiology of this 'protoendotherm' may help to elucidate ancient patterns that led to 'modern' (sustained) endothermy. We searched for, and characterized the molecular basis of NST in warm (27°C) and cold (20°C) acclimated *E. telfairi in vivo* and *in vitro*. Administration of a selective ß3-AR antagonist (SR59230A) suppressed rewarming rates from torpor after cold acclimation, indicating involvement of adrenergically mediated nonshivering thermogenesis (NST). Next, morphological analysis revealed a BAT-like depot in proximity to the gonads. The proton leak of isolated BAT mitochondria could be inhibited by GDP, suggesting UCP1-dependent proton conductance and, hence, the presence of functional BAT, which appeared recruitable by cold acclimation. Molecular analysis confirmed the tissue specific expression of UCP1 in tenrecs (etUCP1). We cloned and stably transfected etUCP1 in HEK293 cells. Isolated mitochondria of etUCP1 HEK293 cells showed inducible proton conductance using palmitate, and GDP-sensitivity, similar to mitochondria containing mouse UCP1. For the search of functional differences, we established bioenergetic measurements in intact HEK293 cells using plate-based respirometry, allowing high-throughput approaches for small molecule modulators. In the initial experiments, we show that the UCP1 activator TTNPB, a retinoic acid analog, is plasma membrane diffusible and allows direct specific activation of tenrec and mouse UCP1.Taken together, we show that *E. telfairi* possesses functional, UCP1-dependent brown adipose tissue, which may facilitate active rewarming from hypothermic states and support high body temperature for parental care. Substantial evolutionary distance between tenrecs and modern mammals provides a new window to study the evolution of structure-function relationships of UCP1.

Molecular characterization of nonshivering thermogenesis in a 'protoendothermic' mammal, the Lesser hedgehog tenrec (*Echinops telfairi*)

Rebecca Oelkrug[1], Nadja Goetze, Cornelia Exner, Goutham Ganjam, Saskia Müller, Maria Kutschke, Matthias Tschöp, Gerhard Heldmaier, Martin Jastroch and Carola W. Meyer

(1) Department of Animal Physiology, Faculty of Biology, Philipps-Universität, Karl-von-Frisch Strasse 8, 35043 Marburg, Germany

The molecular events that facilitated the evolutionary transition from ecto- to endothermia in vertebrates are still unknown. The Lesser hedgehog tenrec, *Echinops telfairi* is considered a 'protoendothermic' mammal because of its ectothermic-like body temperature patterns. Interestingly, females maintain constantly high body temperatures (~33°C) during pregnancy and periods of parental care, demonstrating regulatory heat production. Thus, understanding the thermophysiology of this 'protoendotherm' may help to elucidate ancient patterns that led the way to 'modern'(sustained) endothermy.
We studied warm (27°C) and cold (20°C) acclimated *E. telfairi in vivo* and observed pronounced daily cycles of hypothermia and hypometabolism, confirming that animals were torpid for most of the day. In cold acclimated tenrecs SR59230A, a selective ß3-AR antagonist suppressed rewarming rates from torpor by 50%, indicating involvement of adrenergically mediated nonshivering thermogenesis (NST). A large, brown adipose tissue (BAT)-like depot was found in proximity to the gonads, and molecular analysis confirmed the expression of UCP1. The proton leak of isolated BAT mitochondria could be inhibited >50% by GDP, suggesting UCP1-dependent proton conductance and, hence, the presence of functional BAT. The cold induced recruitment of BAT thermogenesis was associated with higher UCP1 expression and increased oxidative capacity by mitochondrial remodelling. Mitochondria of HEK293 cells transfected with tenrec (etUCP1) cDNA constructs showed a similar regulation of uncoupling activity as HEK293-mitochondria containing mouse UCP1, despite substantial evolutionary distance between these two species.
In summary the NST of *E. telfairi* is UCP1-dependent, recruitable with cold acclimation, and significantly contributes to rewarming from torpor at cold ambient temperatures (50% of peak rewarming). However, sustained endothermia during reproduction and the atypical location of the major BAT depot in the abdominal region also suggests that BAT thermogenesis is relevant for reproductive success in this heterothermic species. Thus, our findings indirectly support the parental care model in the evolution of endothermy.

Molecular characterization of nonshivering thermogenesis in a 'protoendothermic' mammal, the Lesser-hedgehog tenrec (*Echinops telfairi*)

Rebecca Oelkrug[1], Nadja Goetze[1], Gerhard Heldmaier[1], Martin Jastroch[2] and Carola W. Meyer[1,2]

[1] *Department of Animal Physiology, Faculty of Biology, Philipps-Universität, Karl-von-Frisch Strasse 8, 35043 Marburg, Germany*
[2] *Institute for Diabetes and Obesity, Helmholtz Zentrum Munich, German Research Center for Environmental Health (GmbH), Munich, Germany*

The molecular events and mechanisms that facilitated the evolutionary transition from ecto- to endothermia in vertebrates are still unknown but must have involved the development of endogenous heat production. The Lesser-hedgehog tenrec, *Echinops telfairi*, is considered 'protoendothermic' as a result of ectothermic-like body temperature patterns. We studied metabolic responses of *E. telfairi in vivo* and observed daily cycles of hypothermia ranging from 21° to 33°C body temperature (Ta: 20°C). Rewarming rates from torpor were independent of ß3-adrenergic stimulation (judged with inhibitor SR59230A), emphasizing that classical adaptation of thermogenesis as found in brown adipose tissue (BAT) of rodents was absent. However, we found brown adipose-like tissue predominantly located in the abdominal cavity. Molecular analysis confirmed the expression of UCP1 mRNA and protein. The proton leak of isolated mitochondria could be inhibited more than 50% by GDP, suggesting UCP1-dependent proton conductance. Taken together, BAT in *E. telfairi* appears to be consistent with the thermogenic function as found in rodents, but does not display the typical thermogenic adaptation. We are currently comparing UCP1 specific activity of *E. telfairi* with mouse (*Mus musculus*) in HEK293 cells to explore whether differences in physiological heat production are reflected on the molecular evolution of UCP1.

Deutsche Zoologische Gesellschaft
102. Jahrestagung

Induced torpor in UCP1-KO mice

Rebecca Oelkrug, Rosalie Morisset, Sebastian Busse, Gerhard Heldmaier, Carola W. Meyer

Department of Animal Physiology, Faculty of Biology, Philipps-Universität, Karl-von-Frisch Strasse 8, 35043 Marburg, Germany

Endotherms exposed to cold ambient temperatures display two fundamentally different forms of endogenous heat production: shivering and non shivering thermogenesis (NST). A large proportion of NST is generated in the mitochondria of the brown adipose tissue (BAT) where UCP1 (uncoupling protein 1) dissipates mitochondrial proton motive force as heat. In small mammals this avenue of heat production is further assumed to support arousal during torpid or hibernating states.
In order to assess the significance of functional BAT for mammalian torpor we investigated mice with a targeted ablation of the UCP1 gene (genetic background C57BL/6). A combination of cold exposure (18°C) and removal of food was used to induce torpor in wild-type (WT; n=7) and UCP1-KO mice (n=5). Upon energetic challenge, all individuals entered long deep torpor bouts lasting more than 11 hours. There was no difference in torpor depth (min. T_b 19-20°C) or minimal metabolic rate during torpor (6-7 mlO_2/h) between genotypes. A vibrational stimulus to the cage induced alarm arousal to normothermia in all mice. The rewarming rates of UCP1 KO mice, however were 50% lower (0.083°C/min) than those recorded in WT mice (0.165°C/min).
Our results indicate that loss of functional BAT in mice reduces thermogenic capacity but does not impair the use of torpor with respect to the entry and depth. Thus, torpor behavior and arousal from torpor in daily heterotherms is not intimately connected with the expression of UCP1.

ZUSAMMENFASSUNG

Säugetiere und Vögel sind in der Lage eine konstant hohe Körpertemperatur (~35-42°C) unabhängig von der sie umgebenden Außentemperatur zu regulieren und aufrecht zu erhalten, sie sind endotherm (Heldmaier et al. 1990). Das Prärogativ der Endothermie ermöglichte es ihnen, während ihrer Radiation weite Teile der Welt zu kolonisieren und sich auch dort anzusiedeln, wo landlebende ektotherme Wirbeltiere keine Überlebenschance haben.

Endotherme Säugetiere verteidigen ihre Körpertemperatur durch zwei Mechanismen der körpereigenen (endogenen) Wärmebildung, zum einen durch das Muskelzittern und zum anderen durch die zitterfreie Wärmebildung. Beim Muskelzittern reagiert das zervikale Rückenmark auf einen Kältestimulus und vermittelt die Aktivierung von antagonistisch arbeitenden Muskelgruppen. Es kommt zu einer Leerlaufkontraktion und chemische Energie, in Form von ATP, wird in Wärme anstatt mechanischer Arbeit umgesetzt (IUPS-Thermal-Commission 2003). Das Kältezittern findet hauptsächlich in der Peripherie des Körpers statt, es verhindert eine zielgerichtete Lokomotion und zerstört die isolierende Luftschicht im Fell, was den Wärmeverlust über die Körperoberfläche erhöht (Hart 1952, Heldmaier et al. 1989). Letzteres ist vor allem für kleine Säugetiere, aufgrund ihres unvorteilhaften Oberflächen-Volumenverhältnisses, energetisch nachteilhaft. Die zitterfreie Wärmebildung wird dagegen als effizienterer Weg zur endogenen Wärmebildung beschrieben, da sie den Wärmeverlust über die Körperoberfläche nicht beeinflusst (Cannon und Nedergaard 2004). Sie wird maßgeblich von kleinen Säugetieren, vor allem von Winterschläfern und Neugeborenen, zur Aufrechterhaltung einer konstanten Körpertemperatur genutzt (Cannon 1980, Himms-Hagen 1984).

Der Ort der zitterfreien Wärmebildung ist das braune Fettgewebe (Nicholls und Locke 1984), das primär im dorso-zervikalen Bereich exprimiert und deshalb häufig als Heizjacke bezeichnet wird (Heldmaier et al. 2012). Das braune Fettgewebe unterscheidet sich vom weißen Fettgewebe durch eine verstärkte Vaskularisierung, multilokuläre Fetttröpfchen und die einzigartige Expression des Entkopplerproteins 1 (*uncoupling protein 1*, UCP1). Es besitzt nur geringe Mengen an ATP-Synthase, um Ernährungsäquivalente in zelluläre Energieäquivalente umzuwandeln (Cannon and Vogel 1977). Zitterfreie Thermogenese wird durch die Ausschüttung von Noradrenalin aus postganglionären Nervenenden des sympathischen Nervensystems aktiviert (Fig. 1 Introduction). Noradrenalin bindet an spezifische β3-adrenerge Rezeptoren auf der Oberfläche der braunen Adipozyten, woraufhin ein G-Protein gekoppelter Signalweg aktiviert wird, an dessen Ende Triglyzeride zu Fettsäuren abgebaut werden. Diese freigesetzten Fettsäuren dienen als Substrat für die in den Mitochondrien ablaufende β-Oxidation und als Aktivatoren von UCP1. UCP1 wird in der inneren Mitochondrien-membran von braunen Adipocyten exprimiert und entkoppelt dort die oxidative Phosphorylierung von der ATP-Synthese durch die Erschaffung eines Protonenlecks, daraufhin wird Wärme anstelle von ATP gebildet. Die von UCP1 vermittelte Wärmebildung ist ausschlaggebend für die Funktion des braunen Fettgewebes.

Die kritische Rolle von UCP1 für die vom braunen Fett vermittelte zitterfreie Wärmebildung wurde in Studien an BL6-Mäusen, in denen durch homologe Rekombination das UCP1 Gen ausgeknockt wurde, nachgewiesen (Enerback et al. 1997, Golozobouva et al. 2001). UCP1 defiziente Mäuse können kein funktionales UCP1-Protein exprimieren und sind deshalb nicht in der Lage, ihre Körpertemperatur bei akuter Kälteexposition (4°C) langfristig zu verteidigen. Dennoch können auch UCP1-KO Mäuse in Kälte zu überleben, wenn sie zuvor an moderate Kälte (18°C) akklimatisiert wurden (Golozoubova et al. 2006). Dies weist daraufhin, dass längerfristig andere physiologische Mechanismen den Ausfall von UCP1 kompensieren können. Einige Studien deuten auf einen beschleunigten metabolischen Umsatz im weißen Fettgewebe oder zusätzliche Calciumzyklen in der Skelettmuskulatur hin (Grannemann 2003, Meyer et al. 2010, Ukropec et al. 2006, Shabalina et al. 2010). Diese alternativen thermogenetischen Mechanismen scheinen weniger effizient und nachteilig zu sein, denn die mittlere Überlebensrate von UCP1 defizienten Mäusen ist im Vergleich zu Wildtypmäusen erheblich reduziert (Golozobouva et al. 2001).

Langanhaltende Kälteexposition stimuliert die Proliferation des braunen Fettgewebes und verbessert seine Thermogeneseleistung durch eine erhöhte UCP1 Expression und die Rekrutierung seiner oxidativen Kapazität (Klingenspor 2003, Fig. 2 Introduction); ein Prozess, der als adaptive Thermogenese bezeichnet wird (Lowell and Spiegelman 2000). Die adaptive Thermogenese ermöglicht es Säugetieren, ihre Thermogenesekapazität individuell an die vorherrschenden saisonalen Bedingungen anpassen. Dies ist ein Hauptcharakteristikum der thermoregulatorischen Aufgaben des braunen Fettgewebes in eutherischen Säugetieren.

Zitterfreie Wärmebildung ist nicht nur wichtig für die Aufrechterhaltung einer konstanten Körpertemperatur bei Kälteexposition, sondern auch beim Erwachen (*arousal*) aus hypothermen und hypometabolen Phasen, wie dem Winterschlaf oder der Tagesschlaflethargie (Torpor, Fig. 3 Introduction, Cannon and Nedergaard 2004). Beides sind physiologische Verhalten, mit denen Säugetiere bis zu 98% ihres täglichen Energieverbrauchs einsparen können (Wang 1989, Ruf and Heldmaier 1992, Geiser 2004, Heldmaier et al. 2004). Die Tagesschlaflethargie ist definiert als ein spontanes Torporereignis, das innerhalb von 24 Stunden beendet ist. Beim Winterschlaf hingegen handelt es um die Aneinanderreihung mehrerer Torporereignisse, wobei ein einzelnes Torporereignis bis zu 30 Tage andauern kann (Bieber and Ruf 2009). Eine ganze Winterschlafperiode kann mehrere Monate betragen. Viele kleine Säugetiere nutzen Torpor oder den Winterschlaf als Antwort auf sinkende Umgebungstemperaturen oder eine temporäre Nahrungsknappheit im Winter. Besonders Vertreter der modernen Säugetierordnung Eutheria aus den nördlichen Breiten wurden eingehend auf ihre Kapazität zur zitterfreien Wärmebildung und ihr Winterschlafverhalten untersucht. Dies führte dazu, dass die Expression von braunem Fett und die Fähigkeit zur zitterfreien Wärmebildung als Prärogativ der eutherischen Säugetiere diskutiert wurden (Cannon und Nedergaard 2004). Es soll ihnen die Migration in kältere holarktische Regionen ermöglicht haben, einen experimentellen Nachweis für diese Hypothese gibt es bislang nicht. Torpor und Winterschlaf konnten jedoch mittlerweile auch bei phylogenetisch älteren Arten aus afrotropischen Regionen detektiert werden (Dausmann et al. 2004, Mzilikazi and Lovegrove 2004). Auch diese Arten nutzen Torpor und Winterschlaf als physiologische Anpassungen an saisonal bedingte Nahrungsknappheit oder sinkende Außentemperaturen im Winter.

Neuere Studien zeigen zudem, dass die Expression von UCP1 bis zum evolutionären Ursprung der Knochenfische zurückgeführt werden kann (Jastroch et al. 2005). Eine primär thermogenetische Funktion in ektothermen Fischen ist eher unwahrscheinlich. Demzufolge ist es möglich, dass UCP1 einen Funktionswandel im Laufe der Evolution vollzogen hat. Die nächsthöhere Säugetierunterklasse bei der UCP1 und braunes Fett detektiert wurde, sind die Beuteltiere (Jastroch et al. 2008), jedoch scheint ihrem braunen Fett das Hauptcharakteristikum der adaptiven Thermogenese zu fehlen (keine Kälteanpassung, Polymeropolous et al. 2012). In Afrotheriern, die zur Unterklasse der höheren Säugetiere zählen, wurde braunes Fett und UCP1 bei Östlichen Klippen-Elefantenspitzmäusen in einer Laborstudie detektiert (*Elephantulus myurus*, Mzilikazi et al. 2007), aber auch sie zeigten keine Form der adaptiven Thermogenese. Der Nachweis der adaptiven Thermogenese gelang erst bei einem anderen Vertreter der Afrotherier, den Hottentotten-Goldmullen (*Amblysomus hottentottus longiceps*, Scantleburry et al. 2008). Goldmulle leben unterirdisch in einem thermisch gepufferten Höhlensystem, exogene Wärmequellen (z.B. Sonnenbaden) fehlen und die Tiere sind vermutlich mehr auf endogene Wärmebildungsmechanismen angewiesen als ihre oberirdisch lebenden Vertreter. Adaptive Thermogenese in Goldmullen scheint somit nicht repräsentativ für die allgemeine thermoregulatorische Fähigkeit der gesamten Überordnung Afrotheria zu sein. Der evolutionäre Ursprung der UCP1 vermittelten Thermogenese konnte also bis jetzt noch nicht eindeutig geklärt werden.

Ziel dieser Doktorarbeit war es die Bedeutung des braunen Fettgewebes, über seine anerkannte Funktion hinaus, in Säugetieren zu charakterisieren. Besonders die Rolle von aktivem UCP1 während des Aufwachvorgangs auf dem Torpor und in der Prävention von reaktiven Sauerstoffradikalen während der zitterfreien Wärmebildung standen im Fokus dieser Arbeit. Um den evolutionären Ursprung von UCP1 und braunem Fett besser zu verstehen,

wurden Studien an zwei Vertretern der phylogenetisch ursprünglichen Überordnung Afrotheria durchgeführt. Anhand dieser Ergebnisse sollte ein neues Licht auf die Evolution des braunen Fettgewebes geworfen werden. War wirklich die Migration in kältere, holarktische Regionen der Hauptgrund seiner Entstehung? Die vorliegende Arbeit ist in vier Kapitel gegliedert, deren Inhalt im Folgenden zusammengefasst wird.

KAPITEL 1: TORPOR PATTERNS, AROUSAL RATES, AND TEMPORAL ORGANIZATION OF TORPOR ENTRY IN WILDTYPE AND UCP1-ABLATED MICE

R. OELKRUG ∞ G. HELDMAIER
C.W. MEYER

In eutherischen Säugetieren wird dem braunen Fettgewebe eine essentielle Rolle für das Erwärmen der Körpertemperatur aus dem Torpor und dem Winterschlaf zugesprochen. Interessanterweise treten Torpor und Winterschlaf auch bei älteren taxonomischen Gruppen auf, die kein klassisches braunes Fett besitzen und sich demzufolge nicht mittels UCP1 vermittelter Thermogenese aus dem Torpor erwärmen können, zum Beispiel bei Monotremen und Beuteltieren (Fig. 3D Introduction, Hayward and Lisson 1992, Jastroch et al 2008, Nicol et al. 2008). Welchen evolutionären Vorteil die Expression von braunem Fett und UCP1 für das Torporverhalten einer Spezies hat, konnte jedoch bislang nicht eindeutig geklärt werden (Lyman and O´Brian 1986, Stone and Purvis 1992). Diesen Sachverhalt näher zu beleuchten, war Ziel dieser Studie.

Dafür arbeitete ich mit Wildtyp- und UCP1-KO Mäusen desselben genetischen Hintergrunds (CL57/B6J, Enerback et al. 1997), wodurch ich den Effekt der UCP1-Expression auf das Torporverhalten und die Aufwach- und Aufheizraten aus dem Torpor innerhalb derselben Art untersuchen konnte. Mäuse zeigen im Gegensatz zu dsungarischen Zwerghamstern (*Phodopus sungorus*) oder Fettschwanzmakis (*Microcebus murinus*) keinen obligatorischen Torpor während der Wintermonate. Bei ihnen handelt es sich um eine fakultative, physiologische Antwort, die durch Futterentzug und Kälte im Labor induziert werden kann (Hudson and Scott 1979, Webb et al. 1982, Swoap et al. 2006, Dikic et al. 2008). Um Torpor auszulösen wurden die Versuchstiere bis zu 48 Stunden gefastet und zu vier unterschiedlichen Zeitpunkten (6:00, 12:00, 18:00, 24:00 Uhr) wurde ihnen ein Kältestimulus (30°C auf 18°C) zur Torporinduktion gegeben. Unerwarteter Weise traten beide Gruppen bereits 20 Minuten nach dem Umschalten der Außentemperatur in den Torpor ein, wobei der Grad der Hypothermie (19.5-26.7°C) und Hypometabolie (5-22 $ml O_2 * h^{-1}$) zwischen beiden Genotypen vergleichbar war. Auch die UCP1-KO Mäuse konnten aus dem Torpor aufwachen, jedoch zeigten sie, im Vergleich zu den Wildtypmäusen, um 50% reduzierte Erwärmungsraten. Infolgedessen dauerte das Aufwachen aus dem Torpor bei ihnen signifikant länger (39 min vs. 70 min) und kostete 60% mehr Energie. Dadurch belegten meine Daten eindeutig die Hypothese, dass schnelles Erwärmen aus dem Torpor weniger kostenaufwendig ist als langsames (Stone and Purvis 1992, Mc Kechnie and Wolf 2004). Sowohl die Wildtypmäuse als auch die UCP1-KO Mäusen zeigten kein direktes Torporereignis nach dem Absenken der Außentemperatur um 18:00 Uhr im Gegensatz zu den anderen drei Uhrzeiten. Dies deutet daraufhin, dass der circadiane Beginn der nächtlichen Aktivitätsperiode nicht überschrieben werden konnte und dass Torpor in Mäusen an einen ultradianen Rhythmus gebunden ist.

Diese Studie belegte eindeutig, dass die Expression von funktionalem braunem Fett ein schnelleres und energetisch günstigeres Aufwachen aus dem Torpor ermöglicht, dessen Eintritt aber nicht beeinflusst. Phylogenetisch ältere Arten, die kein funktionales braunes Fett exprimieren, greifen vermehrt auf exogene Wärmequellen (wie die Sonnenstrahlung) während des Aufwachvorganges zurück (Mzilikazi et al. 2002). Möglicherweise ist dies ein Kompensationsmechanismus, der es ihnen erlaubt, auch ohne braunes Fett schnell und mit reduzierten Kosten aus dem Torpor aufzuwachen. Schlussfolgernd war die Expression von aktivem braunem Fettgewebe vielleicht vorteilhaft für das Torporverhalten in nördlichen Breiten, aber nicht notwendige Voraussetzung.

KAPITEL 2: UNCOUPLING PROTEIN 1 DECREASES SUPEROXIDE PRODUCTION IN BROWN ADIPOSE TISSUE MITOCHONDRIA

R. OELKRUG ∞ M. KUTSCHKE
G. HELDMAIER ∞ C.W. MEYER
M. JASTROCH

Wie bereits erwähnt, katalysiert UCP1 die Freisetzung der im Protonengradienten gespeicherten Energie als Wärme. UCP1-defiziente Mäuse können zwar in Kälte überleben, haben jedoch eine deutlich erniedrigte Lebenserwartung im Vergleich zu Wildtypmäuse des gleichen genetischen Hintergrunds, was die Frage nach den Vorteilen der durch UCP1 vermittelten Thermogenese aufwirft. Nach der „free radical theory of aging" könnte ein Anstieg von schädlichen Sauerstoffradikalen (*reactive oxygen species*, ROS) potentiell die Lebensdauer eines Organismus einschränken (Harman 1956, 1972). Superoxide und reaktive Sauerstoffspezies entstehen primär durch abspringende Elektronen an den Atmungskomplexen der Mitochondrien, maßgeblich an Komplex I, III und der Glycerol-3-Phosphatdehydrogenase. Durch Kälte steigen die oxidative Kapazität und die Thermogeneseleistung des braunen Fettgewebes an, wodurch die Wahrscheinlichkeit einer oxidativen Schädigung innerhalb der Zelle zunehmen könnte. Durch die Generierung eines Protonenlecks könnte jedoch aktiviertes UCP1 den Protonengradienten so reduzieren, dass es zwar zu einem erhöhten Durchfluss von Elektronen über die Komplexe der Atmungskette kommt, aber zu keinem erhöhten Radikaldruck. Dieses sogenannte „milde Entkoppeln" wird zurzeit intensiv und kontrovers in der Literatur diskutiert. Einige Studien befürworten eine Funktion von UCPs bei der ROS Prävention (Echtay et al. 2002, Echtay et al. 2003), während andere Studien speziell eine Rolle von UCP1 im Schutz vor reaktiven Sauerstoffspezies ablehnen (Silva et al. 2005, Shabalina 2006).

Zur weiteren Evaluierung einer möglichen Funktion von UCP1 in der ROS Prävention wurden Mitochondrien aus dem braunen Fettgewebe von warm (30°C) und kalt (5°C) akklimatisierten Wildtyp- und UCP1-KO Mäusen isoliert und anschließend ihre Atmungs- und Superoxidproduktionsraten *in vitro* bestimmt. Durch Zugabe von Modulatoren der Atmungskette und UCP1 konnten die Seiten der Superoxidproduktion innerhalb der Mitochondrien bestimmt werden. UCP1 reduzierte die Superoxidproduktion an der I_Q-Seite von Komplex I um ~40-50%, an der Glycerol-3-Phosphatdehydrogenase um ~20% und an anderen Seiten, wie dem Q-Pool oder Komplex III, um 50-70%. Durch Kälteakklimatisierung stieg die Protonenumsatzrate in Wildtypmitochondrien um 300% an. Bedingungen, unter denen die Superoxidproduktion ebenfalls ansteigen sollte. Meine Studie zeigte jedoch, dass UCP1 die Superoxidproduktion um bis zu 96% reduzierte. Durch die Entkopplung der Atmungskette von der ATP-Synthese wurde vermutlich die Wahrscheinlichkeit des „reversen Elektronentransport" vermindert und somit die Superoxidproduktion an Komplex I der Atmungskette reduziert. Interessanterweise war die bei den Wildtypen beobachtete, kälteinduzierte Erhöhung der Substratoxidation in braunen Fettmitochondrien von UCP1-defizienten Mäusen unterdrückt. Sie zeigten erniedrigte Superoxidproduktionsraten. Wahrscheinlich ist dies ein Schutzmechanismus, der die Anreicherung von ROS im braunen Fettgewebe von UCP1-defizienten Mäusen verhindern sollte.

Meine Ergebnisse demonstrierten deutlich, dass das Entkoppeln der Atmungskette ein physiologisch relevanter Mechanismus ist, um den oxidativen Stress im braunen Fett während der β-Oxidation (Thermogenese) zu reduzieren. Es ist denkbar, dass in der Evolution eine Selektion für die Implementierung von UCP1 als Schutz vor ROS im braunen Fettgewebe stattfand. Unterstützt wird diese Hypothese durch die Entdeckung von ursprünglichen UCP1 Orthologen in Ektothermen (Jastroch et al. 2005), in denen eine primäre Funktion von UCP1 für die endogene Wärmebildung unwahrscheinlich ist.

KAPITEL 3: SEASONAL CHANGES IN THERMOGENESIS OF A FREE-RANGING AFROTHERIAN SMALL MAMMAL, THE WESTERN ROCK ELEPHANT SHREW (*ELEPHANTULUS RUPESTRIS*)

R. OELKRUG ∞ C.W. MEYER
G. HELDMAIER ∞ N. MZILIKAZI

Wie bereits oben erwähnt, treten Torpor und die Expression von braunem Fettgewebe auch bei phylogenetisch älteren Säugetierordnungen der südlichen Breiten auf (Mzilikazi and Lovegrove 2004, Mzilikazi et al. 2007). Demzufolge ist es wahrscheinlich, dass auch sie Formen der zitterfreien Wärmebildung während der saisonalen Anpassung an den Winter (adaptive Thermogenese) oder während des Aufwärmvorganges aus hypometabolen und hypothermen Phasen nutzen. Um die Funktion des braunen Fettgewebes in phylogenetisch älteren Arten aus afrotropischen Regionen besser zu verstehen, beschäftigte ich mich in dieser Studie mit den thermoregulatorischen Kapazitäten von Westlichen Klippen-Elefantenspitzmäusen aus Südafrika. Basierend auf meinen Hauptforschungsinteressen, der Bedeutung des braunen Fettgewebes in Säugetieren (nicht nur in Eutheriern) und den evolutionären Umständen, die zu seiner Entwicklung geführt haben, interessierte mich vor allem:

1) Wie ausgeprägt ist die saisonale metabolischen Anpassung in Arten afrotropischer Regionen?
2) Wie weitverbreitet sind Formen der adaptive Thermogenese innerhalb der Überordnung Afrotheria?

In dieser Studie wurden Westliche Klippen-Elefantenspitzmäuse (*Elephantulus rupestris*) im Freiland (Gamkaberg Nature Reserve, Oudtshoorn, Südafrika) untersucht, so dass artifizielle Effekte einer Laborhaltung ausgeschlossen werden konnten. Westliche Klippen-Elefantenspitzmäuse gehören zur Überordnung der Afrotheria. Sie sind ideale Kandidaten zur Untersuchung von saisonalen metabolischen Anpassungen, da sie zu den kleinsten Vertretern der Afrotheria zählen und in einem sehr saisonalen Habitat, mit Regen während der Wintermonate, leben (Fig. 4 Introduction).

Entgegen der Erwartungen zeigten die untersuchten Elefantenspitzmäuse eine sehr ausgeprägte Fähigkeit, sich den energetisch höher werdenden Anforderungen während der Wintermonate anzupassen. Sowohl ihr Basalstoffwechsel als auch ihre metabolische Antwort auf einen Kältestimulus waren im Winter im Vergleich zum Sommer gesenkt, was auf eine Verbesserung der Fellisolierung oder eine Reduktion der Körpertemperatur während der Wintermonate hindeutete. Beides führt zu einer gesenkten Wärmeabgabe über die Körperoberfläche und somit zu einer Reduzierung der thermoregulatorischen Kosten. Bemerkenswerter Weise trat Torpor während der Winter- und während der Sommermonate auf, dabei schienen nicht nur sinkende Außentemperaturen und ein reduziertes Nahrungsangebot ausschlagende Faktoren für den Eintritt in den Torpor zu sein. Eine genauere Analyse der Daten ergab, dass Regen oder eine erhöhte Luftfeuchtigkeit als physikalischer Stimulus für den Eintritt in den Torpor eine wichtige Rolle spielten. Eine erhöhte Luftfeuchte zerstört die isolierende Luftschicht im Fell und führt dadurch zu einer erhöhten Wärmeabgabe. Die daraus entstehenden, erhöhten thermoregulatorischen Kosten können durch spontanen Torpor gesenkt werden. Bislang hat nur eine Studie von einem Zusammenhang zwischen Regen und Torpor berichtet (Körtner und Geiser 2000). Dieses Phänomen sollte in nachfolgenden Studien weiter validiert werden.

An den Winter adaptierte Tiere zeigten nicht nur eine erhöhte Torporfrequenz, sondern auch niedrigere minimale Körpertemperaturen (niedrigste aufgezeichnete Körpertemperatur: 11.9°C). Des Weiteren konnte die extreme Flexibilität der Westlichen Klippen-Elefantenspitzmäuse während des *arousals* aus dem Torpor beobachtet werden. Von Östlichen Klippen-Elefantenspitzmäuse (*Elephantulus myurus*) war bislang bekannt, dass Elefantenspitzmäuse exogene Wärmequellen (Sonnenbaden) nutzen um aus dem Torpor aufzuwachen (Mzilikazi and Lovegrove 2002). Die hier untersuchte Art nutzte jedoch meistens körpereigene Wärmebildungsmechanismen um aus dem Torpor zu erwachen und besonders

ausgeprägt war dieses Verhalten während des Winters. Östliche Klippen-Elefantenspitzmäuse leben in einem Habitat mit Regen während der Sommermonate. Es wäre denkbar, dass die härteren Bedingungen im Habitat von Westlichen Klippen-Elefantenspitzmäusen zu einer Form der körpereigenen Wärmebildung (adaptive Thermogenese) während der Wintermonate geführt haben.

Zur weiteren Evaluation dieser Hypothese bestimmte ich die Kapazität zur zitterfreien Wärmebildung von an den Sommer und an den Winter adaptierter Elefantenspitzmäuse. Zur Induktion der maximalen zitterfreien Wärmebildung erhielten die Tiere eine Injektion mit Noradrenalin, dem Neurotransmitter, der vom sympathischen Nervensystem zur Aktivierung des braunen Fetts ausgeschüttet wird. Als Bestätigung meiner Hypothese zeigten an den Winter adaptierte Tiere eine 1.8fach höhere Wärmebildungskapazität als an den Sommer adaptierte Tiere. Der eindeutige Nachweis dafür, dass adaptive Thermogenese ein weitverbreitetes Charakteristikum in der saisonalen Anpassung von afrotherischen Säugetieren ist. Darüber hinaus bestätigten weitere Analysen, dass ihre Fähigkeit zur adaptiven Thermogenese einen hohen Grad an thermoregulatorischer Plastizität aufweist; vergleichbar mit den thermoregulatorischen Fähigkeiten eutherischer Säugetiere der nördlichen Breiten. Ein evolutionäres Szenario, in dem braunes Fett und adaptive Thermogenese primär zur Besiedlung holarktischer Regionen entstanden sind, erscheint vor diesem Hintergrund sehr unwahrscheinlich.

BROWN FAT IN A ´PROTOENDOTHERMIC´ MAMMAL FUELS THE PARENTAL CARE MODEL OF MAMMALIAN EVOLUTION

R. OELKRUG ∞ N. GOETZE ∞ C. EXNER
L. YANG ∞ G.K. GANJAM ∞M. KUTSCHKE ∞ S. MÜLLER ∞ S. STÖHR
M.H. TSCHÖP ∞ P.G. CRICHTON ∞ G. HELDMAIER ∞ M. JASTROCH
C.W. MEYER

Adaptive Thermogenese ist ein weitverbreitetes Charakteristikum der saisonalen Anpassung afrotherischer Säugetiere und konnte bislang nicht in phylogenetisch ursprünglicheren Arten, wie zum Beispiel Beuteltieren, nachgewiesen werden. Es ist demnach wahrscheinlich, dass innerhalb der Säugetierphylogenie voll funktionales braunes Fett das erste Mal bei den Afrotheriern auftrat. Demzufolge hat UCP1 seine volle thermogenetische Funktion an einem Punkt nach der Transition der Beuteltiere entwickelt. Die ursprünglichste Form von „modernem UCP1 und braunem Fett“ müsste demnach innerhalb der Afrotheria zu finden sein. Es gibt eine Gruppe von Säugetieren, die zwischen das Evolutionsstadium fakultativ endothermer Reptilien und endothermer Säugetieren gestellt werden kann. Diese sogenannten „protoendothermen“ Säugetiere zeichnen sich durch eine sehr hohe Flexibilität in ihrem thermoregulatorischen Verhalten und den fakultativen Nutzen von Ektothermie zur Energieeinsparung aus (Grigg et al. 2004). Braunes Fett konnte bei ihnen bislang nicht nachgewiesen werden. Der kleine Igeltenrek (*Echinops telfairi*) ist ein protoendothermes Säugetier, das zur Überordnung Afrotheria zählt (Fig. 5 Introduction). Er lebt endemisch auf Madagaskar und ist der ideale Modellorganismus bei der Untersuchung einer direkten Verbindung zwischen Endothermie und der Evolution von voll funktionalem braunem Fettgewebe.

Die Körpertemperatur des kleinen Igeltenreks ist stark an die Umgebungstemperatur gekoppelt und zeigt reptilien-ähnliche Verläufe (Lovegrove and Genin 2008). Durchgängig hohe (~32°C) Körpertemperaturen werden nur von Weibchen während Perioden der Reproduktion und der elterlichen Fürsorge erreicht (Poppitt et al. 1994). Auch wenn kleine Igeltenreks Formen der endogenen Thermogenese nur sehr opportunistisch zu nutzen scheinen, konnte β3-adrenerge Inhibierung die Aufwärmraten aus dem Torpor *in vivo* erniedrigten; der erste Hinweis auf eine Rolle der zitterfreien Wärmebildung beim *arousal* aus dem Torpor und die mögliche Expression von braunem Fettgewebe. Bei der anschließenden Präparation der Versuchstiere konnte braunes Fettgewebe anatomisch nachgewiesen werden. Ungewöhnlicher Weise befanden sich die größten braunen Fettdepots in der Nähe der Gonaden, wohingegen sie sich bei Nagetieren im Hals-Nacken Bereich befinden. In diesen

braunen Fettdepots konnte eine Rekrutierung der oxidativen Kapazität nach Kälteakklimatisation und ein hohes Protonenleck, das durch UCP1 katalysiert wurde, nachgewiesen werden. Weiteres bioenergetisches Profiling von Tenrek UCP1 ergab die gleiche thermogenetische Potenz wie modernes Maus UCP1, unabhängig von der großen phylogenetischen Distanz zwischen den beiden UCP1 Orthologen. Demnach besitzen auch primitive, protoendothermen Säugetiere voll funktionales braunes Fett. Sie nutzen es nur nicht zur dauerhaften Aufrechterhaltung einer konstant hohen Körpertemperatur.

Die Präsenz von aktivem gonadalen braunem Fett und die erhöhten Körpertemperaturen trächtiger Tenrekweibchen (Poppitt et al. 1994) deuten daraufhin, dass braunes Fett beim kleinen Igeltenrek primär eine Rolle bei der Jungaufzucht spielt. Meine Daten unterstützen dadurch ein evolutionäres Szenario, in dem aktive Selektion zu einer erhöhten Inkubationstemperatur des Fötus und sekundär zu einer Erhöhung der Körpertemperatur geführt hat. Dies ist eine Bekräftigung der elterlichen Fürsorgen Theorie der Evolution der Endothermie (*parental care theory*, Farmer 2000). Eine Reduzierung der Nachwuchs-sterblichkeit und eine Beschleunigung des juvenilen Wachstums ist der effektivste Weg, um die Fitness einer Art zu verbessern (Kozlowski 1992). Die Theorie der elterlichen Fürsorge greift eben diesen Aspekt auf und postuliert, dass es durch eine Verbesserung der Brutpflege (erhöhte Inkubationstemperatur, bessere Versorgung der Jungen) zur Evolution der Endothermie kam (Farmer 2000). Eine direkte Ursache für die Evolution eines distinkten thermogenetischen Organs wie dem braunen Fett wurde in diesem Kontext jedoch noch nie untersucht.

Basierend auf meinen Daten entwickelten wir ein neues Schema zur Evolution der Endothermie, in dem die vom braunen Fett vermittelte zitterfreie Wärmebildung zu einer verbesserten Inkubation und Brutpflege des Nachwuchses geführt hat. Dies ermöglichte die Radiation erster ursprünglicher Eutherier und führte zur Entstehung der ersten obligat endothermen Säugetiere. Die weitere Entwicklung und funktionelle Spezialisierung des braunen Fettgewebes, in Richtung Aufrechterhaltung einer konstant hohen Körpertemperatur, führte erst dann zur Erschließung weiterer ökologischer Nischen und zur Migration in holarktische Gebiete (Fig. 7 Scope of the PhD-thesis).

REFERENZEN

Bieber C. and Ruf T. (2009) *Summer dormancy in edible dormice (Glis glis) without energetic constraints.* Naturwissenschaften 96: 165-171.

Cannon B. and Vogel G. (1977) *The mitochondrial ATPase of brown adipose tissue. Purification and comparison with the mitochondrial ATPase from beef heart.* FEBS Lett 76: 284–289.

Cannon B. (1980) *Nonshivering thermogenesis in the newborn.* Molec Aspects Med 3: 119-223.

Cannon B. and Nedergaard J. (2004) *Brown adipose tissue: function and physiological significance.* Physiol Rev 84: 277–359.

Dausmann K.H., Glos J., Ganzhorn .JU. and Heldmaier G. (2004) *Physiology: hibernation in a tropical primate.* Nature 429: 825–826.

Dikic D., Heldmaier G. and Meyer C.W. (2008) *Induced torpor in different strains of laboratory mice.* In: Hypometabolism in animals: torpor. hibernation and cryobiology, eds. Lovegrove B.G. and McKechnie A.E., University of KwaZulu-Natal, Pietermaritzburg: 223–230.

Echtay K.S., Roussel D., St-Pierre J., Jekabsons, M. B., Cadenas et al. (2002) *Superoxide activates mitochondrial uncoupling proteins. Nature* 415: 96–99.

Echtay K.S., Esteves T.C., Pakay J.L., Jekabsons M.B., Lambert A.J. et al. (2003) *A signalling role for 4-hydroxy-2-nonenal in regulation of mitochondrial uncoupling.* EMBO J 22, 4103–4110.

Enerback S., Jacobsson A., Simpson E.M., Guerra C., Yamashita H. et al. (1997) *Mice lacking mitochondrial uncoupling protein are cold-sensitive but not obese.* Nature 387: 90–94.

Farmer C.G. (2000) *Parental care: the key to understanding endothermy and other convergent features in birds and mammals.* Am Nat 155: 326-334.

Geiser F. (2004) *Metabolic rate and body temperature reduction during hibernation and daily torpor.* Annu Rev Physiol 66: 239–274.

Golozoubova V., Hohtola E., Matthias A., Jacobsson A., Cannon B. et al. (2001) *Only UCP1 can mediate adaptive nonshivering thermogenesis in the cold.* FASEB J 15: 2048–2050.

Golozoubova V., Cannon B. and Nedergaard J. (2006) *UCP1 is essential for adaptive adrenergic nonshivering thermogenesis.* Am J Physiol Endocrinol Metab 291: E350–E357.

Granneman J.G., Burnazi M., Zhu Z. and Schwamb L.A. (2003) *White adipose tissue contributes to UCP1-independent thermogenesis.* Am J Physiol Endocrinol Metab 285: E1230–1236.

Grigg G.C., Beard L.A. and Augee M.L. (2004) *The evolution of endothermy and its diversity in mammals and birds.* Physiol Biochem Zool 77: 982-997.

Harman D. (1956) *Aging: a theory based on free radical and radiation chemistry.* J Gerontol 11: 298–300.

Harman D. (1972) *Free radical theory of aging: dietary implications.* Am J Clin Nutr 25: 839–843.

Hayward J.S. and Lisson P.A. (1992) *Evolution of brown fat: its absence in marsupials and monotremes.* Can J Zool 70: 171–179.

Hart J.S. (1952) *Effects of temperature and work on metabolism, body temperature, and insulation: results with mice.* Can J Zool 30: 90-98.

Heldmaier G., Steinlechner S., Ruf T., Wiesinger H. and Klingenspor M. (1989) Photoperiod and thermoregulation in vertebrates: body temperature rhythms and thermogenic acclimation. J Biol Rhythms 4: 251-265.

Heldmaier G., Klaus S. and Wiesinger H. (1990) *Seasonal adaptation of thermoregulatory heat production in small mammals.* In: Thermoreception and Temperature Regulation, eds. Bligh J. and Voigt K., Springer, Berlin, Heidelberg, New York: 235-243.

Heldmaier G., Ortmann S. and Elvert R. (2004) Natural hypometabolism during hibernation and daily torpor in mammals. Respir Physiol Neurobiol 141: 317–329.

Heldmaier G., Neuweiler G. and Rössler W. (2012) *Vergleichende Tierphysiologie.* Springer-Verlag Berlin, Heidelberg.

Himms-Hagen J. (1984) Nonshivering thermogenesis. Brain. Res Bull 12: 151-160.

Hudson J.W. and Scott I.M. (1979) *Daily torpor in the laboratory mouse, Mus musculus var. albino.* Physiol Zool 52: 205–218.

IUPS-Thermal-Commission (2003) *Glossary of terms for thermal physiology.* 3rd ed. Thermal Biol 28: 75–106.

Jastroch M., Wuertz S., Kloas W. and Klingenspor M. (2005) *Uncoupling protein 1 in fish uncovers an ancient evolutionary history of mammalian nonshivering thermogenesis.* Physiol Genomics 22: 150-156.

Jastroch M., Withers K.W., Taudien S., Frappell P.B., Helwig M. et al. (2008) *Marsupial uncoupling protein 1 sheds light on the evolution of mammalian nonshivering thermogenesis.* Physiol Genomics 32: 161–169.

Klingenspor M. (2003) *Cold-induced recruitment of brown adipose tissue thermogenesis.* Exp Physiol 88: 141–148.

Körtner G. and Geiser F. (2000) *Torpor and activity patterns in free-ranging sugar gliders Petaurus breviceps (Marsupialia).* Oecologia 123: 350 - 357.

Kozlowski J. (1992) *Optimal allocation of resources to growth and reproduction: implications for age and size at maturity.* Trends Ecol Evol 7: 15-19.

Lovegrove B.G. and Genin F. (2008) *Torpor and hibernation in a basal placental mammal, the Lesser Hedgehog Tenrec Echinops telfairi.* J Comp Physiol B 178:691–698.

Lowell B.B. and Spiegelman B.M. (2000) *Towards a molecular understanding of adaptive thermogenesis.* Nature 404: 652-660.

Lyman C.P. and O'Brian R.C. (1986) *Is brown fat necessary?* In: Living in the Cold: Physiological and Biochemical Adaptations, eds. Heller H.C., Musacchia X.J. and Wang L.H.C. Elsevier, New York: 116-119.

McKechnie A.E. and Wolf B.O. (2004) *The energetics of the rewarming phase of avian torpor.* In: Life in the Cold: Evolution, Mechanism, Adaptation and Application, eds. Barnes B.M. and Carey H.V., University of Alaska, Fairbanks: 265-273.

Meyer C.W., Willershauser M., Jastroch M., Rourke B.C., Fromme T., Oelkrug R. et al. (2010) *Adaptive thermogenesis and thermal conductance in wild-type and UCP1-KO mice.* Amer J Physiol 299: R1396-1406.

Mzilikazi N., Lovegrove B. and Ribble D.O. (2002)

Exogenous Passive Heating during Torpor Arousal in Free-Ranging Rock Elephant Shrews, Elephantulus myurus. Oecologica 133: 307-314.

Mzilikazi N. and Lovegrove B.G. (2004) *Daily torpor in free-ranging rock elephant shrews, Elephantulus myurus: a year-long study.* Physiol Biochem Zool 77:285–296.

Mzilikazi N., Jastroch M., Meyer C.W. and Klingenspor M. (2007) *The molecular and biochemical basis of nonshivering thermogenesis in an African endemic mammal, Elephantulus myurus.* Am J Physiol 293: R2120–R2127.

Nicholls D.G., Locke R.M. (1984) *Thermogenic mechanisms in brown fat.* Physiol Rev 64:1-64.

Nicol S.C., Morrow G. and Andersen N.A. (2008) *Hibernation in monotremes: a review*. In: Hypometabolism in Animals: Hibernation, Torpor and Cryobiology, eds. Lovegrove B.G. and McKechnie A.E. University of KwaZulu-Natal, Pietermaritzburg: 251-262.

Polymeropoulos E.T., Jastroch M. and Frappell P.B. (2012) *Absence of adaptive nonshivering thermogenesis in a marsupial, the fat-tailed dunnart (Sminthopsis crassicaudata).* J Comp Physiol B 182: 393-401.

Poppitt S.D., Speakman J.R., Racey P.A. (1994) *Energetics of Reproduction in the Lesser hedgehog tenrec, Echinops telfairi (Martin).* Physiol Zool 67: 976-994.

Ruf T and Heldmaier G (1992) *The Impact of Daily Torpor on Energy Requirements in the Djungarian Hamster, Phodopus sungorus.* Physiol Zool 65: 994 - 1010.

Scantlebury M., Lovegrove B.G., Jackson C.R., Bennett N.C. and Lutermann H. (2008) *Hibernation and non-shivering thermogenesis in the Hottentot golden mole (Amblysomus hottentottus longiceps).* J Comp Physiol B 178: 887–897.

Shabalina I.G., Petrovic N., Kramarova T.V., Hoeks J., Cannon B. et al. (2006) *UCP1 and defense against oxidative stress. 4-Hydroxy-2-nonenal effects on brown fat mitochondria are uncoupling protein 1-independent.* J Biol Chem 281: 13882–13893.

Shabalina I.G., Hoeks J, Kramarova TV, Schrauwen P, Cannon B et al. (2010) *Cold tolerance of UCP1-ablated mice: A skeletal muscle mitochondria switch toward lipid oxidation with marked UCP3 up-regulation not associated with increased basal, fatty acid- or ROS-induced uncoupling or enhanced GDP effects.* Biochim Biophys Acta 1797: 968–980.

Silva, J. P., Shabalina, I. G., Dufour, E., Petrovic, N., Backlund, E. et al. (2005) *SOD2 overexpression: enhanced mitochondrial tolerance but absence of effect on UCP activity*. EMBO J 24: 4061–4070.

Stone G.N. and Purvis A. (1992) *Warm-up rates during arousal from torpor in heterothermic mammals: physiological correlates and a comparison with heterothermic insects.* J Comp Physiol B 162: 284–295.

Swoap S.J., Gutilla M.J., Liles L.C., Smith R.O. and Weinshenker D. (2006) *The full expression of fasting-induced torpor requires beta 3-adrenergic receptor signalling.* J Neurosci 26: 241–245.

Ukropec J., Anunciado R.P., Ravussin Y., Hulver M.W. and Kozak L.P. (2006) *UCP1-independent thermogenesis in white adipose tissue of coldacclimated Ucp1-/- mice.* J Biol Chem 281: 31894–31908.

Wang L.C.H. (1989) *Ecological, physiological and biochemical aspects of torpor in mammals and birds.* In: Animal Adaptation to Cold. Advances in Comparative and Environmental Physiology, ed.Wang L.C.H., Springer Verlag, Heidelberg: 361-401.

Webb G.P., Jagot S.A. and Jakobson M.E. (1982) *Fasting-induced torpor in Mus musculus and its implications in the use of murine modelsfor human obesity*. Comp Biochem Physiol 72: 211–219.

CURRICULUM VITAE

Die Seiten 150-155 (Curriculum Vitae) enthalten persönliche Daten. Sie sind deshalb nicht Bestandteil der Online-Veröffentlichung.

Die Seiten 150-155 (Curriculum Vitae) enthalten persönliche Daten. Sie sind deshalb nicht Bestandteil der Online-Veröffentlichung.

Die Seiten 150-155 (Curriculum Vitae) enthalten persönliche Daten. Sie sind deshalb nicht Bestandteil der Online-Veröffentlichung.

Die Seiten 150-155 (Curriculum Vitae) enthalten persönliche Daten. Sie sind deshalb nicht Bestandteil der Online-Veröffentlichung.

Die Seiten 150-155 (Curriculum Vitae) enthalten persönliche Daten. Sie sind deshalb nicht Bestandteil der Online-Veröffentlichung.

Die Seiten 150-155 (Curriculum Vitae) enthalten persönliche Daten. Sie sind deshalb nicht Bestandteil der Online-Veröffentlichung.

DANKSAGUNG

Die Seiten 156-157 (Danksagung) enthalten persönliche Daten. Sie sind deshalb nicht Bestandteil der Online-Veröffentlichung.

Die Seiten 156-157 (Danksagung) enthalten persönliche Daten. Sie sind deshalb nicht Bestandteil der Online-Veröffentlichung.

EIGENE BEITRÄGE ZU VERÖFFENTLICHTEN TEILEN DER ARBEIT

Laut §8, Absatz 3 der Promotionsordnung der Philipps-Universität Marburg (Fassung vom 12.4.2000) müssen bei den Teilen der Dissertation, die aus gemeinsamer Forschungsarbeit entstanden sind, „die individuellen Leistungen des Doktoranden deutlich abgrenzbar und bewertbar sein." Dies betrifft die Kapitel 1–4 und die Liste der weiteren wissenschaftlichen Arbeiten. Die Beiträge werden im Folgenden detailliert erläutert.

KAPITEL 1: TORPOR PATTERNS, AROUSAL RATES, AND TEMPORAL ORGANIZATION OF TORPOR ENTRY IN WILDTYPE AND UCP1-ABLATED MICE

- Durchführung aller Experimente
- Auswertung und statistische Analyse von allen Daten mit Beratung durch Dr. Carola Meyer und Prof. Dr. Gerhard Heldmaier
- Anfertigung von 90% der Abbildungen, 10% wurden von Dr. Carola Meyer erstellt
- Anfertigung des Manuskriptes in Zusammenarbeit mit Dr. Carola Meyer und Prof. Dr. Gerhard Heldmaier

Dieses Kapitel wurde in der vorliegenden Form am 19.04.2010 beim **JOURNAL OF COMPARATIVE PHYSIOLOGY B** eingereicht und am 01.08.2010 online publiziert:

Oelkrug R., Heldmaier G. and Meyer C.W. (2011) Torpor patterns, arousal rates, and temporal organization of torpor entry in wildtype and UCP1-ablated mice. J Comp Physiol B 181: 137-145.

KAPITEL 2: UNCOUPLING PROTEIN 1 DECREASES SUPEROXIDE PRODUCTION IN BROWN ADIPOSE TISSUE MITOCHONDRIA

- Durchführung aller Experimente
- Auswertung und statistische Analyse von allen Daten mit Beratung durch Dr. Martin Jastroch, Dr. Carola Meyer und Prof. Dr. Gerhard Heldmaier
- Anfertigung von allen Abbildungen
- Anfertigung des Manuskriptes in Zusammenarbeit mit Dr. Martin Jastroch und Prof. Dr. Gerhard Heldmaier

Dieses Kapitel wurde in der vorliegenden Form am 12.03.2010 beim **JOURNAL OF BIOLOGICAL CHEMISTRY** eingereicht und am 16.07.2010 publiziert.

Oelkrug R., Kutschke M., Meyer C.W., Heldmaier G. and Jastroch M. (2010) Uncoupling protein 1 decreases production of reactive oxygen species in brown adipose tissue mitochondria. J Biol Chem 289: 21961- 21968.

KAPITEL 3: SEASONAL CHANGES IN THERMOGENESIS OF A FREE-RANGING AFROTHERIAN SMALL MAMMAL, THE WESTERN ROCK ELEPHANT SHREW (*ELEPHANTULUS RUPESTRIS*)

- Durchführung von allen Freilandarbeiten und Experimenten
- Implantation von 80% der Versuchstiere, die restlichen 20% wurden von M.sc. Stacey Hallam operiert
- Auswertung und statistische Analyse von allen Daten mit Beratung durch Dr. Nomakwezi Mzilikazi, Dr. Carola Meyer und Prof. Dr. Gerhard Heldmaier
- Anfertigung von allen Abbildungen
- Anfertigung des Manuskriptes in Zusammenarbeit mit Dr. Carola Meyer, Dr. Nomakwezi Mzilikazi und Prof. Dr. Gerhard Heldmaier

Dieses Kapitel wurde in dieser Form am 07.08.2011 beim **JOURNAL OF COMPARATIVE PHYSIOLOGY B** eingereicht und am 12.02.2012 online publiziert.

Oelkrug R., Meyer C.W., Heldmaier G. and Mzilikazi N. (2012) Seasonal Changes in Thermogenesis of a Free-ranging Afrotherian Small Mammal, the Western rock elephant shrew (Elephantulus rupestris). J Comp Physiol B 18: 715-727.

KAPITEL 4: BROWN FAT IN A ´PROTOENDOTHERMIC´ MAMMAL FUELS THE PARENTAL CARE MODEL OF MAMMALIAN EVOLUTION

- Durchführung von 80% der Experimente
- In Zusammenarbeit durchgeführte Experimente:

  Implantation der Versuchstiere: Dr. Cornelia Exner
  Atmungsmessungen an isolierten BAT-Mitochondrien: B.sc. Nadja Goetze
  Western Blots: Sigrid Stöhr und Saskia Müller
  Herstellung von *inclusion bodies*: Dr. Lee Yang und Dr. Paul Crichton

- Auswertung und statistische Analyse von allen Daten mit Beratung durch Dr. Martin Jastroch und Dr. Carola Meyer
- Anfertigung von allen Abbildungen
- Anfertigung des Manuskriptes in Zusammenarbeit mit Dr. Martin Jastroch, Dr. Carola Meyer und Prof. Gerhard Heldmaier.

Dieses Kapitel wurde in der vorliegenden Form am 27.12.2012 beim **JOURNAL OF NATURE COMMUNICATIONS** eingereicht und befindet sich derzeit unter Begutachtung.

WEITERE WISSENSCHAFTLICHE ARBEITEN

ADAPTIVE THERMOGENESIS AND THERMAL CONDUCTANCE IN WILD-TYPE AND UCP1-KO MICE.

- Implantation von Versuchstieren mit temperatursensitiven Minimittern

Diese Arbeit wurde in der vorliegenden Form am 08.09.2010 im **AMERICAN JOURNAL OF REGULATORY, INTEGRATIVE AND COMPARATIVE PHYSIOLOGY** online publiziert.

Meyer C.W., Willershäuser M., Jastroch M., Rourke B., Fromme T., Oelkrug R., Heldmaier G. and Klingenspor M. (2010) Adaptive thermogenesis and thermal conductance in wild-type and UCP1-KO mice. Am J Physiol Regul Integr Comp Physiol 299: R1396-1406.

HIBERNATION IN FREE RANGING AFRICAN WOODLAND DORMICE, GRAPHIURUS MURINUS.

- Durchführung von Freilandarbeiten in Zusammenarbeit mit Dr. Nomakwezi Mzilikazi (Feb. 2009)

- Messung der Stoffwechselraten von 9 Tieren (Feb. 2009)

Diese Arbeit wurde in der vorliegenden Form im August 2012 im Buch **LIVING IN A SEASONAL WORLD – THERMOREGULATORY AND METABOLIC ADAPTATIONS** publiziert.

Mzilikazi N., Madikiza Z., Oelkrug R. and Baxter R. (2012) Hibernation in free ranging African woodland dormice, Graphiurus murinus. T. Ruf et al. (eds.), Living in a Seasonal World, eds. Ruf T. et al., Springer, Berlin, Heidelberg, chapter 4: 41-50.

HYPOTHALAMIC GLYCOGEN SYNTHASE KINASE 3B HAS A CENTRAL ROLE IN THE REGULATION OF FOOD INTAKE AND GLUCOSE METABOLISM.

- Einführung von Dr. Goutham K. Ganjam und M.sc. Manon Krüger in die indirekte Kalorimetrie

- Unterstützung bei der Datenaufnahme und Auswertung der indirekten Kalorimetrie

Diese Arbeit wurde in der vorliegenden Form am 01.10.2012 im **BIOCHEMICAL JOURNAL** publiziert.

Benzler J., Ganjam G.K., Krüger M., Pinkenburg O., Kutschke M., Stöhr S., Steger J., Koch C.E ., Oelkrug R., Schwartz M.W., Sheperd P.R. and Tups A. (2012) Hypothalamic glycogen synthase kinase 3β has a central role in the regulation of food intake and glucose metabolism. Biochem J 447: 175–184.

P62 LINKS BETA-ADRENERGIC INPUT WITH MITOCHONDRIAL FUNCTION.

- Präparation von braunem Fettgewebe

Diese Arbeit wurde in der vorliegenden Form am 02.01.2013 im **JOURNAL OF CLINICAL INVESTIGATIONS** publiziert.

Mueller T.D., Lee S. J., Jastroch M., Kabra D., Stemmer K., Aichler M., Abplanalp B., Ananthakrishnan G., Bhardwaj N., Collins S., Divanovic S., Endele M., Finan, Gao Y., Habegger K.M., Hembree J., Heppner K.M., Hofmann S., Holland J., Küchler D., Kutschke M., Krishna R., Lehti M., Oelkrug R., Ottaway N., Perez-Tilve D., Raver C., Walch A.K., Schriever S.C., Speakman J., Tseng Y., Diaz-Meco M., Pfluger P.T., Moscat J. and Tschöp M.H. (2013) p62 links beta-adrenergic input with mitochondrial function. J Clin Invest 123: 469–478.

Die Abfassung der Dissertation in englischer Sprache wurde vom Dekan des Fachbereiches Biologie am 27.11.2012 genehmigt.

ERKLÄRUNG

Hiermit versichere ich, dass ich meine Dissertation

“NEW PERSPECTIVES ON THE SIGNIFICANCE OF BROWN ADIPOSE TISSUE IN MAMMALS”

(„NEUE EINBLICKE IN DIE EVOLUTION DES BRAUNEN FETTGEWEBES DER SÄUGETIERE”)

selbstständig, ohne unerlaubte Hilfe angefertigt und mich keiner anderen als der von mir ausdrücklich bezeichneten Quellen und Hilfen bedient habe.

Die Dissertation wurde in der jetzigen oder in einer ähnlichen Form noch bei keiner anderen Hochschule eingereicht und hat noch keinen sonstigen Prüfungszwecken gedient.

Marburg, den 14.06.2013

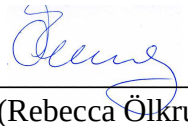

(Rebecca Ölkrug)